# Molecular characterization of quiescent cancer cells

**Ting La**

A thesis submitted in fulfilment of the requirements

for the degree of

Doctor of Philosophy in Medicine Biochemistry

School of Biomedical Sciences and Pharmacy

University of Newcastle

May 2019

# DECLARATION

**STATEMENT OF ORIGINALITY**

*I hereby certify that the work embodied in the thesis is my own work, conducted under normal supervision. The thesis contains no material which has been accepted, or is being examined, for the award of any other degree or diploma in any university or other tertiary institution and, to the best of my knowledge and belief, contains no material previously published or written by another person, except where due reference has been made. I give consent to the final version of my thesis being made available worldwide when deposited in the University's Digital Repository, subject to the provisions of the Copyright Act 1968 and any approved embargo.*

Ting La

**ACKNOWLEDGMENT OF AUTHORSHIP**

*I hereby certify that the work embodied in this thesis contains published paper of which I am a joint author. I have included as part of the thesis a written declaration endorsed in writing by my supervisor, attesting to my contribution to the joint publication/s/scholarly work.*

*By signing below I confirm that Ting La contributed majorly to the paper entitled "A p53-responsive microRNA network promotes cellular quiescence".*

Xu Dong Zhang

## DEDICATION

I dedicate this thesis to my husband Dr. Tao Guo for his endless support and motivation throughout my PhD candidature.

**ACKNOWLEDGEMENTS**

I would like to thank my supervisors Professor Xu Dong Zhang, Dr. Lei Jin and A/Professor Tao Liu for their support and guidance throughout my PhD candidature. Their encouragement, constructive criticism, and incredible enthusiasm have provided me a solid foundation to build on my passion for cancer research.

Special thanks must go to my colleague Margaret Farrelly, a very good partner of doing experiments, who worked with me to establish the dual-fluorescence knock-in (KI) cell lines.

Thanks must go to all my colleagues and friends at the Melanoma Research Laboratory, Xu Guang Yan, Jia Yu Wang, Chun Yan Wang, Hamed Yari, Fen Liu, Yuan Yuan Zhang, Hessam Tabatabaee, Yu Chen Feng, Simonne Sherwin, Lei Jin and Chen Chen Jiang.

I would also like to thank Professor Toshio Kitamura (University of Tokyo, Tokyo, Japan), Drs. Hiroyuki Miyoshi and Atsushi Miyawaki (RIKEN Brain Science Institute, Japan), Dr Michael Carnell (Biomedical Imaging Facility, UNSW), Ms Nicole Cole (The University of Newcastle, Australia), Dr Joshua Brzozowski (The University of Newcastle, Australia) and Dr. Thorne R (The University of Newcastle, Australia) for their assistance in this study.

A very special thank you goes to the security in the University of Newcastle who helped me many times whenever I need.

Last but not least, again I would like to express my gratitude towards my family members and my friends for their love and support. Without them, the completion of my PhD would not have been possible.

# List of Publications Included as part of this Thesis

La T, Liu GZ, Farrelly M, Cole N, Feng YC, Zhang YY, Sherwin SK, Yari H, Tabatabaee H, Yan XG, Guo ST, Liu T, Thorne RF, Jin L, Zhang XD. A p53-responsive microRNA network promotes cancer cell quiescence. Cancer Res. 2018 Dec 1;78(23):6666-6679.

# List of Other Publications during PhD Candidature

1. La T, Liu GZ, Farrelly M, Cole N, Feng YC, Zhang YY, Sherwin SK, Yari H, Tabatabaee H, Yan XG, Guo ST, Liu T, Thorne RF, Jin L, Zhang XD. A p53-responsive microRNA network promotes cancer cell quiescence. Cancer Res. 2018 Dec 1;78(23):6666-6679.

2. Wang JY, Liu GZ, Wilmott JS, La T, Feng YC, Yari H, Yan XG, Thorne RF, Scolyer RA, Zhang XD, Jin L. Skp2-Mediated Stabilization of MTH1 Promotes Survival of Melanoma Cells upon Oxidative Stress. Cancer Res. 2017 Nov 15;77(22):6226-6239

3. Liu F, Jiang CC, Yan XG, Tseng HY, Wang CY, Zhang YY, Yari H, La T, Farrelly M, Guo ST, Thorne RF, Jin L, Wang Q, Zhang XD. BRAF/MEK inhibitors promote CD47 expression that is reversible by ERK inhibition in melanoma. Oncotarget. 2017 May 9;8(41):69477-69492.

4. Wang JY, Jin L, Yan XG, Sherwin S, Farrelly M, Zhang YY, Liu F, Wang CY, Guo ST, Yari H, La T, McFarlane J, Lei FX, Tabatabaee H, Chen JZ, Croft A, Jiang CC, Zhang XD. Reactive Oxygen Species Dictate the Apoptotic Response of Melanoma Cells to TH588. J Invest Dermatol. 2016 Nov;136(11):2277-2286.

5. Wang CY, Guo ST, Wang JY, Yan XG, Farrelly M, Zhang YY, Liu F, Yari H, La T, Lei FX, Jin L, Zhang XD, Jiang CC. Reactivation of ERK and Akt confers resistance of mutant BRAF colon cancer cells to the HSP90 inhibitor AUY922. Oncotarget. 2016 Aug 2;7(31):49597-49610.

## Conferences during PhD Candidature

**Oral presentations:**

1. **La T.** A genomic editing approach for purification of viable quiescent cancer cells. Australian Association of Chinese Biomedical Scientist (AACBS) annual meeting, Sydney, Australia, 28th October, 2018

2. **La T**. A genomic editing approach for purification of viable quiescent cancer cells. School of Biomedical Sciences & Pharmacy Seminar, Callaghan, Australia, 7th September, 2018

3. **La T**. Towards targeting quiescent melanoma cells. The Australasian Melanoma Conference 2016, Sydney, Australia, 28th October, 2016

**Poster presentations:**

1. **La T,** Jin L, Zhang XD. Metabolic approaches to target cancer dormancy. 3rd Australian Cancer and Metabolism Meeting. Sydney, Australia, 21th May, 2019.

2. **La T**, Farrelly M, Cole C, Feng Y. Tabatabaee H, Thorne R, Liu T, Jin L, Zhang XD. Isolation and characterisation of viable quiescent cancer cells. 31st Lorne Cancer Conference 2019. Lorne, Australia, 15th February, 2019.

3. **La T**, Farrelly M, Nico N, Feng Y, Tabatabaee H, Lei J, Zhang XD. A p53‐responsive microRNA network promotes cancer cell quiescence. 2018 Hunter Cancer Research Symposium. New Lambton Heights, Australia, 1st November, 2018.

4. **La T.** A genomic editing approach for purification of viable quiescent cancer cells. American Association for Cancer Research annual meeting. Chicago, America, 15th, April, 2018.

5. **La T**, Farrelly M, Liu T, Lei J, Zhang XD. A genomic editing approach for purification of intact quiescent cancer cells. 2017 Hunter Cancer Research Symposium. New Lambton Heights, Australia, 24th November, 2017.

6. **La T,** Farrelly M, Wang JY, Wang CY, Yan XG, Zhang YY, Liu F, Yari H, Lei FX, Jiang CC, Liu T, Jin L, Zhang XD. Towards targeting quiescent melanoma cells. 2016 Hunter Cancer Research Symposium. New Lambton Heights, Australia, 25th November, 2016.

# List of abbreviations

| | |
|---|---|
| 2,4-DNP | 2,4-Dinitrophenol |
| 3’ UTR | 3’ un-translated region |
| 5’ UTR | 5’ un-translated region |
| ACC | Acetyl CoA carboxylase |
| AGRF | Australia Genome Research Facility |
| AML | Acute myeloid leukemia |
| AMPK | AMP-activated protein kinase |
| ANGPTL4 | Angiopoietin-like 4 |
| APC | Anaphase-promoting complex |
| APOBEC1 | Apolipoprotein B mRNA editing enzyme, catalytic polypeptide 1 |
| APS | Ammonium persulphate |
| ATP | Adenosine triphosphate |
| BAY87-2243 | 1-cyclopropyl-4-(4-[(5-methyl-3-(3-[4-(trifluoromethoxy)phenyl]-1,2,4-oxadiazol-5-yl)-1H-pyrazol-1-yl)methyl]pyridin-2-yl)piperazine |
| BC | Breast cancer |
| BE3 | The third generation base editor |
| BM | Bone marrow |
| BMIF | Biomedicain Imaging Facility |
| C | Cycling |
| C9ORF3 | Chromosome 9 open reading frame 3 |
| CAC1 | CDK2 associated cullin domain 1 |
| cAMP | Cyclic adenosine monophosphate |

| | |
|---|---|
| CCCP | Carbonyl cyanide 3-chlorophenylhydrazone |
| CDC20 | Cell Division Cycle 20 |
| CDH1 | Cadherin 1 |
| CDK | Cyclin dependent kinase |
| CDKI | Cyclin-dependent kinase inhibitor protein |
| CDKN1B | Cyclin Dependent Kinase Inhibitor 1B |
| CDS | Coding sequence |
| Cdt1 | Chromatin licensing and DNA replication factor 1 |
| CI/KIP | CDK interacting protein/Kinase inhibitory protein |
| Cks1 | Cyclin-dependent kinases regulatory subunit 1 |
| COL27A1 | Collagen alpha-1 (XXVII) chain |
| CRISPR | Clustered regularly interspaced short palindromic repeats |
| crRNA | CRISPR RNA |
| CTC | Circulating tumour cell |
| DAPI | 4′,6-diamidino-2-phenylindole |
| DBD | DNA-binding domain |
| DDR | DNA damage response |
| DE | Differential expression |
| DMKG | Dimethyl α-Ketoglutarate |
| DNA | Deoxyribonucleic acid |
| DNMT3A | DNA methyltransferase 3A |
| DSB | Double-strand breaks |
| DTC | Disseminated tumor cells |
| ECL | Electrogenerated chemiluminescence |

| | |
|---|---|
| ECM | Secrete extracellular matrix |
| EDTA | Ethylenediaminetetraacetic acid |
| EMT | Epithelial-to-mesenchymal transition |
| ER | Estrogen receptor |
| ESC | Embryonic stem cell |
| FACS | Fluorescence-activated cell sorter |
| FCS | Fetal Calf Serum |
| FHA | Forkhead-associated domain |
| FOX | Forkhead box |
| FUCCI | Fluorescence Ubiquitin Cell Cycle Indicator |
| G1 phase | Gap 1 phase |
| G2 phase | Gap 2 phase |
| GAPDH | Glyceraldehyde 3-phosphate dehydrogenase |
| GFP | Green fluorescent protein |
| GSEA | Gene set enrichment analysis |
| HD | Homologous recombination |
| HDAC | Histone deacetylase |
| HDR | Homology-directed repair |
| HeLa.pK | HeLa cells with CDKN1B fused with the EGFP gene and MKI67 with the mCherry gene |
| HES1 | Hes Family BHLH Transcription Factor 1 |
| HRP | Horseradish peroxidase |
| HSC | Hematopoietic stem cell |
| INK4 | INhibitors of CDK4 |
| IP | Immunoprecipitation |

| | |
|---|---|
| IPA | Ingenuity Pathway Analysis |
| iTRAQ | Isobaric tags for relative and absolute quantification |
| KI | Knock-in |
| KPC | Kip1 ubiquitination-promoting complex |
| KRAB | Krüppel associated box |
| LC-MS | Liquid chromatography–mass spectrometry |
| lncRNA | Long noncoding RNA |
| LR domain | Leucine/arginine-rich C-terminal domain |
| LSD1 | Lys-specific histone demethylase 1 |
| M phase | Mitotic phase |
| MAPK | Mitogen-activated protein kinase |
| Mel-RM.pK | Mel-RM cells with CDKN1B fused with the EGFP gene and MKI67 with the mCherry gene |
| miRNA | microRNAs |
| MRD | Minimal residual disease |
| NES | Nuclear exportation signal |
| NGS | Next-generation sequencing |
| NHEJ | Nonhomologous end joining |
| NIFK | Nucleolar Protein Interacting With The FHA Domain Of MKI67 |
| NK | Natural killer |
| NLS | Nuclear localization signal |
| ORF | Open reading frame |
| OXPHOS | Oxidative phosphorylation |
| PAM | Protospacer adjacent motif |
| PBS | Phosphate-buffered saline |

| | |
|---|---|
| PCL | Perichromosomal layer |
| PCR | Polymerase chain reaction |
| PFT-α | Pifithrin-α |
| PI | PAM interacting |
| PI | Propidium iodide |
| PI3K | Phosphoinositide 3-kinase |
| PKA | protein kinase A |
| PLDR | Potentially lethal damage |
| Plk | Polo-like protein kinase |
| PP1 | Protein phosphatase 1 |
| PP1 | Protein phosphatase 1 |
| pRb | phosphorylated Retinoblastoma |
| Q | Quiescent |
| QC | Quality control |
| Rb | Retinoblastoma |
| RBPJ | Recombination Signal Binding Protein For Immunoglobulin Kappa J Region |
| RNA | Ribonucleic acid |
| RNAi | RNA interference |
| RNA-Seq | RNA sequencing |
| RVD | Repeat-variable di-residue |
| S phase | Synthesis Phase |
| SA | Senescence-associated |
| SCF complex | Skp, Cullin, F-box containing complex |
| SDS-PAGE | Sodium dodecyl sulphate-polyacrylamide gel electrophoresis |

| | |
|---|---|
| sgRNA | Small guide RNA |
| Skp2 | S-phase kinase-associated protein |
| STR | Short tandem repeat |
| T7E1 | T7 Endonuclease I |
| TALEN | Transcription activator-like effector nuclease |
| TF | Transcription factor |
| TGFβ | Transforming growth-factor beta |
| tracrRNA | Trans-acting antisense RNA |
| TSB | Tris-buffered saline |
| TSP | Thrombospondin |
| TTFA | 2-Thenoyltrifluoroacetone |
| VEGF | Vascular endothelial growth factor |
| WTSS | Whole transcriptome shotgun sequencing |
| ZFN | Zinc-finger nuclease |
| β-gal | β-galactosidase |

# Table of contents

## Contents

# List of figures

# List of tables

# Synopsis

Relapse following initial remission, especially metastasis, is currently a major cause in cancer-related death and occurs in virtually every types of anti-cancer therapy. The tumour recurrence is mainly due to the wake-up of the residual cancer cells, which are remaining quiescent during remission after conventional treatment. Quiescent cancer cells are inherently resistant to cell death and refractory to therapeutic drugs. Specifically targeting quiescent cancer cells by uncover the characteristics would be a promising way to eradicate cancer completely. Nevertheless, the mechanisms responsible for the resistance of quiescent cancer cells to cell death remain largely undefined. This is primarily due to the lack of understanding of their biological characteristics as a consequence of technical hurdles in the isolation and analysis of viable quiescent cells

Quiescent cells characteristically express high levels of the cyclin-dependent kinase (CDK) inhibitor p27. This thesis includes two systems of isolation quiescent cancer cells. First, a model system encompassing an mVenus-tagged p27 mutant lacking the CDK-binding domain (mVenus-p27K$^{-}$) together with a mCherry-tagged truncated mutant of chromatin licensing and DNA replication factor 1 (hCDT1) [mCherry-hCDT1(30/120)] that is exclusively expressed in cells in G0 and G1 phases was employed to isolate putative mVenus-p27K$^{-high}$/mCherry-hCDT1(30/120)+ mouse melanoma cells. By using this system, we identified a p53-responsive microRNA network that promotes cellular quiescence in both mouse and human melanoma cells.

Building on this, we took advantage that quiescent cells are also characteristically negative for the proliferation marker Ki67 to develop a CRISPR/Cas9-based system, in which a green fluorescent protein (EGFP) gene is fused with endogenous *CDKN1B*, the gene encoding p27, and a red fluorescent protein (mCherry) gene, with endogenous *MKI67*, the gene encoding Ki67 in the genome of human melanoma cells. By using this system, we have successfully isolated viable p27$^{high}$/Ki67$^{-}$ human melanoma cells using FACS that were verified to be authentic quiescent cells.

This system provides us with an exceptional tool for further characterization of the biological properties of quiescent melanoma cells.

By analysing the transcripts and protein profiles in the isolated quiescent and cycling cancer cells, we found that in comparison with cycling cancer cells, the quiescent cancer cells generate energy relying on oxidative phosphorylation (OXPHOS) rather than glycolysis. Of note, by employing OXPHOS inhibitor, quiescent melanoma cells either arrested by serum starvation or by various MAPK inhibitors are dramatically sensitive to apoptosis. Overall, towards targeting quiescent cancer cells by inhibiting OXPHOS may be exploited to overcome cellular quiescence induced cancer recurrence.

# Chapter one

# General Introduction

## 1.1 Tumour dormancy

### 1.1.1 Overview

Despite the dramatic development of new technologies and cancer therapeutics since the commencement of the 'War on Cancer' in 1971, cancer is still one the major causes of human death. There are many types of cancer treatment in currently used. Patients with cancer are usually treated with a combination of several kinds of treatments. Surgery is a procedure in which a surgeon removes cancer from a patients' body. Radiation therapy is a kind of treatment that depends on an accurate dose of radiation to kill cancer cells and shrink tumours. While chemotherapy relies on different kinds of drugs to kill cancer. In comparison with surgery and radiation therapy, chemotherapy works on the whole body. Targeted therapy was created according to the abnormal activation of special genes of pathway in specific types of cancer. For example, BRAF somatic missense mutations occur in 66 % of malignant melanomas and at lower frequency in a wide range of human cancers[1]. The activating mutations of BRAF result in the enhancer of the mitogen-activated protein kinase (MAPK) pathway, thereby enhancing tumour growth and facilitates tumour progression. Drugs specifically targeting mutant BRAF (vemurafenib, dabrafenib etc.) were found to shrink or slow the growth of melanoma[2]. An emerging treatment strategy, immunotherapy, is a type a therapeutic that boost the ability of immune system to kill cancer cells.

Generally speaking, all above therapeutics have a striking outcome of killing or shrinking tumours. Nevertheless, fatal recurrence or relapse for a variety of cancers can occur years and even decades later after remission, in most cases results in metastatic disease, the major cause of cancer-related deaths[3, 4, 5].

In metastasis, cancer cells break away from the initial site where they first formed (primary cancer), overcome many kinds of barriers (blood, lymph system etc.), and finally, colonize in

another part of body[6]. Metastatic tumours usually develop during the late stage of cancer. Of note, the lungs are the common organ that metastasis occurs frequently[7, 8]. In comparison with primary tumours, metastatic tumours usually increase the chance of death, which is mainly due to the broaden colonization in the body so that it is out of control of different types of treatments[9].

### 1.1.2 The metastatic cascade

Metastasis is associated with as much as 90% of cancer-related mortality[10]. Cancer metastasis occurs through a sequential series of events known as the metastatic cascade. The cancer cells need overcome seven bottlenecks to finally form a micrometastasis: invasion, intravasation, dissemination into the circulation and survival, arrest at the distant site, extravasation, tumour initiation, and finally, outgrowth and clinical manifestation (Fig. 1.1)[10, 11, 12]. These functions are not only limited to cell-autonomous traits, but also highly depend on the interaction of the metastatic cell with the tumour and host stroma.

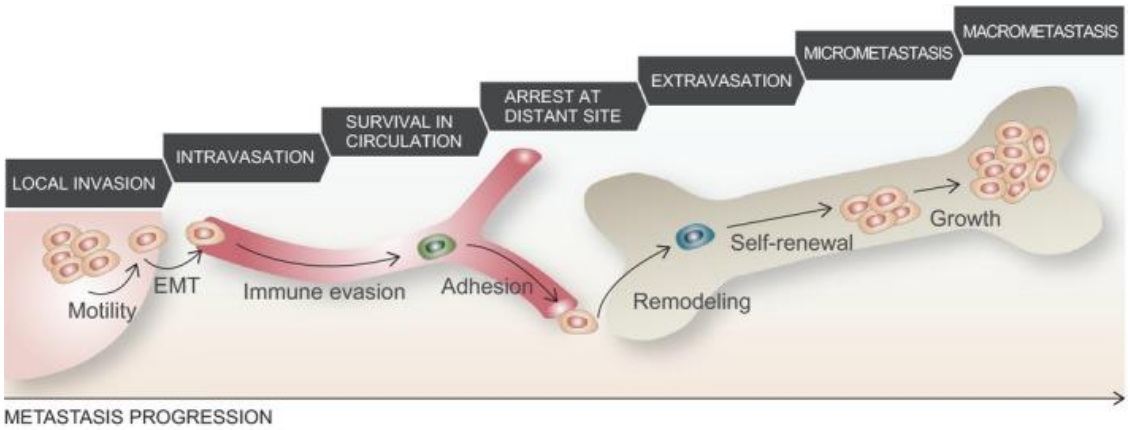


Figure 1.1. The metastatic cascade. Metastasis progresses through the sequence of steps that promote malignant cells, from primary tumour, to disseminate and colonize distant organ. Acquisition of each step is driven by specific cellular functions. Cascade steps are indicated in grey blocks, cell autonomous functions important in each step in black, circulating tumour cell in green, and disseminated tumour cell in blue. Adapted from Roger Gomis (2015)[11]

First, the primary cancer cells achieve the ability of movement by alteration of cytoskeleton, which called invasion. At the same time, they secrete extracellular matrix (ECM) remodelers to

facilitate the cancer cells escaping from the original sites[13, 14]. Furthermore, the other cells in tumour stroma, macrophages and fibroblasts, also secrete pro-migratory factors to enhance the migration of cells from their original sites[15, 16].

Intravasation is the second step of metastasis, which means the cancer cells, after invasion, go through the basal membrane into a blood or lymphatic vessel[17]. In this step, the cancer cells lose their epithelial features, such as adhesion and polarization, followed by gain of mesenchymal features, including migratory and invasive properties, in a process called epithelial-to-mesenchymal transition (EMT). Epithelial cells express high levels of E-cadherin, whereas mesenchymal cells express high levels of N-cadherin, fibronectin and vimentin. These markers are typically used to detect cancer cell migratory ability[18]. In addition, successful intravasation also requires the formation of new vasculature in the primary tumour by the angiogenesis promoters. This kind of vasculature is often leaky and coated by abnormal pericytes which makes it accessible for metastatic cells[19]. Moreover, metastatic cells secrete factors that further increase vessel permeability, such as transforming growth-factor beta (TGFβ), thereby facilitating their entry into the circulation[20]. This is a very selective procedure since the circulatory and lymphatic systems are very hostile to cancer cells. As a consequence, large numbers of cancer cells are killed because of immune natural killer (NK) cells and mechanical damage[21].

We call the cancer cells shed into the vasculature or lymphatics as circulating tumour cell (CTC). A variety of research methods have been developed to isolate and enumerate CTCs, however, they are difficult to study as CTCs usually don't divide[22]. Extensive clinical testing performed using this method shows that the presence of CTCs is a strong prognostic factor for overall survival in patients with metastatic breast, colorectal or prostate cancer[23].

After reaching the secondary site, metastatic cells are arrested in the microvasculature of the host organ prior to extravasation. Extravasation in bone or liver is promoted by extrinsic factors such as the permeability of capillaries. In order to cross the vessel wall, composed of endothelial cells,

basement membrane and tissue-specific cells, cancer cells usually secrete factors to increase the permeability of the endothelium. For example, angiopoietin-like 4 (ANGPTL4) disrupts cell junctions in the vascular endothelium[24].

Once metastatic cells extravasate and settle in the secondary site as disseminated tumour cells (DTCs), they must adapt to the microenvironment of the host organ in order to achieve homing to a distant location to form a micrometastasis. Organ-specific extrinsic factors, including stroma cells, ECM, cytokines, and growth factors, compromise the survival of DTCs[11]. In order to extravasate to a more permissive microenvironment, metastatic cells alter the cell-autonomous trait that facilitate homing and survival by altering SRC tyrosine kinase signaling[25, 26]. Also, in this stage, the cells need escape the checking from immune system[27].In many tumour types DTCs are quiescent for many years before the micrometastase overgrowth to be a macrometastase to be clinical detectable.

### 1.1.3 Remission and cancer dormancy

The extensive period time after conventional treatments and before recurrence is called remission. This means that dormant tumour cells, which induce relapse, are undetectable and asymptomatic in this stage. Broadly speaking, the minimal residual tumours are in clinical cancer dormancy (Fig. 1.2). Cancer dormancy includes tumour mass dormancy and cellular dormancy[28]. Tumour mass dormancy represent a balance between tumour cell proliferation and cell death which maintains the stability of tumour volume or mass[29, 30]. Cellular dormancy or solitary cell dormancy is the individual cancer cells entering a state of temporary cell-cycle arrest[5].

One of the earliest observations of cancer relapse following tumour removal can be traced to ancient Rome when the physician, Celsus, noted the recurrence of certain types of cancers, which he referred to as carcinomas, stating that “after excision, even when a scar has formed, none the less the disease has returned, and caused death”[5]. It was further noticed that the appearance of

secondary tumours over 5 years following surgery is likely to be the result of cancer cells lying in the state of "temporary mitotic arrest"[31]. Over the past several decades, more cases of relapse have been documented[32, 33, 34, 35, 36, 37]. But the knowledge is still too limited to overcome cancer recurrence.

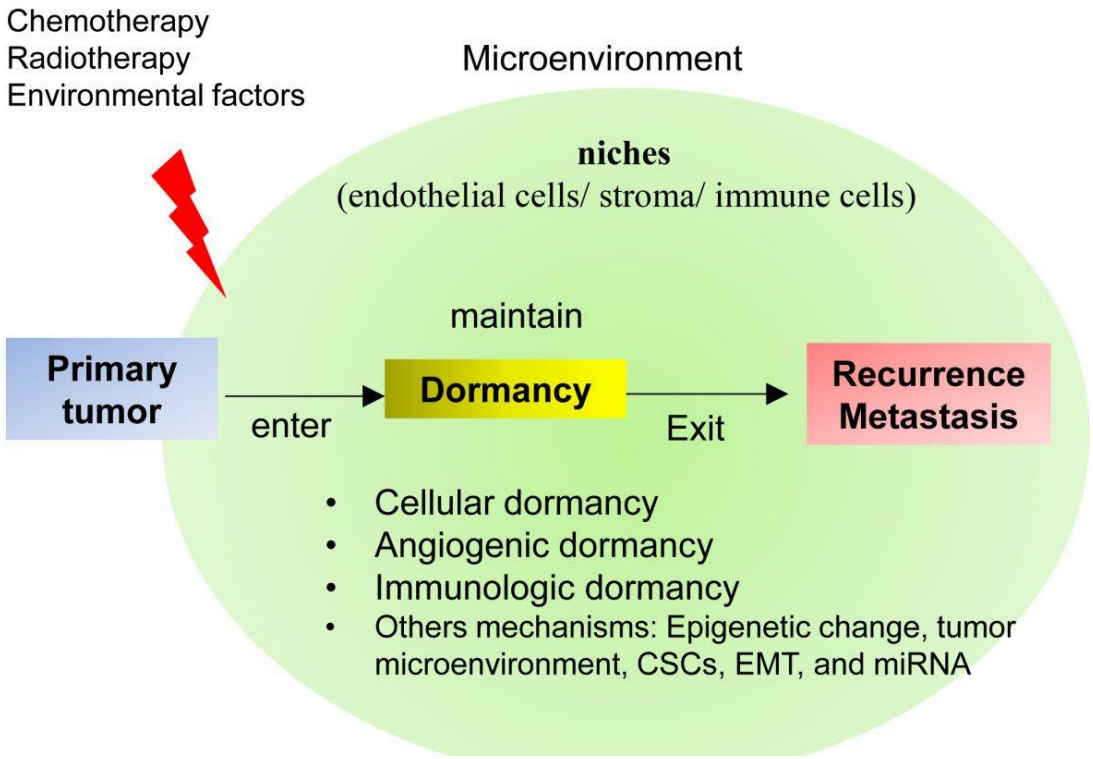


Figure 1.2. A schematic illustration of cancer dormancy and recurrence metastasis**.** Tumour dormancy can lead to tumour recurrence locally or to metastasis at a distant site. Dormancy can be induced by more than one mechanism: cellular dormancy (quiescence), angiogenic dormancy (tumour mass size limit), and immunologic dormancy (immunosurveillance, balance between proliferation and apoptosis). Others mechanisms, such as epigenetic change, tumour microenvironment, CSCs, EMT, and miRNA, also may involve in tumor dormancy. A tumor microenvironment that is altered (such as by frontline treatment) can mediate tumor cell entrance into, maintenance, and exit from dormancy through interaction with cells at niches, such as endothelial cells, stroma, or immune cells. Adapted from Sih-han Wang (2013)[38].

### 1.1.4 Primary and metastatic dormancy

Cancer dormancy does not only exist in the period of time before cancer recurrence. There is enough evidence to illustrate that local tumour dormancy occurs prior to establishment of the primary cancer[39]. Post-mortem examination of random sections of autopsied tissues from men and women who did not have cancer revealed frequent "small cacinomata", with the proportion dramatically higher than the percentage of the persons who were diagnosed with cancer. For example, 39% of the women in their 40s displayed histological signs of breast cancer according to the post-mortem examination, however, only 1% of the women at this age range really get diagnosed with breast cancer[40]. In addition, 100% of the thyroid glands from cancer-free people, aged from 50 to 70 years, were found to have *in situ* carcinomas, whereas the chance of thyroid cancer in this age group is only 0.1%[41].

There is also evidence of metastatic tumour dormancy prior to the establishment of primary cancer. Clinically, this is referred to as "cancer of unknown primary"[42], which accounts for 3-55% of all malignancies. For instance, patients with stage M0 breast cancer could relapse after complete resection of their primary tumour, and their metastatic tumour had significantly fewer genetic abnormalities than the primary tumour[39, 43]. It was reported that in these patients, primary cancer could not be identified after histopathologic review of biopsy material and CT scan, but full-body imaging identified metastatic lesions that were confirmed by biopsy[42].

Cancer dormancy occurring during the formation of a primary cancer are usually not aggressive. These dormant tumours are never exposed to conventional treatment. The main reason of dormancy comes from the microenvironment where the tumour is located, such as the lacking of nutrition or too strong immune system[5, 44]. While dormant tumours occurring after the treatment of the primary tumour are from cells that have survived various kinds of therapeutics which usually achieve certain extent of adaptation to treatment. Therefore, it remains an important challenge to treating recurrent metastatic tumours.

### 1.1.5 Potential models of tumour dormancy

Current experimental models of cancer dormancy can be subdivided into two general categories reflecting different growth kinetics. The first type, known as tumour mass dormancy, represents stagnation of overall tumour growth, which is maintained by the equilibrium of proliferation and cell death[29, 30]. This results in retarded growth of tumours, caused by the lack of new vasculature around the tumours or efficient immunosurveillance. The second type, known as cellular dormancy, which means a reversible cell cycle exiting.

#### *1.1.5.1 Tumour mass dormancy*

Tumour mass dormancy includes both angiogenic dormancy and immunologic dormancy. Once tumours reach a certain tumour mass size that requires more than the normal tissue vasculature can provide, the tumour mass induces angiogenesis to meet its nutrient demands. However, not all tumours have this capability and therefore are unable to grow beyond a certain size[38]. Malignant cells can remain clinically undetectable for years before undergoing an "angiogenic switch" which is regulated by pro-angiogenic factors and anti-angiogenic factors (Fig.1.3)[44]. Pro-angiogenic factors which promote angiogenesis, including vascular endothelial growth factor (VEGF), platelet-derived growth factor, fibroblast growth factor and angiopoietin. Anti-angiogenic factors, which are against pro-angiogenic factors including thrombospondin (TSP), endostatin, vasculostatin and angiostatin[45].

An early pioneer of this model, Judah Folkman, suggested that human bodies are constantly keeping small tumours in check by preventing their ability to recruit new blood supply[41]. The direct evidence of angiogenic dormancy was obtained from the use of microscopic and macroscopic technologies to track the endothelial cell marker. This experiment indicated that large tumours had well-organized vascular structures, whereas small tumours had few small

vessels[46]. However, the critical role of angiogenic dormancy in metastatic dormancy is less convincing. Assessment of GFP-tagged CTCs cancer cells suggested that CTCs most likely to embed and grow in sites enriched in oxygen, close to endothelial vessels[47]. This hints that other mechanisms besides angiogenic dormancy are needed to explain cancer dormancy.

Another explanation regarding cancer dormancy is the idea of immunologic dormancy. A current model explaining the role of immune system in cancer progression is a three stage process: elimination, equilibrium and escape[5]. Elimination means cancer cells are recognized and eliminated by the immune system. Certain tumour cells may not be completely eliminated, however their net growth is restricted by immunity control, resulting in a state of equilibrium and maintenance of tumour cells in dormancy. During Equilibrium, some tumour cells may induce a host-protective immune response, or their antigen expression (recognized by adaptive immunity via T-cell effectors) may be modified to adapt to the host immune system. In this case, the edited tumour cells can escape from immunosurveillance and eventually become clinically detectable and lead to tumour recurrence[48, 49].

There are also many cases support immune dormancy. It is well known that after receiving organ donation, immunosuppression is a vital process for patients so as to not reject the new organ. It is reported that metastatic melanoma developed 1 to 2 years post-transplantation in two allograft recipients receiving kidneys from the same donor, who had been treated for primary melanoma 16 years before death and was considered disease-free at time of organ donation[50].

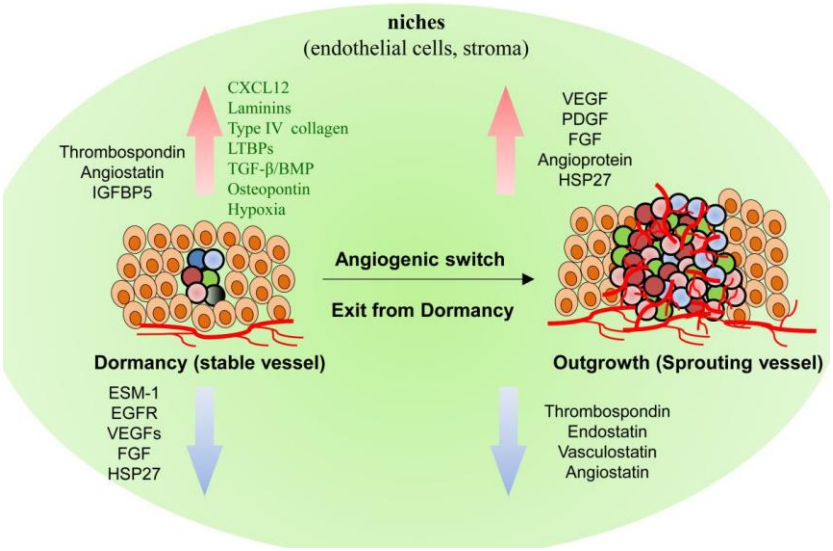


Figure 1.3. Angiogenic dormancy**.** At niches, dormancy can be induced through signaling between DTCs, endothelial cells, and stroma with both upregulation and downregulation of multiple factors and signaling axes. DTCs enter dormancy with a vascular structure that is stable and non-angiogenic. In contrast, a sprouting vascular structure triggers tumor cells to exit from dormancy following an "angiogenic switch" in microenvironment, leading to tumor outgrowth and recurrence or metastasis. BMP, bone morphogenetic protein; CXCL12, Chemokine (C-X-C motif) ligand 12; EGFR, epithelial growth factor receptors; ESM-1, endothelial specific marker 1; FGF, fibroblast growth factor; HSP27, heat shock protein 27; IGFBP5, insulin-like growth factor binding protein 5; LTBPs, latent transforming growth factor β binding protein; PDGF, platelet-derived growth factor; TGF-β, transforming growth factor β; VEGFs, vascular endothelial growth factors. Adapted from Sih-han Wang (2013)[38].

### *1.1.5.2 Cellular dormancy*

Cellular dormancy, or solitary cell dormancy, refers to single tumour cells that are in a temporary quiescent state, or at G0 phase of the cell cycle. The common trait between quiescent cells and senescence cells is that both of these cells are not dividing. However, only quiescent cells have the ability of cell cycle re-entry.

In patients with prolonged clinical dormancy, the presence of dormant cells is often identified by the lack of cellular proliferation marker Ki67, as well as the lack of apoptotic markers[51]. Analysis

of human tumour tissue samples of breast cancer patients undergoing neoadjuvant chemotherapy, revealed a significant enrichment for dormant cells in tissue samples of patients after exposure to chemotherapy compared with those in the same individual before treatment[52]. Further, isolation and characterization of CTCs from breast cancer patients have also demonstrated that many of these cells are dormant or have limited proliferative capacity[22, 51]. The quiescent cellular population of tumours poses a barrier to the success of many cancer therapies. For example, quiescent cancer cells (colon adenocarcinoma) are resistance to chemotherapeutic drug vinblastine, doxorubicin, cisplatin and 5-fluorouracil (5-FU) [53]. Therefore, in order to specifically target quiescent cancer cells, we need to better characterise the differences between cycling and quiescent cancer cells.

## 1.2 Cell cycle

### 1.2.1 Overview

Cellular dormancy is closely related with the cell cycle. The cell cycle is a series of events that take place in a cell, leading to duplication of its DNA and division of cytoplasm and organelles to produce two daughter cells. In mammalian somatic cells, the cell cycle is divided into two main stages: interphase and mitotic (M) phase. Interphase is the stage where a cell grows and accumulates nutrients to prepare DNAs, RNAs, proteins, and the other materials, which are necessary for mitosis. In the mitotic phase, replicated chromosomes and cytoplasm split into two daughter cells. In summary, interphase is the phase that cell prepares to divide while mitotic phase is the phase in which the cell separates into two daughter cells.

Interphase, also called preparatory phase or intermitosis, proceeds in three stages: G1 phase, S phase and G2 phase (Fig. 1.4). Typically, interphase lasts for at least 91% of the total time required for the cell cycle. The duration of G1 is highly variable, even among different cells of the same

species[54]. In this phase, the cell increases its supply of proteins, increases the number of organelles (such as mitochondria, ribosomes), and grows in size. S phase starts when DNA synthesis commences and results in the duplication of all the chromosomes. The RNA transcription and protein synthesis are extremely low in S phase, except for the production of histone. G2 phase occurs after DNA replication and is a period of protein synthesis and rapid cell growth to prepare the cell for mitosis. Mitosis (M phase) is a relatively short period of the cell cycle and is highly regulated. The replicated DNA from the S phase will be divided equally into two daughter cells.

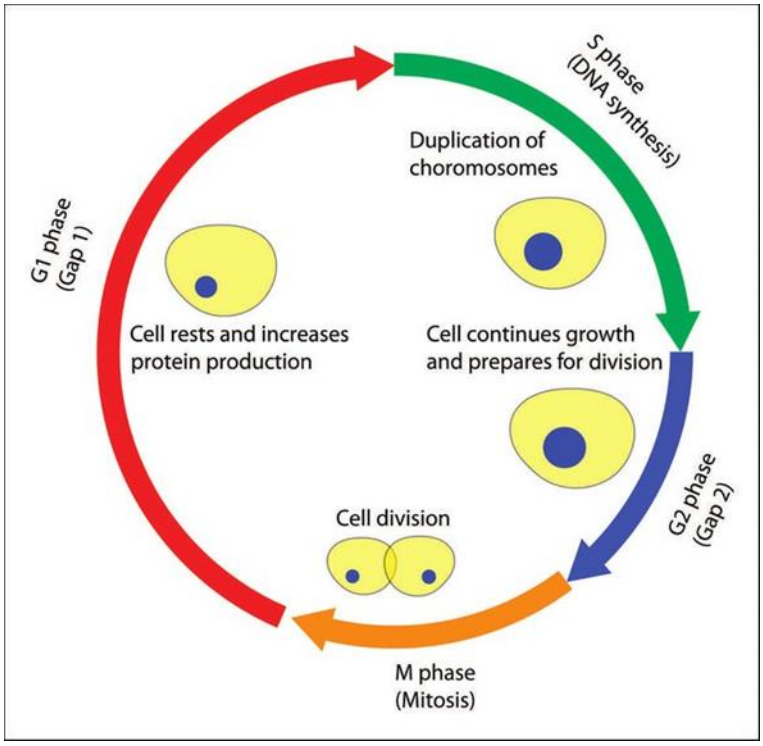


Figure 1.4. A simplified representation of the eukaryotic cell cycle. During the different phases of the cycle the cells undergo a variety of significant changes, such as protein increase in the G1 phase, chromosome duplication in the S phase, ensuring that the cell is ready for division in G2 phase, and process of cell division in the M phase. Adapted from Schie IW (2013)[55].

### 1.2.2 Cell cycle checkpoint

The cell cycle is a highly regulated series events, where cells use information, both internal and external to the cell, to decide whether to proceed with cell division[56]. This regulation makes sure that cells do not divide under unfavourable conditions (for instance, when their DNA is damaged, or when there is not enough room for more cells in a tissue or organ)[57]. A major part of this regulation involves the cell cycle checkpoints where the cell examines the internal and external information to decide whether to go forward with the next step of the cell cycle or not[58].

Generally, there are three checkpoints in cell cycle. The first one is G1/G0 checkpoint, which determines the successful transition from G1/G0 phase to S phase, and is the main checkpoint for a cell[58]. Once the cell passes this checkpoint, it becomes committed to undergoing the cell cycle. In this checkpoint, cells mainly check with the nutrients to make sure it is enough to finalize a whole cell cycle. Information including cell size, external molecular signals and DNA integrity are also checked. If a cell fails to pass this checkpoint, it may leave cell cycle and enter a resting stage called G0 phase or quiescent phase[59].

The G2 checkpoint occurs late in the G2 phase, just before M phase, to make sure a successful completion of M phase will be achieved. Cells arrest at this checkpoint when there are some mistakes about DNA integrity and replication. The cell will attempt to fix the problems, unless the damage is irreparable, in which the cell will undergo apoptosis[58]. The common rule is that the damaged DNA is not passed to the daughter cells. The M checkpoint is also known as the spindle checkpoint. Here, the cell examines whether all the sister chromatids are correctly attached to the spindle microtubules. If a chromosome is misplaced, the cell will pause mitosis, allowing time for the spindle to capture the stray chromosome.[58]

The internal and external cues trigger signalling pathways inside the cell that activate, or inactivate, a set of core proteins that move the cell cycle forward to make sure the cell cycle checkpoints are passed. These core proteins are Cyclins and cyclin dependent kinases (CDKs)[60].

### 1.2.3 Cyclins and CDKs

Cell cycle transitions are driven by periodic destruction of key cell cycle regulators, with the ubiquitin proteasome system playing a central role in this process[61]. Cyclins are among the most important cell cycle regulators. They are a group of related proteins, and there are four basic types found in humans and most other eukaryotes: G1 cyclins, G1/S cyclins, G2 cyclins and M cyclins (Fig. 1.5). Each cyclin is associated with a particular phase. The levels of the different cyclins vary considerably across the cell cycle. Cyclin D (G1 cyclins), Cyclin E (G1/S cyclins), Cyclin A (G2 cyclins) and Cyclin B (M cyclins) are the four major cyclins that are well studied (Fig. 1.5). Cyclin is destroyed by ubiquitin-dependent proteolysis[62].

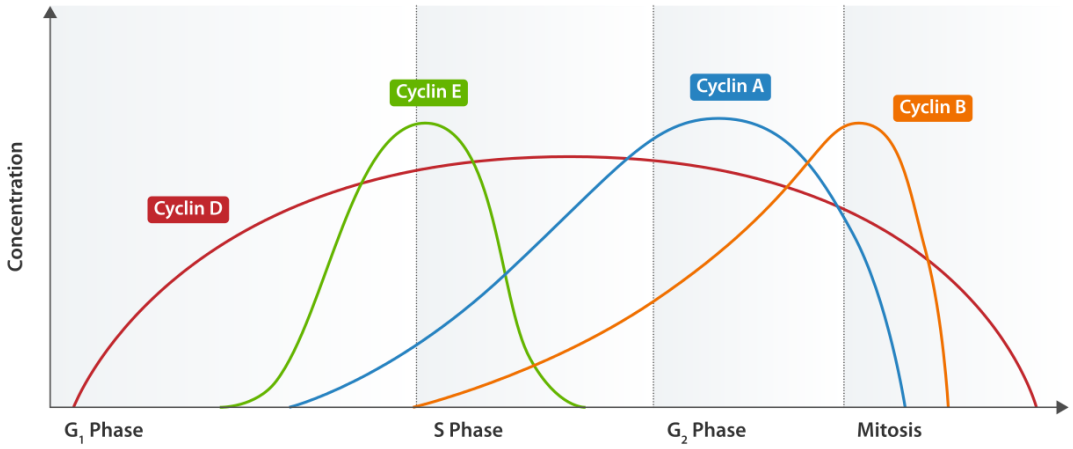


Figure 1.5. Expression of human cyclins through the cell cycle. Adapted from Wikipedia: https://en.wikipedia.org/wiki/Cyclin

The regulation of cyclins throughout the cell cycle depends on the ubiquitination and degradation. Usually, CDKs work as kinases to modify the target proteins at downstream are activated by the binding of the specific cyclins. In general, CDKs keep a constant level across the cell cycle and the activations are regulated by the levels of cyclins[60].

Cyclin-dependent kinase inhibitor proteins (CDKIs) are proteins that can bind with the cyclin-CKDs complex to inhibit the function of CDKs (Table 1.1). The mammalian CIP/KIP family of CDK inhibitors (CKIs) comprises three proteins; p21(Cip1/WAF1), p27(Kip1), and p57(Kip2), that bind and inhibit cyclin-CDK complexes, which are key regulators of the cell cycle[63]. These CKIs are usually regulated by proteasome-mediated degradation, which is tightly controlled by multiple ubiquitin ligases. In this thesis, the ligase specifically regulating G0 phase, which is closely associated with cellular dormancy, will be reviewed later.

Table 1.1. Cyclin-dependent kinase inhibitor proteins

(https://en.wikipedia.org/wiki/Cyclin-dependent_kinase_inhibitor_protein)

| Protein | Gene | Interacts with |
|---|---|---|
| P16 | CDKN2A | Cyclin-dependent kinase 4, Cyclin-dependent kinase 6 |
| P15 | CDKN2B | Cyclin-dependent kinase 4 |
| P18 | CDKN2C | Cyclin-dependent kinase 4, Cyclin-dependent kinase 6 |
| P19 | CDKN2B | Cyclin-dependent kinase 4, Cyclin-dependent kinase 6 |
| P21/WAF1 | CDKN1A | Cyclin E1/Cyclin-dependent kinase 2 |
| P27 | CDKN1B | Cyclin D3/Cyclin-dependent kinase 4, Cyclin E1/Cyclin-dependent kinase 2 |
| P57 | CDKN1C | Cyclin E1/Cyclin-dependent kinase 2 |
| KAP | CDKN3 | Cyclin-dependent kinase 2 |

### 1.2.4 G0 phase

After mitosis, a cell has three options: (1) to continue the cell cycle and enter S phase; (2) stop the cell cycle and enter G0 phase for undergoing differentiation; (3) become arrested in G1 phase, allowing the cell to enter G0 phase or re-enter cell cycle[64]. In cellular dormancy, the residual cancer cells, after conventional treatment, choose a resting state at G0 phase to avoid the double burden from cells dividing and the unfriendly microenvironment. G0 phase is a cellular state outside of the replicative cell cycle. We also call the cells at G0 phase as quiescent cells.

Many cells in the body are highly differentiated cells which are at G0 phase, for example, muscle cells. These highly differentiated cells are in an irreversible G0 phase. It is the reversibility of G0 phase in quiescent cancer cells that induce cancer recurrence. The major characteristics of quiescent cancer cells are unknown. However, some common molecules and pathways that regulate the entry of G0 phase and the re-entry of cell cycle may be involved.

### 1.2.5 APC/Skp2/p27

The anaphase-promoting complex (APC) is a cell cycle-regulated ubiquitin ligase that assembles multiubiquitin chains on regulatory proteins, such as securin and cyclins, and thereby targets them for destruction by the 26S proteasome[65]. $APC^{cdc20}$ plays a very important role in mitosis to ensure the successful separation of sister chromatids. While cdc20 (Cell Division Cycle 20) is being degraded since anaphase, together with Cyclin B, after which, in G0 and G1 phase, dephosphorylated Cdh1 replaces cdc20 as the major substrate (Fig. 1.6).

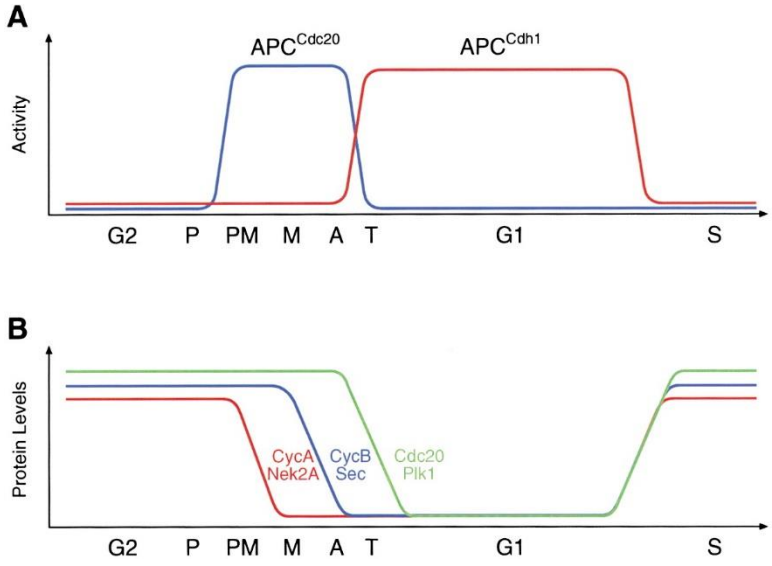


Figure 1.6. APC-Mediated Proteolysis during the Cell Cycle. Adapted from Jan-Michael Peters (2002)[66].

S-phase kinase-associated protein 2 (Skp2) as a major substrate of $APC^{cdh1}$ at G0 and early G1 phase so that skp2, and its co-factor Cks1, are not stable during G0 and early G1 phase[67]. However, p27 is accumulated during these phases due to the decreased levels of Skp2. P27 is coded by Cyclin Dependent Kinase Inhibitor 1B (CDKN1B). It is a CKD inhibitor that binds to and prevents the activation of cyclin E-CDK2 or cyclin D-CDK4 complexes, and thus controls cell cycle progression of cell cycle re-entry. As a substrate of E3 ligase Skp2, p27 enriches in G0 phase and is degraded as cells start a new cell cycle (Fig. 1.7)[68]. More details will be reviewed in section 1.4.

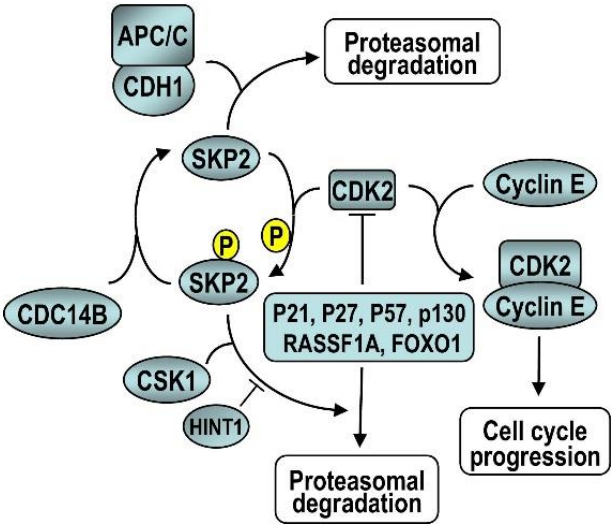


Figure 1.7. Schematic representation of the Skp2 effect on cell cycle regulation. Adapted from Diego F.Calvisi (2009)[69].

### 1.2.6 Rb/E2F pathway

The retinoblastoma gene was identified as the first tumour suppressor. It is now thought to play a fundamental role in cellular regulation, and is the target of tumorigenic mutations in many cell types. Rb is phosphorylated and dephosphorylated during the cell cycle; the hyperphosphorylated (inactive) form predominates in proliferating cells, whereas the hypophosphorylated (active) form is generally more abundant in quiescent or differentiating cells[70].

E2F is a group of genes that codifies a family of transcription factors (TFs)[71]. Three of them are activators: E2F1, E2F2 and E2F3a. Six others act as suppressors: E2F3b, E2F4-8. All of them are involved in the cell cycle regulation and synthesis of DNA in mammalian cells. The E2F proteins contain several evolutionarily conserved domains found in most members of the family. These domains include a DNA binding domain, a dimerization domain which determines interaction with the differentiation-regulated transcription factor proteins, a transactivation domain enriched in acidic amino acids, and a tumour suppressor protein association domain which is embedded

within the transactivation domain. E2F1, E2F2 and E2F3 have an additional cyclin binding domain which promotes the transcriptions of cyclins and is associated with the cell cycle[71].

E2F/Rb pathway is in charge of G1/S transition (Fig. 1.8). In the absence of phosphorylated Rb (pRb), Rb always bind with E2F1 to prevent it working as a transcriptional factor to promote gene transcription[72]. When cells pass the G1 checkpoint and are ready to commence a new cell cycle, Cyclin D and Cyclin E are always upregulated. CDK4 and CDK2 are activated partially because of the degraded p27. In this case, Rb is inactivated by phosphorylation, catalysed by CDKs in complex with cyclin parterners[73]. The pRb loses the ability to bind with E2F1 so that E2F1 can boost the transcription of a series genes that facilitate cell proliferation, such as Cyclin A. When cells enter into cell cycle, proliferating marker Ki67 will be upregulated[72].

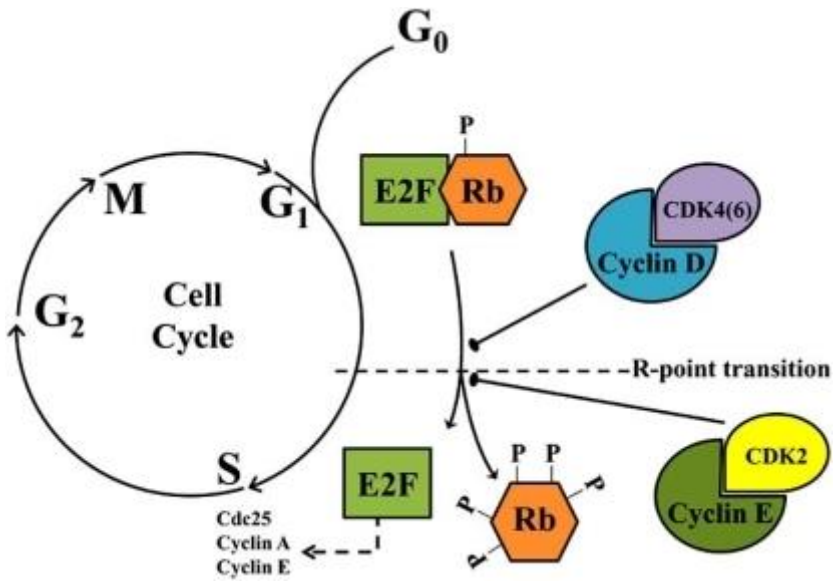


Figure 1.8. The Rb/E2F pathway. Sequential phosphorylation by kinase complexes Cyclin D:Cdk 4/6 and Cyclin E:Cdk 2, respectively, causes conformational changes to the Rb structure and release of E2F. The release of E2F is necessary for the expression of S-phases genes. Adapted from Kyle K. Biggar (2009)[74].

There are also some other pathways regulate cell cycle, which are also very critical for G0 phase, including the MAPK and PI3K/AKT pathways. Because they are well studied in the other publications and irreverent to my project, I do not review them in this thesis.

## 1.3 FUCCI

### 1.3.1 Overview

Fluorescence Ubiquitin Cell Cycle Indicator (FUCCI), based on the rule that the $SCF^{Skp2}$ complex (Skp, Cullin, F-box containing complex) is a direct substrate of the $APC^{Cdh1}$ complex but also functions as a feedback inhibitor of $APC^{Cdh1}$ [75]. These two ligase activities oscillate reciprocally during the cell cycle. The $APC^{Cdh1}$ complex is active in the late M and G1 phases and targets Geminin for degradation, while the $SCF^{Skp2}$ complex is active in the S and G2 phases and targets Cdt1 for degradation[76, 77]. Due to cell cycle-dependent proteolysis, protein levels of Geminin and Cdt1 oscillate inversely. Previous data shows that Cdt1 levels are highest during G1, while Geminin levels are highest during the S, G2, and M phases (Fig. 1.9A)[78]. Using the FUCCI system, Sakaue-Sawano et al. harnessed the above principle to develop fluorescence-fused truncated Cdt1(30-120) and Geminin(1-110) to mark G1 and G2/S/M phases separately (Fig. 9B)[76].

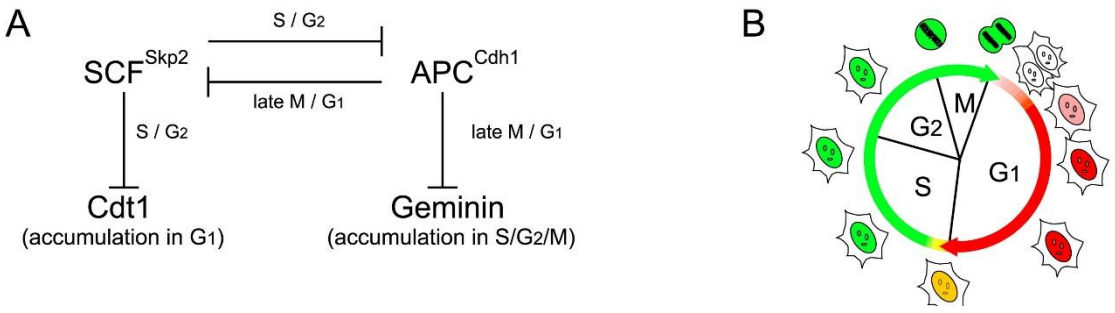


Figure 1.9. FUCCI. A, Cell-cycle regulation by $SCF^{Skp2}$ and $APC^{Cdh1}$ maintains bistability between G1 and S/G2/M phases. B, A fluorescent probe that labels individual G1 phase nuclei in

red (mKO2-hCdt1 (30-120)) and S/G2/M phase nuclei green (mAG-hGem(1-110)). Adapted from Asako Sakaue-Sawano (2008)[76].

Sakaue-Sawano et al. also used mAG-hGem(1-60), which locates both to the nucleus and cytoplasm to visualize the overall cell morphology[79]. Because it is the degradation monitor between the balance of $SCF^{Skp2}$ and $APC^{Cdh1}$ E3 ligase activities, the above system is called FUCCI(SA). In 2017, Sakaue-Sawano et al. induced a fluorescence-labelled hCdt1 (1-100) Cy(-) which can track cells at S phase sharply. Since it is the balance between $CUL4^{Ddb1}$ and $APC^{Cdh1}$ E3 ligase activities, it is called FUCCI (CA)[80]. The difference between hCdt1(30-120) and hCdt1(1-100)Cy(-) is that at M and G2 phase, the truncated Cdt1 can only can be partially degraded, so that in these phases, both of the green and red fluorescence are shown, producing a yellow overlay. In this case, only cells at S phase turn green (Fig. 1.10).

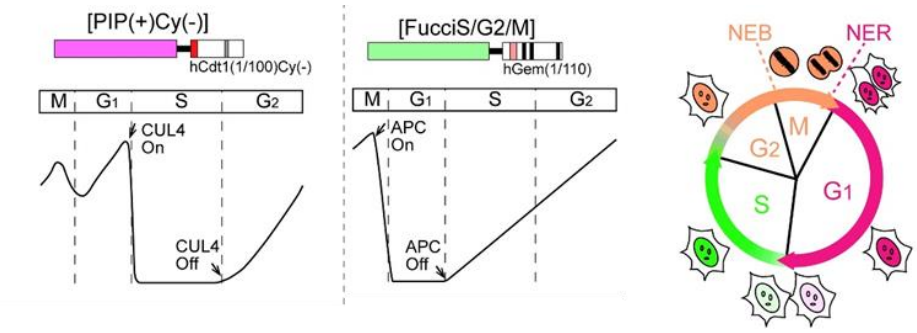


Figure 1.10. FUCCI (CA). Adapted from Asako Sakaue-Sawano (2017)[80].

### 1.3.2 Application of FUCCI

In recent years, the FUCCI system has been adapted to several model systems including flies, fish, mice, and plants, making this technology available to a wide range of researchers for studies of diverse biological problems (Fig.1.11)[81]. Additionally, a major advantage of genetically encoded biosensors is that they allow the generation of transgenic organisms that can be used in various experimental setups and thus, provide valuable resources for the research community[81]. The

FUCCI technology is widely applicable in cell biology and therefore it is not surprising that several FUCCI-expressing cell lines have been developed (Table 1.2). The most obvious application of these cell lines is to use the FUCCI sensors as a means for determining whether a certain treatment alters the duration of specific cell cycle phases.

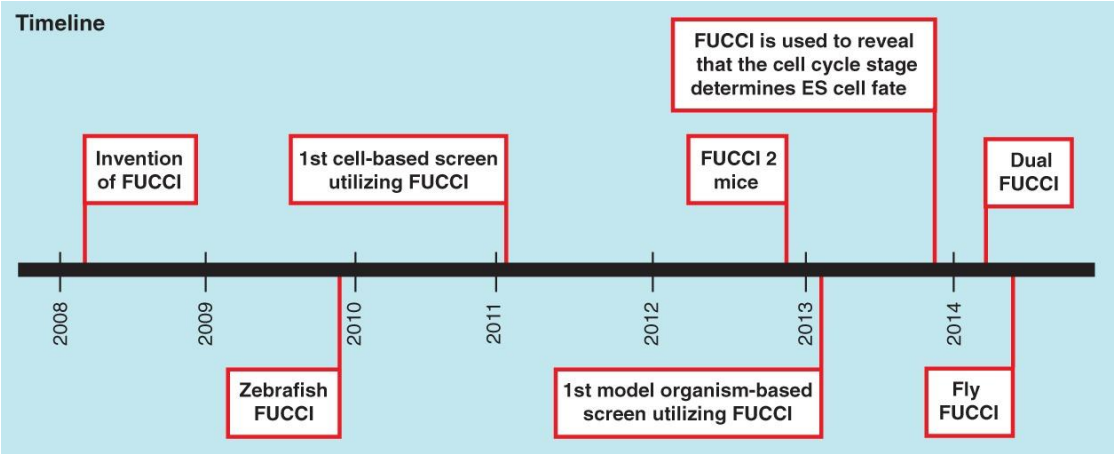


Figure 1.11. Timeline illustrating the invention of the different FUCCI variants and the key discoveries that have been made with them. Adapted from N. Zielke (2015)[81].

**Table 1.2. FUCCI-Expressing Cell Lines**. Adapted from N. Zielke (2015)[81].

| Cell line | Description | Species of Origin |
|---|---|---|
| BJ-hTert | Foreskin fibroblasts | Human |
| EndoC-βH2 | Pancreatic β cells | Human |
| hESC H9 | Embryonic stem cells | Human |
| hESC WA09 | Embryonic stem cells | Human |
| HeLa | Cervical cancer cells | Human |
| HCT116 | Colon cancer cells | Human |
| MKM45 | Stomach adenocarcinoma cells | Human |
| RPE-1 | Retinal pigment epithelial cells | Human |
| B16 | Melanoma cells | Mouse |
| D2A1 | Mammary cancer cells | Mouse |
| L1210 | Lymphocytic leukemia cells | Mouse |
| mESC CGR8 | Embryonic stem cells | Mouse |
| mESC E14 | Embryonic stem cells | Mouse |
| NIH 3T3 | Fibroblast cells | Mouse |
| NMuMG | Normal murine mammary gland cells | Mouse |
| S2-R+ | Derived from late embryos | *Drosophila* |

### 1.3.3 mVenus-p27K$^-$

Even though FUCCI, as a cell cycle indicator, is widely used, the hCdt1(30-120) not only labels G1 phase, but is also an indicator of the early S phase[76]. Therefore, it is hard to distinguish the cells at G0 phase from the cells at the other phases. The transition between G0 and G1 is particularly difficult to visualize. Toshihiko Oki et al. constructed the mVenus-fused CDK binding domain mutant p27 (mVenus-p27K$^-$) as an indicator to visualize G0 cells and the G0-G1 transition[82]. P27 is highly expressed at G0 phase and degraded gradually at G0-G1 transition[63]. It is tightly controlled by Kip1 ubiquitination-promoting complex (KPC) and SCF$^{Skp2}$. Therefore, p27 is a good indicator of quiescent cells. However, the transfected full length p27 can inhibit cell growth as a CDK inhibitor[82, 83]. In Oki's article[82], they tried 4 types constructs (Fig. 1.12). Finally, mVenus-p27K- showed good quality to indicate G0 phase and G0-G1 transition. Combined with mCherry-hCdt(30-120). G0 cells were isolated[82].

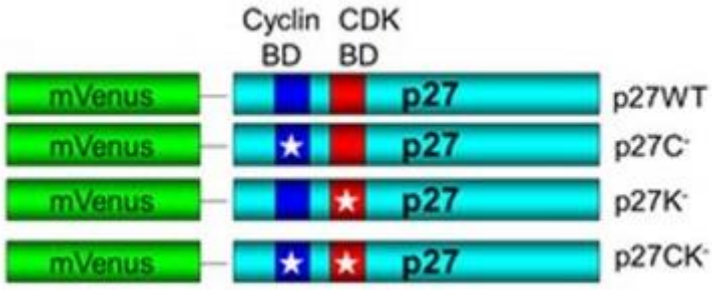


Figure 1.12. Various constructs with concatenated mVenus and p27. Adapted from Toshihiko Oki (2014)[82].

The disadvantage of this system is that it can only be used in mouse cells. The reason is unknown. In consideration of the conservation issues, we can only use this system to study particular genes that are conserved between human and mouse, which include some coding genes and miRNAs[84]. Long noncoding RNAs (lncRNAs) are not conserved, and therefore are not suitable in this system.

## 1.4 p27

### 1.4.1 Overview of p27

There exists a tightly controlled interaction between cyclin, CDKs and CDKIs control cell cycle progression. There are two families of mammalian CKIs: the INK4 (INhibitors of CDK4) and CI/KIP (CDK interacting protein/Kinase inhibitory protein) family[85]. P27 belongs to CIP/KIP family. The members in INK4 family, $p16^{INK4a}$, $p15^{INK4b}$, $p18^{INK4c}$, $p19^{INK4d}$, are inhibitors of CDK4 and CDK6, which specifically inhibit G1 phase cyclin-CDKs. The CIP/KIP family are made up of three proteins, $p21^{cip1/waf1}$, $p27^{kip1}$ and $p57^{kip2}$, which interact with a wide range of cyclin-CDKs to control more aspects of the cell cycle. P27 can bind with cyclin A, cyclin B, cyclin D and cyclin E in all cell phases (Fig. 1.13). But it play a very vital role at G0 phase[63].

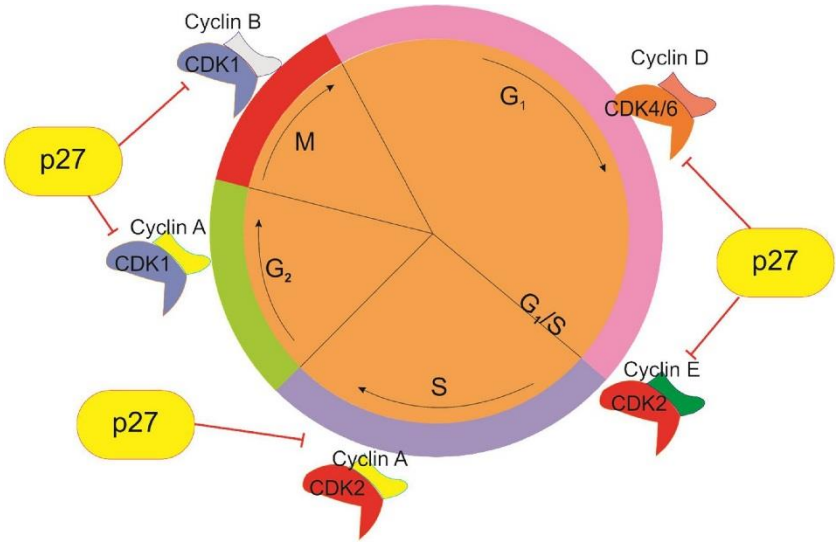


Figure 1.13. P27 interacts with multiple proteins in cell cycle. P27 can interact whit diverse Cyclin-dependent kinases and their cyclin regulatory subunits in different stage of cell cycle and regulate their activity. Adapted from Maryam Abbastabar (2018)[86].

The expression of p27 can be transcriptionally and post-translationally regulated, however, is regulated mainly by proteolysis. P27 is a major protein that regulates the cell cycle. The

subcellular location of p27 offer the different functions of p27. In addition, it also play roles in apoptosis, cytoskeleton assembly and cell movement[87].

### 1.4.2 Genomic CDKN1B organization and p27 protein domain structure

In 1994, p27 was found to inhibit the activity of CDK2 in mink lung epithelial cells as a 27 kDa protein[88]. P27 is located on the short arm of chromosome 12. There is a nuclear exportation signal (NES) at the N-terminal and a nuclear localization signal (NLS) at C-terminal (Fig. 1.14). The N-terminus contains a highly conserved region (residues 28-89). This is a cell cycle inhibitory region including cyclin and CDK binding domains. Mutant part of the amino acids in this region will result in loss of binding to CDK/cyclin complex. P27 contains multiple sites that can be phosphorylated. The subcellular location and functional activation mainly depend on the phosphorylation of these sites.

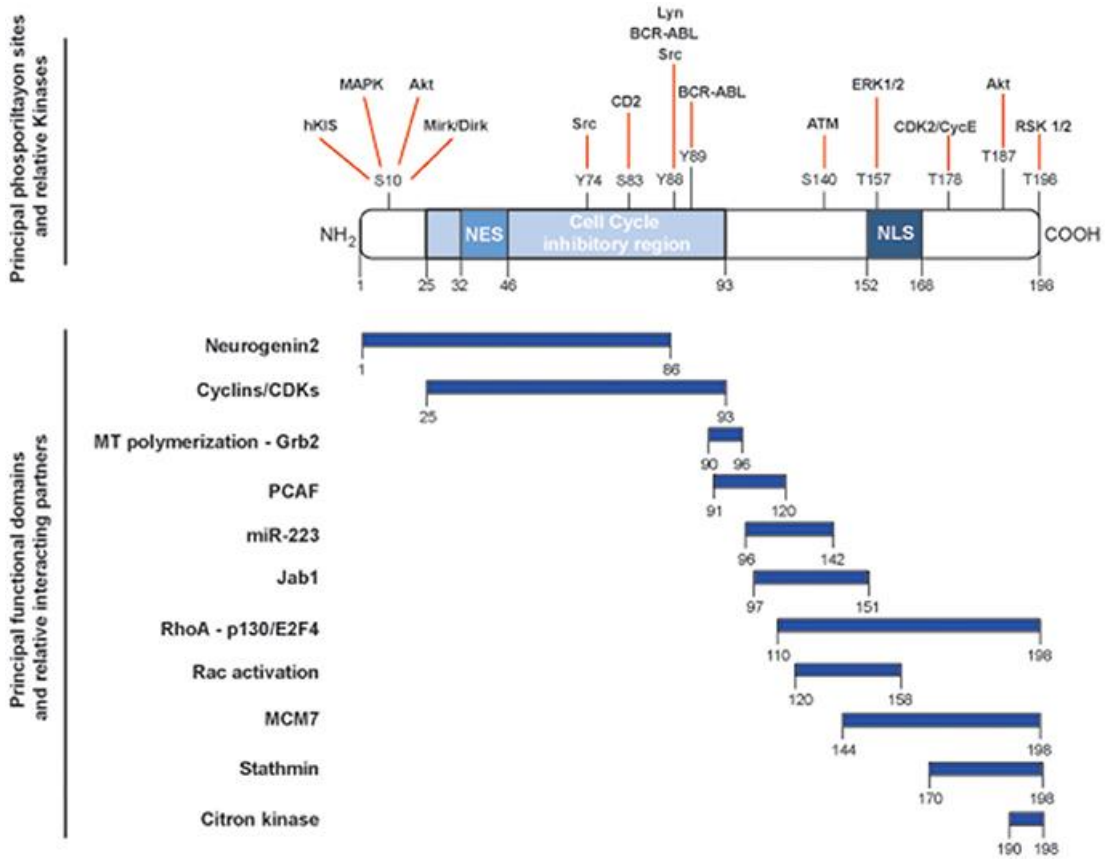


Figure 1.14. Schematic representation of the main functional domains and phosphorylation sites of p27. P27 protein is composed by 198 amino acids and contains a nuclear exportation signal (NES) at the N-terminus and a nuclear localization signal (NLS) at the C-terminus. Key phosphorylation sites and corresponding kinases are depicted in the upper part of the figure and linked with red lines. The cell cycle inhibitory region is comprised between amino acids 25and 93 and is necessary for the binding to cyclin/CDK complexes. Known functional domains and relative interacting protein/microRNA are reported below and highlighted by blue rectangles. Adapted from Martina Cusan (2018)[89].

### 1.4.3 Transcriptional regulation of p27

The transcriptional modulation of p27 plays a minor role in p27 level. It has been reported that several transcription factors (TFs) promote or repress the transcription of p27 (Fig. 1.15). FOX (Forkhead box) proteins are a family of transcription factors that play a critical role in regulating the expression of genes involved in cell growth, proliferation, differentiation, and longevity. A

sequence of 80-100 amino acids forming the forkhead box to binds to DNA. IL-3 inhibits Foxo3a activity in a PI3K-depedent manner. FOXO3a results a significant increase in p27 promoter activity and mRNA levels as well as protein levels in Ba/F3 cell lines[90].

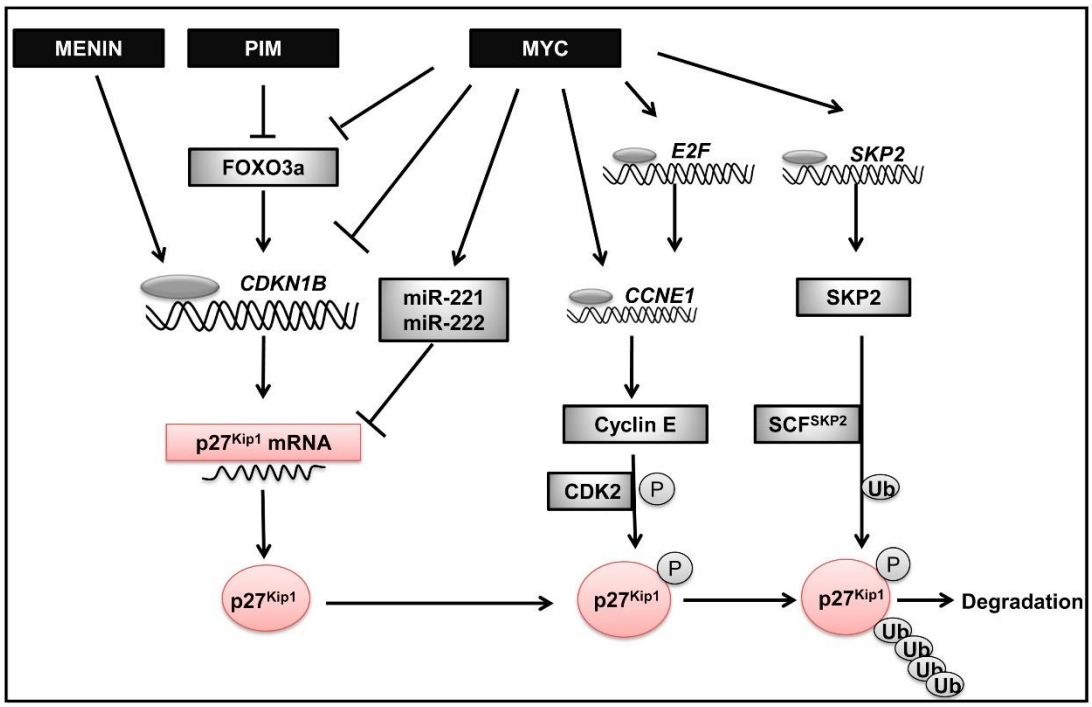


Figure 1.15. Transcriptional and post-translational regulation of p27Kip1 by MYC, PIM and MENIN. Adapted from Su Su Thae Hnit (2015)[87].

Menin is a tumour suppressor which is associated with multiple endocrine neoplasia type 1 (MEN-1 syndrome)[91]. The menin protein is encoded by the *MEN1* gene and associates with and modulates the histone methyltransferase activity of a nuclear protein complex to activate gene expression. In pancreatic islet cells, menin directly binds to the p27 promoter region and increases the methylation of lysine 4 (Lys-4) in histone H3 (H3K4)[92].

Myc is a family of regulator genes and proto-oncogenes that encode for transcription factors. In cancer, c-myc is often constitutively expressed. Myc regulates the expression of p27 at different levels. First, c-Myc can bind to p27 promoter directly to supress the transcription of p27[93]. In addition, Chandramohan et al. found that c-Myc inhibits FOXO3a-mediated activation of p27

promoter via physical association[94]. Secondly, Myc promotes the transcription of miRNA-221 and miRNA-222, which further target p27 mRNA[95, 96]. Furthermore, Myc has effects on p27 protein degradation via the regulation of Skp2, CUL1 and E2F transcription factors[97, 98, 99, 100].

### 1.4.4 Translational regulation of p27

The 5' un-translated region (5' UTR) of p27 contains an internal ribosome entry site (IRES), which is regulated by several proteins[101]. NSun2 methylates the 5' UTR of p27 mRNA at cytosine, thus repressing the translation of p27[102]. Polypyrimidine tract-binding protein (PTB) binds to the 5' UTR to promote the translation of p27[103] while the binding of HuD repress the translation of p27[104, 105]. There are also several miRNAs and lncRNAs regulate the translation of p27 (Table 1.3).

**Table 1.3. Examples of non-coding RNAs that influence on p27.** Adapted from Maryam Abbastabar (2018)[86].

| nc RNA | Down- or up regulation in cancer | Mechanism | Cancer association |
|---|---|---|---|
| Mir-24-3p | up | Bind to CDKN1B 3′ UTR and inhibit its translation | Laryngeal squamous cell carcinoma |
| Mir-221/222 | up | bind to CDKN1B 3′ UTR and inhibit its translation | Hepatocellular carcinoma, breast cancer |
| miR-340 | down | Induces the stabilization of p27by targeting SKP2/ inhibition of PUM1 and PUM2 | Non-small cell lung cancer |
| MiR-196a | up | Bind to CDKN1B 3′ UTR and inhibit its translation | Gastric cancer |
| Mir148-a | up | - | Gastric cancer |
| Mir-940 | up | Bind to CDKN1B 3′ UTR and inhibit its translation | Cervical cancer |
| lncRNA AC026166.2-001 | down | Acts as a sponge of miR-24-3p and regulates the expression of p27 and cyclin D1. | Laryngeal squamous cell carcinoma |
| LncRNA SNHG6 | up | Epigenetically silencing p27 through interacting with PRC2 | Gastric Cancer |

### 1.4.5 Phosphorylation of p27 at Thr187 promotes $SCF^{SKP2}$-dependent degradation in the nucleus.

The phosphorylation of p27 at Thr187 is necessary for proteasome-mediated degradation by $SCF^{skp2}$. During G0 and early G1 phases, the accumulation of Cdh1 facilities the degradation of Skp2 by $APC^{Cdh1}$ complex[67, 75]. While Skp2 is upregulated, there is a decrease of Cdh1 during cell cycle re-entry. The degradation of p27 during cell cycle re-entry is caused by the increased Skp2, which needs a series accurate modifications. It is associated with the Skp2 protein level and p27 Thr187 phosphorylation but not the non-phosphorylated peptide[106]. Unlike other known SCF substrates, p27 ubiquitination also requires the accessory protein Cyclin-dependent kinases regulatory subunit 1 (Cks1)[107]. Cks1 is a co-factor of Skp2 and is necessary for Skp2 to recognise p27 (Fig. 1.16)[108, 109]. In addition, like Skp2, the unstable Cks1 in G0 and early G1 phase is also due to the degradation of $APC^{Cdh1}$ complex[67]. The degradation of p27 by Skp2 occurs in nucleus.

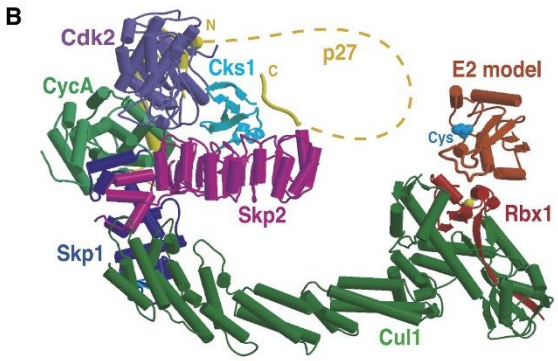


Figure 1.16. Model of the $SCF^{Skp2}$-Cks1-p27Kip1-Cdk2-cyclin A complex. Adapted from Bing Hao (2005)[107].

Since p27 inhibits cyclin E(A)/CDK2 activity, the involvement of CDK2 in p27 degradation appears, at a first glance, quite obscure. In 1997, R J Sheaff et al. found that expression of cyclin E-CDK2 in murine fibroblasts causes phosphorylation of the CDK inhibitor p27Kip1 at T187,

and that cyclin E-CDK2 can directly phosphorylate p27 T187 *in vitro*. Furthermore, they found cyclin E-CDK2-dependent phosphorylation of p27 results in elimination of p27 from the cell, allowing cells to transit from G1 to S phase[110].

The process of p27 degradation during cell cycle re-entry is also a highly regulated series events. When p27 bind with the inactive CDK2 and Cyclin A/E complex, the Tyr[88] phosphorylation of p27, which is induced by the non-receptor tyrosine kinases Src, Lyn, Bcr-Abl, and Jak2, help the ejection of p27 from the CDK2 catalytic pocket. Subsequently, CDK phosphorylate T187 of p27 which recruits Cks1 and the co-factor Skp2 to commence ubiquitination followed by proteasome degradation (Fig. 1.17).

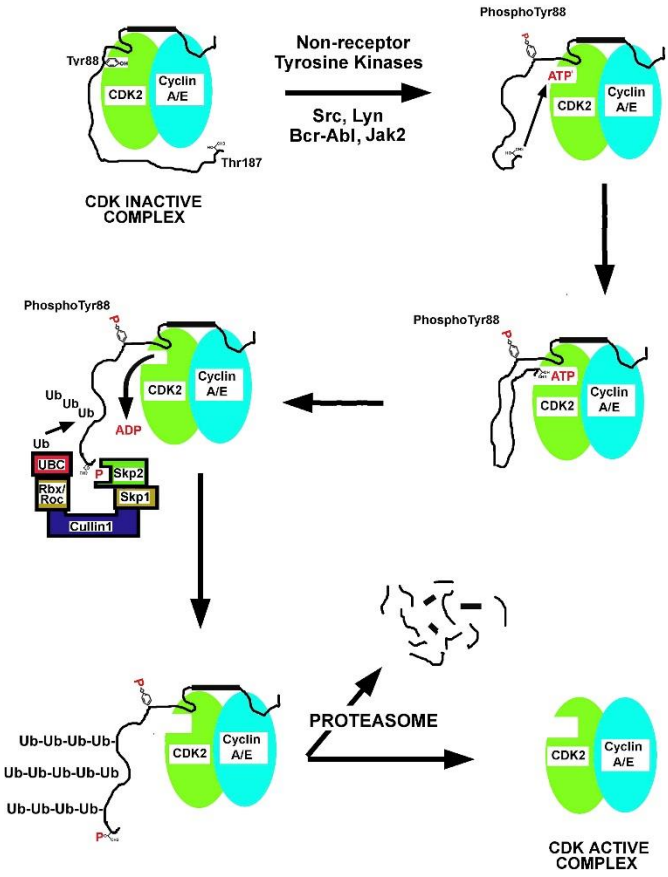


Figure 1.17. Mechanism of activation of p27Kip1/cyclin/CDK by non-receptor tyrosine kinases. Adapted from Debora Bencivenga (2017)[111].

### 1.4.6 Phosphorylation of p27 at Ser10 promotes KPC-dependent degradation in the cytoplasm.

As a cell exits from the G0 phase, p27 is degraded by the proteasome pathway in nucleus. However, the degradation also occurs in Skp2 knockout cells. This hints that there is another mechanism used to decrease the expression of p27. Since p27 is exported from nucleus to the cytoplasm in this case, there must be a Skp2-independent pathway occurring in the cytoplasm. It was finally confirmed that it is the E3 complex KPC (Kip1 ubiquitination-promoting complex) that plays this role in cytoplasm[63].

The phosphorylation of p27 at Ser10 is necessary for cytoplasmic localization and recruits the carrier protein CRM1 for nuclear export[112]. Jab1 is also a key molecule for p27 nuclear-to-cytoplasmic shuttling[113].

KPC, consisting KPC1 and KPC2, is located in cytoplasm. KPC1 contains a RING-finger domain, and KPC2 contains an ubiquitin-like domain and two ubiquitin-associated domains. Inactivation of KPC by itself has little effect on cell cycle progression; however, co-inactivation of KPC and Skp2 inhibits the G1-to-S phase transition, indicating that the two E3s act redundantly to allow cell cycle re-entry[114]. One mechanism for p27 nuclear export to allow KPC-mediated degradation is via p27 binding to cyclin D2–CDK4/6, which is translocated to the cytoplasm during G1 phase in response to the phosphorylation of cyclin D2[115]. Further, P27 also can be degraded by EE6-AP and PIRH2[116, 117].

### 1.4.7 P27 and cell apoptosis

As a CKI, the major function of p27 is working as a cell cycle regulator. It can also have an effect on proliferation, differentiation and cell death. A number of studies have suggested that apoptosis accumulates in the G1 phase of the cell cycle[118, 119, 120]. Keiju Hiromura et al. reported that in

mesangial cells and fibroblasts, apoptosis is increased when the levels of the p27 are absent or reduced[121]. The explanation is that p27 protects cells from apoptosis by maintaining CDK2 inactivity.

## 1.5 Ki67

### 1.5.1 Overview of Ki67

Ki67 is encoded by the *MKI67* gene in human and is also known as antigen KI-67. It was first identified via an antibody raised against Hodgkin's lymphoma cell nuclei[122]. Ki67 is a nuclear protein and is generally expressed strongly in proliferating cells and poorly in quiescent cells[122]. As such, Ki67 is one of the most widely used markers of proliferation in oncology[123, 124].

### 1.5.2 Ki67 structure

Ki67 contains several conserved functional regions: N-terminal forkhead-associated (FHA) domain, a protein phosphatase 1 (PP1)-binding domain, a large central region comprising tandem repeats, and a C-terminal LR (leucine/arginine-rich) chromatin-binding domain (Fig. 1.18)[125]. The FHA domain is a motif that preferentially recognizes phosphorylated protein epitopes[126]. This FHA domain in Ki67 can bind with kinesin-like motor protein Hklp2/Kifl5 and nucleolar protein NIFK[126, 127], which are critical for the maintenance of spindle bipolarity[128] and cancer metastasis[129], respectively.

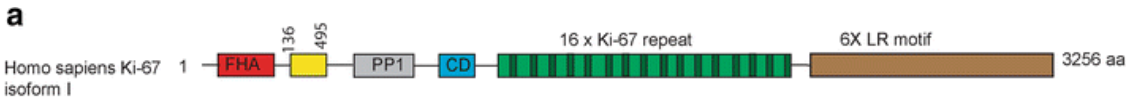


Figure 1.18. A schematic diagram of human Ki-67 structure. Adapted from Xiaoming Sun (2018)[130].

Ki67 contains a canonical protein phosphatase 1 (PP1)-binding motif[131]. Ki67 binds with PP1γ on chromosomes during anaphase, which is a critical step during mitotic exit for the removal of histone phosphorylation[132]. The central region of Ki67 is comprised of tandem repeats that contain residues phosphorylated by CDK1 during mitosis. Furthermore, Ki67's mitotic localization and *in vitro* DNA binding affinity are affected by phosphorylation[133]. At the onset of mitosis, Ki-67 becomes hyperphosphorylated and thereby binds less avidly to DNA, and is highly mobile on the chromosome periphery until anaphase[134]. Ki-67 has a weakly conserved leucine/arginine-rich C-terminal domain (LR domain) which can bind to DNA *in vitro* and is required for association with chromosomes in living cells[135].

### 1.5.3 Transcriptional and post-translational regulation of Ki67

Ki67 was initially thought to be undetectable in cells in the G0 phase[136]. However, it was later confirmed that this was not accurate[137], and that Ki67 is still expressed in the G1/G0 phases, but expression is higher in the S/G2/M phases[137]. Zambon et al. used a ki67 promoter to ectopically express GFP in mouse embryonic stem cells (ESCs), HEK293A and HT1080 cells. The GFP expression, under variety conditions, indicates that the Ki67 promoter can be used to identify proliferating subpopulations of live cells[138]. This hints that the transcription of Ki67 occurs in a cell cycle-dependent manner.

The core promoter of Ki67 is from −223 to +12 nt relative to the transcriptional initiation site, which is the TATA-less, GC-rich region[139]. Bisulfite sequencing and methylation-specific PCR (MSP) were used to generate the methylation profile of the Ki-67 promoter *in vitro* and *in vivo*, indicating that the Ki67 promoter is hypomethylated[140]. Comparatively, DNA microarray analysis revealed that Ki67 is transcriptional controlled by E2F[141]. However, there have been no further studies to elucidate the relationship between Ki67 and E2F. Sp1 was another transcription factor found to regulate the transcriptional expression of Ki67[139]. Transcription factor Sp1 is a zinc

finger transcription factor that binds to GC-rich motifs of many promoters and was reported to be involved in the maintenance of the methylation-free status of CpG islands[142]. The post-translational regulation of Ki67 is seldom reported. However, there are three $APC^{Cdh1}$ binding sites in human Ki67 isoform 1 and two in Ki67 isoform 2. Mouse Cdh1 is coded by *Fzr1* gene. The *Fzr1* knockout MEFs express high and homogeneous levels of Ki67 compared to *Fzr1* heterozygous mice, indicating that Ki67 is regulated by $APC^{Cdh1}$[143].

### 1.5.4 The localisation and function of Ki67

The function of Ki67 during the cell cycle is still unknown. Though experiments with antisense oligonucleotides and antibodies against MKI67 revealed a decreased rate of cell division, indicating the important role of this protein in cell cycle[125], depletion of Ki67 in human HeLa and U2OS cells did not alter cell cycle distribution[143]. Furthermore, proliferation of human MCF-10A epithelial breast or DLD-1 colon cancer cells were not affected by loss of Ki67, although clonogenic growth of highly diluted cell populations were decreased[144]. These studies raised the possibility that the contributions of Ki67 to cell cycle progression could be cell type specific, at least in human cells[130].

However, some assumptions based on the localization and protein-protein interactions have been proven. First, the nucleolar localization of Ki67 is believed to be responsible for enhancing the high rates of ribosomal synthesis during cell proliferation[145, 146] and the sequestration of MKI67 protein within nucleoli until mitosis starts again[145]. Second, Ki67 coats on the chromosomes in mitosis. In mitosis, a proteinaceous sheath, termed the perichromosomal layer (PCL), exists at the outer surfaces of individual chromosomes[147]. Several studies have found that Ki67 is required for the formation of the human PCL. Acute depletion of Ki67 in human cells caused dispersal of all other PCL components[131, 143]. The function of PCL is to protect the chromosomal surface during mitosis. First of all, disruption of the PCL upon Ki67 depletion delocalizes nucleolar components

during mitosis, which in turn leads to their asymmetric distribution in daughter cells[131]. Secondly, Ki67 prevents the aggregation of mitotic chromosomes[135].

### 1.5.5 Ki67 and cancer

Ki67 is well known as a proliferation marker in the clinic to assess how aggressive a tumour is. The best studied examples in this content are carcinomas of the prostate and the breast. The Ki67 labeling index is an independent prognostic factor for survival rate, which includes all stages and grade categories. The scoring system is based on the percentage of tumour cells stained by an antibody. Multiple clinical laboratories have reported the successful use of Ki67 as a diagnostic tool[148, 149]. Expression of Ki67, as evaluated by immunostaining, has become the gold standard, with a cut off level of between 10 and 14% positively‐stained cells defined as high-risk in terms of prognosis[150, 151]. The St. Gallen Consensus in 2009 considered the Ki67 labelling index important for selecting the addition of chemotherapy to endocrine therapy in hormone receptor‐positive breast cancers. In addition, tumours may be classified as low, intermediate, and highly proliferating, according to the Ki67 labelling index of $\leqslant$ 15%, 16%–30%, and >30%, respectively[152].

## 1.6 CRISPR/Cas9

### 1.6.1 A brief history of genome editing

Genome editing (also called gene editing) refers to a group of technologies that give scientists the ability to alter the DNA of an organism. These technologies allow genetic material to be added, removed, or altered at particular locations in the genome. Several approaches to genome editing have been developed.

Zinc-finger nuclease (ZFN) was the first generation of genome editing technology, which was popular before 2010[153]. The DNA-binding domain of ZFNs is comprised of zinc-finger proteins, which each binding to approximately three DNA bases. Different combinations of zinc-finger proteins bind to different sequences of DNA, although it is hard to predict exactly where they will bind without testing them first. The nuclease component of ZFNs is normally a FokI nuclease, which cuts the DNA (Fig. 1.19).


Figure 1.19. Zinc Finger Nuclease (ZFN). ZFN consists of two functional domains: a.) A DNA-binding domain comprised of a chain of two-finger modules, each recognizing a unique hexamer (6 bp) sequence of DNA. Two-finger modules are stitched together to form a Zinc Finger Protein, each with specificity of ≥ 24 bp. b.) A DNA-cleaving domain comprised of the nuclease domain of Fok I. When the DNA-binding and DNA-cleaving domains are fused together, a highly-specific pair of 'genomic scissors' are created. Adapted from sigma (https://www.sigmaaldrich.com/life-science/zinc-finger-nuclease-technology/learning-center/what-is-zfn.html).

Transcription activator-like effector nuclease (TALEN) were the next generation genome editing technology, and were developed in 2011, becoming popular in 2012. However, TALEN was quickly replaced by more cost-effective technology, the Clustered Regularly Interspaced Short Palindromic Repeats (CRISPR) system. The mechanism of TALEN is similar to ZFN, however, the DNA-binding domain of TALENs is made of transcription activator-like effector (TALE) domains (Fig. 1.20)[154, 155].

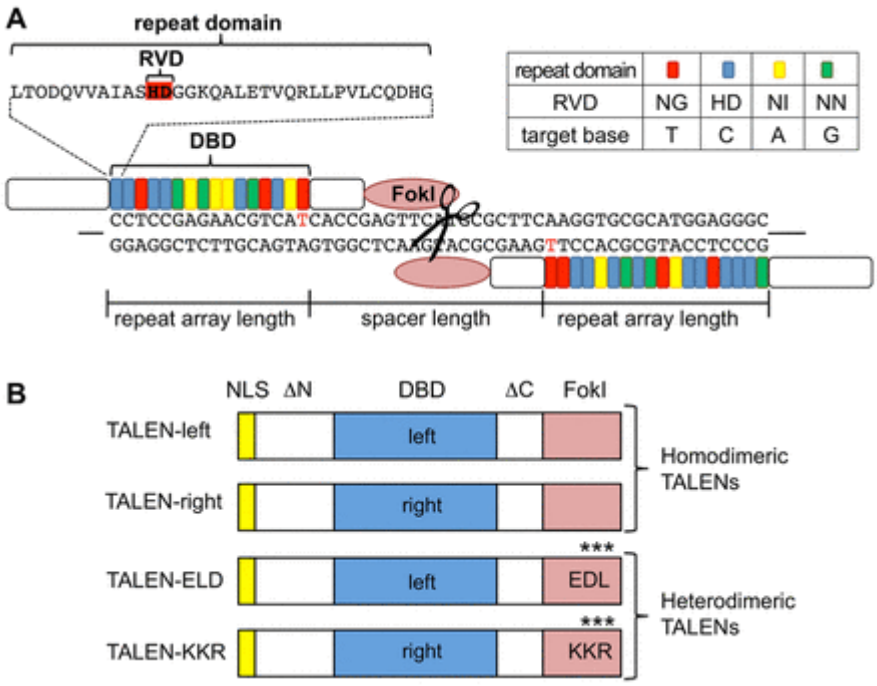


Figure 1.20. Schematic illustration of the TALEN system. A. Binding of the customized TALENs on the genome. The DNA-binding domain (DBD) is composed of repeat domains. Each repeat domain consists of 34 a.a. residues and recognizes one nucleotide. Among the 34 a.a. residues, a set of the 12th and 13th residues is referred to as repeat-variable di-residue (RVD) and functions as a determiner for nucleotide recognition of the domain. The repeat domains containing NG, HD, NI, and NN recognize T, C, A, and G and are shown with red, blue, yellow, and green boxes, respectively. Length of the DNA-binding site (named "repeat array length") and length between two DNA-binding sites (named "spacer length") were important parameters for target recognition and dimerization of TALENs on the genome. T at position 0 of the DNA-binding sequence was shown in red. B. Domain structure of homodimeric and heterodimeric TALENs. GoldyTALEN scaffold was used as a backbone. Both TALEN-left and TALEN-right for homodimeric TALENs contain a wild-type FokI domain. TALEN-ELD and TALEN-KKR for heterodimeric TALENs contain a mutated FokI domain ELD and KKR, respectively. ΔN and ΔC indicate truncated N-terminal and C-terminal domains of TALEN. Left and right DBDs were customized to bind in close proximity. All of the TALENs have an SV40 NLS. Adapted from Akiko Naitou (2015)[156].

In comparison with ZFN and TALEN, CRISPR/Cas9 is the most cost-effective and efficient system used for genome editing. It is also the most widely used genome editing technology now and is adaptable for use in various species.

### 1.6.2 CRISPR/Cas9

CRISPR/Cas9 was adapted from a naturally occurring genome editing system in bacteria. Bacteria and archaea have evolved RNA-mediated adaptive defence systems, termed clustered regularly interspaced short palindromic repeats (CRISPR)/CRISPR-associated (Cas), that protect organisms from invading viruses and plasmids[157, 158]. Approximately 40% of bacteria and 90% of archaea possess CRISPR/Cas systems to confer resistance to foreign DNA elements[159]. These defence systems rely on small RNAs for sequence-specific detection and silencing of foreign nucleic acids. CRISPR/Cas systems are composed of cas genes, organized in operon(s), and CRISPR array(s), consisting of genome-targeting sequences (called spacers) interspersed with identical repeats[159]. CRISPR/Cas9 belongs to the type II CRISPR/Cas system (Fig. 1.21). Cas9 contains at least two nuclease domains, a RuvC-like nuclease domain near the amino terminus and the HNH nuclease domain in the middle of the protein[159]. The Cas9 HNH nuclease domain cleaves the complementary strand, whereas the Cas9 RuvC-like domain cleaves the noncomplementary strand. Thus, the Cas9 nuclease creates DNA double stranded breaks Fig. 1.21).

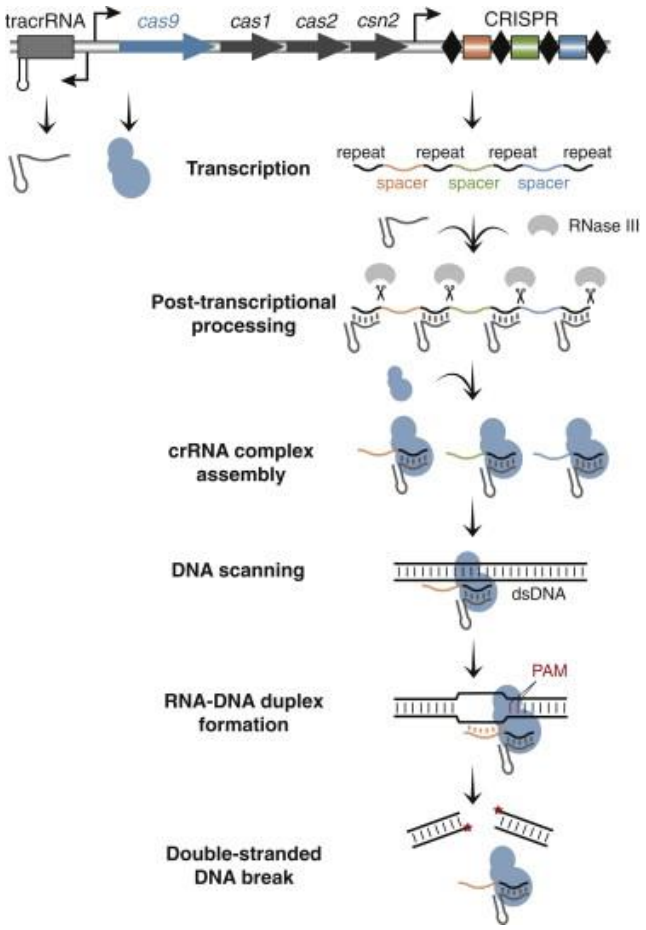


Figure 1.21. Mechanism of the Type II CRISPR System from S. pyogenes**.** The system consists of a set of CRISPR-associated (Cas) proteins and a CRISPR locus that contains an array of repeat-spacer sequences. All repeats are the same and all spacers are different and complementary to the target DNA sequences. When the cell is infected by foreign DNA elements, the CRISPR locus will transcribe into a long precursor transcript, which will be cleaved into smaller fragments. The cleavage is mediated by a trans-acting antisense RNA (tracrRNA) and the host RNase III. After cleavage, one single protein, Cas9, recognizes and binds to the cleaved form of the crRNA. Cas9 guides crRNA to DNA and scans the DNA molecule. The complex is stabilized by basepairing between the crRNA and the DNA target. In this case, Cas9 causes double-stranded DNA breaks due to its nuclease activity. This usually removes cognate DNA molecules, and cells confer immunity to certain DNA populations. Adapted from Lei S. Qi (2013)[160].

Based on the mechanism of the Type II CRISPR System, in 2012, Martin Jinek et al. found that the mature CRISPR RNAs (crRNAs) that are base-paired to trans-activating crRNA (tracrRNA) forms a two-RNA structure that directs the CRISPR-associated protein Cas9 to introduce double-

stranded breaks in target DNA[161]. In addition, site-specific cleavage occurs at locations also determined by the target protospacer DNA (referred to as small guide RNA in later sections) and a short motif (referred to as the protospacer adjacent motif (PAM)) juxtaposed to the complementary region in the target DNA[161]. The crRNA/tracrRNA duplex can be replaced by single chimeric RNA. This raised the exciting possibility of developing a simple and versatile RNA-directed system to generate dsDNA breaks for genome targeting and editing. Furthermore, in 2013, Le Cong et al. engineered two different type II CRISPR/Cas systems and demonstrated that Cas9 nucleases can be directed by short RNAs to induce precise cleavage at endogenous genomic loci in human and mouse cells[162]. In this article, the authors codon-optimized the *S. pyogenes Cas9 (SpCas9)* and confirmed that only Cas9 and chimeric RNA with specific small guide RNA (sgRNA) are sufficient to achieve targeted cleavage of mammalian chromosomes. Additionally, they verified that cells can repair the CRISPR/Cas9 induced DSB (double-strand breaks) not only by nonhomologous end joining (NHEJ) but also by homology-directed repair (HDR). In comparison with NHEJ, HDR can induce precise repair that exactly meets researcher's aims of genome editing. Le Cong et al. also validated that the editing of multiple genome sites is feasible. They edited *EMX1* and *PVALB* genes by insertion two sgRNAs in one vector[162]. George Church's group also published similar work in Science simultaneously[163].

### 1.6.3 The application of CRISPR/Cas9

After the publication of the two Science papers, CRISPR/Cas9 for genome editing has been used in a wide range of organisms, including baker's yeast (Saccharomyces cerevisiae)[164, 165], the opportunistic pathogen *Candida albicans*[166, 167], *Danio rerio*[168], *Drosophila melanogaster*[169, 170], *Harpegnathos saltator*[171] and *Ooceraea biroi*[172], *Aedes aegypti*[173], *Caenorhabditis elegans*[174], plants[175], mice[176], monkeys[177] and human embryos[178]. Excluding base editing, this system has also been utilized to manipulate transcription and epigenetic modification, genome-scale screening, cell therapy and human embryo modification[179].

In response to CRISPR/Cas9 induced DSBs, cellular DNA repair processes result in random insertions or deletions at the site of DNA cleavage through HDR or NHEJ, depending on the presence or absence of homologous DNA template, respectively. The low efficiency of HDR make precise mutation correction more unpredictable. Komor AC et al. engineered fusions of CRISPR/Cas9 and a cytidine deaminase enzyme that retain the ability to be programmed with a guide RNA, do not induce dsDNA breaks, and mediate the direct conversion of cytidine to uridine, thereby effecting a C→T (or G→A) substitution (Fig. 1.22)[180]. The optimized system was called the third generation base editor (BE3). Furthermore, BE4 was designed based on BE3 to increase the efficiency of C:G to T:A base editing by approximately 50%, while halving the frequency of undesired by-products with respect to those generated by BE3[181].

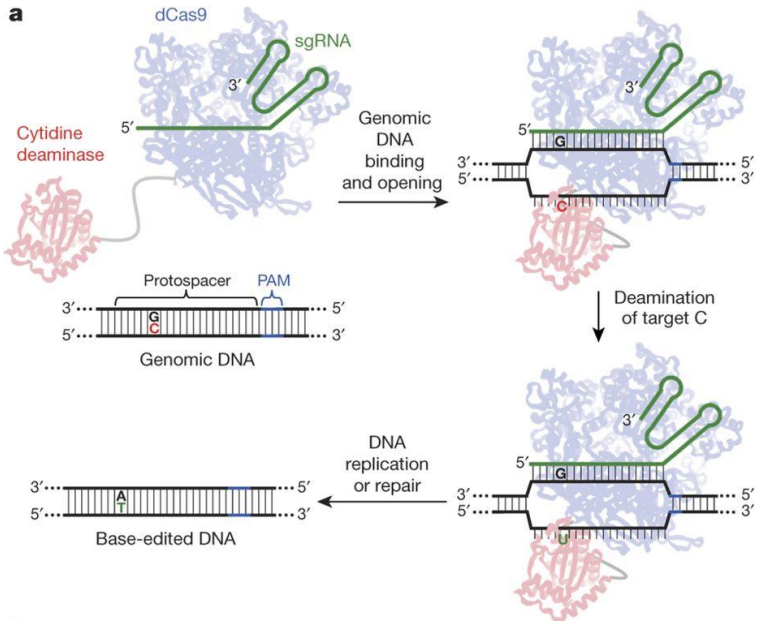


Figure 1.22. Base editing strategy of BE3. DNA with a target C (red) at a locus specified by a guide RNA (green) is bound by dCas9 (blue), which mediates local DNA strand separation. Cytidine deamination by a tethered Apolipoprotein B mRNA editing enzyme, catalytic polypeptide 1 (APOBEC1) enzyme (red) converts the single-stranded target C→U. The resulting G:U heteroduplex can be permanently converted to an A:T base pair following DNA replication or DNA repair. Adapted from Alexis C. Komor (2016)[180].

The dCas9 protein is a Cas9 variant which is capable of binding to the target sequence, but unable to cleave its target[160]. This protein has been adopted as a DNA-binding platform for transcription modulation and epigenetic editing, and engineered by using a variety of effector domains. For example, dCas9 was used by fusion with conventional transcriptional activators, such as VP64, p65, or a subunit of RNA polymerase, to active the transcription of some genes[182, 183]. Opposingly, dCas9 can block target gene transcription by fusing a repressive effector domain, such as the Kruppel-associated box (KRAB)[184, 185]. KRAB repression is mediated by repressive histone modifications such as H3K9me3. By utilizing epigenome modifying repressors, including Lys-specific histone demethylase 1 (LSD1)[186], histone deacetylase (HDAC)[187], DNA methyltransferases DNMT3A and MQ1[188, 189], and mSin3 interaction domains[190], the scope of applying CRISPR repression has been extended to epigenetic editing.

RNA interference (RNAi) screening is limited by incompletely abrogated gene expression and high off-target effects, resulting in false positive[191]. CRISPR can be adapted for genome-scale screening by combining Cas9 with pooled-guide RNA libraries and next-generation sequencing (NGS)[192, 193]. These screens utilize pooled sgRNA libraries generated by cloning chip-synthesized oligonucleotides, which cover the entire human or mouse transcriptome, into lentiviral vectors. Upon transduction of the libraries into cells, sgRNAs induce a selectable phenotype that can be identified by NGS[179]. Further, CRISPR/Cas9 has been used in the field of cell therapy, mainly involving immune cell therapy[194] and stem cell therapy[195].

### 1.6.4 Cas12 and Cas13

During the first wave of the CRISPR revolution, it was all about Cas9 which belongs to the type II CRISPR/Cas system. While the nucleases belonging to type V and type VI CRISPR/Cas also be used for gene editing. Cas12, also known as Cpf1, is a nuclease that has a RuvC domain but not an HNH domain. The molecular weight of Cas12 is smaller than Cas9 and it does not need

tracrRNA. Moreover, it has RNase activity and can recognize a different PAM sequence which is at the upstream of its target (Fig. 1.23)[196]. Cas13 belongs to the type VI system and is utilized to edit RNA (Fig. 1.23)[197]. Many applications have also been built using Cas13s in mammalian cells, including transcript knockdown, live-cell transcript imaging[198], and RNA base editing[197].

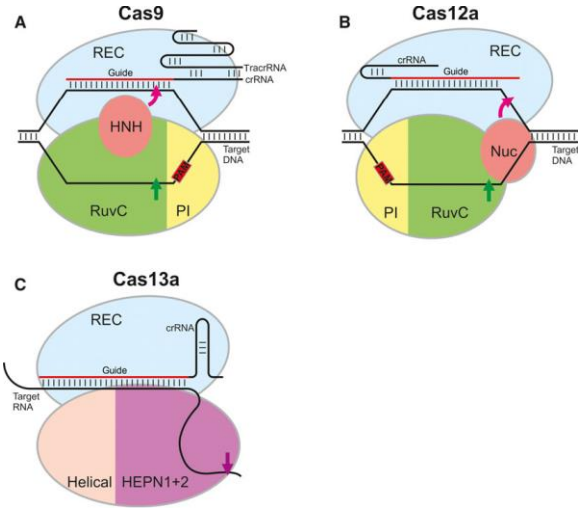


Figure 1.23. Schematic comparison of Cas proteins in their native forms. A. The CRISPR/Cas9 system mediates its function via the single effector Cas9 and two small RNAs, the crRNA and tracrRNA. Upon hybridization, the crRNA::tracrRNA complex associates with the Cas9 nuclease and binds to its recognition site upstream of the PAM sequence. DNA binding is mediated by the 20-nucleotide guide sequence of the crRNA. The Cas9 nuclease induces a blunt-ended DSB 3 bp upstream of the PAM sequence. Recognition of the crRNA::tracrRNA::target complex is mediated by the REC (recognition) lobe, the PI (PAM interacting) domain is responsible for PAM recognition. The DSB is mediated by the HNH and RuvC nuclease domains, with the HNH domain cleaving the target and the RuvC domain cleaving the nontarget strand. B. The CRISPR/Cas12a system mediates its function via the single effector Cas12a and a single crRNA. Upon association of Cas12a and crRNA, the complex binds to its recognition site downstream of the PAM sequence. DNA binding is mediated by a 23–25-nucleotide guide sequence of the crRNA. The Cas12a nuclease induces a staggered-ended DSB distal from the PAM sequence. Recognition of the crRNA::target complex is mediated by the REC (recognition) lobe, the PI domain is responsible for PAM recognition. The DSB is mediated by the Nuc and RuvC domains, with the Nuc domain cleaving the target strand after the 18th bp downstream of the PAM and the RuvC domain cleaving the nontarget strand after the 23rd bp downstream of the PAM (in case of FnCas12a). C. The CRISPR/Cas13 system (Cas13a shown) mediates its function via the single effector Cas13 and a single crRNA. Upon association of Cas13 and crRNA, the complex binds to its recognition site within the target RNA mediated by the guide sequence of the crRNA. The catalytic site is located at the outside of the protein facing the surrounding solution, leading to cleavage of the target RNA remote from the recognition site. Recognition of the crRNA::target complex is mediated by the REC (recognition) lobe, cleavage of the target RNA by the HEPN domain. Adapted from Patrick Schindele (2018)[199].

## 1.7 Rationale, hypothesis and aims

Recurrence after initial treatment resulting from residual quiescent cancer cells is a major obstacle in the curative treatment of cancer. While targeting quiescent cells in combination with existing therapeutic drugs is emerging as a promising strategy to improve the therapeutic efficiency. If a molecular network encompassing not only proteins but also noncoding RNAs which is essential for survival of quiescent cancer cells is uncovered, targeting key components of the network renders quiescent cancer cells sensitive to killing by conventional anti-cancer therapy will be possible.

We hypothesize quiescent cancer cells can by isolated according to the fluorescence labelled genes which are specifically accumulated in quiescent or cycling phases. The labellings are either depend on ectopic expression or gnomically knock-in. The pathways are involved in regulating the quiescent status of cancer cells can be targeted to sensitize the killing of quiescent cancer cells. The aims of this PhD thesis is to test these hypotheses.

Aims

1. To isolate intact quiescent cancer cells.
2. To characterize molecular signatures of quiescent compared with cycling melanoma cells
3. To define the functional significance of miRNAs in cellular dormancy.
4. To confirm pathways that contribute to quiescence maintenance and drug resistance.

# Chapter two

# Materials and methods

# 2. Material and methods

## 2.1. Tissue culture

### 2.1.1. Cell lines

Human melanoma cells were isolated from patient biopsies of the Calvary Mater Newcastle and Sydney Melanoma Units. Mel-RM was from bowel. Mel-FH, Mel-RMu, Mel-CV and Mel-JD were from lymph nodes[200]. MM200 was established from primary melanoma and gifted from Dr Pope and Dr Parsons (Queensland Institute for Medical Research, QLD, Australia). IgR3 was isolated from primary melanoma and was obtained from Dr. Hope (Genetics Department, University of Adelaide, SA, Australia). Sk-Mel-28 (skin) cell line was bought from the American Type Culture Collection (ATCC). ME1007 and ME4405, isolated from primary melanoma lesions, were kindly gifted from Dr. Giorgio Parmiani (National Cancer Institute, Milan, Italy). All human melanoma cell lines were cultured in Dulbecco's modified Eagle's medium (DMEM) containing 5% fetal calf serum (FCS) (Commonwealth Serum Laboratories, Parkville, VIC, Australia) at 37℃ in a humidified atmosphere of 5% $CO_2$. Human melanocytes HMMn-MP and HEMn-DP were purchased form Clonetics (Edward Kellar, VIC, Australia) and were cultured in melanocyte medium (Gibco, Invitrogen, Mulgrave, VIC, Australia) under the same conditions. All cell lines were examined every 2 months for mycoplasma contamination.

### 2.2.2 Establishment of primary melanoma cell Lines

Fresh melanoma tumour samples were handled under sterile conditions in class Ⅱ biosafety hoods. The fresh melanoma tissues were cut into small pieces and cells were pressed out of tumour segments with the flat end of a 10-ml syringe plunger and teased out into DMEM containing antibiotics (penicillin, 100µg/ml; streptomycin, 100µg/ml and amphotericin B 250ng/ml). The

cell suspension was centrifuged on Ficoll-Paque (Pharmacia) at 2500 rpm for 30 min at room temperature to remove fibrous or other non-cellular debris. Viable cells at the interface of the Ficoll-Paque and medium were collected and washed twice with phosphate buffer saline (PBS) before culturing in DMEM with 10% FCS. The cultured cells were treated with 100µg /ml gentamycin (Sigma-Aldrich, Castle Hill, NSW, Australia) against fibrolasts and incubated for 45 min on ice with a murine Mab against human CD45 (Silenius) and with MAb against human fibroblasts (Sera-Lab). The melanoma cell suspension was washed, checked for viability by trypan blue exclusion and for leukocyte contaminants by staining with MAb against human CD45-FITC (Silenius). Some of the fresh isolates were cultured in a 75-cm flask and when cells were confluent were called P1 cells. For subculture, the cells from a confluent flask were distributed into three flasks. When confluent, these were referred to as P2 cells, and so on.

## 2.2 Antibodies and other reagents

A list of antibodies and other reagents that were used in this thesis are shown in Tables 2.1 and 2.2, respectively.

**Table 2.1. List of antibodies**

| Antibody | Catalogue No. | Company |
|---|---|---|
| Phospho-Rb (Ser807/811) (D20B12) XP® Rabbit mAb | #8516 | Cell Signalling Technology (Beverly, MA) |
| Phospho-Rb (Ser807/811) antibody | #9308 | Cell Signalling Technology (Beverly, MA) |
| cyclin D1 antibody (H-295) | sc-753 | Santa Cruz Biotechnology (Santa Cruz, CA) |
| Cdk2 (D-12) | sc-6248 | Santa Cruz Biotechnology (Santa Cruz, CA) |
| p21 Waf1/Cip1 (12D1) Rabbit mAb | #2947 | Cell Signalling Technology (Beverly, MA) |
| p27 antibody (F-8) | sc-1641 | Santa Cruz Biotechnology (Santa Cruz, CA) |
| p27 Kip1 (D69C12) XP® Rabbit mAb | #3686S | Cell Signalling Technology (Beverly, MA) |
| GFP (D5.1) XP® Rabbit mAb | #2956 | Cell Signalling Technology (Beverly, MA) |
| GAPDH antibody (6C5) | sc-32233 | Santa Cruz Biotechnology (Santa Cruz, CA) |
| Ki-67 (D3B5) Rabbit mAb | #9129 | Cell Signalling Technology (Beverly, MA) |
| Goat anti-Rabbit IgG(H+L) Secondary antibody, Alexa Fluor | A-11008 | Thermo Fisher Scientific (Waltham, MA) |
| APC anti-mouse Ki-67 antibody | 652406 | BioLegend (San Diego, CA) |
| APC Rat IgG2a, K Isotype Ctrl antibody | 400512 | BioLegend (San Diego, CA) |
| Skp2 (D3G5) XP® Rabbit mAb | #2652 | Cell Signalling Technology (Beverly, MA) |
| p27 KIP 1 (phospho T187) antibody | ab75908 | Abcam (Cambridge, United Kingdom) |
| p27 KIP 1 (phospho S10) antibody | ab62364 | Abcam (Cambridge, United Kingdom) |
| p27 KIP 1 (phospho T198) antibody | ab64949 | Abcam (Cambridge, United Kingdom) |
| CKS1 antibody | ab130529 | Abcam (Cambridge, United Kingdom) |
| C10orf46 antibody [EPR16094] | ab190799 | Abcam (Cambridge, United Kingdom) |
| p53 antibody (DO-1) | sc-126 | Santa Cruz Biotechnology (Santa Cruz, CA) |
| Monoclonal ANTI-FLAG® M2 antibody produced in mouse | F3165 | Sigma-Aldrich (St. Louis, MO) |
| Phospho-CDK2 (Thr160) antibody | #2561 | Cell Signalling Technology (Beverly, MA) |

**Table 0.1. List of Recombinant Proteins and other Reagent**

| Proteins/Reagents | Source |
|---|---|
| Sodium Chloride (NaCl) | Ajax Finechem (Seven Hills, NSW, Australia) |
| TRIS | Ajax Finechem (Seven Hills, NSW, Australia) |
| Methanol | Ajax Finechem (Seven Hills, NSW, Australia) |
| Glycine | Ajax Finechem (Seven Hills, NSW, Australia) |
| TaqMan Universal Master Mix II | Applied Biosystems (Mulgrave, VIC, Australia) |
| 30% Acrylamide/Bis Solution | Bio-Rad (Regents Park, NSW, Australia) |
| Protein Assay Dye | Bio-Rad (Regents Park, NSW, Australia) |
| Agar Powder | Bioline (Alexandria, NSW, Australia) |
| Annexin V | BD Pharmingen (San Diego, CA, USA) |
| VisionBlue Quick Cell Viability | BioVision (Mountain View, CA, USA) |
| Fetal Calf Serum (FCS) | Commonwealth Serum Laboratories (Parkville, VIC, Australia) |
| DH5α Competent Cells | Invitrogen (Carlsbad, CA, USA) |
| Lipofectamine 3000 | Invitrogen (Carlsbad, CA, USA) |
| Opti-MEM | Invitrogen (Carlsbad, CA, USA) |
| Luminata Crescendo Western HRP | Merck Millipore (Kilsyth, VIC, Australia) |
| CellTiter-Glo assay Kit | Promega (San Luis Obispo, CA, USA) |
| ISOLATE II Plasmid Mini Kit | Bioline (Alexandria, NSW, Australia) |
| ISOLATE II RNA Mini Kit | Bioline (Alexandria, NSW, Australia) |
| qScript cDNA SuperMix | Quantabio (Beverly, MA, USA) |
| Protease Inhibitor Cocktail | Roche Diagnostics (Castle Hill, NSW, Australia) |
| Ammonium Persulphate | Sigma-Aldrich (Sydney, NSW, Australia) |
| Ampicillin | Sigma-Aldrich (Sydney, NSW, Australia) |
| BSA | Sigma-Aldrich (Sydney, NSW, Australia) |
| Crystal Violet | Sigma-Aldrich (Sydney, NSW, Australia) |
| Ethanol (Molecular Biology Grade) | Sigma-Aldrich (Sydney, NSW, Australia) |
| NP-40 | Sigma-Aldrich (Sydney, NSW, Australia) |
| Propidium Iodide | Sigma-Aldrich (Sydney, NSW, Australia) |
| Puromycin | Sigma-Aldrich (Sydney, NSW, Australia) |
| Trametinib | Selleckchem (Redfern, NSW, Australia) |
| 2,4-DNP | Sigma-Aldrich (Sydney, NSW, Australia) |
| Olgomycin A | Sigma-Aldrich (Sydney, NSW, Australia) |
| Metformin hydrochloride | Sigma-Aldrich (Sydney, NSW, Australia) |
| CCCP | Sigma-Aldrich (Sydney, NSW, Australia) |
| Triton X-100 | Sigma-Aldrich (Sydney, NSW, Australia) |
| T ween-20 | Sigma-Aldrich (Sydney, NSW, Australia) |
| Vemurafenib | Selleckchem (Redfern, NSW, Australia) |
| SCR7 | Xcess Biosciences (San Diego, CA, USA) |

## 2.3 Cell viability assay

### 2.3.1 MTS assay

Cell viability of melanoma cells were determined using VisionBlue Quick Cell ViabilityAssay. Melanoma cells ($5x10^3$ cells/well) were seeded in flat-bottomed 96-well plates overnight prion to treatments. 10 µl of VisionBlue™ (BioVision, Mountain View, CA, USA) reagent was added to each well and then incubated at 37°C in a humidified atmosphere of 5% $CO_2$ for 1-3 hours. Fluorescence was detected by a microplate reader (Synergy 2, Bio Tek, Winooski, VT, USA) at excitation 530nm and emission 590nm.

### 2.3.2 CellTiter-Glo assay

CellTiter-Glo Assay can also be used for examining cell viability of melanoma cells. $5x10^3$ cells were seeded in each well of a 96-well plate (white) overnight before treatment. CellTiter-Glo reagent and plate were first equilibrated at room temperature for 30 minutes before adding equal CellTiter-Glo reagent to each well of cell culture medium. After mixing on an orbital shaker for 2 minutes, the plates were incubated at room temperature for a further 10 minutes to stabilize the luminescence. The luminescence intensity was measured by Synergy 2 multidetection microplate reader.

## 2.4 Cell proliferation assays

### 2.4.1 BrdUrd Incorporation assay

BrdUrd cell proliferation assays were carried out using an assay kit (Cell Signaling Technology) as per the manufacturer's instructions. Briefly, cells were seeded at $5 \times 10^3$/ well in 96-well plates overnight before treatment as indicated. BrdUrd (10 µmol/L) was added and cells were incubated for 4 hours before BrdUrd assays were carried out. Absorbance was read at 450 nm using a Synergy 2 multidetection mircroplate reader.

### 2.4.2 Colony formation assay

Melanoma cells ($1x10^3$/well) were seeded in a 6-well plate overnight before respective treatments. The culture medium was changed to fresh DMEM containing 5% FCS to allow cells to grow for 10-14 days. As colonies formed, cells were washed twice with ice-cold PBS before fixing with ice-cold methanol for 10 minutes on ice. After incubation, methanol was discarded and cells were stained with 0.5% crystal violet solution for 15 minutes at room temperature. Cells were then washed with distilled water multiple times until crystal violet dye no longer washes off. Plates were allowed to dry overnight at room temperature in the dark. The photos were captured by Bio-Rad Versa-doc image system (Bio-Rad, Regents Park, NSW, Australia).

## 2.5 Apoptosis

### 2.5.1 PI-Annexin V Staining

Apoptosis was measured by staining with the Annexin V/propidium iodide (PI) Apoptosis Detection Kit (BD Biosciences) according to the manufacture's protocols. 5 x $10^4$ melanoma cells were seeded per well in 24-well plates overnight before treatment. Cells were harvested with trypsin and washed twice with ice-cold PBS before resuspending in binding buffer (10mM Hepes/NaOH, pH 7.4; 140mM NaCl; 2.5 mM $CaCl_2$) at a density of 1 x $10^6$ cell/ml. 100 µl of cells (1 x $10^5$) were then transferred into a falcon polystyrene tube and stained with 5 µl of Annexin V-FITC and 5 µl of PI following with incubation in the dark at room temperature for 15minutes. After incubation, cells were diluted with 400 µl of binding buffer and samples were analysed by flow cytometry (FACScanto, Becton Dickinson, Sunnyvale, CA, USA) within one hour.

### 2.5.2 PARP and Caspase 3 cleavage

The cleavage of PARP and Caaspase 3 were detected by Western blotting. In briefly, whole cell protein was extracted and subjected to SDS PAGE. Then the proteins on the gel were transferred to a nitrocellulose membranes. PARP (BD Biosciences, 556494) and Caspase 3 (Enzo Life Sciences, AAP-113) antibodies were incubated and the blots were detected by ImageReader LAS-4000 (Fujifilm Corporation, Japan).

## 2.6 Western blotting

### 2.6.1 Whole cell protein extraction

Cells (2×105/well) were seeded in 6-well plates and were allowed to grow overnight before treatment at the indicated time points. Cells were trypsinized and washed with PBS before resuspending in ice-cold lysis buffer (10mM Tris-HCl, pH 7.4; 140mM NaCl; 0.5mM CaCl2; 0.5mM MgCl2; 0.02% NaN3; 1% NP-40; 1x protease inhibitor cocktail (Roche DiagnostuBIocs, Castle Hill, NSW, Australia)). Cell lysates were vortexed vigorously and incubated on ice for 30 minutes followed by centrifuging at 13,000 rpm for 30 minutes at 4ºC. The supernatants containing proteins were transferred to new tubes. Protein concentrations were measured by Bio-Rad Protein Assay Dye Reagent Concentrate (Bio-Rad, 500-0006) and detected with a spectrophotometer (Thermo Fisher Scientific, GENESYS™ 10S UV-Vis Spectrophotometer).

### 2.6.2 SDS-PAGE

Sodium dodecyl sulphate-polyacrylamide gel electrophoresis (SDS-PAGE) was used for separating proteins. The Mini-PROTEAN 3 electrophoresis system was purchased from Bio-Rad (Bio-Rad, Regents Rark, NSW, Australia). Gels (7.5-15%) with a thickness of 1.5mm were

prepared and used for separating 10-250kDa proteins. Each gel consists of two layers, resolving gel (resolving gel buffer (1.5M Tris, pH8.8; 30% acrylamide solution; 10% ammonium persulphate (APS); N,N,N',N'-tetramethylethylenediamine (TEMED)) and stacking gel (stacking gel buffer (800mM Tris, pH 6.8; 30% acrylamide solution, 10% SDS, 10% APS, TEMED). The resolving gel buffer was mixed well and poured into between spacer and short plates. Distilled water was topped on the resolving gel for removing air bubbles. When the resolving gel had polymerised, the stacking gel buffer was layered over the resolving gel before placing a multi-well comb into the stacking gel buffer. After polymerisation was completed, the comb was removed and gel was mounted in an electrophoresis apparatus. 30-100 µg proteins were mixed with an equal volume of 2 × SDS- PAGE loading buffer (4 x Tris CI/SDS, pH 6.8; 20% glycerol; 0.001% bromophenol blue; 4% SDS; 0.02%- mercapto ethanol) before boiling the mixture for 3 minutes at 100°C. Samples were loaded into wells with unstained and/or pre-stained protein molecular weight markers (Bio-Rad, Regents Park, NSW, Australia) and then electrophoresed in pre-cold SDS running buffer (25mM Tris, 200mM glycine, 0.1% SDS).

### 2.6.3 Western Blot

When the electrophoresis was completed, proteins on the SDS-polyacylamide gels were transferred onto 0.45 µm nitrocellulose membranes (Bio-Rad, Regents Park, NSW, Australia) in transferring buffer (20mM Tris, 150mM glycine, 20% methanol) via the Mini Trans-Blot electrophoretic transfer cell (Bio-Rad, Regents Park, NSW, Australia) at 100V for 2 hours. Non-specific interactions in the nitrocellulose membranes were incubated with 5% milk /BSA containing Tris-buffer saline supplement with Tween-20 (TBS-T) at room temperature for an hour. Membranes were then incubated with primary antibodies on a shaker overnight at 4°C. The next day, membranes were washed three times with TBS-T for 20 minutes each time and incubated with horseradish peroxidase-conjugated secondary antibody at room temperature for 2 hours. Membranes were washed three times again with TBS-T before exposure to Lumunata Crescendo

Western HRP (Merck Millipore, Kilsyth, VIC, Australis). Images were captured by using the ImageReader LAS-4000 (Fujifilm Corporation, Japan).

## 2.7 The establishment a fluorescent knock-in cell lines.

### 2.7.1 Plasmids

We constructed sgRNA expression vectors by inserting annealed oligonucleotide including target sequences and adaptor sequence into BsmBI-digested lentiCRISPR v2 (Addgene plasmid #52961) containing human codon-optimized SpCas9 expression cassette and a human U6 promoter driving the expression of the chimeric sgRNA.

Donor DNA fragments were synthesized (HuaGene Biotech Co., Ltd, Shanghai) and inserted into *pEASY* Blunt-Zero vector (TransGen Biotech). CDKN1B/GFP donor was linearized by PstI-HF (NEB, R3140L) and MKI67/mCherry donor was linearized by SpeI-HF (NEB, R3133L) before nucleofection.

**Supplementary data 2.1**

CDKN1B/GFP donor DNA sequence:

Homology arms

EGFP

Mutated nucleotides (synonymous mutations)

ACGTGCGAGTGTCTAACGGGAGCCCTAGCCTGGAGCGGATGGACGCCAGGCAGGC

GGAGCACCCCAAGCCCTCGGCCTGCAGGAACCTCTTCGGCCCGGTGGACCACGAAG

AGTTAACCCGGGACTTGGAGAAGCACTGCAGAGACATGGAAGAGGCGAGCCAGCG

CAAGTGGAATTTCGATTTTCAGAATCACAAACCCCTAGAGGGCAAGTACGAGTGGC

AAGAGGTGGAGAAGGGCAGCTTGCCCGAGTTCTACTACAGACCCCCGCGGCCCCCC

AAAGGTGCCTGCAAGGTGCCGGCGCAGGAGAGCCAGGATGTCAGCGGGAGCCGCC

CGGCGGCGCCTTTAATTGGGGCTCCGGCTAACTCTGAGGACACGCATTTGGTGGAC

CCAAAGACTGATCCGTCGGACAGCCAGACGGGGTTAGCGGAGCAATGCGCAGGAA

TAAGGAAGCGACCTGCAACCGACGgtaatgacccttcccaaccatagaatgtgtttggggccccgctttgcctgct

ggagggtgttaaccttagcttgcttttcggcgtattctgatttagctttgggagagctaactttattggtcttaggtgttcagtgctacctggccca

ctgcttgtctgtttgtgacttttaagtcagaaactggagatggtaagatccgataatttccctaacttaatacatcgcggtccctctcactagcaa

ctcctaggtatgtgacaaagttgggatgtttatcaacggtccgcctcctggctagggaaagagctctggggcggagaatgcactttctgttttt

tgaaaacaacctcattttgtgcccttaaaagccactggggatgacggatccaggattgtgggtggaggtagtgggtttttcatcccctgacta

tggggccaacttctgccagccattgtttttttctaataaagattgtgtgttctttttaaaaatttcccctgcgcttagATTCTTCTACTCA

AAACAAAAGAGCCAACAGAACAGAAGAAAATGTTTCAGACGGTTCCCCAAATGCC

GGTTCTGTGGAGCAGACGCCCAAGAAGCCTGGCCTCAGAAGACGTCAAACAATGG

TGAGCAAGGGCGAGGAGCTGTTCACCGGGGTGGTGCCCATCCTGGTCGAGCTGGAC

GGCGACGTAAACGGCCACAAGTTCAGCGTGTCCGGCGAGGGCGAGGGCGATGCCA

CCTACGGCAAGCTGACCCTGAAGTTCATCTGCACCACCGGCAAGCTGCCCGTGCCC

TGGCCCACCCTCGTGACCACCCTGACCTACGGCGTGCAGTGCTTCAGCCGCTACCCC

GACCACATGAAGCAGCACGACTTCTTCAAGTCCGCCATGCCCGAAGGCTACGTCCA

GGAGCGCACCATCTTCTTCAAGGACGACGGCAACTACAAGACCCGCGCCGAGGTG

AAGTTCGAGGGCGACACCCTGGTGAACCGCATCGAGCTGAAGGGCATCGACTTCAA

GGAGGACGGCAACATCCTGGGGCACAAGCTGGAGTACAACTACAACAGCCACAAC

GTCTATATCATGGCCGACAAGCAGAAGAACGGCATCAAGGTGAACTTCAAGATCCG

CCACAACATCGAGGACGGCAGCGTGCAGCTCGCCGACCACTACCAGCAGAACACC

CCCATCGGCGACGGCCCCGTGCTGCTGCCCGACAACCACTACCTGAGCACCCAGTC

CGCCCTGAGCAAAGACCCCAACGAGAAGCGCGATCACATGGTCCTGCTGGAGTTCG

TGACCGCCGCCGGGATCACTCTCGGCATGGACGAGCTGTACAAGTAAACAGCTCGgt

gggttgatcactaaaggagcacgcactggaacccggggccttcagacctcacgatacctgatcttactggttgctggcaaattaaaagctta

tggggttttgttttgtttatacttcgtgaggtcaaaaaagtagcaatggggaaggctggggatacggtaattcctcagagtttctatgcccaga

gatactttctcttcaaactgttgaccagagcagctacttgtaacccaggccccatcgggtaggaaggtcgtttccctgtgagtcccactaaaa

cgtgttgggagcaataggttctttgcccatccgaacaagaactagggtactccctcagtccgaattaatgagaattaatttcctagaggttcag

cttgagtcggtaacagattttgagccatacatggaaaaatggcaaatacatgattaagtttcaattttgaggggggaatgtttggtagaaattgct

catctttggttatgcaagggattagagatgtgaataggatggtatgttgtgttctttgacattttaataaactgtcactttccctgttgtctcctaagt

ttggagagagaaggaaccagtatttgcaaaaaccaaatggaaagataaaaaagttactaaagtttctacagaatttctggtaacactgaagtt

gcaaagcagaagttaaattaactcttgtcagtaagcaatccaggaacacgtcagccagtgtatgctaattgtgccgtaacagggtgatttgg

atatttgtaggggaaatgggtagtaaatatcaagactggtgaccgtaggtcagcccagcacaaaggaagtggagatttttccatgcacaag

aatctgatcactgtaaatagctaatttgaataattcagtccccagataaccaacatgggttggttattcataataaactacatattttaatagtttatt

agcttcctttagaccaagactgtgacctctttattttctaaagcacacacgtagtttagcatatgaggcgataaaatattgatgttaacttttaaat

ccccagttataaaaattttaaaataacagggattaaggtgagattcaggtttgttgtgtctttaaattgtatatgtgacttcacatatctttttcagcg

cttatacaaaacggcactatagaacctccattttacagcaccatatgaagtgggaaaattaggtgaaaattttcctgaagcaaccttaacatgc

gcagcccttg

MKI67/mCherry donor DNA sequence:

Homology arms

mCherry

agcaaacgaaactcatgtagcaataacctcttcagatacagaattctggcaagtacagctgtccagacagaccctcttcggcacaaactag

gaagcttcaactgccaagaaaaggaaagattcccaggtgtccccagtacctgctgcatagccaggcagccagtggaggggggagggctt

gtgtgtctggatggtgggcaggaagtcctagtggggagatgcccatagactgttccagagagggaagaggagaggctcaagaagggca

ctgatgcccacacaggtgtcctaagtcagagactgtacttctggggcaggctggaagcagaagacacccgacagtgccagacaaggtcc

tagaaaccacaggcacaccagggacgcaacagctgacgtgggtcagcacgttcacccgtcgagtcttacaataaaacgcaggctccag

gcgcttaccgaattcacagtctggaaggtgctgcttcctcagaatgaaaccaaagaagggtgaaagcgaatcttttaactaggatgattcct

aaacacagagcaaccaggcccaaggctgagccaggcctggtgtgttctgccgggggcgttccagcctcttctcacacacaagcaccca

ggagacgcccaacacacacatgctcctctttgccgagctcttcggtgggtgtcggtagtcctagaaaatgcatatataagatagatttttcca

gtaagaagcttgtagccatgcttttcaccatggttcctctcccttagccaaggggtgagaactactgcaagagtaaaggccaaggcaggtct

cctgcatgcaagttgggcatgcttctgtctacaggggttccttggtttaggagacccaaaagacttaatcctggttggattcacttttctgagt

gacatttttagtttgtgaaaatgtgtgcatcgatgaagaaattttattatgaattagcttaaaaatgcattaggaacttctgtatgaaaagatcac

attatttaagtgtaaaaaaactgcataataaaagcagttcaagtcaagaaaaacaatgttaatggaatatattttaaaacttatttccaacctcaa

aattaattttctgcaactaaggacctgcataatacctagtaagcctttggggttttgcagaggaggtcgattctaaaaatgggtgtttaaattact

taagagttctatttttttttcttcccacacaggctgaggacaatgtgtgtgtcaagaaaataagaaccagaagtcatagggacagtgaagatatt

ATGGTGAGCAAGGGCGAGGAGGATAACATGGCCATCATCAAGGAGTTCATGCGCT

TCAAGGTGCACATGGAGGGCTCCGTGAACGGCCACGAGTTCGAGATCGAGGGCGA

GGGCGAGGGCCGCCCCTACGAGGGCACCCAGACCGCCAAGCTGAAGGTGACCAAG

GGTGGCCCCCTGCCCTTCGCCTGGGACATCCTGTCCCCTCAGTTCATGTACGGCTCC

AAGGCCTACGTGAAGCACCCCGCCGACATCCCCGACTACTTGAAGCTGTCCTTCCC

CGAGGGCTTCAAGTGGGAGCGCGTGATGAACTTCGAGGACGGCGGCGTGGTGACC

GTGACCCAGGACTCCTCCCTGCAGGACGGCGAGTTCATCTACAAGGTGAAGCTGCG

CGGCACCAACTTCCCCTCCGACGGCCCCGTAATGCAGAAGAAGACCATGGGCTGGG

AGGCCTCCTCCGAGCGGATGTACCCCGAGGACGGCGCCCTGAAGGGCGAGATCAA

GCAGAGGCTGAAGCTGAAGGACGGCGGCCACTACGACGCTGAGGTCAAGACCACC

TACAAGGCCAAGAAGCCCGTGCAGCTGCCCGGCGCCTACAACGTCAACATCAAGTT

GGACATCACCTCCCACAACGAGGACTACACCATCGTGGAACAGTACGAACGCGCC

GAGGGCCGCCACTCCACCGGCGGCATGGACGAGCTGTACAAGTAACAGAAAAATC

GAACTGGGAAAAATATAATAAAGTTAGTTTTGTGATAAGTTCTAGTGCAGTTTTTGT

CATAAATTACAAGTGAATTCTGTAAGTAAGGCTGTCAGTCTGCTTAAGGGAAGAAA

ACTTTGGATTTGCTGGGTCTGAATCGGCTTCATAAACTCCACTGGGAGCACTGCTGG

GCTCCTGGACTGAGAATAGTTGAACACCGGGGGCTTTGTGAAGGAGTCTGGGCCAA

GGTTTGCCCTCAGCTTTGCAGAATGAAGCCTTGAGGTCTGTCACCACCCACAGCCA

CCCTACAGCAGCCTTAACTGTGACACTTGCCACACTGTGTCGTCGTTTGTTTGCCTA

TGTCCTCCAGGGCACGGTGGCAGGAACAACTATCCTCGTCTGTCCCAACACTGAGC

AGGCACTCGGTAAACACGAATGAATGGATGAGCGCACGGATGAATGGAGCTTACA

AGATCTGTCTTTCCAATGGCCGGGGGCATTTGGTCCCCAAATTAAGGCTATTGGAC

ATCTGCACAGGACAGTCCTATTTTTGATGTCCTTTCCTTTCTGAAAATAAAGTTTTGT
GCTTTGGAGAATGACTCGTGAGCACATCTTTAGGGACCAAGAGTGACTTTCTGTAA
GGAGTGACTCGTGGCTTGCCTTGGTCTCTTGGGAATACTTTTCTAACTAGGGTTGCT
CTCACCTGAGACATTCTCCACCCGCGGAATCTCAGGGTCCCAGGCTGTGGGCCATC
ACGACCTCAAACTGGCTCCTAATCTCCAGCTTTCCTGTCATTGAAAGCTTCGGAAGT
TTACTGGCTCTGCTCCCGCCTGTTTTCTTTCTGACTCTATCTGGCAGCCCGATGCCAC
CCAGTACAGGAAGTGACACCAGTACTCTGTAAAGCATCATCATCCTTGGAGAGACT
GAGCAC

### 2.7.2 Cell culture.

Mel-RM and HeLa cells were maintained in DMEM with 5% fetal calf serum (FCS). Mel-RM were obtained as previous described[200]. HeLa and HEK293T cells were obtained from ATCC. All cell lines were verified to be free of mycoplasma contamination every 3 months and were authenticated by short tandem repeat (STR) profiling in April 2018 by Australia Genome Research Facility (AGRF).

### 2.7.3 Transfection

For T7 Endonuclease I (T7E1) assay, HEK293T cells were transfected with Lipofectamine 3000 Reagent (Thermo Fisher) according to the manufacturer's protocol. For the genome editing of Mel-RM and HeLa cells, $1\times10^6$ cells to were subjected electroporation with Nucleofector II (Lonza) and Cell Line Nucleofector® Kit R (25 RCT) (Lonza, VCA-1001).We monitor Mel-RM cells by program G-016 for and HeLa cells by program A-028 with 2.5 µg lentiCRISPR v2 plasmid and 2.5 µg linearized donor vectors for 4 pulses of each cell lines. In order to increase the homologues recombination, 2 µg/ml puromycin and 10 µM SCR7 were incubated with cell for 24 hours after the cells recovered from electroporation.

### 2.7.4 Flow cytometry

For the single cell sorting to get a specific genetic background coloy, six to eight days after electroporation, the cells were trypsinized and suspended in sorting beffer (5 mM EDTA, 25 mM Hepes, 1% FCS in PBS). GFP or mCherry positive cells were gated and each single cell was sorted into 96-well plates.

For detecting the shift of the fused protein, the selected positive cells were seed in 24-well plate. Twenty-four hours later, cells were treated with or without serum starvation or MEK inhibitor (GSK1120212) for indicated periods. Then the cells were harvested and suspended in PBS.

For quiescent and cycling cells were sorted for RNA sequencing or proteomics, the cells were treated by indicated treatment and periods and then were suspended in sorting buffer (5 mM EDTA, 25 mM Hepes,1% FCS in PBS). $GFP^{+}$/$mCherry^{-}$ cells were sorted as quiescent cells while the others were cycling cells.

### 2.7.5 Genotyping and sequence analysis

Marker insertion into CDKN1B and MKI67 locus was confirmed by PCR with 2×TransTaq®-T PCR SuperMix (TransGen Biotech). Sequence analysis was done by AGRF. All primers were listed in Table 2.3

**Table 2.3. Primers for T7E1 assay and genotyping**

| Primer | Sequence (5'-3') | Amplicon (bp) |
|---|---|---|
| p27 T7E1-F | GCTTGCTTTTCGGCGTATTCTGATT | 721 |
| p27 T7E1-R | AGCCTTCCCCATTGCTACTTTTTTG | |
| p27 up-F | TCTTTTGGCTCCGAGGGCAGTC | 1878 |
| p27 up-R | CGCTTCTCGTTGGGGTCTTTGCT | |
| p27 full-F | TTTTTTTGAGAGTGCGAGAGAGGC | 2804/3521 |
| p27 full-R | GGTCAAAGGCAAGTGGGAAATAAAT | |
| Ki67 T7E1-F | TGTCTACAGGGGTTCCTTGGTTT | 830 |
| Ki67 T7E1-R | GGACATAGGCAAACAAACGACG | |
| Ki67 up-F | TTGGAAAGGCAGAAGGAACAGAAGT | 1850 |
| Ki67 up-R | CAGGATGTCCCAGGCGAAGG | |
| Ki67 full-F | GTGAGAGTTCCTGGTCAGTGGGG | 2958/3666 |
| Ki67 full-R | TGGATGACGCTGTGAGAACCCTA | |

### 2.7.6 Time lapse photos

Live cell images were taken in Biomedicain Imaging Facility (BMIF) in UNSWby Zeiss Celldiscoverer 7. Mel-RM.pK (Mel-RM cells with CDKN1B fused with the EGFP gene and MKI67 with the mCherry gene) and HeLa.pK (HeLa cells with CDKN1B fused with the EGFP gene and MKI67 with the mCherry gene) cells were cultured as above, plated onto glass-bottom plates (Cellvis, P06-1.5H-N), and imaged in no phenol red DMEM (Thermo Fisher Scientific, 21063) with 5% FCS on Zeiss Celldiscoverer 7 with a 20× 0.95-NA objective every 15 minutes at 37°C and 5% $CO_2$. Videos and photos were exported by ZEN.

## 2.8 Whole genome sequencing

Mel-RM.pK (RG28) cells were subject 50× whole genome sequencing to confirm the offtarget which are induced by sgRNAs. First, the genomic DNA of Mel-RM and Mel-RM.pK cells were extracted by Wizard® Genomic DNA Purification Kit (Promega, A1120). The quality of the genomic DNA were confirmed by NanoDrop, Qubit dsDNA HS Assay Kit and agarose Electroresis. Second, the samples passed QC (quality control) were subjected to fragmentation

(Covaris S220) and library construction (NEBNext® Ultra™ II DNA Library Prep Kit for Illumina®). The libraries that passed library QC were subjected to HiSeq Sequencing.

The on-target and off-target sites were analysed by Genewiz (Suzhou,China).

## 2.9 Whole transcriptome sequencing

The cycling and quiescent cells were subjected to RNA isolation. Total RNA was isolated using the ISOLATE II RNA Mini Kit (Bioline, BIO-52073) according to the manufacturer's instructions. Briefly, 350 µl of lysis buffer RLY and 3.5 µl β-ME were added to cell pellet and vortex vigorously. After filtered by ISOLATE II Filter, the homogenised lysates were mixed well with an equal volume of 70% ethanol and then the mixture was transferred into ISOLATE II RNA Mini columns. The columns were centrifuged at 11,000 × g for 30 seconds, washed once with Membrane Desalting Buffer (MEM) before incubating with DNAse I for half an hour. The columns were washed by RW1 and RW2 provided by the kit sequentially. RNAs were finally eluted with 50 µl of RNase-free water. RNA samples were quantitated with NanoDrop 2000 spectrophotometer (Thermo Scientific, Scoresby, VIC, Australia) and stored at -80°C before use.

The RNAs were dried to powder by Rotational Vacuum Concentrator (MARTIN CHRIST, RVC 2-25) in RNA stable tubes (Biomatrica, San Diego, CA) for delivery. Technical duplicates were set for each sample (cycling and quiescent). The workflow of sequencing is shown in Figure 2.1

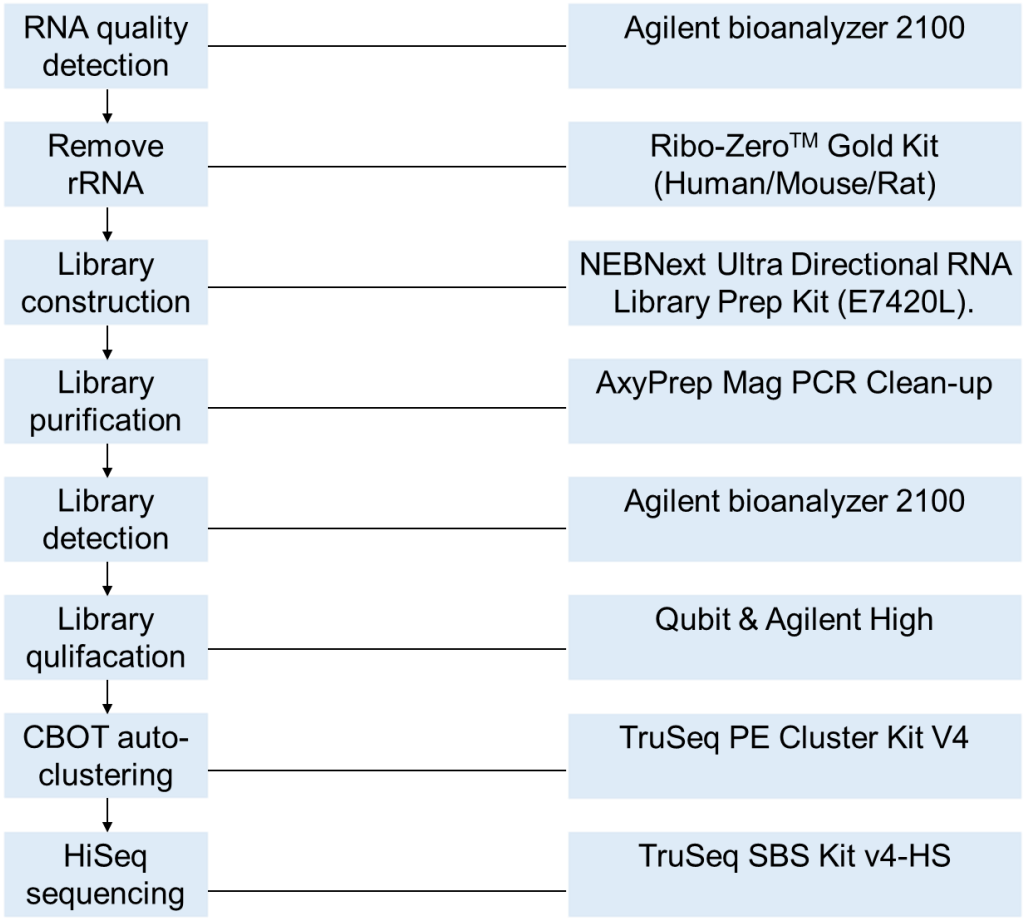


Figure 2.1. Transcriptome sequencing experimental workflow

A transcriptome includes all the RNAs a cell transcribes in a certain functional state: encoding mRNAs and non-coding RNAs. Researches on non-coding RNAs mainly focuses on small RNA, IncRNA and cirRNA, which has regulation effects in gene transcription. Leveraging the next generation transcriptome sequencing technology, mRNA, IncRNA, circRNA and small RNA in the same sample can be analyzed simultaneously to investigate the transcriptional regulation behind biological activities. The study on the interaction between coding and noncoding RNAs is very powerful in scientific research as well as result validation. The raw data was cleaned and analysed according to the workflow in Figure 2.2.

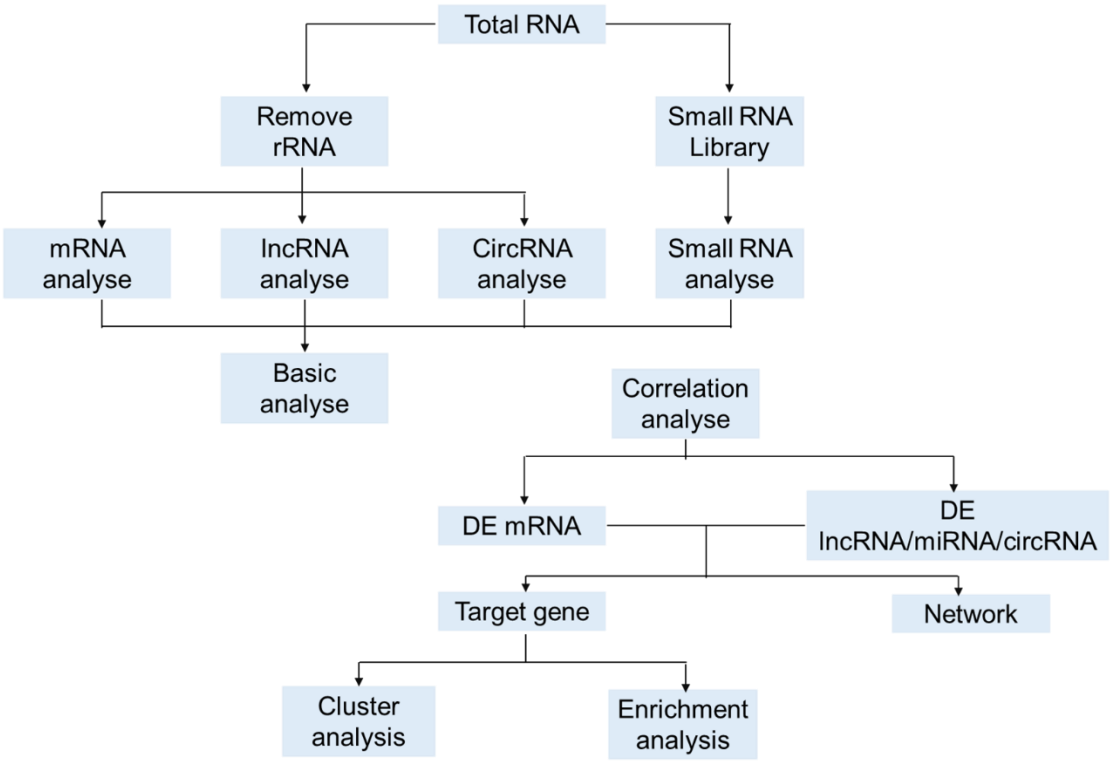


Figure 2.2. Whole transcriptome analysis workflow

## 2.10 Proteomics

Isobaric tags for relative and absolute quantification (iTRAQ) is utilized here to quantity the differential expressed proteins. 4-plex iTRAQ was performed by Proteomics International (Western Australia). Technical duplicates were set for cycling and quiescent cancer cells (Table 2.4).

**Table 2.4. Repeat experimental design for 4-plex**

| Label | 114 | 115 | 116 | 117 |
|---|---|---|---|---|
| Sample name | Cycling-1 | Cycling-2 | Quiescent-1 | Quiescent-2 |

### 2.10.1 Sample preparation

In detail, the sorted cell pellets were lysis by Lysis Buffer 2 ( 0.2% IGEPAL, 0.2% Triton X, 0.2% w/v CHAPS, 75 mM NaCl, 1 mM EDTA, protease inhibitors in PBS) on ice for 1 hour. The debris were centrifuged at 13,000g for 10 min at 4°C. After that, the supernatants are transferred to new tubes and the protein concentrations were measured by Bio-Rad Protein Assay Dye Reagent Concentrate (Bio-Rad, 500-0006) and detected with a spectrophotometer (Thermo Fisher Scientific, GENESYS™ 10S UV-Vis Spectrophotometer). For each technique duplicates, 135 µg protein was precipitated by acetone. The protocol of acetone precipitation of proteins is shown as following. First, mixing the lysate with four times the sample volume of cold acetone and sit it at -20°C overnight. Second, centrifuge the mixture for 10 minutes at 13000g in 4 °C. Before send out in dry ice for further experiments, 10 µl acetone should be remained to keep the pellet moist.

### 2.10.2 Proteome Mapping by 1D LC-MS

The protein samples were acetone precipitated, reduced, alkylated and trypsin digested according to the iTRAQ protocol (Sciex). Pooled sample (2 µg, which was 10% of each sample) was analysed by electrospray ionisation mass spectrometry using the Shimadzu Prominence nano HPLC system (Shimadzu) coupled to a 5600 TripleTOF mass spectrometer (Sciex). Peptides were loaded onto an Agilent Zorbax 300SB-C18, 3.5 µm (Agilent Technologies) and separated with a linear gradient of water/acetonitrile/0.1% formic acid (v/v).

### 2.10.3 Differential Expression by iTRAQ analysis

The protein samples were acetone precipitated, reduced, alkylated and trypsin digested according to the iTRAQ protocol (Sciex). The samples were then labelled using the iTRAQ reagents as Table 2.5.

**Table 2.5. The labelling of the samples.**

| Sample name | Amount of protein supplied (µg) | Sample reference | Amount of protein labelled (µg) | iTRAQ reagent |
|---|---|---|---|---|
| Cycling-1 | -135 | A | 36.5 | 114 |
| Cycling-2 | -135 | B | 36.5 | 115 |
| Quiescent-1 | -135 | C | 36.5 | 116 |
| Quiescent-2 | -135 | D | 36.5 | 117 |

All labelled samples were combined to make a pooled sample. Peptides were desalted on a Strata-X 33 µm polymeric reversed phase column (Phenomenex) and dissolved in a buffer containing 2% acetonitrile 0.1% formic acid before separation by high pH on an Agilent 1100 HPLC system using a Zorbax C18 column (2.1 × 150 mm). Peptides were eluted with a linear gradient of 20mM ammonium formate, 2% ACN to 20mM ammonium formate, 90% ACN at 0.2ml/min. The 95 fractions were concatenated into 12 fractions and dried down. Each fraction was analysed by electrospray ionisation mass spectrometry using the Shimadzu Prominence nano HPLC system (Shimadzu) coupled to a 5600 TripleTOF mass spectrometer (Sciex). Peptides were loaded onto an Agilent Zorbax 300SB-C18, 3.5 µm (Agilent Technologies) and separated with a linear gradient of water/acetonitrile/0.1% formic acid (v/v).

### 2.10.4 Data analysis

Spectral data were analysed using ProteinPilot™ 5.0 Software (Sciex) against: Database: SwissProt; Taxonomy: Homo sapiens (Human); Version: April 2017; 20,199 sequences.

## 2.11 Gene Set Enrichment Analysis (GSEA) and (Ingenuity Pathway Analysis) IPA analysis

GSEA software was downloaded from http://software.broadinstitute.org/gsea/index.jsp. The whole mRNA expression list were ranked and uploaded as the instruction. IPA was purchased from QIAGEN. The usage of the software followed the instruction.

# Chapter three A p53-responsive microRNA network promotes cellular quiescence

## Acknowledgement of Collaboration

I hereby certify that other researchers have collaborated and contributed to the work embodied in this Chapter.

This original article was accepted into *Cancer Research* for publication on 2nd October 2018. I, Ting La, was the first authors of this manuscript, with the exception of the following: Primary melanoma cells established from patients' tumour biopsies were cultured by Ms. Margaret Farrelly. Cell sorting were carried out by Nicole Cole.

The work embodied in this Chapter attests and clearly identifies the nature of intellectual input to be included as part of the overall thesis. Therefore, this work will be discussed further in Chapter Three.

_____

Ting La

## 3.1 Abstract

Cancer cells in quiescence (G0 phase) are resistant to death and re-entry of quiescent cancer cells into the cell cycle plays an important role in cancer recurrence. Here we show that two p53-responsive microRNAs (miRNAs) utilize distinct but complementary mechanisms to promote cancer cell quiescence through facilitating p27 stabilization. Purified quiescent B16 mouse melanoma cells expressed higher levels of miRNA-27b-3p and miRNA-455-3p relative to their proliferating counterparts. These miRNAs were subsequently found to be similarly increased in diverse types of human cancer cell lines upon induction of quiescence. Inhibition of miRNA-27b-3p or miRNA-455-3p reduced, whereas its overexpression increased, the proportion of quiescent cells, indicating that these miRNAs promote cancer cell quiescence. In accordance, cancer xenografts bearing miRNA-27b-3p or miRNA-455-3p mimics were retarded in growth. Mechanistic investigations showed that miRNA-27b-3p targeted cyclin-dependent kinase regulatory subunit 1 leading to reduction in p27 polyubiquitination mediated by Skp2, whereas miRNA-455-3p targeted CDK2 associated cullin domain 1 that enhanced CDK2-mediated phosphorylation of p27 necessary for its polyubiquitination. Of note, the gene encoding miRNA-27b-3p was embedded in the intron of the *Chromosome 9 open reading frame 3* gene that was transcriptionally activated by p53. Similarly, the host gene of miRNA-455-3p *collagen Type XXVII alpha-1 chain* appeared also a p53 transcriptional target. Collectively, our results identify miRNA-27b-3p and miRNA-455-3p as important regulator of cancer cell quiescence in response to p53 and suggest that manipulating miRNA-27b-3p and miRNA-455-3p may constitute novel therapeutic avenues for improving outcomes of cancer treatment.

## 3.2 Introduction

Despite the advance in cancer treatment using molecularly targeted therapies and resurgence of immunotherapy, relapse following initial disease remission remains an unsolved problem[201]. Recurrent and metastatic cancer lesions often undergo a period of dormancy[29], which can be conceptually classified into two models[5]. The first is tumour mass dormancy whereby the rate of tumour cell proliferation is balanced by the rate of programmed cell death, mostly apoptosis, caused by the lack of vasculature (angiogenic dormancy) and/or anti-cancer immune responses (immunologic dormancy)[5] . The second is cellular dormancy resulting from cell-intrinsic or extrinsic mechanisms leading to a state of quiescence where cells exit the cell cycle and are reversibly arrested in G0 phase. These models are not mutually exclusive. In particular, it is cellular dormancy that renders cancer cells fundamentally resistant to cell death and refractory to therapeutics [5]. Consequently, curative cancer treatment requires therapies that either sustain the dormant state or effectively kill quiescent cancer cells.

Molecular signatures of cellular quiescence in some types of cells, such as hematopoietic stem cells and fibroblasts have been documented[202, 203, 204, 205]. Although changes in gene expression/activation vary depending on cell type and context, quiescent cells generally display reduction in the expression of pro-proliferation genes and upregulation of genes encoding CDK inhibitors and those associated with remodeling the extracellular environment[206, 207]. A variety of signal pathways, such as the MEK/ERK and p38 pathways contribute to regulation of cellular quiescence in cancer[208, 209, 210]. These pathways commonly converge on modulation of the Rb-E2F bistable switch that is a master regulator of cell cycle progression[211]. Noticeably, the tumor suppressor p53 also plays a role in regulating quiescence, but the mechanisms involved remain to be fully understood [212].

Genetic ablation of the microRNA processing enzyme Dicer results in quiescence exit in some cell types[213, 214], suggesting that miRNAs are required to regulate cellular quiescence. Indeed, a number of miRNAs including miR-126 and miR-489 are involved in maintaining cellular quiescence[213, 215], whereas miR-195 and miR-497 act to induce quiescence in skeletal muscle stem cells [216]. Moreover, miR-125 and miR-29 regulate cellular quiescence in fibroblasts[217]. Of note, some miRNAs impinge on Rb-E2F activity though directly sequestering CDK inhibitors. For example, miR-221 and miR-222 promotes the transition from quiescence to proliferation through targeting the CDK inhibitors p27 and p57[95].

Here we demonstrate that the p53-responsive miRNAs, miRNA-27b-3p and miRNA-455-3p, promote cellular quiescence through facilitating stabilization of p27 utilizing distinct but complementary pathways. First, miRNA-27b-3p targets Cks1, a cofactor of Skp2 that is important for p27 polyubiquitination and subsequent degradation[108]. Secondly, miRNA-455-3p targets CDK2 associated cullin domain 1 (CAC1) that promotes the kinase activity of CDK2 leading to phosphorylation of p27 for Skp2-mediated polyubiquitination[218, 219]. Thus, the manipulation of miRNA-27b-3p and miRNA-455-3p to maintain or disrupt cancer cell quiescence may provide potential avenues to improve the therapeutic efficacy of systemic cancer treatments.

## 3.3 Materials and methods

### 3.3.1 Cell culture

The human melanoma cell lines Mel-RM, Sk-Mel-28, A375 and mouse melanoma cell line B16 were cultured in DMEM containing 5% FCS[200]. HEK293T, A549, MCF7, HeLa, WiDr, HT29, HCT116, U2OS cells were obtained from ATCC and cultured according to ATCC instructions. All cell lines were verified to be free of mycoplasma contamination every 3 months and were authenticated by short tandem repeat (STR) profiling in April 2018 by Australian Genome Research Facility (AGRF). The passage numbers of all the cell lines used in this paper are less than 30 after thawing.

### 3.3.2 Antibodies and reagents

Information on antibodies and reagents used in this study is provided in Tables 3.1 & 3.2.

**Table 3.1. List of antibodies**

| Antibody | Catalogue No. | Company |
|---|---|---|
| Phospho-Rb (Ser807/811) (D20B12) XP® Rabbit mAb | #8516 | Cell Signalling Technology (Beverly, MA) |
| Phospho-Rb (Ser807/811) antibody | #9308 | Cell Signalling Technology (Beverly, MA) |
| cyclin D1 antibody (H-295) | sc-753 | Santa Cruz Biotechnology (Santa Cruz, CA) |
| Cdk2 (D-12) | sc-6248 | Santa Cruz Biotechnology (Santa Cruz, CA) |
| p21 Waf1/Cip1 (12D1) Rabbit mAb | #2947 | Cell Signalling Technology (Beverly, MA) |
| p27 antibody (F-8) | sc-1641 | Santa Cruz Biotechnology (Santa Cruz, CA) |
| GAPDH antibody (6C5) | sc-32233 | Santa Cruz Biotechnology (Santa Cruz, CA) |
| Ki-67 (D3B5) Rabbit mAb | #9129 | Cell Signalling Technology (Beverly, MA) |
| Goat anti-Rabbit IgG(H+L) Secondary antibody, Alexa Fluor 488 | A-11008 | Thermo Fisher Scientific (Waltham, MA) |
| APC anti-mouse Ki-67 antibody | 652406 | BioLegend (San Diego, CA) |
| APC Rat IgG2a, K Isotype Ctrl antibody | 400512 | BioLegend (San Diego, CA) |
| Skp2 (D3G5) XP® Rabbit mAb | #2652 | Cell Signalling Technology (Beverly, MA) |
| p27 KIP 1 (phospho T187) antibody | ab75908 | Abcam (Cambridge, United Kingdom) |
| p27 KIP 1 (phospho S10) antibody | ab62364 | Abcam (Cambridge, United Kingdom) |
| p27 KIP 1 (phospho T198) antibody | ab64949 | Abcam (Cambridge, United Kingdom) |
| CKS1 antibody | ab130529 | Abcam (Cambridge, United Kingdom) |
| C10orf46 antibody [EPR16094] | ab190799 | Abcam (Cambridge, United Kingdom) |
| p53 antibody (DO-1) | sc-126 | Santa Cruz Biotechnology (Santa Cruz, CA) |
| Monoclonal ANTI-FLAG® M2 antibody produced in mouse | F3165 | Sigma-Aldrich (St. Louis, MO) |
| Phospho-CDK2 (Thr160) antibody | #2561 | Cell Signalling Technology (Beverly, MA) |

**Table 3.2. List of Reagents**

| Reagent | Catalogue No. | Company |
|---|---|---|
| Cycloheximide | 100183 | MP Biomedicals |
| pifithrin-α | P4359 | Sigma-Aldrich |
| MG132 | M7449-1ML | Sigma-Aldrich |
| Propidium iodide | P4170-1G | Sigma-Aldrich |
| bisBenzimide H 33258 | B2883-100mg | Sigma-Aldrich |
| Pyronin Y | P9172-1G | Sigma-Aldrich |

### 3.3.3 Small interference RNA (siRNA) and short hairpin RNA (shRNA)

siRNAs were obtained from GenePharma (Shanghai, China) and transfected using Lipofectamine 2000 reagent (Invitrogen). The human control and CDKN1A MISSION® shRNA lentiviral transduction particles were purchased from Sigma-Aldrich (Castle Hill, NSW, Australia). Lentiviral particle transduction was carried out as per the manufacturer's protocols. The siRNA and shRNA sequences were listed in Table 3.3.

**Table 3.3. siRNA and shRNA sequences**

| si/shRNA | 5'-3' |
|---|---|
| Ctrl siRNA | UUCUCCGAACGUGUCACGUTT |
| CKS1 siRNA | GGAGUUUGAGUAUCGACAUTT |
| CAC1 siRNA | GGAUGGUGCCAUAGAUCAATT |
| p27 siRNA | GCGCAAGUGGAAUUUCGAUUUTT |
| C9orf3 siRNA-1 | GCUUGAGAGUUCCGGAAUATT |
| C9orf3 siRNA-2 | GGUCUUGCUUCUGGAGCAUTT |
| COL27A1 siRNA-1 | CCAAGCUGUCAGCCAGUAATT |
| COL27A1 siRNA-2 | GGGACUGGCUGGUUAUGAUTT |
| p53 siRNA-1 | CGGCGCACAGAGGAAGAGAAUCUCTT |
| p53 siRNA-1 | CUACUUCCUGAAAACAACGTT |
| Scramble | CAGUACUUUUGUGUAGUACAA |
| Ctrl mimics | UUCUCCGAACGUGUCACGUTT |
| mmu-miR-455-3p mimics | GCAGUCCACGGGCAUAUACAC |
| mmu-miR-455-3p inhibitor | GUGUAUAUGCCCGUGGACUGC |
| mmu-miR-23b-3p mimics | AUCACAUUGCCAGGGAUUACC |
| mmu-miR-23b-3p inhibitor | GGUAAUCCCUGGCAAUGUGAU |
| has-miR-27b-3p mimics | UUCACAGUGGCUAAGUUCUGC |
| has-miR-27b-3p inhibitor | GCAGAACUUAGCCACUGUGAA |
| has-miR-455-3p mimics | GCAGUCCAUGGGCAUAUACAC |
| has-miR-455-3p inhibitor | GUGUAUAUGCCCAUGGACUGC |
| mmu-miR-210-3p mimics | CUGUGCGUGUGACAGCGGCUGA |
| mmu-miR-210-3p inhibitor | UCAGCCGCUGUCACACGCACAG |
| p21 shRNA | CCGGGACAGCAGAGGAAGACCATGTCTCGAGACATGG TCTTCCTCTGCTGTCTTTTTG |
| Ctrl shRNA | CCGGGCGCGATAGCGCTAATAATTTCTCGAGAAATTAT TAGCGCTATCGCGCTTTTT |

### 3.3.4 Plasmids

pMXs-IP-mVenus-p27K$^-$, pGag-pol-IRES-bs$^r$ and pEnv-IRES-puro$^r$ were generous gifts from professor Toshio Kitamura (University of Tokyo, Tokyo, Japan). mCherry-hCdt1(30/120)/ pCSII-EF-MCS was generous gift from Dr. Hiroyuki Miyoshi and Dr.Atsushi Miyawaki (RIKEN Brain Science Institute, Japan). Other plasmids used are detailed in Table 3.4 & 3.5.

**Table 3.4. Lists of plasmids obtained commercially**

| Plasmid | Company | Catalogue No. |
|---|---|---|
| pWZL Neo Myr Flag CDKN1B | Addgene | 20420 |
| pWZL Neo Myr Flag CKS1B | Addgene | 20461 |
| pWZL-Neo-Myr-Flag-DEST | Addgene | 15300 |
| CMV10-3xFlag Skp2 WT | Addgene | 81115 |
| pRK5-HA-Ubiquitin-WT | Addgene | 17608 |
| pRL-SV40P | Addgene | 27163 |
| p3xflag-Myc-CMV-24 | Sigma-Aldrich | E9283 |
| pGL3-C9orf3-(-1500/+100) | Tolo Biotechnology | |
| pGL3-C9orf3-(-1000/+100) | Tolo Biotechnology | |
| pGL3-C9orf3-(-500/+100) | Tolo Biotechnology | |
| pGL3-C9orf3-(-250/+100) | Tolo Biotechnology | |
| pGL3-C9orf3-(-100/+100) | Tolo Biotechnology | |
| pGL3-COL27A1-(-1500/+100) | Tolo Biotechnology | |
| pGL3-COL27A1-(-1000/+100) | Tolo Biotechnology | |
| pGL3-COL27A1-(-500/+100) | Tolo Biotechnology | |
| pGL3-COL27A1-(-250/+100) | Tolo Biotechnology | |
| psiCHECK-2 | Promega | C8021 |
| pGL3-basic | Promega | E1751 |

**Table 3.5. Lists of plasmids constructed in house[a]**

| Plasmid | Bone vector | Material |
|---|---|---|
| psiCHECK-2/CKS1-3'UTR | psiCHECK-2 | NEBuilder® HiFi DNA Assembly Cloning Kit (E5520) |
| psiCHECK-2/CKS1-3'UTR-mut | psiCHECK-2 | NEBuilder® HiFi DNA Assembly Cloning Kit (E5520) |
| psiCHECK-2/CAC1-3'UTR | psiCHECK-2 | NEBuilder® HiFi DNA Assembly Cloning Kit (E5520) |
| psiCHECK-2/CAC1-3'UTR-mut | psiCHECK-2 | NEBuilder® HiFi DNA Assembly Cloning Kit (E5520) |
| pGL3-C9orf3 promoter (-1242/-203) | pGL3-basic | NEBuilder® HiFi DNA Assembly Cloning Kit (E5520) |
| pGL3-C9orf3 promoter (-1242/+33) | pGL3-basic | NEBuilder® HiFi DNA Assembly Cloning Kit (E5520) |
| pGL3-COL27A1 promoter (-762/+158) | pGL3-basic | NEBuilder® HiFi DNA Assembly Cloning Kit (E5520) |
| pGL3-COL27A1 promoter (-981/+95) | pGL3-basic | NEBuilder® HiFi DNA Assembly Cloning Kit (E5520) |
| CAC1 cDNA | P3xflag-Myc-CMV-24 | NEBuilder® HiFi DNA Assembly Cloning Kit (E5520) |
| pWZL Neo Myr Flag CDKN1B T187G | pWZL Neo Myr Flag CDKN1B | DpnI (R0176S) |

a: 1. All insertions or plasmids that amplified by PCR used Q5® High-Fidelity DNA Polymerase (M049L).

2. All plasmids were transformed and extracted from NEB® Stable Competent E. coli (High Efficiency) (C3040H).

### 3.3.5 miRNA profiling and Real-time PCR

Total RNA was isolated using the ISOLATE II RNA Mini Kit (Bioline) according to manufacturer's protocols. RNA sequencing (10M 50SE) was performed to characterize miRNA expression profiles (BGI, Hong Kong). The results have been deposited to the Gene Expression Omnibus (GEO) (GEO accession: GSE118547).

Reverse transcription was undertaken using the qScript cDNA Supermix (Quantabio, 95048) and TaqMan™ MicroRNA Reverse Transcription Kit (ThermoFish Scientific, 4366596) for mRNAs and miRNAs, respectively. qPCR was performed with 20 µl reaction volume using SensiFAST™ SYBR Hi-ROX Kit (Bioline). The 2-ΔΔCT method was applied to calculate the relative expression levels of genes. Primers used are detailed in Supplementary Table 7.

### 3.3.6 Western blotting and Immunoprecipitation (IP)

Western blotting and IP were carried out as described in previous publication [200]. The relative intensity of bands was quantified using Image J and normalized against GAPDH.

### 3.3.7 Serum starvation and contact inhibition

Cell confluence was monitored until the control group reached 70-80% confluence. For serum starvation, cell culture medium was replaced with serum-free medium. For serum replenishment, serum-free medium was replaced by medium containing 5% FCS. For contact inhibition, culture medium was refreshed every 24 hours after cells reached 100% confluence.

### 3.3.8 G0 and G1 cell isolation

pMXs-IP-mVenus-p27K$^-$,pGag-pol-IRES-bs$^r$ and pEnv-IRES-puro$^r$ were used to package retrovirus to deliver mVenus-p27K$^-$ , whereas pMDLg.pRRE, pRSU.pREV, pMD2.g and mCherry-hCdt1(30-120) pCSII-EF-MCS were used to package lentivirus to deliver mCherry-hCdt1(30-120) into cells. Cells were transduced with viral particles carrying mCherry-hCdt1(30-120) and the mCherry-positive cells isolated by fluorescence-activated cell sorter (FACS) were further transduced with viral particles carrying mVenus-p27K$^-$. Cells positive for both mVenus-p27K$^-$ and mCherry-hCdt1(30-120) were selected by the addition of puromycin (3 µg/ml). G0

cells (mVenus-p27K$^{-high}$/mCherry-hCDT1(30/120)$^{+}$) and G1 cells (mVenus-p27K$^{-low}$/mCherry-hCDT1(30/120)$^{+}$ ) were isolated using FACS sorting (FACSAria III, BD).

### 3.3.9 Cell cycle analysis

For Ki67/DNA double staining, cells fixed with cold 70% ethanol at -20 °C for 2 hours were washed with staining buffer (BioLegend, #420201) for three times before stained with APC-conjugated anti-Ki-67 antibody (BioLegend, #652406). After washing, cells were suspended in PI staining buffer and analysed using a flow cytometer (FACSCanto II, BD). Hoechst 33342/Pyronin Y double staining were carried according to protocols described previously [220]. In brief, cells were stained with 2 μg/ml Hoechst 33258 for 45 minutes and 4 μg/ml Pyronin Y for additional 15 minutes. DNA and RNA contents were determined using a flow cytometer (LSRFORTESSA X-20, BD).

### 3.3.10 Clonogenic assay

Cells were seeded in six-well plates at 1000 cells/well. About two weeks later, cells were stained with crystal violet (0.5%). ColonyArea was quantitated using ImageJ-plugin. ColonyArea in cells introduced with Ctrl mimics was arbitrarily designated as 1.

### 3.3.11 Luciferase reporter assay

Reporter activities were measured as per the manufacturer's protocol (Dual-Glo® Luciferase Assay System, Promega). Briefly, psiCHECK-2 vector-based plasmids were co-transfected with miRNA mimics or anti-miRNAs into cells. Alternatively pGL3-basic vector-based plasmids were co-transfected with pRL-SV40P. Firefly and Renilla luciferase activities were recorded using a microplate reader (BioTek, VT).

### 3.3.12 Chromatin Immunoprecipitation (ChIP) assay

Cells were harvested and subjected to ChIP assays according to the manufacturer's protocol (MAGnify™ Chromatin Immunoprecipitation System, ThermoFisher Scientific, 49-2024). PCR products were separated by gel electrophoresis on 2% agarose gel.

### 3.3.13 Senescence

Senescence was detected by staining senescence-associated (SA) β-galactosidase (β-gal) using a Senescence Detection Kit (Sigma-Aldrich, CS0030-1KT). Briefly, cells were washed twice and then fixed at room temperature. After washing, cells were stained with a staining mixture. Slides were then examined using a light microscope and SA-β-gal positive cells were calculated across 5 random high-power fields.

### 3.3.14 Apoptosis

Apoptotic cells were quantitated using the Annexin V/PI Apoptosis Detection Kit (BD Biosciences). In brief, cells in binding buffer were incubated with Annexin V/PI for 15 min before analysis using a flow cytometer (FACSCanto II, BD Biosciences).

### 3.3.15 Xenograft mouse model

The animal experiments were conducted as our previously described with approval from the Animal Research Ethics Committee of Shanxi Cancer Hospital of China [221]. Briefly, male BALB/c nude mice (4-week old; Model Animal Research Centre of Nanjing University, China) were subcutaneously injected with Mel-RM cells with or without stable overexpression of miR-

27b-3p or miR-455-3p ($1 \times 10^7$). Each groups contained 6 mice. Tumour growth was monitored using a calliper.

### 3.3.16 Statistical analysis

Statistical analysis was carried out using GraphPad Prism 7. Statistical significance was analysed by Student's *t*-test and expressed as a P value. $P < 0.05$ were considered to be statistical significance.

## 3.4 Results

### 3.4.1 MiR-27b-3p and miR-455-3p promote cellular quiescence

To isolate cancer cells in the quiescent (G0) state, we employed a model system encompassing an mVenus-tagged p27 deletion mutant lacking the CDK-binding domain (mVenus-p27K$^-$) together with a mCherry-tagged truncated mutant of human chromatin licensing and DNA replication factor 1 (hCDT1) (mCherry-hCDT1(30/120)) [82]. While hCDT1 is exclusively expressed in cells in G0 and G1 phases, p27 is markedly more abundant in G0 compared with G1 cells [222, 223]. After co-introduction of these constructs into B16 mouse melanoma cells, distinctive populations of mVenus-p27K$^{-low}$ and mVenus-p27K$^{-high}$ cells positive for mCherry-hCDT1(30/120) were observed (Fig. 3.1A). The population of mVenus-p27K$^{-high}$ mCherry-hCDT1(30/120)$^+$ cells was enriched by serum starvation or contact inhibition (Fig. 3.1A and Fig. 3.1B), two conditions widely used for induction of cellular quiescence [224], suggesting that this population represented cells in the quiescent state. In support, mVenus-p27K$^{-high}$ mCherry-hCDT1(30/120)$^+$ cells displayed typical G0 features including substantially higher levels of endogenous p27 and p21, but with low Ki67 expression and reduced levels of phosphorylated retinoblastoma protein (pRb), cyclin D1 and cyclin-dependent kinase 2 (CDK2) compared with mVenus-p27K$^{-low}$ mCherry-hCDT1(30/120)$^+$ cells (Fig. 3.1C and 3.1D). Moreover, dual nucleic acid staining (DNA stained with Hoechst-33342, and RNA with Pyronin Y) identified these cells to be diploid with low RNA content (Fig. 3.1E), characteristic of cells in the quiescent state [225].

We then undertook a comparative analysis of miRNA expression profiles between G0 (mVenus-p27K$^{-high}$ mCherry-hCDT1(30/120)$^+$) and G1 (mVenus-p27K$^{-low}$ mCherry-hCDT1(30/120)$^+$) cells isolated using FACS (Fig. 3.1A). Comparing RNA sequencing (RNA-seq) data we derived a list of differentially expressed miRNAs (Table 3.6). Focussing on the most prominently

upregulated miRNAs in G0 cells, we confirmed that four of the five candidate miRNAs were significantly increased in G0 compared to G1 cells using qPCR (Fig. 3.1F). As anticipated, the expression of these miRNAs was also increased in the total unfractionated population of B16 cells, albeit to a lesser extent, under serum starvation or contact inhibition conditions (Supplementary Fig. 3.1A). Since cancer cells *in vivo* frequently encounter poor nutrition microenvironments due to abnormal vasculature [226], we focused on serum starvation as a trigger of cellular quiescence hereafter.

**Table 3.6. A summary of miRNAs that are expressed at higher levels in G0 cells than G1 cells**

| miR | G1 | G0 | p-value | fold-change(log2 |
|---|---|---|---|---|
| mmu-miR-455-3p | 15 | 94 | 5.90E-05 | 2.647698 |
| mmu-miR-27b-3p | 1732 | 8560 | 0 | 2.305172 |
| mmu-miR-322-5p | 36 | 163 | 4.35E-10 | 2.178803 |
| mmu-miR-210-3p | 164 | 718 | 5.51E-46 | 2.130288 |
| mmu-miR-23b-3p | 142 | 579 | 2.40E-30 | 2.027672 |
| mmu-miR-190b-5p | 5 | 20 | 0.003291 | 2 |
| mmu-miR-9769-3p | 5 | 20 | 0.003291 | 2 |
| mmu-miR-8112 | 9 | 35 | 0.000104 | 1.959358 |
| mmu-miR-1249-3p | 25 | 93 | 4.32E-10 | 1.895303 |
| mmu-miR-450b-5p | 35 | 122 | 2.72E-14 | 1.801454 |
| mmu-miR-1949 | 5 | 17 | 0.013344 | 1.765535 |
| mmu-let-7f-1-3p | 4 | 13 | 0.036886 | 1.70044 |
| mmu-miR-335-3p | 318 | 992 | 8.40E-113 | 1.641313 |
| mmu-miR-185-3p | 9 | 28 | 5.81E-05 | 1.63743 |
| mmu-miR-132-3p | 31 | 94 | 4.56E-06 | 1.600393 |
| mmu-miR-676-3p | 5 | 15 | 0.032355 | 1.584963 |
| mmu-miR-874-3p | 193 | 556 | 4.23E-39 | 1.526484 |
| mmu-miR-351-3p | 179 | 502 | 3.79E-34 | 1.487728 |
| mmu-miR-26a-1-3p | 5 | 14 | 0.002937 | 1.485427 |
| mmu-miR-1960 | 5 | 14 | 0.049535 | 1.485427 |
| mmu-miR-322-3p | 375 | 1039 | 1.24E-67 | 1.470233 |
| mmu-miR-7083-5p | 7 | 19 | 0.002034 | 1.440573 |
| mmu-miR-698-5p | 7 | 19 | 0.024145 | 1.440573 |
| mmu-let-7i-3p | 15 | 40 | 3.45E-06 | 1.415037 |
| mmu-miR-143-5p | 35 | 93 | 5.55E-07 | 1.409876 |
| mmu-miR-674-5p | 67 | 175 | 1.14E-11 | 1.385122 |
| mmu-miR-132-5p | 57 | 146 | 1.09E-09 | 1.356935 |
| mmu-miR-503-5p | 1013 | 2561 | 1.70E-141 | 1.338073 |
| mmu-miR-450a-5p | 114 | 285 | 6.65E-17 | 1.321928 |
| mmu-miR-421-3p | 105 | 261 | 1.84E-15 | 1.31366 |
| mmu-miR-351-5p | 4663 | 11377 | 0 | 1.28679 |
| mmu-miR-6904-5p | 7 | 17 | 0.000529 | 1.280108 |
| mmu-miR-505-5p | 82 | 198 | 1.57E-11 | 1.271805 |
| mmu-miR-7015-3p | 8 | 19 | 0.04435 | 1.247928 |
| mmu-miR-326-3p | 40 | 94 | 6.32E-06 | 1.232661 |
| mmu-miR-450a-2-3p | 6 | 14 | 0.002937 | 1.222392 |
| mmu-miR-5122 | 11 | 25 | 0.026275 | 1.184425 |
| mmu-miR-10b-3p | 120 | 272 | 1.05E-13 | 1.180572 |
| mmu-miR-200c-3p | 33 | 74 | 0.000135 | 1.165059 |
| mmu-miR-3473b | 13 | 29 | 0.018585 | 1.157541 |
| mmu-miR-218-1-3p | 15 | 33 | 0.013177 | 1.137504 |
| mmu-miR-21a-3p | 28 | 61 | 0.00079 | 1.123382 |
| mmu-miR-574-3p | 222 | 477 | 1.35E-20 | 1.10343 |
| mmu-miR-30b-5p | 48 | 103 | 1.69E-05 | 1.101538 |
| mmu-miR-338-5p | 7 | 15 | 0.00554 | 1.099536 |
| mmu-miR-542-3p | 23 | 48 | 0.004649 | 1.061401 |
| mmu-miR-195a-5p | 188 | 392 | 3.72E-16 | 1.060121 |

To examine whether the candidate miRNAs are functionally involved in regulation of cellular quiescence, specific anti-miRNA oligonucleotides were used to inhibit their expression.

Strikingly, inhibition of miRNA-27b-3p or miRNA-455-3p but not inhibition of the other miRNAs diminished the induction of quiescence by serum starvation (Fig. 3.1G & H and supplementary Fig. 3.1B.D). In contrast, introduction of miRNA-27b-3p or miRNA-455-3p mimics increased the proportion of cells in G0 phase (Fig. 3.1I & J and supplementary Fig. 3.1E - G). Of note, neither inhibition of miRNA-27b-3p or miRNA-455-3p nor introduction of its mimics triggered cellular senescence or apoptosis (Supplementary Fig. 3.1H & I). Moreover, no additive or synergistic effects on quiescence were observed when both miRNAs were co-manipulated (Fig. 3.1H & J), suggesting that these miRNAs might be functionally interrelated.

Both miRNA-27b-3p and miRNA-455-3p are highly conserved among mammalian species (Supplementary Fig. 3.2), proposing that their biological functions may also be broadly preserved. Indeed, serum starvation similarly increased the levels of these miRNAs in a range of human cancer cell lines, Mel-RM (melanoma), U2OS (osteosarcoma), A549 (lung) and HCT116 (colon), which were reduced to the basal levels after serum replenishment (Fig. 3.2A). Moreover, introduction of anti-miRNA-27b-3p or anti-miRNA-455-3p blunted the induction of quiescence (Fig. 3.2B). This was associated with inhibition of upregulation of p27 and downregulation of Ki67, pRB, cyclin D1 and CDK2 (Fig. 3.2C & D). Conversely, introduction of miRNA-27b-3p or miRNA-455-3p mimics promoted serum starvation induced-quiescence along with upregulation of p27 and reduction in Ki67, pRB, cyclin D1 and CDK2 expression (Fig. 3.2E - G). Noticeably, manipulation of miRNA-27b-3p or anti-miRNA-455-3p did not affect the upregulation of p21 caused serum starvation (Fig. 3.2C & F), suggesting that p21 upregulation in quiescent cells was not associated with these miRNAs. In accordance with induction of cellular quiescence, both miRNA-27b-3p and miRNA-455-3p negatively regulated cell proliferation and clonogenicity (Fig. 3.2H & I). This was mirrored *in vivo* when Mel-RM cells bearing miRNA-27b-3p or miRNA-455-3p mimics were transplanted into nu/nu mice (Fig. 3.2J). Taken together, these results identified miRNA-27b-3p and miRNA-455-3p as facilitators of cancer cell quiescence.

### 3.4.2 MiR-27b-3p and miR-455-3p promote p27 stabilization through downregulating Skp2 and promoting its phosphorylation at Thr187, respectively

Given both miRNA-27b-3p and miRNA-455-3p appeared to regulate p27expression, which is essential for cellular quiescence [227] (Fig. 3.2C & F), we investigated how these miRNAs affect p27 expression. Anti-miRNA oligonucleotide-mediated inhibition of either miRNA accelerated the turnover rate of the p27 protein (Fig. 3.3A), whereas introduction of miRNA-27b-3p or miRNA-455-3p mimics prolonged its half-life time (Supplementary Fig.3.3A). These manipulations did not influence the expression of p27 mRNA (Supplementary Fig. 3.3B). Rather, inhibition of miR-27b-3p or miR-455-3p was associated with increased p27 polyubiquitination (Fig 3.3B & Supplementary Fig. 3.3C). This infers that the p27 upregulation caused by miRNA-27b-3p and miRNA-455-3p is associated with inhibition of p27 polyubiquitination that prevents its degradation [106].

Interestingly, inhibition of miRNA-27b-3p but not miRNA-455-3p prolonged the half-life time of the Skp2 protein, whereases introduction of miRNA-27b-3p mimics accelerated Skp2 protein turnover rate (Fig. 3.3C and Supplementary Fig. 3.3D ), suggesting that posttranslational regulation of p27 by miRNA-27b-3p may involve Skp2. Indeed, knockdown of Skp2 counteracted the accelerated p27 turnover associated with inhibition of miRNA-27b-3p (Fig. 3.3D), whereas overexpression of Skp2 abolished the prolonged p27 half-life time triggered by miRNA-27b-3p mimics (Supplementary Fig. 3.3E). These results consolidated the functional association between miRNA-27b-3p and Skp2-mediated regulation of p27. Intriguingly, Skp2 knockdown and overexpression also diminished the changes in the p27 turnover rate caused by anti-miRNA-455-3p and miRNA-455-3p mimics, respectively (Fig. 3.3E and Supplementary Fig. 3.3F), suggesting that miRNA-455-3p-mediated promotion of p27 stabilization also requires Skp2.

Since p27 phosphorylation at Thr187 is necessary for Skp2-mediated polyubiquitination [106], we examined whether miRNA-455-3p affects phosphorylation of p27. Introduction of anti-miRNA-

455-3p but not anti-miRNA-27b-3p enhanced Thr187 phosphorylation of p27, which was associated with a decrease in p27 expression (Fig. 3.3F). In contrast, introduction of miRNA-455-3p mimics reduced p27 phosphorylation at Thr187 (Fig. 3.3G). Of note, neither anti-miRNA-455-3p nor miRNA-455-3p mimics altered the p27 phosphorylation at Ser10 or Thr198 (Fig. 3.3F & G), suggesting that regulation of p27 phosphorylation at Thr187 by miRNA-455-3p is specific. In support, a point mutation of Thr187 disabled the ability of miRNA-455-3p to regulate p27 phosphorylation and its turnover rate (Fig. 3.3H and Supplementary Fig 3.3G & H). Therefore, miRNA-455-3p promotes p27 stability through inhibiting its phosphorylation at Thr187.

### 3.4.3 MiR-27b-3p suppresses Skp2 expression through targeting Cks1, whereas miR-455-3p inhibits p27 phosphorylation through targeting CAC1

In silico analysis showed that amongst predicted targets of miRNA-27b-3p was Cks1, a cofactor of Skp2 that prevents Skp2 auto-ubiquitylation and degradation (Supplementary Fig. 3.4A) [67]. To test whether, as proposed, Cks1 3′UTR is targeted by miRNA-27b-3p, we introduced luciferase reporter plasmids containing the 3′UTR of Cks1 into Mel-RM and A549 cells (Supplementary Fig. 3.4C). The reporter activity was reduced, albeit moderately, by the presence of the 3′UTR of Cks1, which was reversed when the 3′UTR was mutated (Fig. 3.4A), indicating that the 3′UTR of Cks1 was inhibited by endogenous miRNA-27b-3p. In support, co-introduction of anti-miRNA-27b-3p increased, whereas co-introduction of miRNA-27b-3p mimics further reduced the reporter activity (Fig. 3.4A & B). Therefore, miRNA-27b-3p targets the 3′UTR of Cks1. Consistently, introduction of miRNA-27b-3p mimics into Mel-RM and A549 cells down-regulated the levels of endogenous Cks1, whereas introduction of anti-miRNA-27b-3p increased Cks1 expression levels (Fig. 3.4C & D). Moreover, the decreased Skp2 expression in cells treated with miRNA-27b-3p mimics was reversed by overexpression of Cks1 and conversely, the increase Skp2 expression caused by anti-miRNA-27b-3p was abolished by Cks1knockdown (Fig. 3.4E & F). Further supporting the regulatory effect of miRNA-27b-3p on Cks1, the levels of

miRNA-27b-3p were inversely correlated with Cks1 protein expression levels (Supplementary Fig. 3.4D & E).

Interrogation of potential targets of miRNA-455-3p highlighted CAC1 (Supplementary Fig. 3.4B), known to promote the kinase activity of CDK2 [218]. Similar to experiments undertaken with miRNA-27b-3p, we introduced luciferase reporter plasmids of the 3′UTR of CAC1 into Mel-RM and A549 cells (Supplementary Fig.3.4C). The reporter activity was reduced by the presence of the 3′UTR but this was abolished when the 3′UTR was mutated (Fig. 3.4G). Moreover, co-introduction of anti-miRNA-455-3p promoted, whereas co-introduction of miRNA-455-3p mimics further inhibited the reporter activity (Fig. 3.4G & H). In accordance, miRNA-455-3p mimics reduced, whereas anti-miRNA-455-3p upregulated endogenous expression of CAC1 (Fig. 3.4I & J). Therefore, miRNA-455-3p targets the 3′UTR of CAC1. Consistently, co-introduction of miRNA-455-3p mimics reversed the CAC overexpression-triggered enhancement in the kinase activity of CDK2 and phosphorylation of p27 at Thr187 (Fig. 3.4K). In contrast, antagonising miRNA-455-3p increased CDK2 activity and Thr187-phosphorylated p27, which was diminished by knockdown of CAC1 (Fig. 3.4L). Taken together, these results indicate that miRNA-455-3p targets the 3′UTR of CAC1 to attenuate CDK2 activity and thus prevent Thr187 phosphorylation of p27 [219]. Indeed, the expression levels of miRNA-455-3p were inversely correlated with CAC1protein expression levels (Supplementary Fig. 3.4D & F).

### 3.4.4 Co-regulation of miRNA-27b-3p and miRNA-455-3p and their host genes

We examined the mechanisms responsible for regulation of miRNA-27b-3p and miRNA-455-3p. The pre-miRNA-27b-3p is embedded within the last intron of the human *Chromosome 9 open reading frame 3* (*C9ORF3*) gene, whereas the pre-miRNA-455-3p is located to the tenth intron of the human *collagen alpha-1 (XXVII) chain* (*COL27A1*) gene (Supplementary Fig.3.5). Intriguingly, analysis of publicly available expression profiles in 35,763 of cancers of diverse

types acquired from the R2 Genomics Analysis and Visualization Platform revealed that *C9ORF3* and *COL27A1* mRNA expression levels were positively correlated (Fig. 3.5A) (R2: http://r2.amc.nl), consistent with the correlative relationship between the expression of miRNA-27b-3p and miRNA-455-3p identified in a panel of human cancer cell lines (Fig. 3.5B). Indeed, knockdown of *C9ORF3* and *COL27A1* inhibited the expression of miRNA-27b-3p and miRNA-455-3p, respectively (Fig. 3.5C & D). In support, both *C9ORF3* and *COL27A1* were upregulated by serum starvation and this upregulation was diminished after serum replenishment (Fig. 3.5E). Moreover, knockdown of *C9ORF3* or *COL27A1* diminished induction of quiescence by serum starvation (Fig. 3.5F). Thus not only are miRNA-27b-3p and miRNA-455-3p concurrently regulated with their host genes but more generally these observations suggest that transcriptional regulation of *C9ORF*3 or *COL27A1* expression may potentially be controlled though a common mechanism.

### 3.4.5 p53 transcriptionally regulates miRNA-27b-3p and miRNA-455-3p

We sought to map the active regions in the proximal promoters of the miRNA-27b-3p and miRNA-455-3p host genes. Luciferase reporter assays using constructs having incremental deletions spanning ~1500 bases upstream down to 100 bp downstream of the *C9ORF*3 gene transcription start site showed that the -250 ~ -100 segment was the shortest region that remained active in Mel-RM cells undergoing serum starvation (Fig. 3.6A). By use of the same approach, the -1000 ~ -500 fragment was identified to be the shortest region of the *COL27A1* gene that remained transcriptionally active in in serum-starved cells (Fig. 3.6B). Importantly, serum replenishment decreased the transcriptional activities of the -250 ~ -100 segment of the *C9ORF*3 gene and the -1000 ~ -500 fragment of the *COL27A1* gene (Fig. 3.6C & D), confirming that these genes are transcriptionally responsive to serum starvation.

Examination of the minimally active promoter regions of both genes showed that they shared in common consensus binding sites for p53 (Supplementary Fig. 3.6A). One putative p53 binding site (-157 to -143 bp) was identified at the -250 ~ -100 segment of the *C9ORF*3 gene whereas the -1000 ~ -500 segment of the *COL27A1* gene also contained three consensus p53 binding sites (-929 to -915 bp, -919 to -905 bp and -814 to -800 bp) (Supplementary Fig.3.6A). We analysed whether the p53-binding sites (p53-BSs) contained within the respective reporter constructs were responsible for the increased transcriptional activity in response to serum starvation. Deletion of the p53-BS in the *C9ORF*3 reporter construct diminished its transcriptional activity (Fig. 3.6E), whereas deletion of the p53-BSs in the *COL27A1* construct similarly abolished its transcriptional activity (Fig. 3.6F). Together these findings suggest that p53-mediated regulation underpins the increased expression of *C9ORF3* and *COL27A1* in quiescent cells and by inference, the increased expression of miRNA-27b-3p and miRNA-455-3p.

Further reporter assay experiments showed that enforced overexpression of wild-type p53 enhanced the reporter activity of both *C9ORF*3 and *COL27A1* reporters while the p53ΔTA mutant (lacking the transactivation domain) did not augment transcription (Fig. 3.6G). In addition, knockdown of p53 or treatment with the small molecule inhibitor of p53 transcriptional activity, pifithrin-α (PFT-α), inhibited activation of the p53-BS-containing luciferase reporters of both genes (Fig. 3.6H & I), confirming that the response of the p53-BSs to induction of quiescence is mediated by p53. This was supported by binding of p53 to the p53-BSs at both genes, which was enhanced by serum starvation (Fig. 3.6J). Therefore, the putative p53-BSs are responsive to p53 that was increased upon induction of quiescence (Supplementary Fig. 3.6A) [228] . In accordance, p53 knockdown or treatment with PFT-α reduced the endogenous expression levels of *C9ORF3* and *COL27A1* (Supplementary Fig. 3.6B & C).

We tested whether p53 is similarly important for miRNA-27b-3p and miRNA-455-3p expression. Since p53 is also essential for miRNA processing [229], we examined its effect on the expression of pri-miRNA-27b-3p and pri-miRNA-455-3p. Knockdown of p53 or treatment with PFT-α

downregulated pri-miRNA-27b-3p and pri-miRNA-455-3p and abolished their upregulation in response to serum starvation (Fig. 3.6K and L). Conversely, overexpression of p53 promoted the expression of these pri-miRNAs in cells with or without serum starvation or contact inhibition (Fig. 3.6M). Therefore, binding of p53 to the p53-BSs at the *C9ORF3* and *COL27A1* gene transcriptionally upregulates miRNA-27b-3p and miRNA-455-3p in response to induction of cellular quiescence. Of note, although the expression levels of miRNA-27b-3p and miRNA-455-3p and their host genes appeared to correlate with wild-type p53 protein expression in cancer cell lines (Supplementary Fig. 3.6D &E), analysis of publicly available datasets acquired from the TCGA did not show any significant relationship between the expression levels of these miRNAs and the *TP53* mutational status or wild-type p53 mRNA expression levels in human melanoma (Supplementary Fig. 3.6F & G), implicating that miRNA-27b-3p and miRNA-455-3p are also subjected to regulations by mechanisms other than p53.

### 3.4.6 p53 drives cellular quiescence through miRNA-27b-3p and miRNA-455-3p

Knockdown of p53 reduced the proportion of quiescent cells, phenocopying introduction of anti-miRNA-27b-3p or anti-miRNA-455-3p (Fig. 3.2B & Supplementary Fig. 3.7A). In contrast, overexpression of p53 promoted quiescence, similar to introduction of miRNA-27b-3p or miRNA-455-3p mimics (Fig. 3.2E & Supplementary Fig. 3.7B). Co-introduction of miRNA-27b-3p or miRNA-455-3p mimics reversed the reduction in quiescence caused by p53 knocked down, whereas co-introduction of anti-miRNA-27b-3p or anti-miRNA-455-3p blocked promotion of quiescence by overexpression of p53 (Fig. 3.7A & B), confirming that p53-induced cellular quiescence is mediated through these miRNAs. Similar to p53, the *C9ORF3* and *COL27A1* genes appeared to play a role in regulating cellular quiescence through miRNA-27b-3p and miRNA-455-3p, respectively, as knockdown of C9ORF3 inhibited quiescence, which was reversed by introduction of miRNA-27b-3p, whereas overexpression of miRNA-455-3p mimics

diminished the reduction in quiescent cells caused by knockdown of COL27A1 (Supplementary Fig. 3.7C & D).

Knockdown of p53 also resulted in downregulation of p27 that was associated with shortened half-life of the protein, whereas overexpression of p53 increased p27 expression in association with prolonging its half-life (Supplementary Fig. 3.7E & F). The effect of p53 knockdown on p27 expression was diminished by co-introduction of miRNA-27b-3p or miRNA-455-3p mimics (Fig. 3.7C). Consistnely, the effect of p53 overexpression on p27 expression was reduced by co-introduction of anti-miRNA-27b-3p or anti- miRNA-455-3p (Fig. 3.7D). These results further consolidate that p53 promotes p27 stability through these miRNAs. Knockdown of p27 diminished p53-overexpression-casued promotion of cellular quiescence (Fig. 3.7E), whereas overexpression of p27 increased the G0 cell proportion irrespective of the p53 expression status (Fig. 3.7F), indicating that upregulation of p27 is necessary for p53-mediated cellular quiescence. Of note, p21 which plays an important role in p53-mediated cell cycle regulation was involved in p53-mediated cellular quiescence [63, 230], as knockdown of p21 did not alter the proportion of G0 cells even when p53 was overexpressed (Supplementary Fig. 3.7G & H).

### 3.4.7 Figures and legends

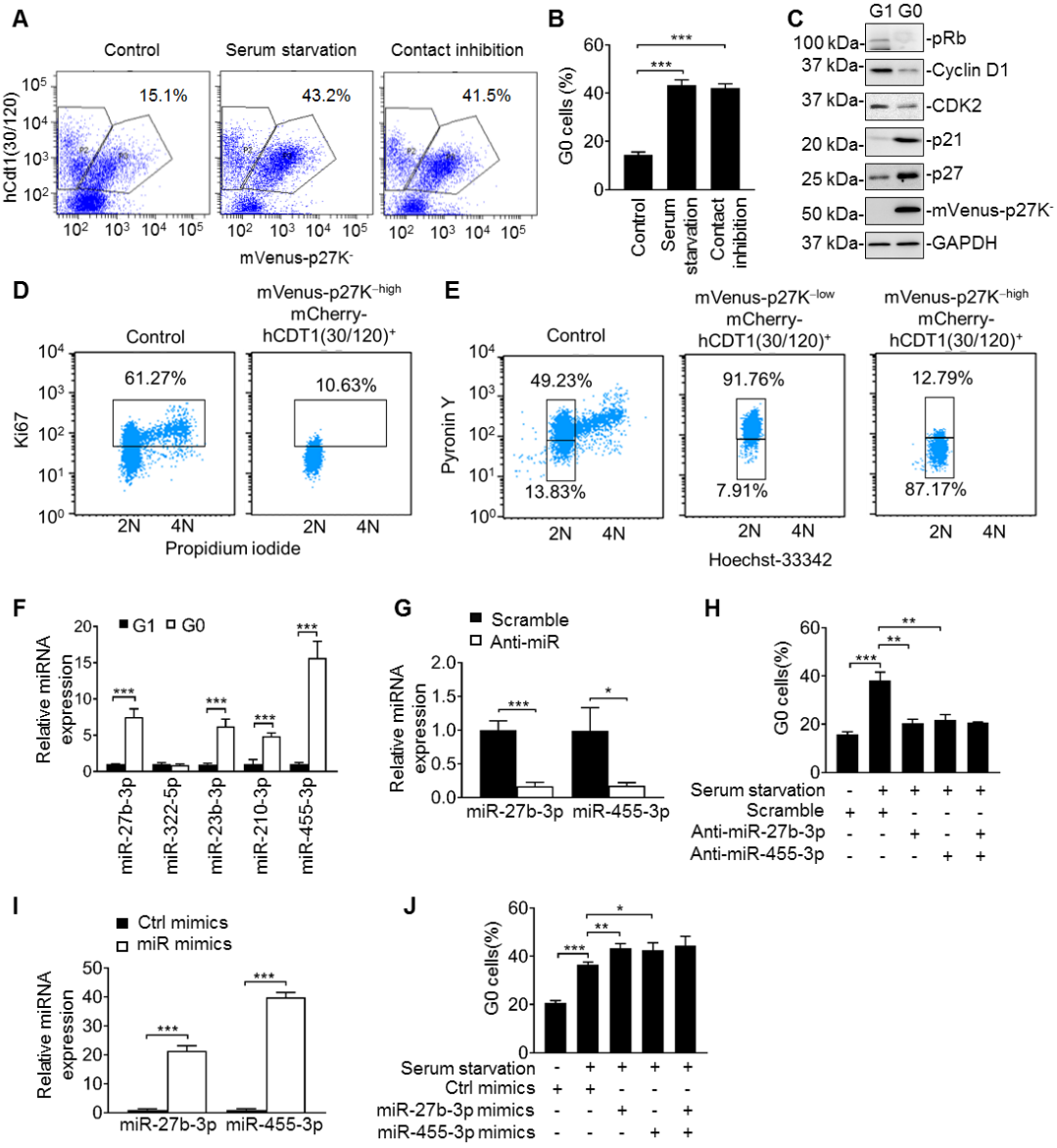


Figure 3.1. MiR-27b-3p and miR-455-3p promote cellular quiescence in B16 cells. **A**, Representative flow cytometric plots of B16 cells stably expressing mCherry-hCdt1(30-120) and mVenus-p27K$^{-}$ cultured under indicated conditions. Numbers represent percentage of quiescent cells. **B**, Quantitation of G0 cells in 3 independent experiments as shown in (A). **C**, Whole cell lysates from sorted G1 and G0 B16 cells were subjected to Western Blotting. **D**, Representative flow cytometric plots of unsorted and sorted mVenus-p27K$^{-high}$/mCherry-hCDT1(30/120)$^{+}$ B16 cells stained with an APC-conjugated anti-Ki67 antibody and propidium iodide. Ki67$^{high}$ cells were gated as proliferating cells. Numbers represent percentage of proliferating cells. **E**,

Representative flow cytometric plots of unsorted (left), sorted mVenus-p27K$^{-low}$ mCherry-hCDT1(30/120)$^{+}$ (middle) and mVenus-p27K$^{-high}$ mCherry-hCDT1(30/120)$^{+}$ (right) B16 cells stained with Hoechst-33342 and Pyronin Y. Pyronin Y$^{high}$ Hoechst-33342$^{low}$ and Pyronin Y$^{low}$ Hoechst-33342 $^{low}$ cells were gated as G1 and G0 cells, respectively. Numbers represent percentage of cells in G1 (higher) or G0 (lower). **F**, Total RNA from sorted G1 and G0 B16 cells were subjected to qPCR analysis. **G**, Total RNA from B16 cells transfected with indicated RNA oligonucleotides were subject to qPCR analysis. **H**, B16 cells transfected with indicated RNA oligonucleotides were cultured with or without serum starvation. Twenty-four hours later, cells were subjected to Hoechst-33342 and Pyronin Y double staining followed by analysis using cytometry. **I**, Total RNA from B16 cells transfected with indicated microRNA mimics were subject to qPCR analysis. **J**, Representative flow cytometric plots of B16 cells transfected with indicated microRNA mimics cultured with or without serum starvation. Twenty-four hours later, cells were subjected to Hoechst-33342 and Pyronin Y double staining followed by analysis using cytometry.

Data shown are either representative (A, C, D and E) or mean ± SEM (B, F, G, H, I and J) of three individual experiments. *, $P<0.05$, **, $P<0.01$, ***, $P<0.001$, Student's *t*-test.

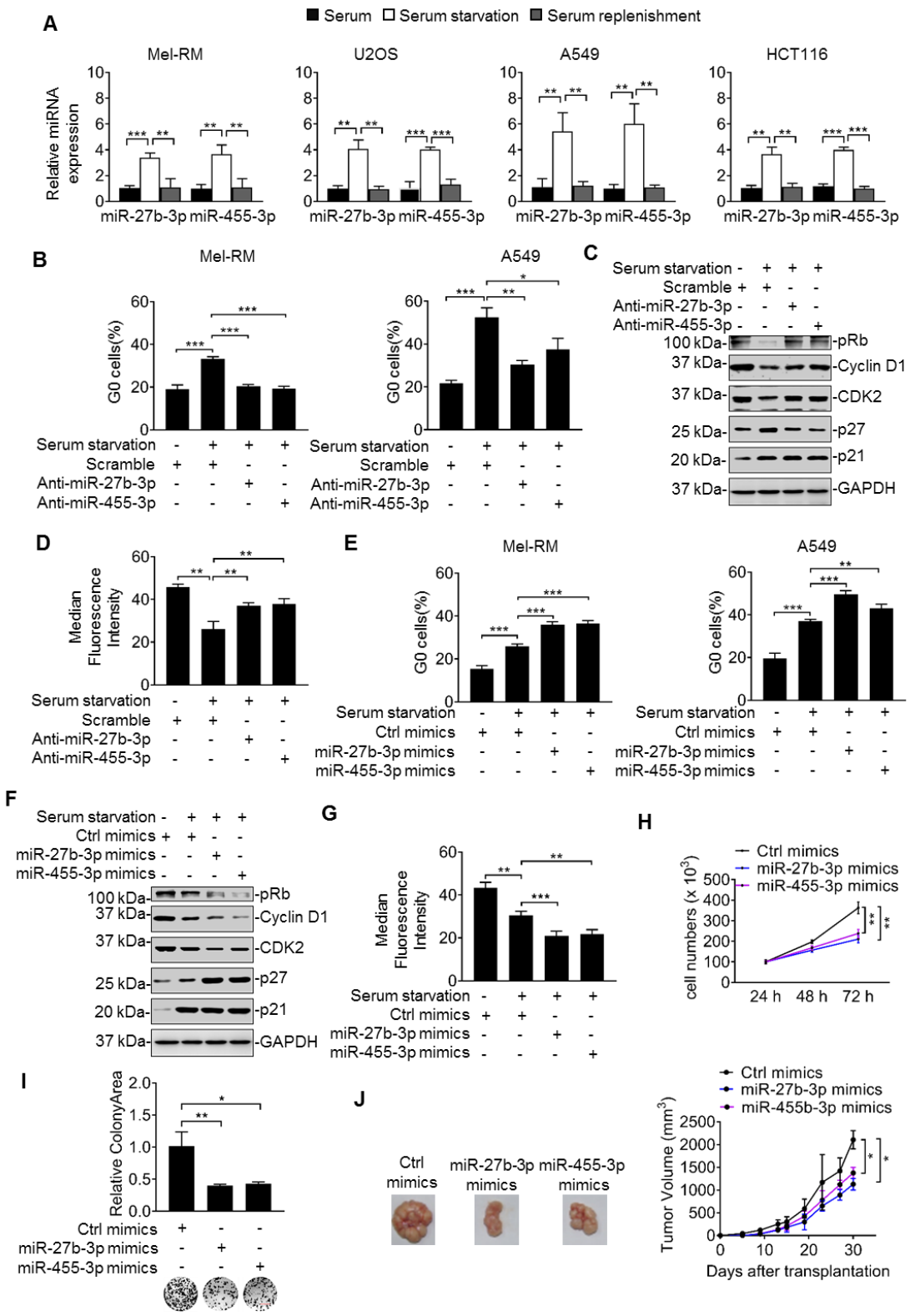


Figure 3.2. MiR-27b-3p and miR-455-3p are up-regulated in quiescent cells and promote cellular quiescence in various human cancer cell lines. **A,** Total RNA from Mel-RM, U2OS, A549 and HCT116 cells cultured with or without serum starvation for 36 hours followed by serum replenishment for another 12 hours were subjected to qPCR analysis. **B,** Mel-RM (left) and A549 (right) cells transfected with indicated RNA oligonucleotides were cultured with or without serum

starvation. Twenty-four hours later, cells were subjected to Hoechst-33342 and Pyronin Y double staining followed by analysis using cytometry. **C,** Whole cell lysates from Mel-RM cells transfected with indicated RNA oligonucleotides cultured with or without serum starvation were subject to Western blotting. **D,** Mel-RM cells transfected with indicated RNA oligonucleotides cultured with or without serum starvation were subjected to staining with an APC-conjugated anti-Ki67 antibody and analysis using flow cytometry. **E,** Mel-RM (left) and A549 (right) cells transfected with indicated anti-miRNA oligonucleotides were cultured with or without serum starvation. Twenty-four hours later, cells were subjected to Hoechst-33342 and Pyronin Y double staining followed by analysis using cytometry. **F,** Whole cell lysates from Mel-RM cells transfected with indicated anti-miRNA oligonucleotides cultured with or without serum starvation were subject to Western blotting. **G,** Mel-RM cells transfected with indicated anti-miRNA oligonucleotides cultured with or without serum starvation were subjected to staining with an APC-conjugated anti-Ki67 antibody and analysis using flow cytometry. **H,** Viable Mel-RM cells were counted in an automated cell counter 24, 48 and 72 hours after transfection with indicated miRNA mimics. **I,** Mel-RM cells transfected with indicated miRNA mimics were subjected to clonogenic assay. ColonyArea was quantitated using ImageJ-plugin; ColonyArea in cells introduced with control (Ctrl) mimics was arbitrarily designated as 1. Scale bar, 1 cm. **J,** Representative photographs (left) and growth curves (right) of tumour xenografts of Mel-RM cells with or without introduction of miR-27b-3p or miR-455-3p mimics. n=6 mice per group.
Data shown are either representative (C, F, I (lower) and J (left)) or mean ± SEM (A, B, D, E, G, H, I (upper) andJ (right)) of three individual experiments. *, $P<0.05$, **, $P<0.01$, ***, $P<0.001$, Student's *t*-test.

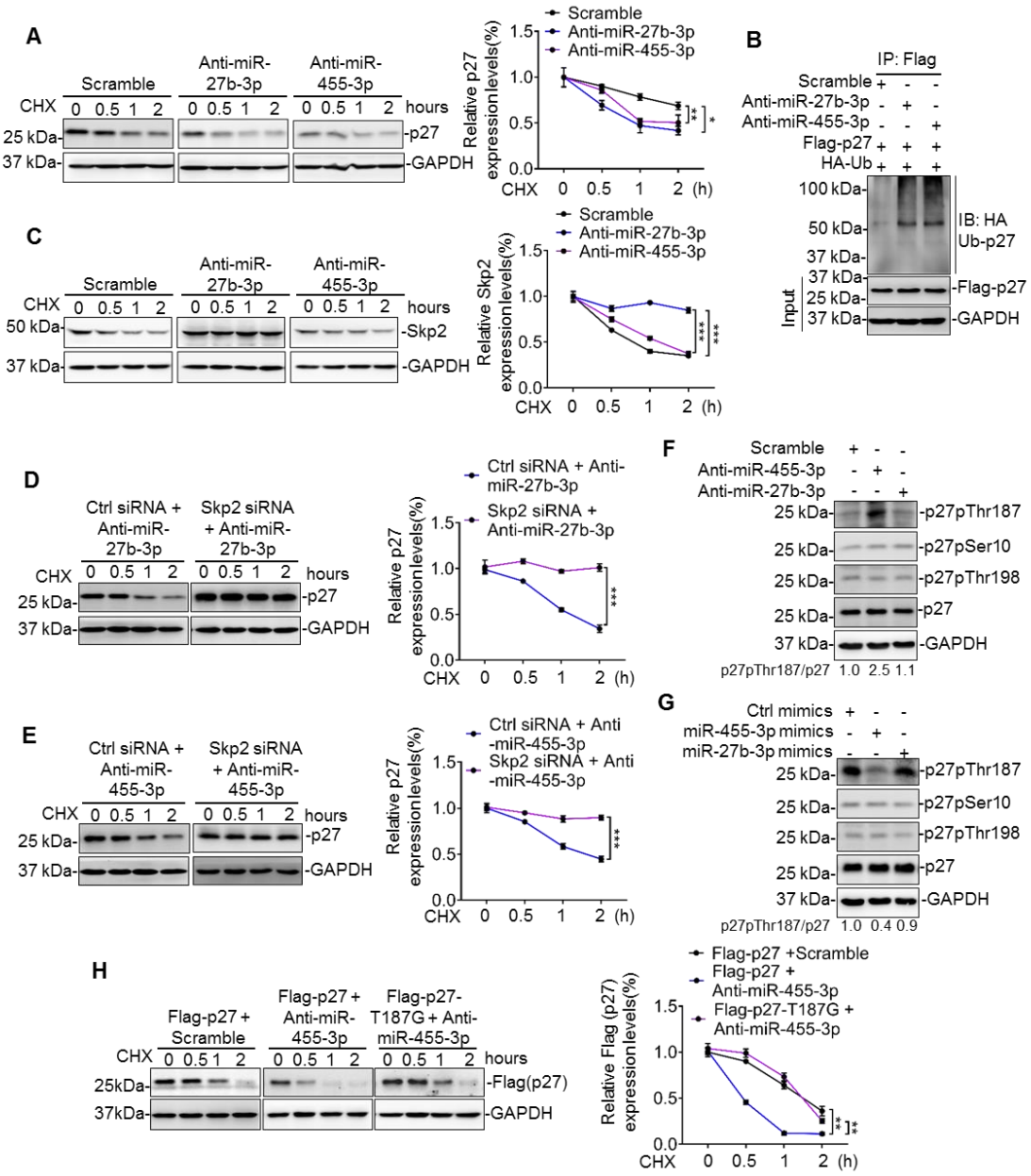


Figure 3.3. MiR-27b-3p and miR-455-3p promote p27 stabilization through downregulating Skp2 and promoting its phosphorylation at Thr187, respectively. **A,** Whole cell lysates from Mel-RM cells transfected with indicated anti-miRNA oligonucleotides treated with cycloheximide (CHX; 5µg/ml) for indicated periods were subjected to Western Blotting. Quantitation of p27 relative to GAPDH expression is also shown (right). **B,** Immunoprecipitates with an antibody against Flag from whole cell lysates of A549 cells transfected with indicated anti-miRNA oligonucleotides and plasmids were subjected to Western blotting. **C,** Whole cell lysates from Mel-RM cells transfected with indicated anti-miRNA oligonucleotides treated with cycloheximide (CHX; 5µg/ml) for indicated periods were subjected to Western Blotting. Quantitation of Skp2 relative to GAPDH expression is also shown (right). **D & E,** Whole cell lysates from Mel-RM cells co-

transfected with indicated anti-miRNA oligonucleotides and siRNAs with or without treatment with cycloheximide (CHX; 5μg/ml) for indicated periods were subjected to Western blotting. Quantitation of p27 relative to GAPDH expression is also shown (right). **F & G,** Whole cell lysates from Mel-RM cells transfected with indicated anti-miRNA (F) or RNA (G) oligonucleotides were subjected to Western Blotting. Numbers represent quantitation of p27 phosphorylated at Thr187 relative to total p27 expression. **H**, Whole cell lysates from Mel-RM cells co-transfected with indicated anti-miRNA oligonucleotides and plasmids with or without treatment with cycloheximide (CHX; 5μg/ml) for indicated periods were subjected to Western blotting. Quantitation of Flag relative to GAPDH expression is also shown (right).

Data shown are either representative (A (left), B, C (left), D (left), E (left), F, G and H (left)) or mean ± SEM (A (right), C (right), D (right), E (right) and H (right)) of three individual experiments. *, $P<0.05$, **, $P<0.01$, ***, $P<0.001$, Student's *t*-test.

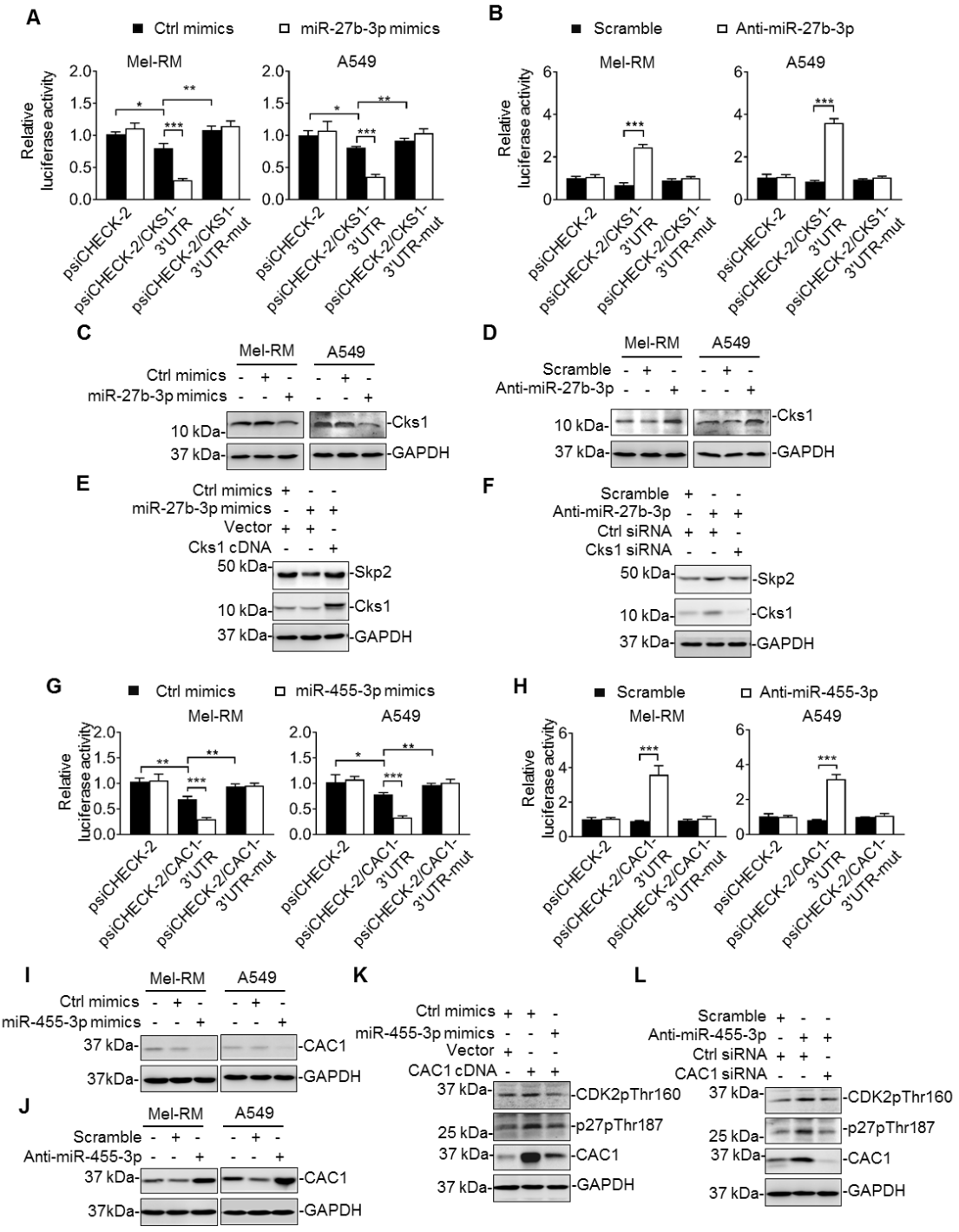


Figure 3.4. MiR-27b-3p suppresses Skp2 expression through targeting CKS1, whereas miR-455-3p inhibits p27 phosphorylation through targeting CAC1. **A,** Luciferase reporter activity measured in Mel-RM (left) and A549 (right) cells after co-transfection with indicated reporter constructs and miRNA mimics. **B,** Luciferase reporter activity measured in Mel-RM (left) and A549 (right) cells after co-transfecting cells with indicated reporter constructs and anti-miRNA oligonucleotides. **C** & **D**, Whole cell lysates from Mel-RM and A549 cells transfected with

indicated miRNA mimics (C) or anti-miRNA oligonucleotides (D) were subjected to Western Blotting. **E**, Whole cell lysates from Mel-RM cells co-transfected with indicated miRNA mimics and cDNAs were subjected to Western blotting. **F**, Whole cell lysates from Mel-RM cells co-transfected with indicated anti-miRNA oligonucleotides and siRNAs were subjected to Western Blotting. **G** & **H**, Mel-RM (left) and A549 (right) cells were co-transfected with indicated reporter constructs and miRNA mimics (G) or anti-miRNA oligonucleotides (H). Twenty-four hours later, reporter activity was measured using luciferase assays. **I & J**, Whole cell lysates from Mel-RM and A549 cells transfected with indicated miRNA mimics (I) or anti-miRNA oligonucleotides (J) were subjected to Western Blotting. **K,** Whole cell lysates from Mel-RM cells co-transfected with indicated miRNA mimics and cDNAs were subjected to Western Blotting. **L,** Whole cell lysates from Mel-RM cells co-transfected with indicated anti-miRNA oligonucleotides and siRNAs were subjected to Western Blotting.

Data shown are either representative (C, D, E, F, I, J, K and L) or mean ± SEM (A, B, G and H) of three individual experiments. *, $P<0.05$, **, $P<0.01$, ***, $P<0.001$, Student's *t*-test.

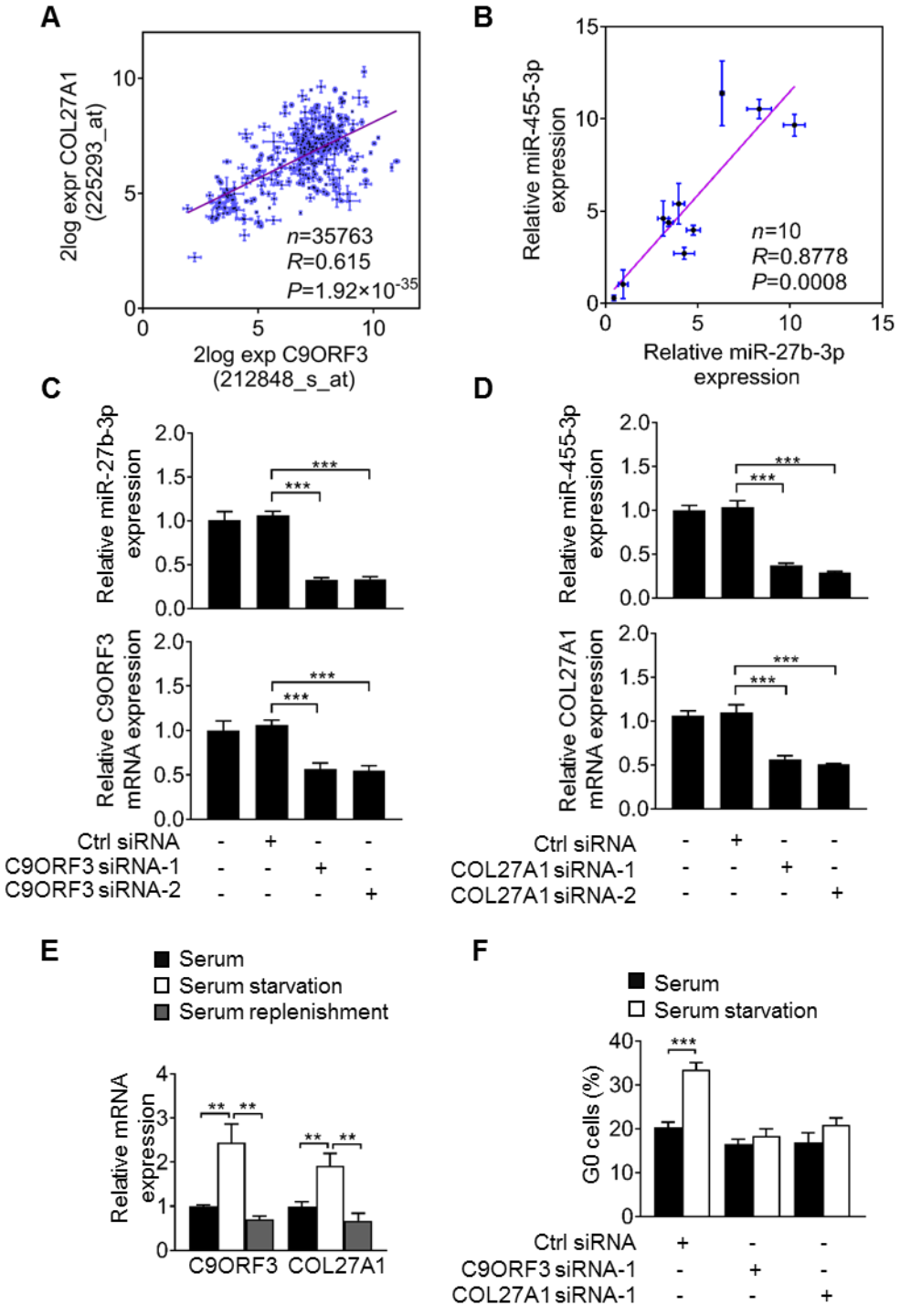


Figure 3.5. Co-regulation of miRNA-27b-3p and miRNA-455-3p and their host genes. **A,** Two-sided Pearson's correlation was employed to analyze the correlation between C9ORF3 and COL27A1 mRNA levels in data from 35763 various cancer patient samples acquired from the R2 Genomics Analysis and Visualization Platform. **B,** Regression analysis showing the positive correlation between miR-27b-3p and miR-455-3p levels in a cell line panel comprised of Mel-RM, Sk-Mel-28, A375, U2OS, A549, MCF7, HeLa, WiDr, HT-29 and HCT116. **C,** Total RNA

from Mel-RM cells transfected with indicated siRNAs were subjected to qPCR analysis of miR-27b-3p (upper) and C9ORF3 (lower) mRNA expression. **D,** Total RNA from Mel-RM cells transfected with indicated siRNAs were subjected to qPCR analysis of miR-455-3p (upper) and COL27A1 (lower) mRNA expression. **E**, Total RNA from Mel-RM cells cultured with or without serum starvation for 36 hours followed by serum replenishment for another 12 hours were subjected to qPCR analysis C9ORF3 and COL27A1 mRNA expression. **F**, Mel-RM cells transfected with indicated siRNAs cultured with or without serum starvation were subjected to Hoechst-33342 and Pyronin Y double staining followed by analysis using cytometry.

Data shown are mean ± SEM (C, D, E and F) of three individual experiments. **, $P<0.01$, ***, $P<0.001$, Student's *t*-test.

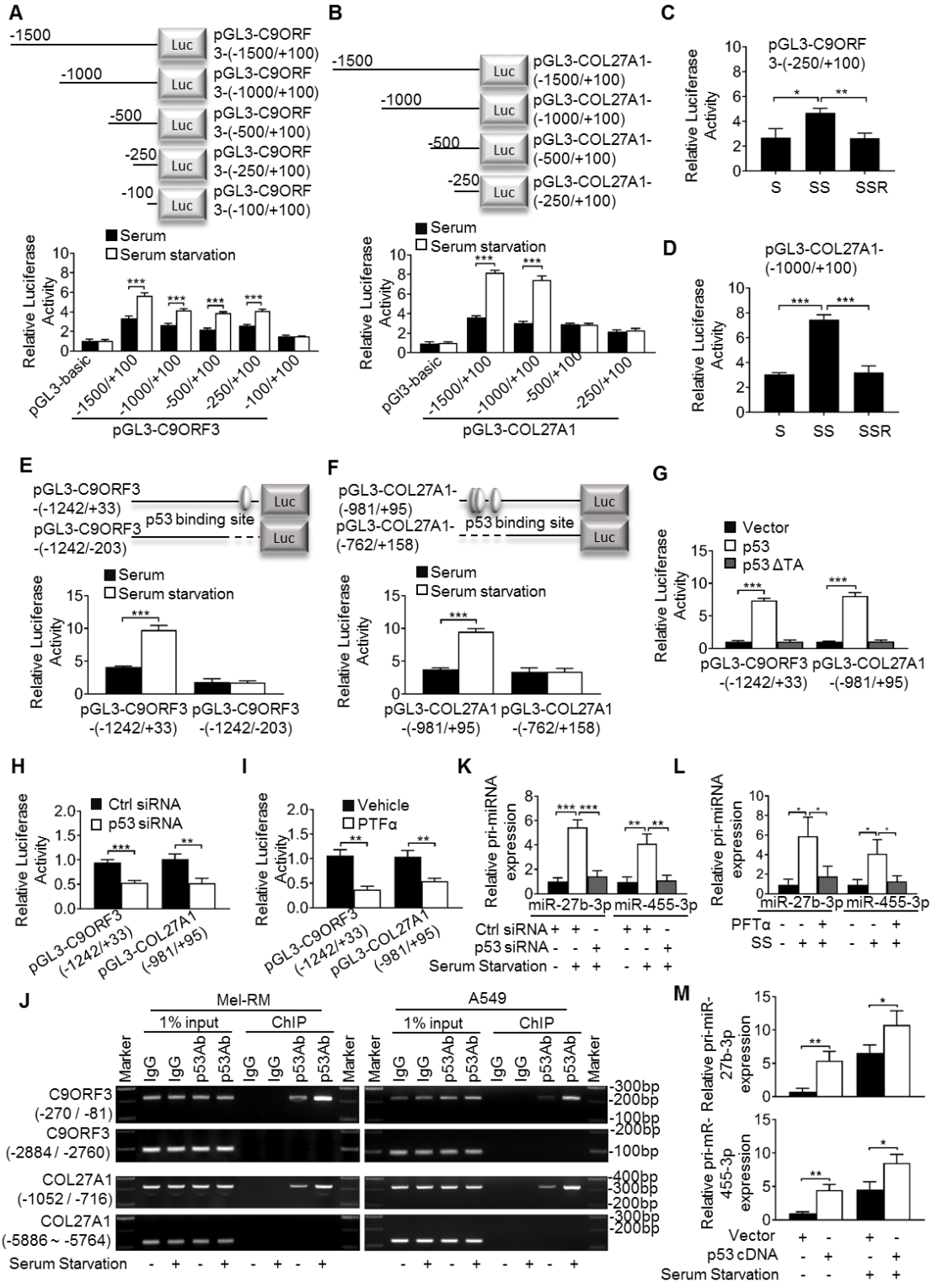


Figure 3.6． p53 transcriptionally regulates miRNA-27b-3p and miRNA-455-3p. **A & B**, Luciferase reporter activity measured in Mel-RM cells transfected with indicated *C9ORF3* (A) or *COL27A1* (B) promoter reporter constructs as illustrated (upper) cultured with or without serum starvation. **C** & **D**, Luciferase reporter activity measured in Mel-RM cells transfected with pGL3-

C9ORF3-(-250/+100) (C) or pGL3-COL27A1-(-1000/+100) (D) cultured with or without serum starvation followed by serum replenishment. S: serum; SS: serum starvation; SSR: Serum replenishment. **E & F,** Luciferase reporter activity measured in Mel-RM cells transfected with wild-type or mutant (lacking p53 binding sites) *C9ORF3* (E) or *COL27A1* (F) reporter constructs as illustrated (upper) cultured with or without serum starvation. **G,** Luciferase reporter activity measured in Mel-RM cells transfected with indicated cDNAs and promoter reporter constructs. 53ΔTA: p53 mutant lacking the transactivation domain. **H & I,** Luciferase reporter activity measured in Mel-RM cells transfected with indicated promoter reporter constructs with or without co-introduction of indicated siRNA (H) or treatment with PTFα (40 nmol/ml). **J,** Mel-RM (left) and A549 (right) cells cultured with or without serum starvation for 36 hours were subjected to chromatin immunoprecipitation (ChIP). **K** & **L,** Total RNA from Mel-RM cells transfected with indicated siRNAs (K) or treated with PTFα (40 nmol/ml) (L) were subjected to qPCR analysis of pir-miR-27b-3p and pri-miR-455-3p. SS: serum starvation. **M,** Total RNA from Mel-RM cells transfected with indicated cDNAs cultured with or without serum starvation were subjected to qPCR analysis of pir-miR-27b-3p (upper) and pri-miR-455-3p (lower).

Data shown are either representative (J) or mean ± SEM (A, B, C, D, E, F, G, H, I, K, L and M) of three individual experiments. *, $P<0.05$, **, $P<0.01$, ***, $P<0.001$, Student's *t*-test.

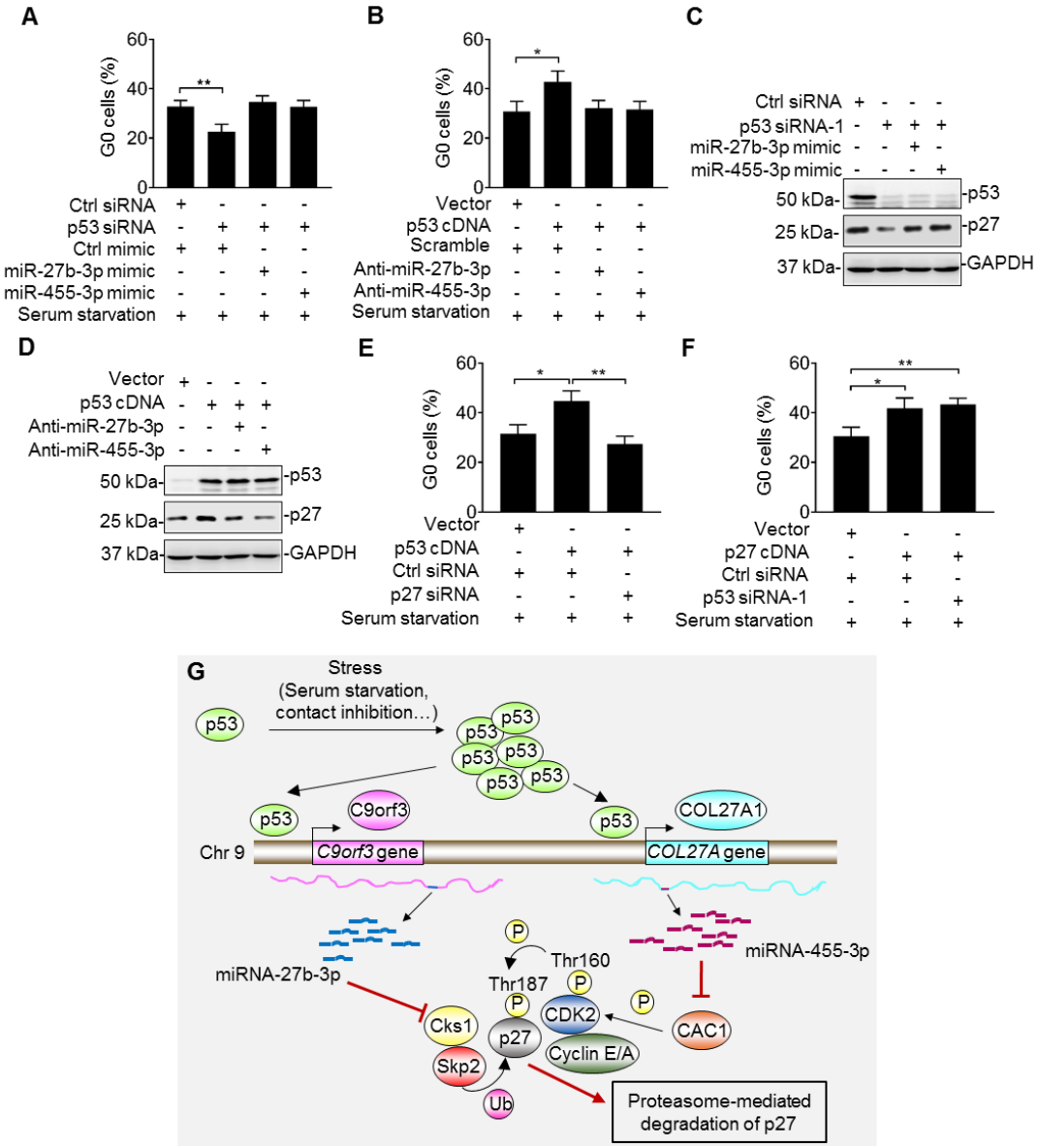


Figure 3.7. p53 drives cellular quiescence through miRNA-27b-3p and miRNA-455-3p. **A & B,** Mel-RM cells co-transfected with indicated miRNA mimics and siRNAs (A) or anti-miRNA oligonucleotides and cDNAs (B) were cultured with serum starvation. Twenty-four later, cells were subjected to Hoechst-33342 and Pyronin Y staining followed by analysis using flow cytometry. **C & D**, Whole cell lysates from Mel-RM cells co-transfected with indicated miRNA mimics and siRNA (C) or anti-miRNA oligonucleotides and cDNA (D) were subjected to Western Blotting. **E & F**, Mel-RM cells co-transfected with p53 cDNA and p27 siRNAs (E) or p27 cDNA and p53 siRNAs (F) were cultured with serum starvation. Twenty-four later, cells were subjected to Hoechst-33342 and Pyronin Y staining followed by analysis using flow cytometry. **G,** A schematic illustration of the identified p53-responsive microRNA network that promotes cellular quiescence.

Data shown are either representative (C and D) or mean ± SEM (A, B, E and F) of three individual experiments. *, $P<0.05$, **, $P<0.01$, Student's *t*-test.

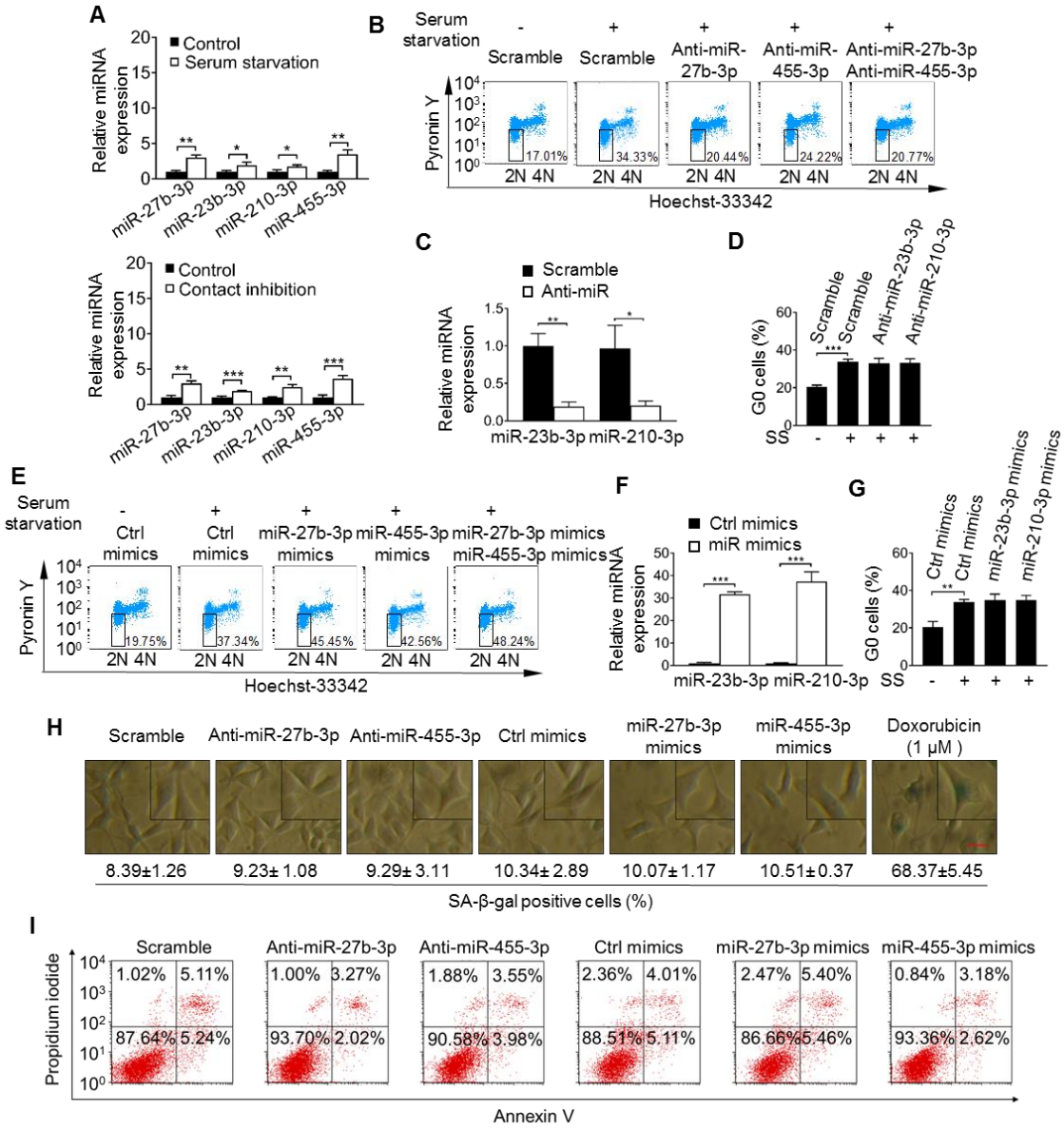


Supplementary Figure 3.1: MiR-27b-3p and miR-455-3p promote cellular quiescence in B16 mouse melanoma cells.

A, Total RNA from B16 cells cultured with or without serum starvation for 36 hours (top) or contact inhibition for 48 hours (bottom) were subjected to qPCR analysis (n = 3, mean ± SEM). *, $P<0.05$, **, $P<0.01$, ***, $P<0.001$, Student's *t*-test. B & E, B16 cells transfected with indicated anti-miRNA oligonucleotides (B) or miRNA mimics (E) were cultured in the presence or absence of serum. Cells were then subjected to Hoechst-33342 and Pyronin Y double staining followed by analysis using cytometry. Pyronin $Y^{low}$ Hoechst-$33342^{low}$ cells were gated as G0 cells. Data shown are representative of three individual experiments. C & F, Total RNA from B16 cells transfected with indicated anti-miRNA oligonucleotides (C) or miRNA mimics (F) were

subjected to qPCR analysis (n = 3, mean ± SEM). *, *P*<0.05, **, *P*<0.01, ***, *P*<0.001. Student's *t*-test. D & G, B16 cells transfected with indicated anti-miRNA oligonucleotides (D) or miRNA mimics (G) were cultured in the presence or absence of serum. Cells were then subjected to Hoechst-33342 and Pyronin Y double staining followed by analysis using cytometry. (n = 3, mean ± SEM). **, *P*<0.01, ***, *P*<0.001, Student's *t*-test. H, B16 cells transfected with indicated anti-miRNA oligonucleotides or miRNA mimics or treated with 1 μM Doxorubicin for 48 hours were subjected to SA-β-galactosidase staining. Quantification of SA-β-galactosidase staining were also shown under figures. Scale bar=25 μm. Data shown are representative of three individual experiments. I, B16 cells transfected with indicated anti-miRNA oligonucleotides or miRNA mimics were subjected to PI/Annexin V apoptosis analysis. Data shown are representative of three individual experiments.

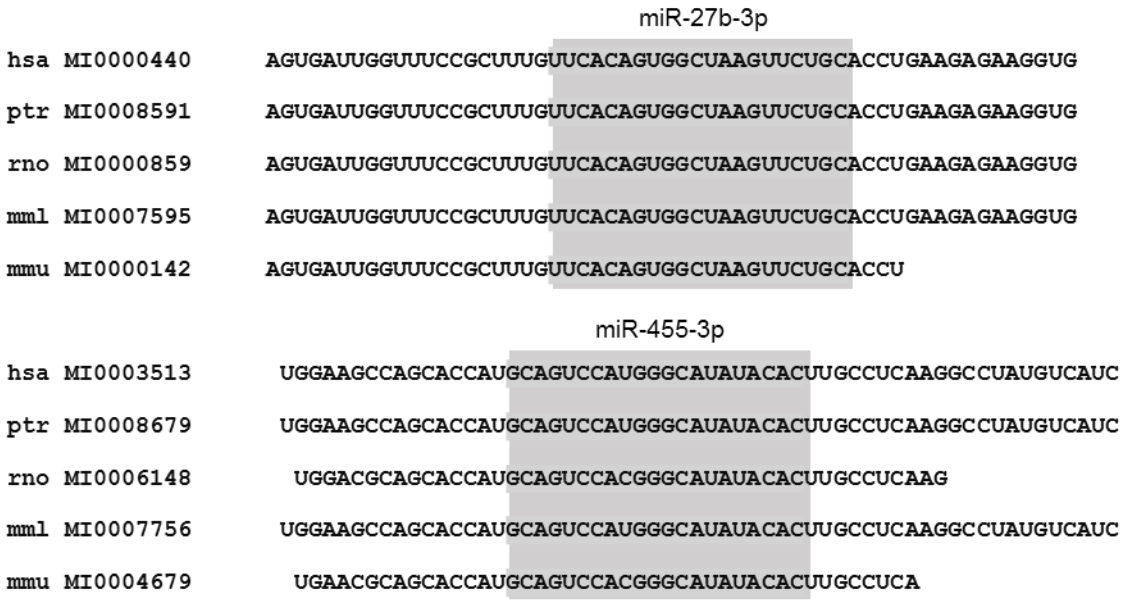


Supplementary Figure 3.2: miR-27b-3p and miR-455-3p are conserved in various mammal species. miR-27b-3p (top) and miR-455-3p (bottom) sequences from five mammal species were aligned using ClustalW serve. Identical nucleic acids residues are shaded in dark grey.

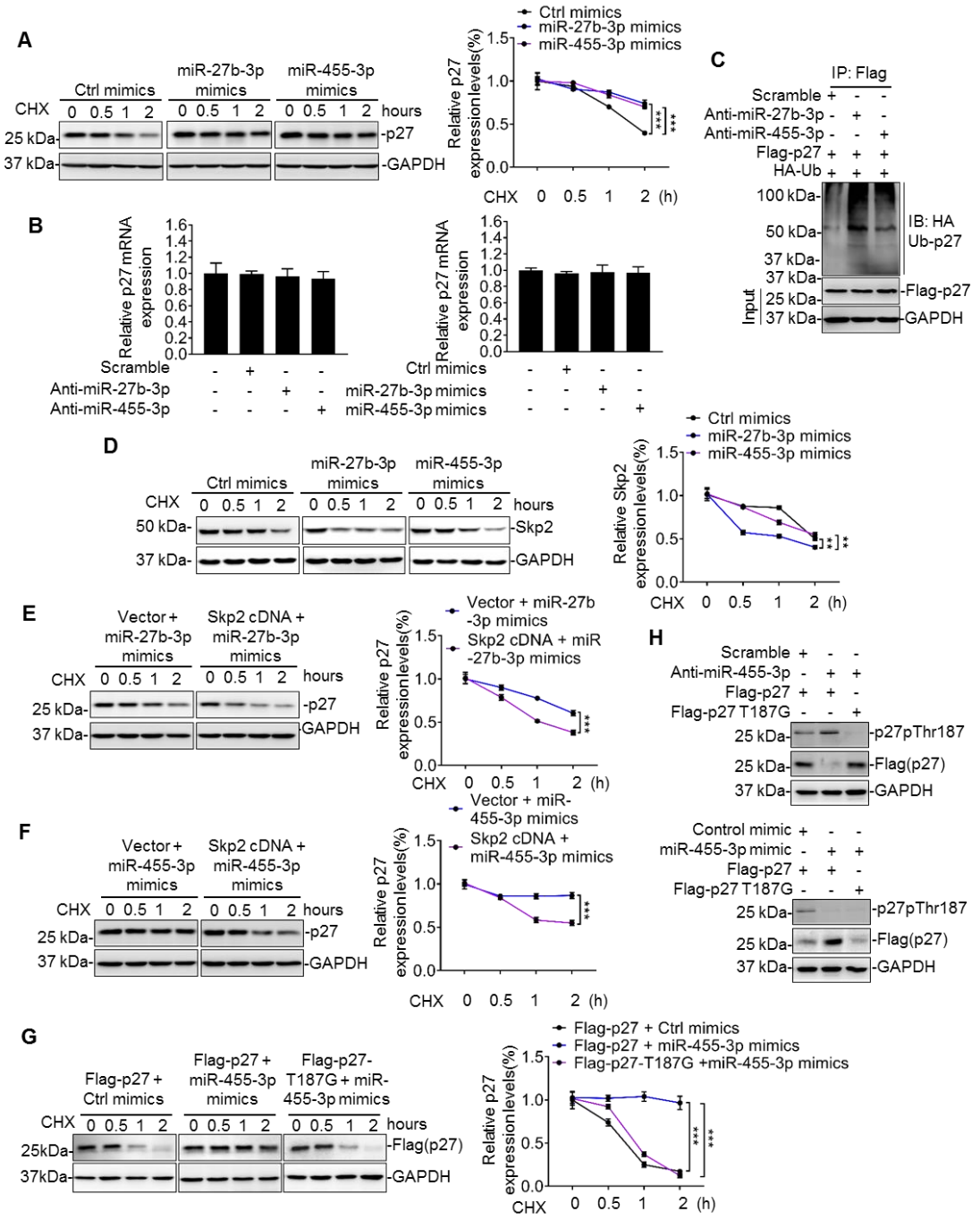


Supplementary Figure 3.3: MiR-27b-3p and miR-455-3p promote p27 stabilization through downregulating Skp2 and promoting p27 phosphorylation at Thr187, respectively

A, Mel-RM cells transfected with indicated miRNA mimics were treated with cycloheximide (CHX; 5µg/ml). Whole cell lysates were subjected to Western Blotting (left). Quantification of p27 relative to GAPDH is also shown (right) (n = 3, mean ± SEM). ***, $P<0.001$, Student's *t*-test. B, Mel-RM cells transfected with indicated anti-miRNA oligonucleotides (left) or miRNA mimics (right) were subjected to qPCR analysis (n = 3, mean ± SEM). Student's *t*-test. C, Mel-

RM cells transfected with indicated anti-miRNA oligonucleotides and cDNAs were subjected to p27 ubiquitination analysis. Data shown are representative of three independent experiments. D, Mel-RM cells transfected with indicated miRNA mimics were treated with cycloheximide (CHX; 5µg/ml). Whole cell lysates were subjected to Western Blotting (left). Quantification of p27 relative to GAPDH is also shown (right) (n = 3, mean ± SEM). **, $P<0.01$, Student's *t*-test. E, Mel-RM cells co-transfected with indicated miRNA mimics and cDNAs were treated with cycloheximide (CHX; 5µg/ml). Whole cell lysates were subjected to Western Blotting (left). Quantification of p27 relative to GAPDH is also shown (right). (n = 3, mean ± SEM). ***, $P<0.001$, Student's *t*-test. F, Mel-RM cells co-transfected with indicated anti-miRNA oligonucleotides and siRNAs were treated with cycloheximide (CHX; 5µg/ml). Whole cell lysates were subjected to Western Blotting (left). Quantification of p27 relative to GAPDH is also shown (right). (n = 3, mean ± SEM). ***, $P<0.001$, Student's *t*-test. G, Mel-RM cells co-transfected with indicated miRNA mimics and Flag-p27 or Flag-p27-T187G were treated with cycloheximide (CHX; 5µg/ml). Whole cell lysates were subjected to Western Blotting (left). Quantification of p27 relative to GAPDH is also shown (right). (n = 3, mean ± SEM). ***, $P<0.001$, Student's *t*-test. H, Mel-RM cells co-transfected with indicated miRNA mimics and Flag-p27 or Flag-p27-T187G were subjected to Western Blotting. Data shown are representative of three individual experiments.

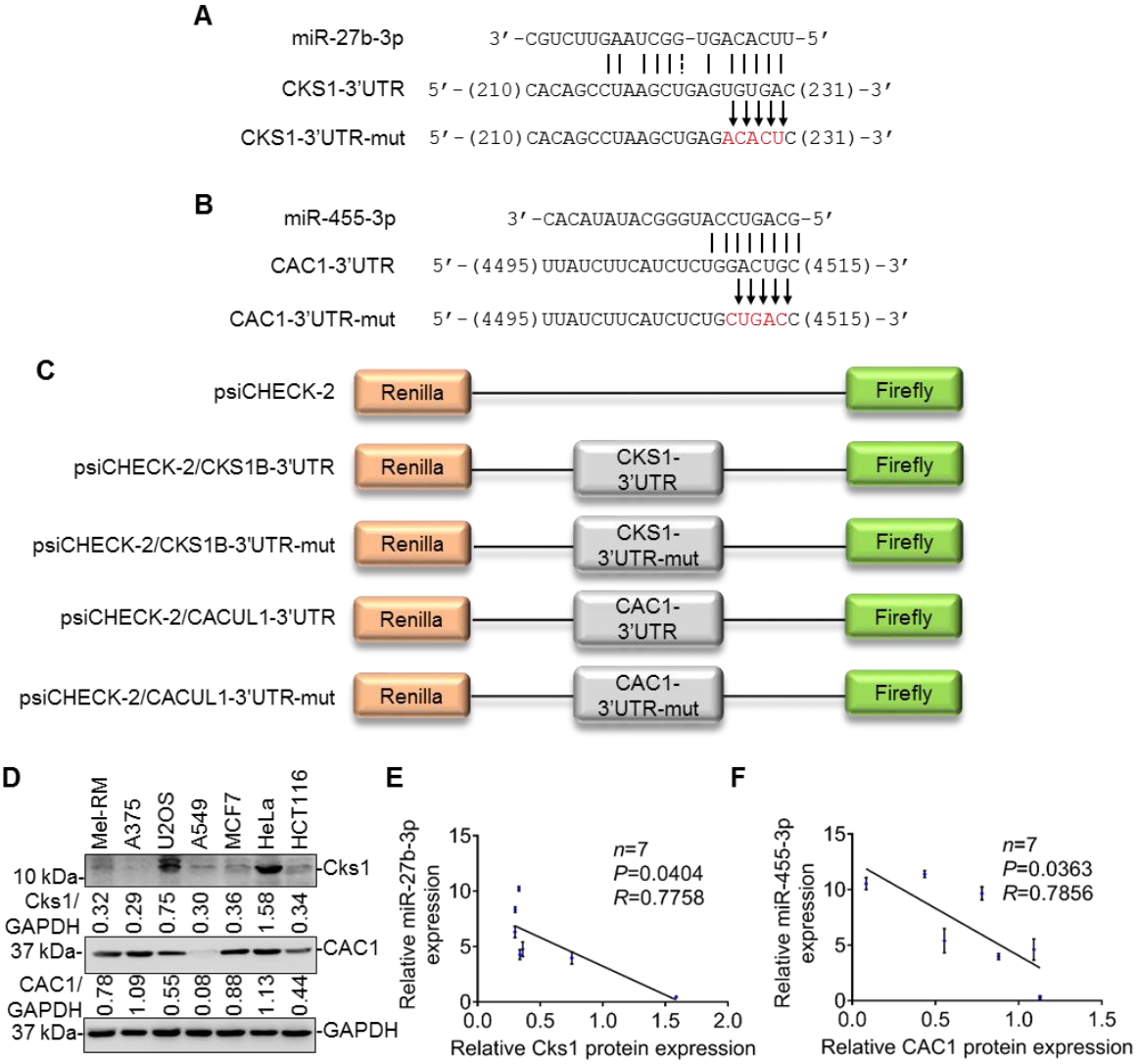


Supplementary Figure 3.4: MiR-27b-3p and miR-455-3p target Cks1 and CAC1, respectively.

**A,** A schematic illustration of base pairing between miR-27b-3p and the 3'UTR of Cks1. Substitution of five consecutive nucleic acids in seed region for mutant reporter construct are shown in red. **B,** A schematic illustration of base pairing between miR-455-3p and 3'UTR of CAC1. Substitution of five consecutive nucleic acids in seed region for mutant reporter construct are shown in red. **C,** A schematic illustration of psiCHECK2–based luciferase reporter constructs. **D,** Whole-cell lysates from indicated cancer cell lines were subjected to Western blotting. Quantification of p27 relative to GAPDH is also shown under figures. Data shown are representative of three individual experiments. **E,** Regression analysis of the relationship between miR-27b-3p expression levels as shown in Fig. 5B and Cks1 protein expression levels as shown in Fig. 5D. **F,** Regression analysis of the relationship between miR-455-3p expression levels as shown in Fig. 5B and CAC1 protein expression levels as shown in Fig. 5D.

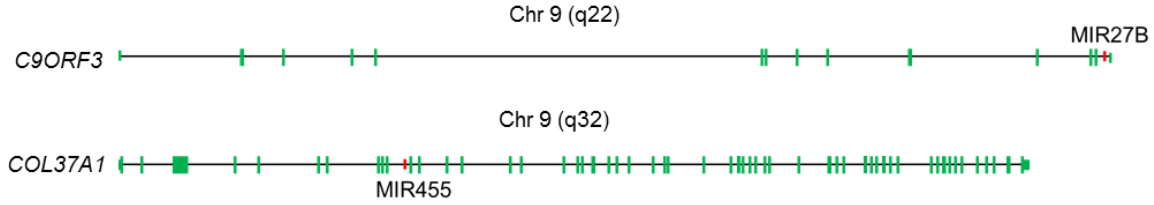


Supplementary Figure 3.5: The genomic locus of miR-27b-3p and miR-455-3p. A schematic illustration showing that miR-27b-3p is embedded within the last intron of the *C9ORF3* gene and miR-455-3p is embedded in the tenth intron of *COL27A1* gene.

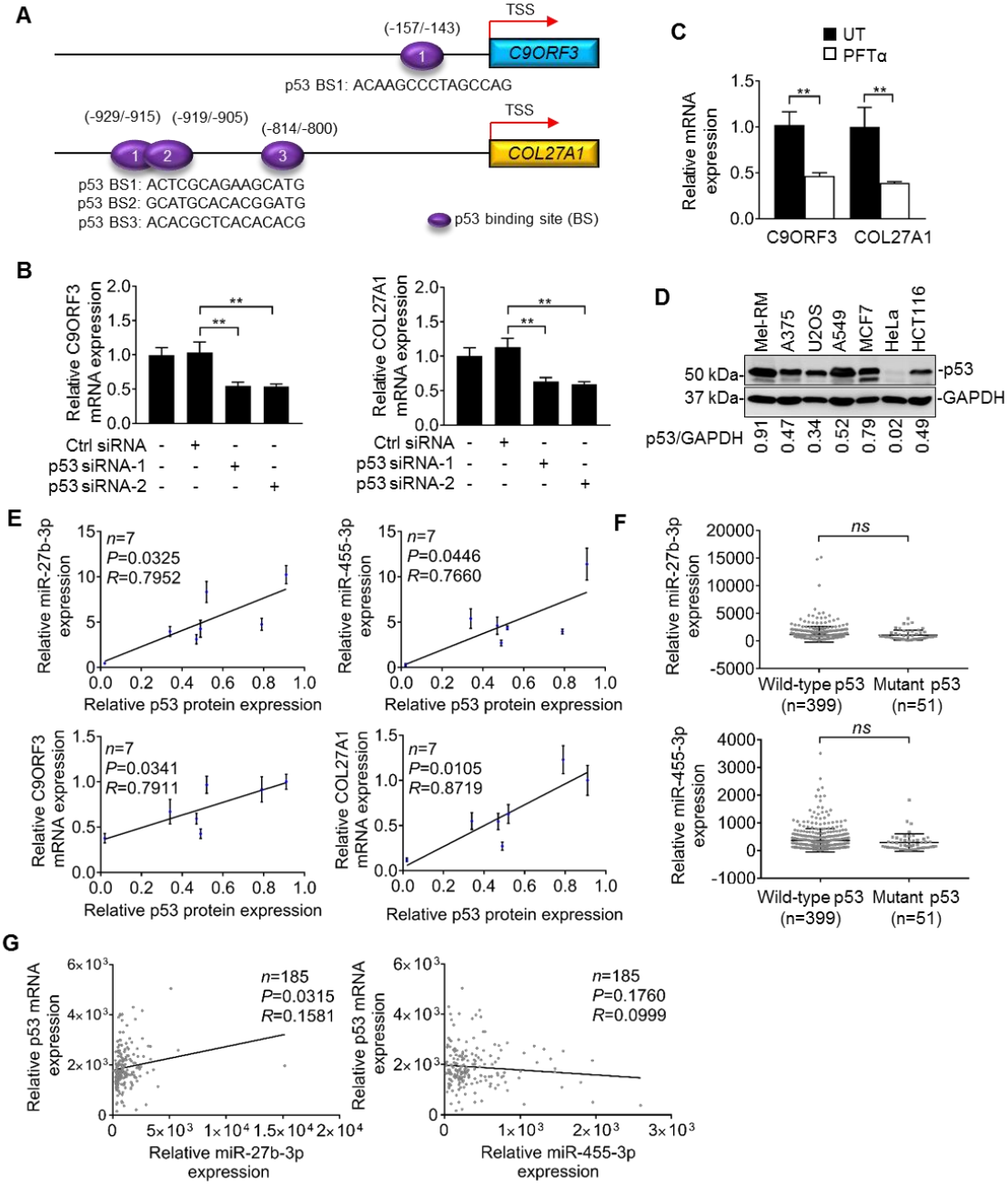

Supplementary Figure 3.6: miR-27b-3p and miR-455-3p are p53-responsive miRNAs.

**A**, A schematic illustration of p53 binding sites on *C9ORF3* and *COL27A1* promoters. **B**, Mel-RM cells transfected with indicated siRNAs were subjected to qPCR analysis of C9orf3 (left) and COL27A1 (right). (n = 3, mean ± SEM). **, $P<0.01$, Student's *t*-test. **C**, Mel-RM cells were treated with PTFα (40 nmol/ml) for 48 hours. Total RNA from cells were subjected to qPCR analysis (n = 3, mean ± SEM). **, $P<0.01$, Student's *t*-test. **D,** Whole cell lysates from the indicated cancer cell lines were subjected to Western blotting**.** Quantification of p53 relative to GAPDH were also shown under figures. **E,** Regression analysis of the relationship between miR-27b-3p and p53 protein levels (upper left panel), miR-455-3p and p53 protein levels (upper right panel), C9ORF3 mRNA and p53 protein levels (lower left panel), and COL27A1 mRNA and p53 protein expression levels (lower right panel). **F,** The relative abundance of miR-27b-3p (top) and miR-455-3p (bottom) were compared between wild-type p53 melanoma (n=399) and mutant p53 melanoma (n=51). Data were adapted from TCGA dataset. n.s., not significant, Student's *t*-test. **G,** Regression analysis of the relationship between miR-27b-3p (left) or miR-455-3p (right) levels and wild-type and diploid p53 mRNA levels. Data were adapted from TCGA dataset. n = 185 clinical samples. Pearson's correlation.

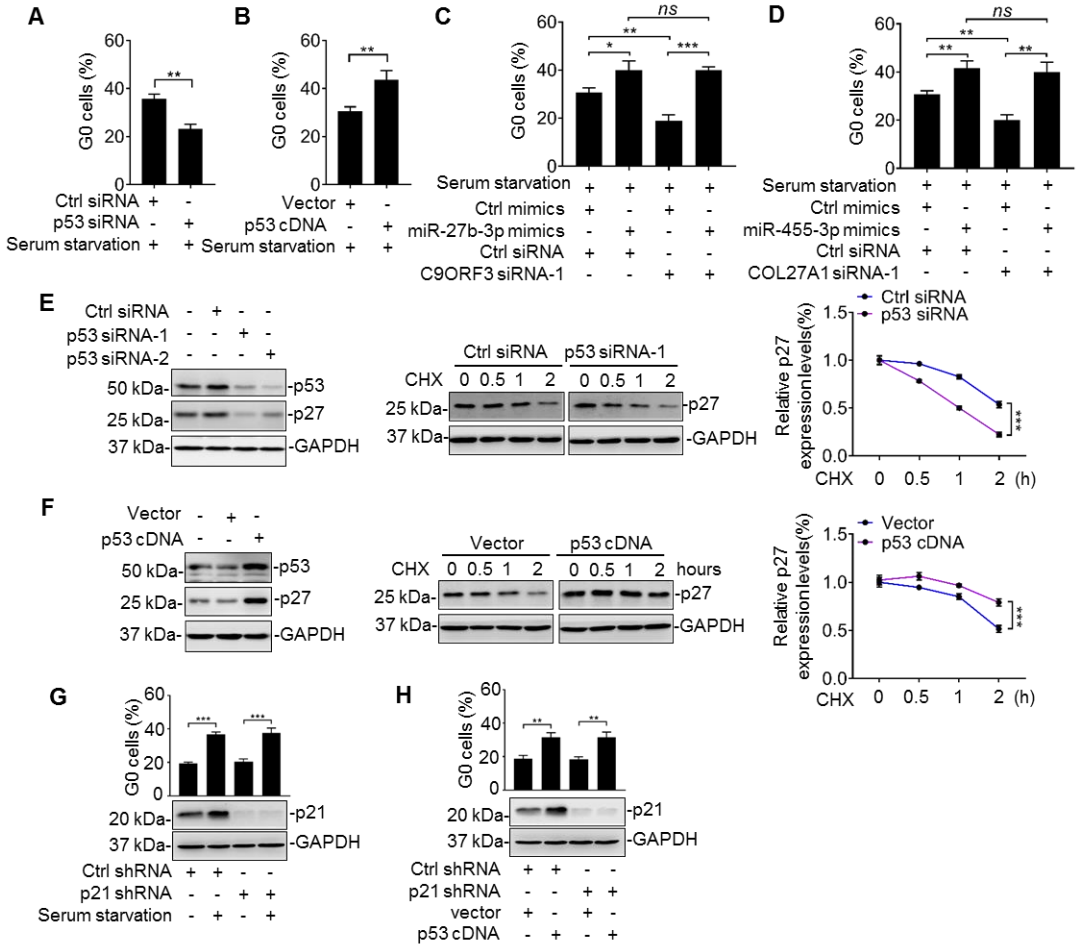


Supplementary Figure 3.7: p53 drives cellular quiescence through miRNA-27b-3p and miRNA-455-3p.

**A & B,** Mel-RM cells co-transfected with indicated p53 siRNAs (A) or p53 cDNAs (B) were cultured in the absence of serum. Cells were then subjected Hoechst-33342 and Pyronin Y double staining followed by analysis using cytometry (n = 3, mean ± SEM). **, $P$<0.01, Student's $t$-test. **C & D**, Mel-RM cells co-transfected with indicated miR-27b-3p mimics and C9ORF3 siRNA (C) or miR-455-3p mimics and COL29A1 siRNA (D) were cultured in the absence of serum. Cells were then subjected to Hoechst-33342 and Pyronin Y double staining followed by analysis using cytometry (n = 3, mean ± SEM). *, $P$<0.05, **, $P$<0.01, ***, $P$<0.001, n.s., not significant, Student's $t$-test. **E & F,** Mel-RM cells transfected with indicated p53 siRNAs (E) or p53 cDNAs (F) were treated with (middle panel) or without (left panel) cycloheximide (CHX; 5µg/ml). Whole cell lysates were subjected to Western Blotting. Quantification of p27 relative to GAPDH is also shown (right panel) (n = 3, mean ± SEM). ***, $P$<0.001, Student's $t$-test. **G**, Mel-RM cells transduced with indicated ctrl shRNA and p21 shRNA were cultured in the presence or absence of serum. Cells were then subjected to Hoechst-33342 and Pyronin Y double staining followed

by analysis using cytometry (top) and Western Blotting (bottom) (n = 3, mean ± SEM). ***, $P<0.001$, Student's *t*-test. **H**, Mel-RM cells stably expressing ctrl shRNA or p21 shRNA were transfected with p53 cDNA or control plasmids. Cells were then subjected to Hoechst-33342 and Pyronin Y double staining followed by analysis using cytometry (top) and Western Blotting (bottom). (n = 3, mean ± SEM). **, $P<0.01$, Student's *t*-test.

## 3.5 Discussion

As the guardian of the genome, p53 responds to cellular stress by promoting cell cycle arrest, either transiently, or permanently to eliminate cells via apoptosis or through senescence [231]. Moreover, the involvement of p53 in regulation of cellular quiescence has been documented in various experimental systems [212, 232]. Nonetheless, most of the previous studies were carried out in arbitrarily defined "quiescent" cells, a total cell population subjected to serum starvation, contact inhibition or growth factor withdrawal [205, 224]. Conceivably these studies encompassed cells that were forcefully arrested in other phases of the cell cycle, in particular, those in G1 phase that are not readily distinguishable from G0 cells by conventional cell cycle analysis approaches [233]. Indeed, while the p53 transcriptional target p21 was shown to be critical for quiescence in some studies [234], we found that p21 was not involved in regulation of cellular quiescence, although it was upregulated in purified G0 cells. It is probable that the role of p21 in p53-mediated cellular quiescence reported in previous studies reflects its contribution to p53-induced G1 phase arrest [235]. Thus, this discrepancy calls for more diligent investigation of the molecular mechanisms involved in the regulation of quiescence. In support, there is increasing evidence showing that purified quiescent (G0) cells express distinct transcript profiles compared with cells in G1 phase [82], although the profiles vary dynamically depending on the depth of quiescence and quiescence inducers in question [211]. By taking advantage of a previously verified experimental system for visualizing G0 to G1 transition [82], we were able to faithfully isolate G0 and G1 cells through co-introducing mVenus-p27K$^-$ that cannot bind to CDK but is still prone to proteosomal degradation and mCherry-hCDT1(30/120) that is specifically expressed in G0 and G1 cells.

We focused on differentially expressed miRNAs between G0 and G1 cells, as a number of previous studies have shown that ablation of the miRNA processing enzyme Dicer promotes quiescence exit[213, 214], pointing to an essential role of miRNAs in regulation of quiescence. Indeed,

the list of miRNAs involved in cellular quiescence is rapidly expanding [95, 213, 215, 216, 236, 237], but results from clearly defined putative G0 cells are currently lacking. Herein we identified miRNA-27b-3p and miRNA-455-3p as positive regulators of cellular quiescence through comparative analysis of highly purified G0 and G1 cells. However, it remains unknown whether these miRNAs function to promote quiescence entry and maintenance or to block quiescence exit. Nevertheless, mechanistic investigation revealed that both miRNA-27b-3p and miRNA-455-3p promoted p27 stabilization through sequestering Skp2-mediated degradation. Skp2 is known to be primarily responsible for degrading p27 in cells that proceed through S phase and afterwards [63, 227], whereas its expression levels are low in cells during the G0 to G1 transition where p27 expression starts to be reduced [67]. It is therefore conceivable that miRNA-27b-3p and miRNA-455-3p are mainly involved in promoting quiescence entry and maintenance. Of note, p27 expression is negatively regulated by miRNA-221 and miRNA-222 that are known to inhibit cellular quiescence [95, 237]. It appears that a comprehensive miRNA network encompassing miRNA-27b-3p, miRNA-455-3p, miRNA-221, miRNA-222 and possibly others yet to be identified play an important bidirectional role in regulating cellular quiescence through controlling p27 expression.

Neither miRNA-27b-3p nor miRNA-455-3p directly targeted the transcript of p27. Instead, miRNA-27b-3p inhibited the expression of Cks1 that binds to Skp2 and prevents it from auto-ubiquitylation and degradation [67]. On the other hand, miRNA-455-3p targeted CAC1 that promotes CDK2 activity leading to increased phosphorylation of p27 at Thr187 which is necessary for polyubiquitination of p27 by Skp2. Therefore, albeit affecting p27 expression indirectly, these miRNAs act cooperatively to ensure that the molecular machinery that drives p27 degradation is under tight control. This interdependent relationship between miRNA-27b-3p and miRNA-455-3p in regulation of p27 also provides a mechanistic explanation as to why co-knockdown or co-overexpression of these miRNAs did not produce additive effects on p27 expression. Since both Cks1 and CAC1 can promote cell cycle progression through interacting

with various CDKs [218, 238], it is foreseeable that targeting Cks1 and CAC1 by miRNA-27b-3p and miRNA-455-3p may have broad negative effects on cell proliferation apart from promoting cellular quiescence.

Interestingly, similar to the correlative relationship between miRNA-27b-3p and miRNA-455-3p expression levels, the transcript levels of the miRNA-27b-3p host gene *C9ORF3* and the miRNA-455-3p host gene *COL27A1* were positively correlated. These observations suggested that *C9ORF*3 and *COL27A1* were likely to be regulated by the same mechanism and we established this to be transcriptional regulation by p53. This not only identified *C9ORF3* along with miRNA-27b-3p and *COL27A1* together with miRNA-455-3p as novel transcriptional targets of p53, but also established these genes and their products as important components of p53-driven networks promoting cellular quiescence. However whether regulation of *C9ORF3* and *COL27A1* by p53 has other effects on cellular processes remains to be investigated. *C9ORF3* encodes an aminopeptidase with its function less understood [239], whereas *COL27A1* encodes protein that is a member of the fibrillar collagens of extracellular matrix proteins.

A practical implication of this study is the potential application in the treatment of cancer. Cellular quiescence is closely related to evasion of cancer cells to killing by systemic treatment, as most of available therapeutics primarily target proliferating cancer cells [240]. Re-entry of quiescent cancer cells into the cell cycle plays an important role in relapse following initial tumour remission [220]. Therefore, curative treatment of cancer requires therapies that either sustain the quiescent state or drive quiescent cells into the cell cycle to render them sensitive to induction of cell death [5, 29]. Accordingly, our results suggest that either promotion of miRNA-27b-3p and miRNA-455-3p expression to force cells to remain in the quiescent state permanently or inhibition

of these miRNAs to have quiescent cells re-enter the cell cycle is a testable approach for improving the therapeutic efficacy of systemic therapeutic agents.

In summary, we have shown in the study that p53 is a driver of quiescence in cancer cells through two interrelated miRNA pathways with potential implications for cancer treatment (Fig. 3.7G). Noticeably, although miRNA-27b-3p and miRNA-455-3p expression is primarily regulated by p53, they are detectable in *TP53*-null cells and those carrying mutant *TP53*, albeit at low levels. Considering that p53 inactivation through mutation or deletion occurs in >50% of human cancers [241], this suggests that unidentified mechanisms may be involved in regulation of the expression of miRNA-27b-3p and miRNA-455-3p that function independently of p53 to regulate cellular quiescence.

# Chapter Four The establishment of CDKN1B-EGFP and MKI67-mCherry HD KI Mel-RM subline

## 4.1 Introduction

In order to further uncover the characteristics of human quiescent cancer cells, especially the contributions of long noncoding RNAs (lncRNAs), which is not conservative, we need a system which can isolate human quiescent cancer cells directly by labelling human cancer cells. FUCCI system based on the oscillate expression of Cdt1 and geminin which are tightly controlled by proteasome degradation. It is delivered to the cells by lentivirus, which is an exogenous overexpressed system. Currently, it is widely used in various species. However, this system cannot specifically label the cells at G0 phase. On the other hand, the functional output of the each coding gene is determined by its localization and dynamic interactions with genomic DNA, RNA and protein. For example, the subcellular localization of p53 determines the different functions of p53 which were mediated by the interaction with different proteins[242]. Ectopic overexpression is a notorious concern in conventional and especially in super-resolution fluorescence light microscopy studies because it may cause numerous artifacts including ectopic subcellular localizations, erroneous formation of protein complexes, and others. Nevertheless, the typical overexpression-induced artefacts can be avoided in genome-edited cells[243].

Genome editing techniques which enable to track the expression and the localization of the target gene by fused fluorescence. The possibility of accurate trackage is based on the share of the same promoter, the same transcriptional initial complex, the same transcript, the same localization signal and the same ubiquitination site for degradation between target genes and the fluorescent genes. The strategy is that inserting the full open reading frame (ORF) of a fluorescent gene before the stop codon of the target gene in the genome. Since we don't need the target proteins and fluorescent proteins fold and behave independently, linker peptides (spacers) are not needed here.

P27 is a gene which is upregulated in quiescent cells while degraded when cell cycle re-entry[63]. It can be used as a marker of the cells at G0 phase and G0-G1 transition. While Ki67 is the widely

used proliferation maker which is upregulated in proliferative cells, especially in late G1, S, G2 and M phases. Moreover, it is reported that the Ki67 levels in G0 and early G1 phases are depended on how long an individual cell has spent in G0[137]. Considering the relative higher levels of p27 at G0 and G1 phases, the co-trackage of Ki67 can exclude the cells which at G1 phase that still show a high levels of p27 but already commence the accumulation of Ki67.

In this chapter, I will label the endogenous p27 with an *EGFP* and Ki67 with a red fluorescence (*mCherry*) by CRISPR/Cas9 technnology in human melanoma cell line (Mel-RM) and cervical cancer cell line (HeLa) for the purpose of isolation human quiescent cells. Homologous recombination (HD) was utilized to insert EGFP and mCherry to the genome accurately.

## 4.2 Results

### 4.2.1 The Design of sgRNAs and homologous arms

In order to insert the two fluorescent proteins in the 3' of coding sequence (CDS) of p27 and Ki67, two sgRNAs were designed separately to target the regions which are close to stop codon of the two genes (Table 4.1 & Figure 4.1).

**Table 4.1 Oligonucleotides for generating sgRNA expression vector**

| Oligo | Sequence (5'-3') |
|---|---|
| p27 sgRNA-1-top | CACCGTGCTCCACAGAACCGGCATT |
| p27 sgRNA-1-bottom | AAACAATGCCGGTTCTGTGGAGCAC |
| p27 sgRNA-2-top | CACCGTCAAACGTAAACAGCTCGGT |
| p27 sgRNA-2-bottom | AAACACCGAGCTGTTTACGTTTGAC |
| Ki67 sgRNA-1-top | CACCGTTTGACAGAAAAATCGAACT |
| Ki67 sgRNA-1-bottom | AAACAGTTCGATTTTTCTGTCAAAC |
| Ki67 sgRNA-2-top | CACCGATTTGACAGAAAAATCGAAC |
| Ki67 sgRNA-2-bottom | AAACGTTCGATTTTTCTGTCAAATC |

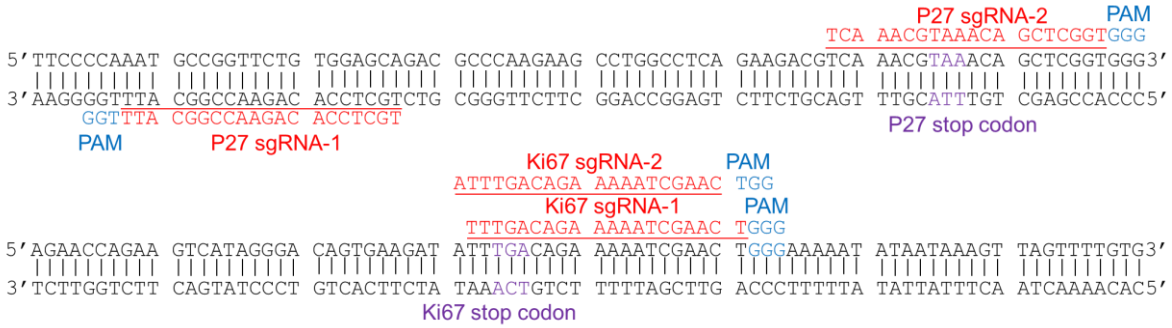


Figure 4.1. The loci of the designed sgRNAs. Red indicates sgRNA. Blue indicates PAM. Purple indicates stop codon.

The annealed oligonucleotides in Table 4.1 were ligated into BsmBI-digested lentiCRISPR v2. To test the cleavage efficiency, we adapted T7E1 assay in HEK293T cells (Fig. 4.2). There is no big difference between the two sgRNAs for p27 and Ki67, the one more close to the stop codon were chose for further study (Figure 4.3 & 4.4).

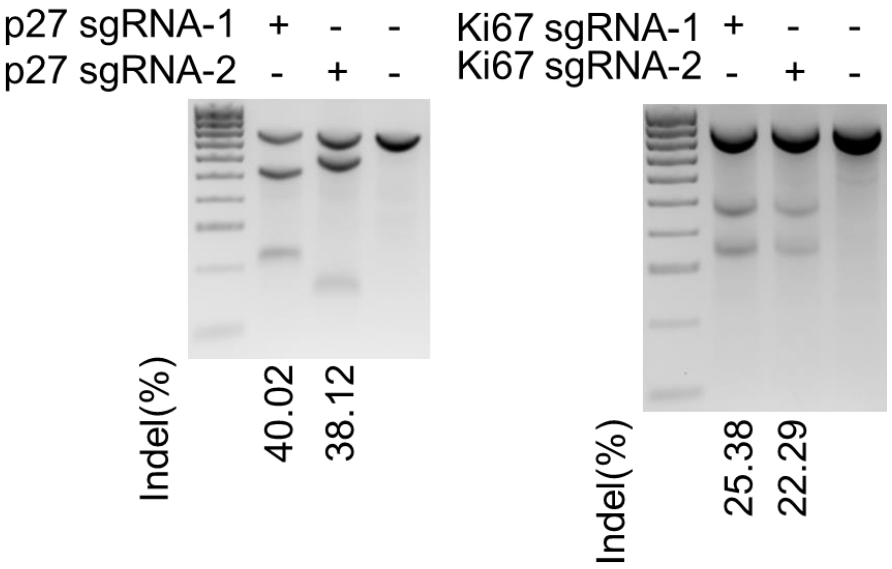


Figure 4.2. T7EI assay for Cas9-medisted indels.

Considering the length of EGFP and mCherry are around 700 bp, the homologous arms should be long enough to make sure HDR. Two donor vectors that carries EGFP flanked by a 1097 bp left arm and 1256 bp right arm (Figure 4.3) and mCherry gene flanked by a 1288 bp left arm and 920 bp right arm were integrated into *pEASY* Blunt-Zero vector (Figure 4.4).

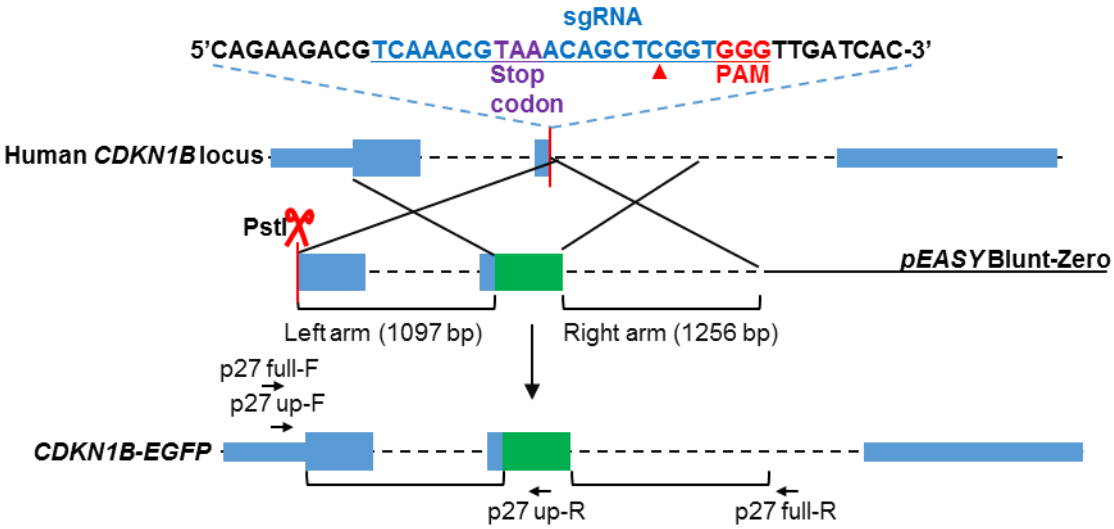


Figure 4.3. The schematic diagram of the strategy to generate CDKN1B-EGFP knock-in cells by homologous recombination. The p27 sgRNA-2 was used to target p27 stop codon region. The donor DNA consisting of EGFP flanked human p27 sequences (left arm and right arm) was used. The primers used for further genotyping are also indicated.

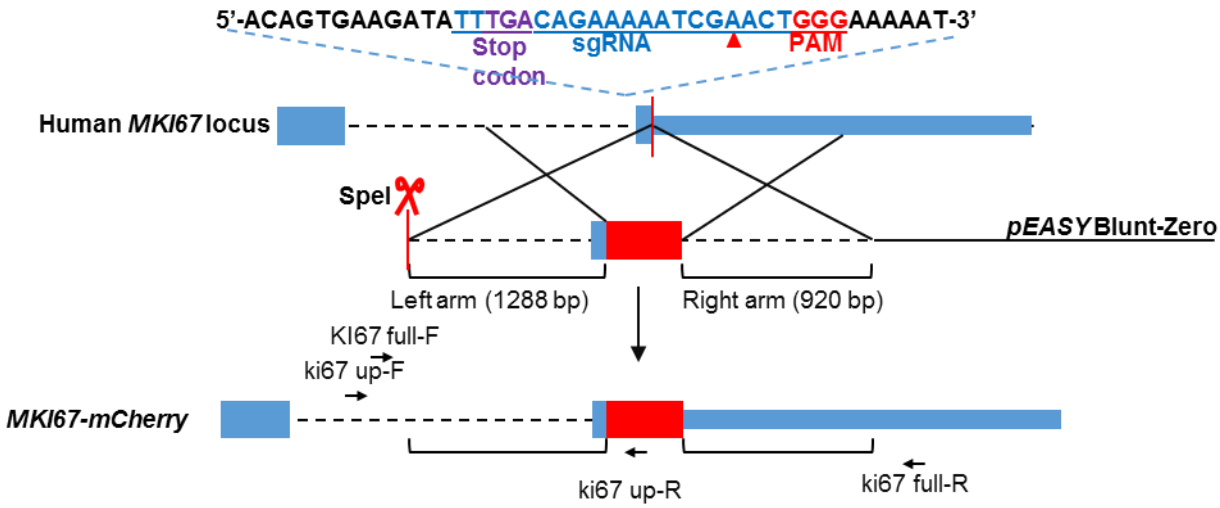


Figure 4.4. The schematic diagram of the strategy to generate MKI67-mCherry knock-in cells by homologous recombination. The Ki67 sgRNA-1 was used to target Ki67 stop codon region. The donor DNA consisting of mCherry flanked human Ki67 sequences (left arm and right arm) was used. The primers used for further genotyping are also indicated.

### 4.2.2 Generation of CDKN1B-EGFP HD KI (knock-in) Mel-RM subline

We Transfected the linearized donor as well as Cas9/sgRNA by nucleofection to Mel-RM (metastatic melanoma cell line, BRAF wild-type). In order to increase the Homology directed repair (HDR) efficiency, puromycin and SCR7 were used. The selected cells were subjected to FACS (Figure 4.5).

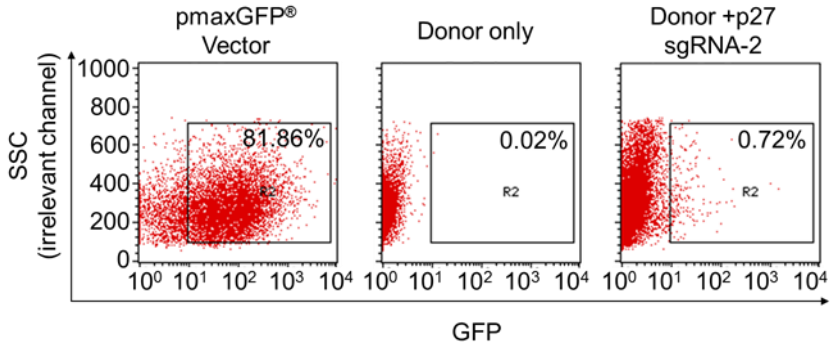


Figure 4.5. The proportions of GFP positive cells after puromycin and SCR7 selection. Each single cells were sorted into each wells of 96 well plate.

After a slight serum starvation, we found that there are 0.72 % GFP positive cells in the cells transfected with both donor plasmid and p27 sgRNA, while only 0.02% GFP positive cells in donor only cells. We sorted each single GFP positive cells in a well of 96-well plate. 288 single cells were seed in 96-well plate (3 plates). Only 81 cells grew up to form colonies. Genotyping by PCR analysis the 81 colonies identified that 44 of the colonies had EGFP insertion (Figure 4.6).

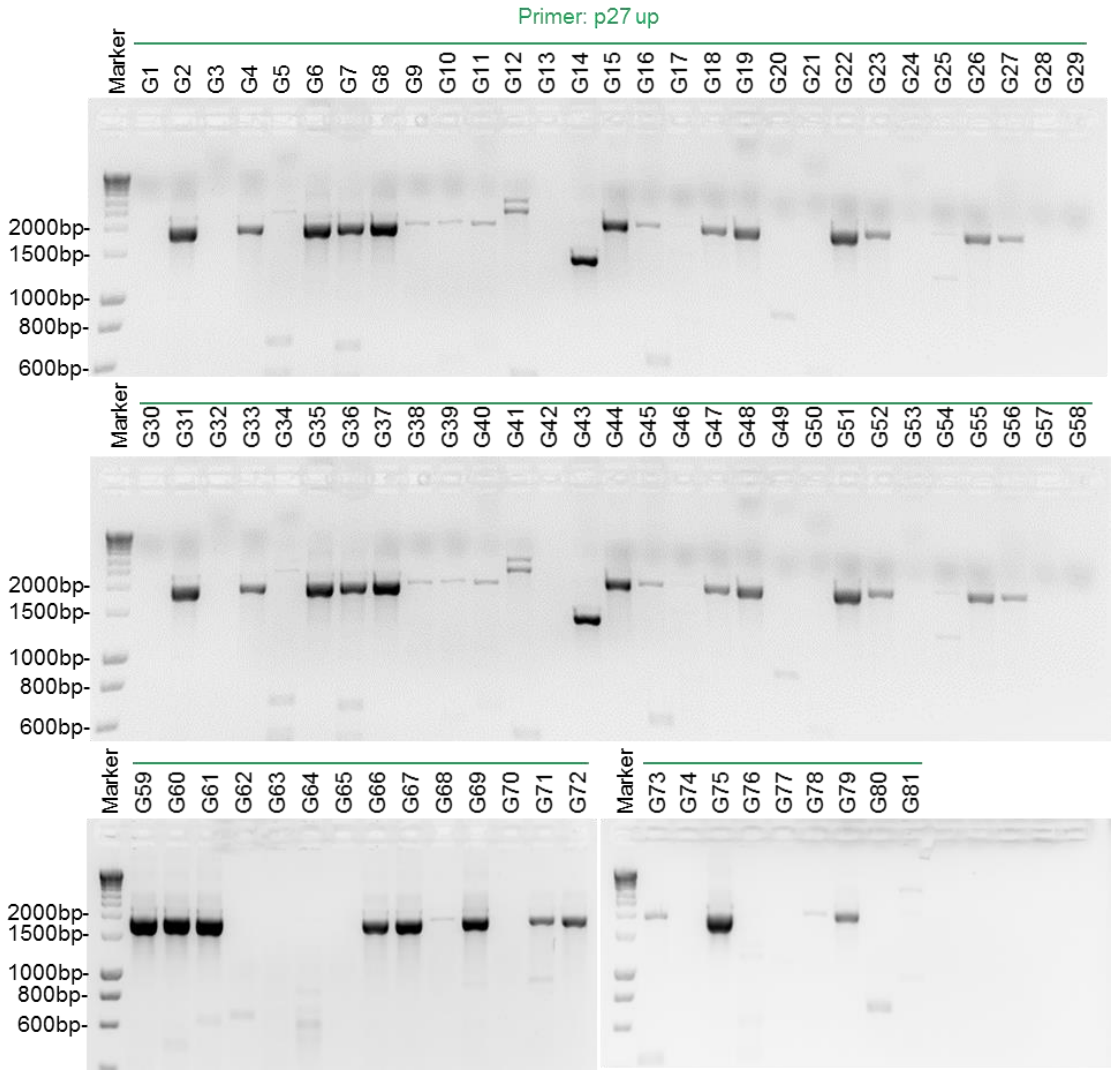


Figure 4.6. Genotyping of the 81colonies by primer p27 up. The total lysate from each single colonies were subjected to PCR by p27 up primers showed in figure 4.3.

Some of these 44 colonies occupied an extremely slow growth ratio or dramatic appearance changing. Finally, we chose 10 colonies to do further verification. Four of them cannot be seen that the increase of GFP intensity after serum starvation and another four were doubted as multiple colonies (not all cell's fluorescence intensity increased) (Figure 4.7). Clone G44 and G55 showed the characteristics of promising candidates, which including similar doubling time and also are sensitive to serum starvation with parental cell (Figure 4.8A & B). However, genotyping demonstrated that G44 is a biallelically integrated clone while G55 is a monoallelically edited clone (Figure 4.8 C). The fused protein p27-EGFP can be both detected by p27 and GFP antibody

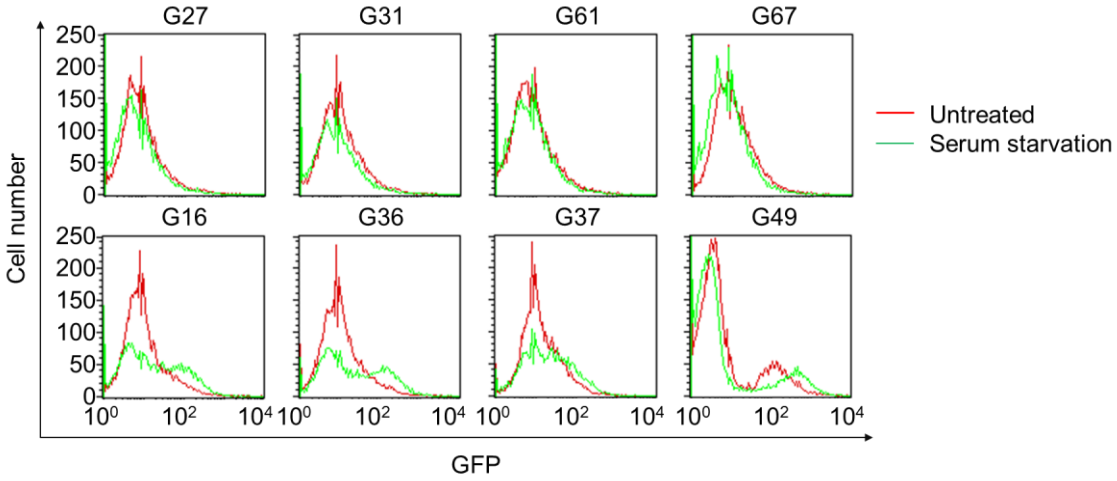


Figure 4.7. Flow cytometer analysis the shift of GFP before and after serum starvation in the 8 colonies. Each sub-cell lines were treated with or without serum starvation were subjected to flow cytometry.

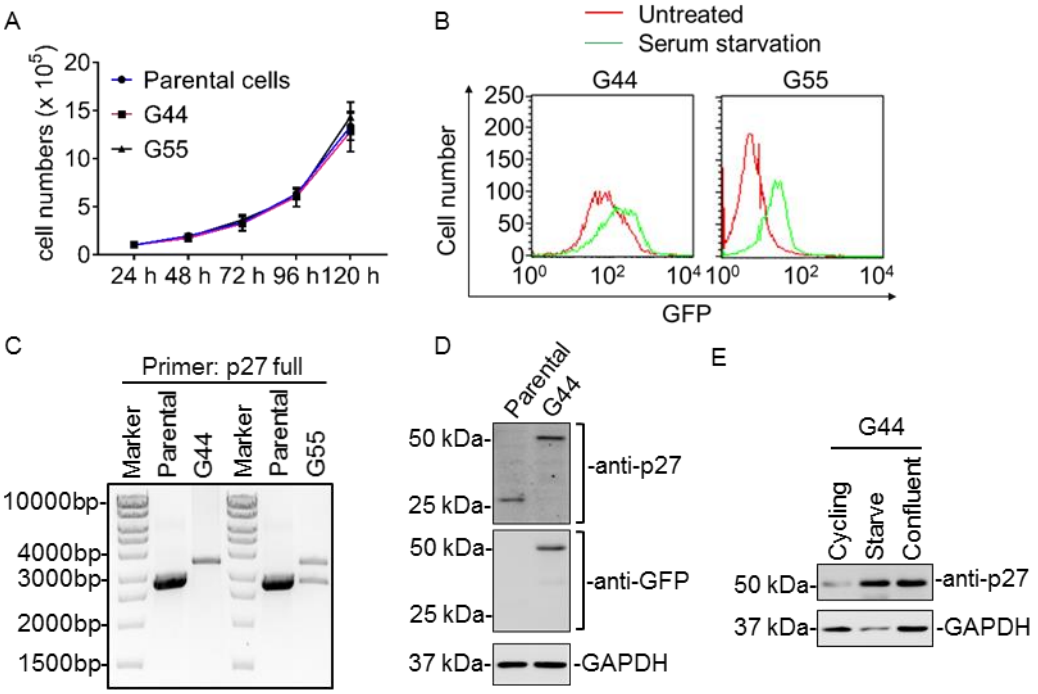


Figure 4.8. Verification of the phenotypes and genotypes of G44 and G55. **A,** Viable cells were counted in an automated cell counter 24, 48, and 72 hours after seeding. **B,** Flow cytometer analysis the shift of GFP before and after serum starvation in the G44 and G55. **C,** The genomic DNAs were extracted from Mel-RM, G44 and G55 cells and subjected PCR. P27 full primers were used. The PCR products were separated by Agarose gel. **D,** Mel-RM and G44 were subjected to Western blotting. **E,** G44 cells were treated with or without serum starvation and contact inhibition were subjected to Western blotting.

(Figure 4.8 D). In addition, the fused protein increased after serum and contact inhibition (Figure 4.8E). But the monoallelically integration G55 is too dim to take photos under microscope (data not shown), we chose G44 for further study (Figure 4.9).

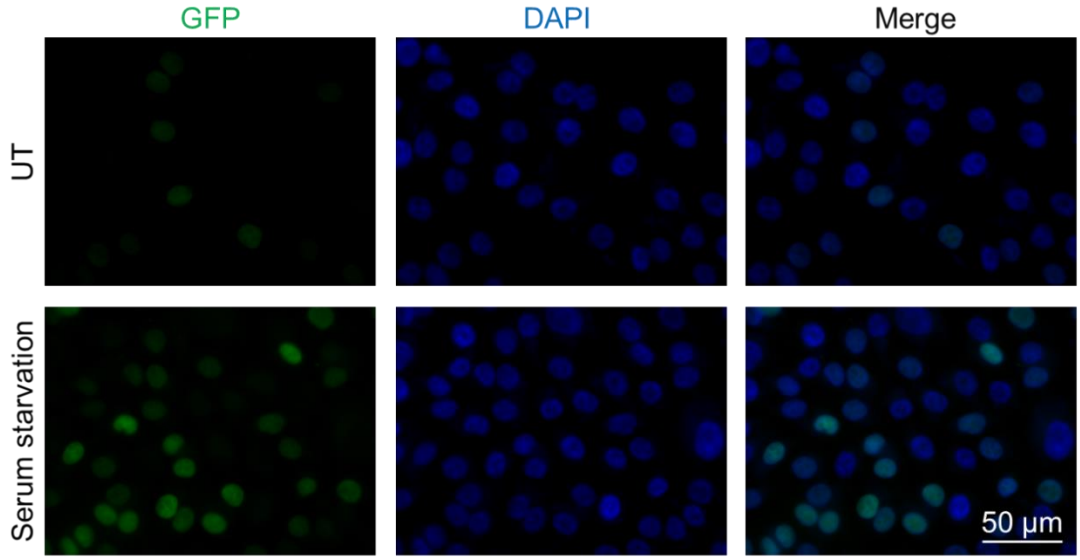


Figure 4.9. The representative images of G44 cell after DAPI staining before and after serum starvation.

### 4.2.3 Generation of MKI67-mCherry HD KI Mel-RM subline

Ki67 is a nuclear protein and encoded by the *MKI67* gene in human. As a cellular marker of proliferation, the protein is present during all active phase of cell cycle, especially, it located to the surface of chromosome in mitosis. The immunostaining of Ki67 exhibited dot-like staining. Nucleofection following with puromycine and SCR7 selection, FACS showed there were 4.83% cells expressed mCherry fluorescence. While the cells only electroporated by donor showed 0.2% mCherry positive cells (Figure 4.10).

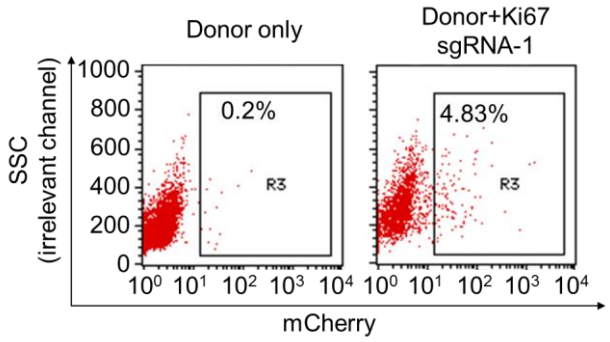


Figure 4.10. The mCherry positive single cells were sorted into each wells of 96 well plate.

We sorted the mCherry positive cells to three 96-well plates. Ninety-four colonies grew up while 35 displayed a mCherry insertion (Figure 4.11A). We picked up the 10 colonies which showed happy appearance and proliferation rate (R6, R36, R37, R39, R51, R53, R63, R67, R75, R92 ) to perform DAPI staining (Figure 4.11B). All the location of ki67/mCherry showed a nuclear- and dot-like pattern. We chose R53 to do further study. Genotyping by primer ki67 full indicated R53 is a biallelically integrated clone (Figure 4.11C). Furthermore, the mCherry fluorescence is sensitive to serum starvation, and MEK inhibitor, which are the two ways to arrest cells to quiescent state (Figure 4.12B). Here, we found MEK inhibitor is a more efficient way to arrest Mel-RM to quiescent cells, which can arrest more than 50% cells during 24 hours and more than 95% cells after 48 hours in G0 phase (Figure 4.12A). Since serum starvation is a gentle method, we use MEK inhibitor for further study.

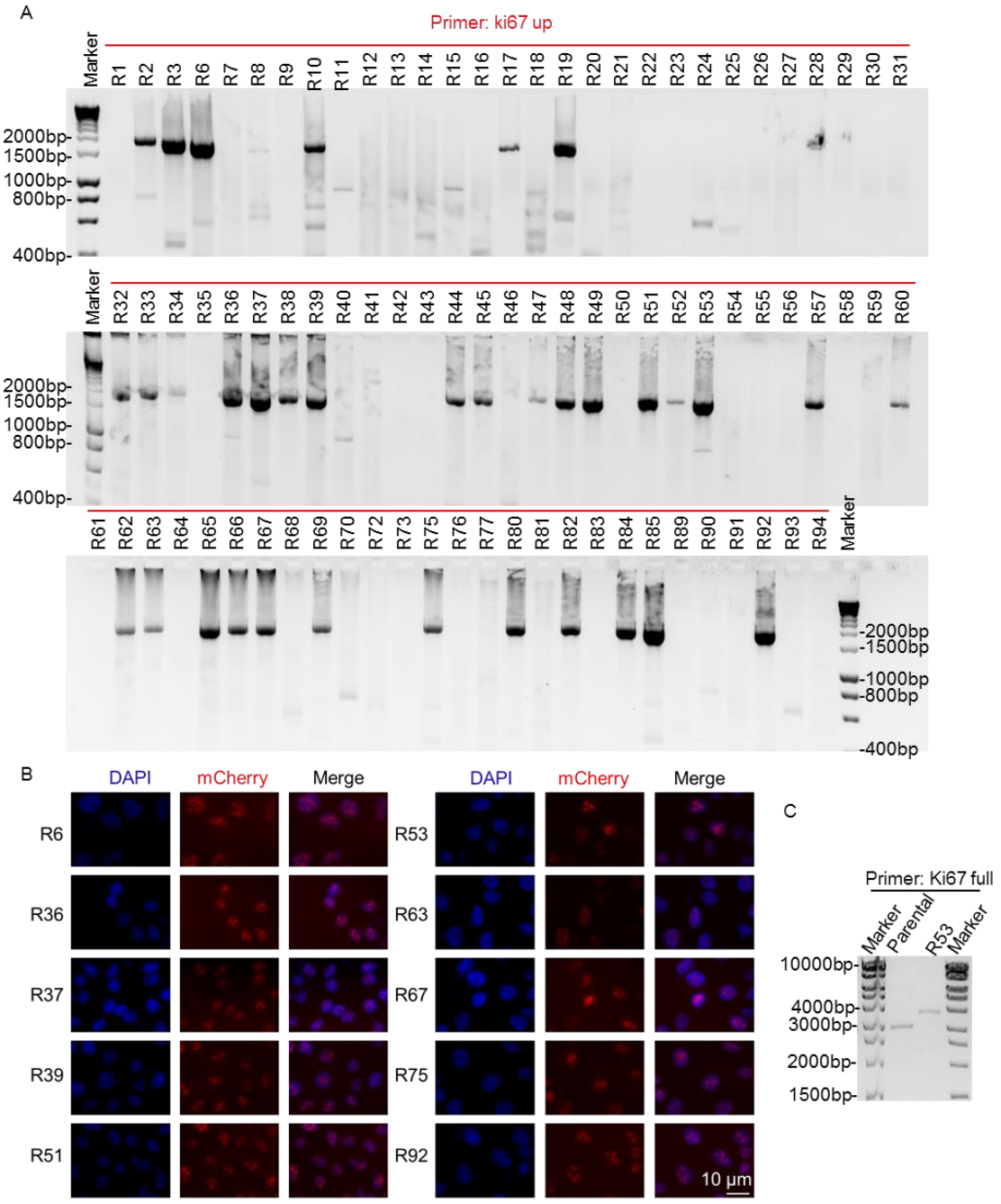


Figure 4.11. The genotyping and phenotyping of Ki67/mCherry cells. A, Genotyping of the 94 colonies by primer Ki67 up. The total lysate from each single colonies were subjected to PCR by Ki67 up primers showed in figure 4.4. B, The representative images of mCherry knock-in cells after DAPI staining. C, The genomic DNAs were extracted from Mel-RM and R53 cells and subjected PCR. Ki67 full primers were used. The PCR products were separated by Agarose gel.

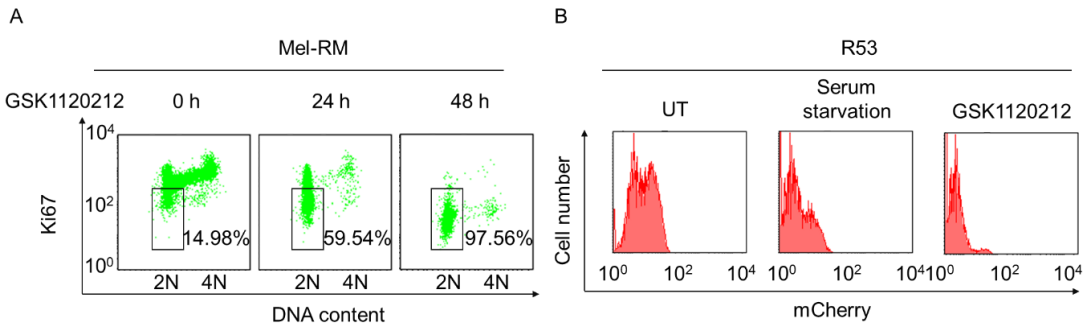


Figure 4.12. Flow cytometer analysis the shift of mCherry before and after serum starvation and MEK inhibitor treatment**. A,** Mel-RM cells were treated by 1μM MEK inhibitor GSK1120212 for indicated periods and subjected to Propidium iodide and Ki67 staining. Diploid and Ki67 negative cells were gated as G0 cells. **B,** R53 cells were treated by serum and 1μM MEK inhibitor GSK1120212 for 48 hours and subjected to flow cytometry analysis.

### 4.2.4 Generation of CDKN1B-EGFP/MKI67-mCherry HD KI Mel-RM subline (Mel-RM.pK)

The above data showed that both CDKN1B-EGFP knock-in and MKI67-mCherry knock-in are workable in Mel-RM cells. Next, we tried knock-in mCherry to G44 as well as knock-in EGFP to R53. The results illustrated both way are feasible. Here, we take integrating EGFP before p27 stop codon in R53 as an example to get the dual-fluorescence insertion. Before starting the next round insertion, we keep culturing the R53 for one month to dilute the retention of lentiCRISPR v2.0/Ki67 sgRNA-1 which includes puromycin resistant gene. Since we usually incubate the cells with puromycin just for 24 hours to kill the untransfected cells, cells are usually re-sensitive to puromycin again after keep feeding for one month. We used the same methods to integrate EGFP to R53. Thirty-six colonies were picked up. Since we have noticed that MEK inhibitor can arrest Mel-RM cell to quiescent state, we used FACS to detect the shift GFP of the 36 coloines before and after GSK1120212 treatment first. According to previous experience (Figure 4.8B), colonies with relative high GFP were collected for further confirmation of the genotypes and phenotypes. However, RG11, RG13 and RG30 were two colonies stand for colonies with dim GFP. Both PCR and Western blotting indicate colony RG28 is a good colonies with both GFP and mCherry knock-

in (Figure 4.13). To make sure the accurate insertion, we amplified the knock-in site by p27 full and ki67 full primer separately by PCR (Figure 4.14). The PCR product were ligated into T vector. The exactly insertion sequences were confirmed by Sanger sequencing. The aligned full sequences are not shown.

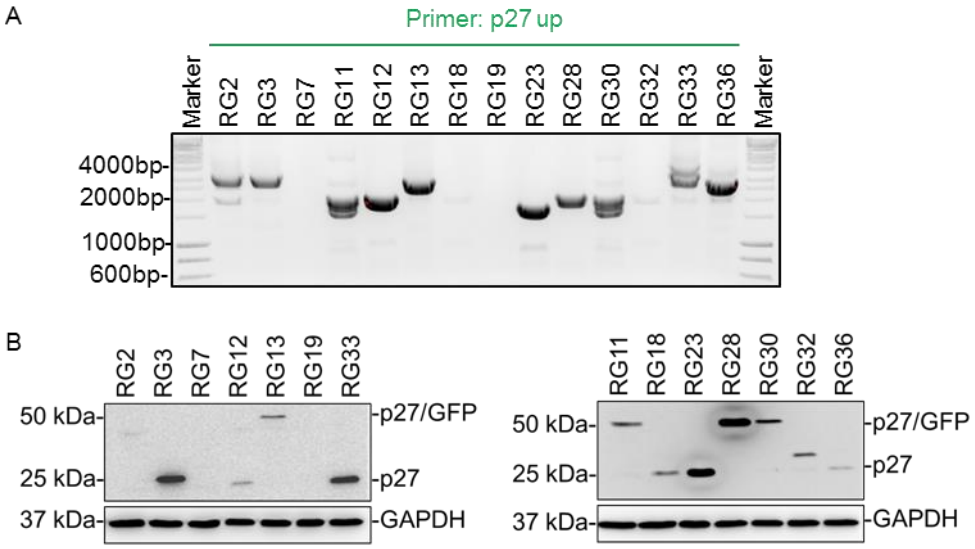


Figure 4.13. Genotyping analysis of the EGFP knock-in in the candidature colonies in Mel-RM cells. **A**, PCR analysis of targeted allele containing the EGFP insertion in the candidature colonies. Primer p27 up were used here. **B,** Western blotting confirm the fused protein p27-EGFP in the candidature colonies.

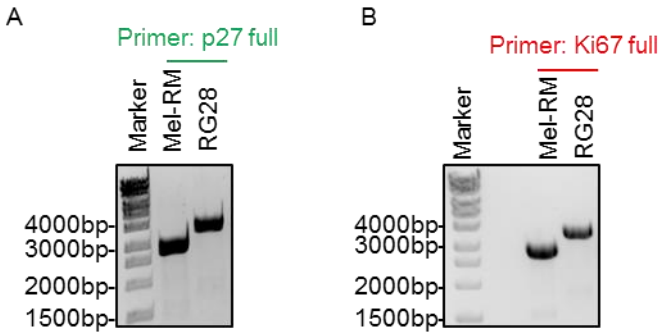


Figure 4.14. Genotyping analysis of the dual-fluorescence knock-in RG28 cells. **A,** PCR analysis of the targeted CDKN1B allele of Mel-RM and RG28 cells. The location of the primers were showed in Figure 4.3. **B,** PCR analysis of the targeted MKI67 allele of Mel-RM and RG28 cells. The location of the primers were showed in Figure 4.4.

### 4.2.5 Generation of CDKN1B-EGFP/MKI67-mCherry HD KI HeLa subline

HeLa cell is a commonly used cell line that is remarkably durable and prolific. It is also a cell line that was used to study cell cycle[76]. We adapted the same strategy to get the dual-knock-in HeLa cells. Thirty-five of forty-eight colonies had EGFP insertion based on PCR (Figure 4.15A). Considering together with the detection of the fused p27-EGFP by Western blotting (Figure 4.15B), we chose AG21 for further mCherry knock-in. Fourteen of 261 colonies were positive inserted according PCR (Data not shown). We verified the location of the fusing proteins under microscope of AG21/R130 cells which performed as expected (seldom cells express highly p27 and most of the cells display a dot-like ki67 expression) (Figure 4.15C). Live cell image shows that the expression and localization of p27 and Ki67 as a cell cycle dependent manner. This is to say that the bright green fluorescence only can be seen after mitosis following nuclear envelope reformation, which means G1 phase. While the intensity of mCherry reach to the peak before cells detached and become round, which represents M phase (Figure 4.15D).

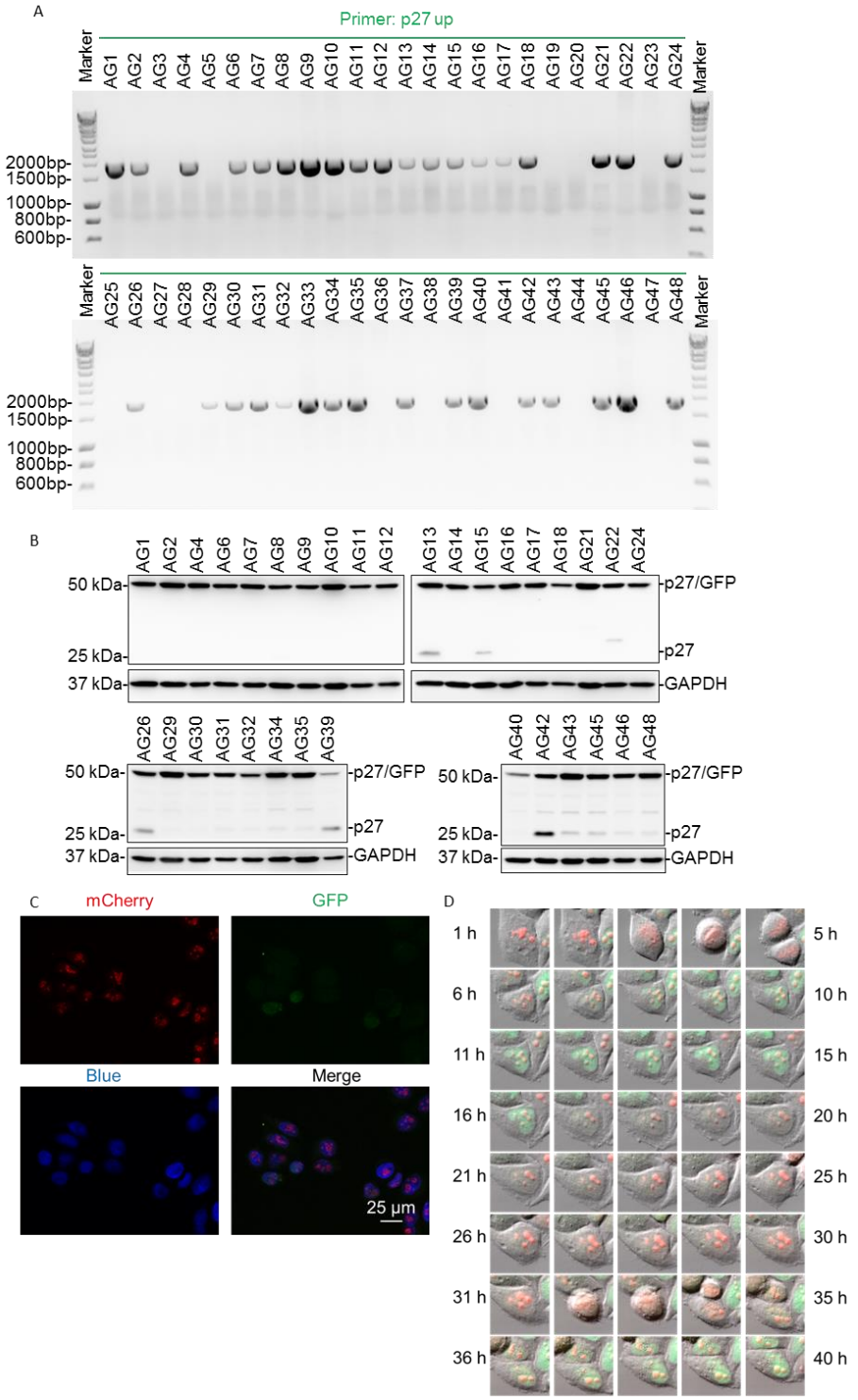


Figure 4.15. The establishment of CDKN1B-EGFP/MKI67-mCherry HD KI HeLa subline. **A,** Genotyping EGPF insertion in HeLa cells by p27 up primer. **B,** Thirty-three colonies were subjected to Western blotting to confirm the fusing protein p27-EGFP. **C,** Representative image of AG21/R130 cells. **D,** Cell cycle-dependent changes in fluorescence of p27-EGFP and Ki67-mCherry in AG21/R130 cells.

### 4.2.6 Off-target detection in Mel-RM.pK (RG28) cells

CRISPR-Cas9 specificity depends on the first 20 bp sgRNA and there is some off-target effect. The method of off-target detection analysis and filtering by the comparison method is as follows: (1) Compare the single experimental group sample with the SNV/Indel of the control sample, and take the unique SNV/Indel site of the experimental group as a potential off-target site. (2) According to the potential off-target site in step (1), the 100 bp sequence upstream and downstream of the site is captured in the reference genome as a potential off-target region. (3) Using the alignment software Blast (version 2.3.0+), the gRNA sequence was aligned with the potential off-target region, allowing up to 6 mismatches, but requiring a 12-bp perfect match before the PAM sequence. (4) Comparison of the mutation sites in the results without the PAM sequence (NRG). (5) Filtration of a mutation site in which a base tandem repeat exists. (6) The retention mutation occurs at the site of the gRNA alignment region (20 bp) as a possible off-target site.

The offer target sites in RG28 were summarized in table 4.2 and table 4.3 for p27 sgRNA-2 and Ki67 sgRNA-1 separately. All the off target happened in intron or intergenically without amino acid changing, which means, have limited effect on the cells.

**Table 4.2. The summary of off target sites induced by p27 sgRNA-2**

| | | | | | | | | | RG28 | | | Mel-RM | |
|---|---|---|---|---|---|---|---|---|---|---|---|---|---|
| #CHROM | POS | REF | ALT | Func | Gene | Exonic Func | AAChange | Homo/Hete | Depth | Frequency | Homo/Hete | Depth | Frequency |
| chr13 | 97876882 | CAAA | CA,C | intronic | MBNL2 | . | . | Hete | 19 | 0.526,0.368 | Homo | 25 | 0.96 |
| chr16 | 33539354 | AT | A | intergenic | LOC390705;ENPP7P13 | . | . | Hete | 44 | 0.795 | Homo | 35 | 0.857 |
| chr16 | 33539356 | T | A | intergenic | LOC390705;ENPP7P13 | . | . | Hete | 44 | 0.795 | Hete | 37 | 0.838 |
| chr2 | 1.09E+08 | C | CT | intergenic | RGPD4;SLC5A7 | . | . | Hete | 40 | 0.65 | Homo | 30 | 0.833 |
| chr3 | 1.68E+08 | G | GTATA,GTA | ncRNA_intronic | EGFEM1P | . | . | Homo | 7 | 1 | Hete | 8 | 0.25,0.625 |
| chr4 | 74068035 | TAA | TA,T | intronic | ANKRD17 | . | . | Hete | 6 | 0.667 | Homo | 9 | 0.778 |
| chr5 | 10738608 | C | T | intronic | DAP | . | . | Hete | 41 | 0.293 | . | . | . |
| chr6 | 1.61E+08 | C | CTT,CT | intergenic | SLC22A2;SLC22A3 | . | . | Hete | 16 | 0.312 | Hete | 12 | 0.333 |
| chr6 | 1.63E+08 | TTTG | T | intronic | PARK2 | . | . | Homo | 12 | 1 | Homo | 34 | 1 |
| chr6 | 1.63E+08 | CTGTGTGTG TGTG | CTGTG,C | intronic | PARK2 | . | . | Hete | 10 | 0.8,0.2 | Homo | 31 | 1 |

Table 4.3. The summary of off target sites induced by Ki67 sgRNA-1

| | | | | | | | | | RG28 | | | RM | |
|---|---|---|---|---|---|---|---|---|---|---|---|---|---|
| #CHROM | POS | REF | ALT | Func | Gene | ExonicFunc | AAChange | Homo/Hete | Depth | Frequency | Homo/Hete | Depth | Frequency |
| chr22 | 26195098 | T | TTGTGTGTG,TTGTGTGTG | intronic | MYO18B | . | . | Hete | 21 | 0.667,0.333 | Hete | 20 | 0.65,0.35 |

Note of table 4.2 and 4.3

(1)CHROM：the chromosome of the site；

(2)POS：the position on the chromosome；

(3)REF：the genotype in the reference genome；

(4)ALT：the genotype of the mutation；

(5)Func：Genomic compartment of the mutation；

(6)Gene: The gene nearest to the mutation；

(7)ExonicFunc：variant type of this site on the exon region of the annotation in the RefGene database；

(8)AAChange: amino acid changes; annotated by each transcript. Information divided by colon meas gene name, transcript name, exon mutation, amino acid position of mutation and protein mutation.

(9)Hete/Home：homozygosity and heterozygosity；

(10)Dp：sequencing depth of the site；

(11)Fre：mutation frequency

## 4.4 Discussion

We have established two cell lines with endogenous p27 fused with EGFP and Ki67 fused with mCherry. By using this system, we can track the expression and localization of endogenous p27 and Ki67 without disturbing the cells. We show that the intensity of the two kinds of fluorescence in Mel-RM cells changes under different conditions, especially after the treatment with MEK inhibitor, which can arrest most of the cells at G0 phase.

HeLa cells divide quicker than Mel-RM cell. It is hard to see the quiescent cells. In addition, it is hard to arrest HeLa cells at G0 phase (Data not shown). We tried lovastatin, which blocks the activity of HMG-CoA reductase, to arrest G0 cells. It can arrest small population of quiescent cells in a short period (24 hours) by low dose (10 μM) (Data not shown). Longer exposure (more than 36 hours) will induce massive apoptosis. Neither serum starvation nor contact inhibition can arrest HeLa cells into quiescent state dramatically. We tested the shift of the two kinds of fluorescence after lovastatin treatment. The shifts were as we expected but slightly. We took live cell images by ZEISS Celldiscoverer 7 of the cells. The two kinds of fluorescence behave a cell cycle-dependent manner. We cannot see any pause of proliferation in HeLa cells under the microscope. None of the two types of fluorescence expresses extremely high or extremely low. This indicates that the accumulation and degradation of the fused proteins are very efficiently. The no stop proliferation also hints that there is no quiescent status in HeLa cells. Therefore, HeLa cell is not a good model to study quiescent cells.

However, this is not the case in Mel-RM cells. In Mel-RM cells, the expression pattern of the two kinds of fluorescence are heterogeneous. We can see in the most of the cells, the two kinds of the fluorescence still behave a cell cycle-dependent manner. While a small population of the cells are always expressing very bright green fluorescence. Furthermore, it seems these cells are not dividing.

In summary, the expression of the two kinds of fluorescence in HeLa cells shows a cell cycle-dependent manner. This indicates that the labelling can be used as a cell cycle indicator. Considering the

complicated and heterogeneous expression pattern of the two kinds of fluorescence in Mel-RM cells, which hints the heterogeneity of this cell lines, especially the small population of the cells which are always showing a high p27 level, we will use Mel-RM as a model to study cellular quiescence. Further explanation will be shown in the following chapters.

# Chapter Five Characterization of the quiescent cancer cells by RNA sequencing and proteomics

## 5.1 Introduction

Flow cytometry is a technique used to detect and measure physical and chemical characteristics of a population of cells or particles by flow cytometer. Cell sorting is one of the main utilizations of flow cytometer. FACS, utilizes flow cytometry to provide a fast, objective and quantitative measurement for sorting a heterogeneous mixture of cells. Since we have labelled the endogenous p27 and Ki67 with GFP and mCherry separately in last chapter, we will adapt FACS to isolate the $p27^{high}/Ki67^{low}$ cells as quiescent cancer cells while the rest population are cycling cells.

Omics, such as genomics, proteomics or metabolomics, aims at the collective characterization and quantification of pools of biological molecules that translate into the structure, function, and dynamics of an organism or organisms.

The transcriptome is the complete set of transcripts in a cell, and their quantity, for a specific developmental stage or physiological condition[244]. It is the relative levels of the transcripts, especially noncoding RNAs, determine cell fate, function and characteristics. It is also critical for understanding development and disease[245]. Here, we employed RNA sequencing (RNA-Seq) to uncover the transcriptome of quiescent cancer cells relative to cycling cancer cells.

RNA-Seq, also called whole transcriptome shotgun sequencing (WTSS), uses NGS to reveal the presence and quantity of RNA in a biological sample at a given moment[246]. The key aims of transcriptomics are: to catalogue all species of transcript, including mRNAs, non-coding RNAs and small RNAs; to determine the transcriptional structure of genes, in terms of their start sites, 5' and 3' ends, splicing patterns and other post-transcriptional modifications; and to quantify the changing expression levels of each transcript during development and under different conditions[245]. The differential expressed genes usually play vital role in the related phenotype.

Proteins are the most vital parts of living organisms, with many functions. The proteome is the entire set of proteins that is produced or modified by an organism or system[247]. Proteomics is the large-scale study of proteins. Proteomics is more complicated than genomics because an organism's genome is more or less constant, whereas proteomes differ from cell to cell and from time to time. This is also the significance of proteomics, which is reveal the mechanism behind different phenotypes. Since the poor correlation between RNA expression and protein levels[248], it is more accurate to use proteomics to assess the distinct profile between different samples. Proteomics confirms the presence of the protein and provides a direct measure of the quantity present.

Not only does the translation from mRNA cause differences, but many proteins also are subjected to a wide variety of chemical modifications after translation. The most common and widely studied post translational modifications include phosphorylation and glycosylation. Many of these post-translational modifications are critical to the protein's function. Phosphorylation modification happens commonly in many enzyme to active the activity of the reaction. It is also very critical in the process of cell signalling. Proteomics can be utilized to determine the set of phosphorylated proteins in particular samples to uncover the active or inactive pathway. In addition to phosphorylated modification. Proteins also can be modified by methylation, acetylation, glycosylation, oxidation, and nitrosylation. Therefore, a proteomics study could become complex in certain circumstance. For example, methods such as phosphoproteomics and glycoproteomics are used to study post-translational modifications.

One major factor affecting reproducibility in proteomics experiments is the simultaneous elution of many more peptides than mass spectrometers can measure[249]. Also, different instruments, software, samples, the methods of sample preparation and et al. contribute to the reproducibility of proteomics[250, 251, 252, 253].

Quantitative mass spectrometry-based proteomic methods enable the measurement of protein abundance changes across multiple proteomes[249]. In this chapter, we employed expression proteomics to find the proteins highly expresses in quiescent cells rather than cycling cells.

Extracting biological insight is as important as omics itself. By analysing the omics data, we can find the most upregulated and downregulated genes. But usually, it is the change of gene sets but not only a unique gene that make big difference.

Ingenuity Pathway Analysis (IPA) can be used to help researchers analyse omics data and model biological systems. The input of IPA is usually the differential expression (DE) gene with strict cut off. While gene set enrichment analysis (GSEA) is a method to identify classes of genes or proteins that are over-represented in a large set of genes or proteins, and may have an association with disease phenotypes. Since cells are always get a tendency to resist change in order to maintain a stable, relatively constant internal environment, a slight activation or inactivation of a pathway maybe enough to induce dramatically phenomenon change. GSEA accept all coding gene expression list, no matter it is differential expressed or not. Thus, even small contribution of one gene can be calculated into the results.

As discussed in last chapter, HeLa.pK cells is not a good model to study quiescent cells, we will focus on Mel-RM. pK cells in these chapter to systematically characterize quiescent cancer cells.

## 5.2 Results

### 5.2.1 Time lapse photos of Mel-RM.pK

Although both of HeLa.pK and Mel-RM.pK subline are came from a single cells, the proliferation of these two sublines are showing different pattern. The dividing of each HeLa.pK cells are non-stop and the doubling time of each cells are very even. Strikingly, the proliferation of Mel-RM.pK cells are heterogeneous. The cells without any treatment represent different doubling time (Fig.5.1). It can be seen that the more p27 or GFP, the longer of the cell cycle (Fig.5.1A & B).

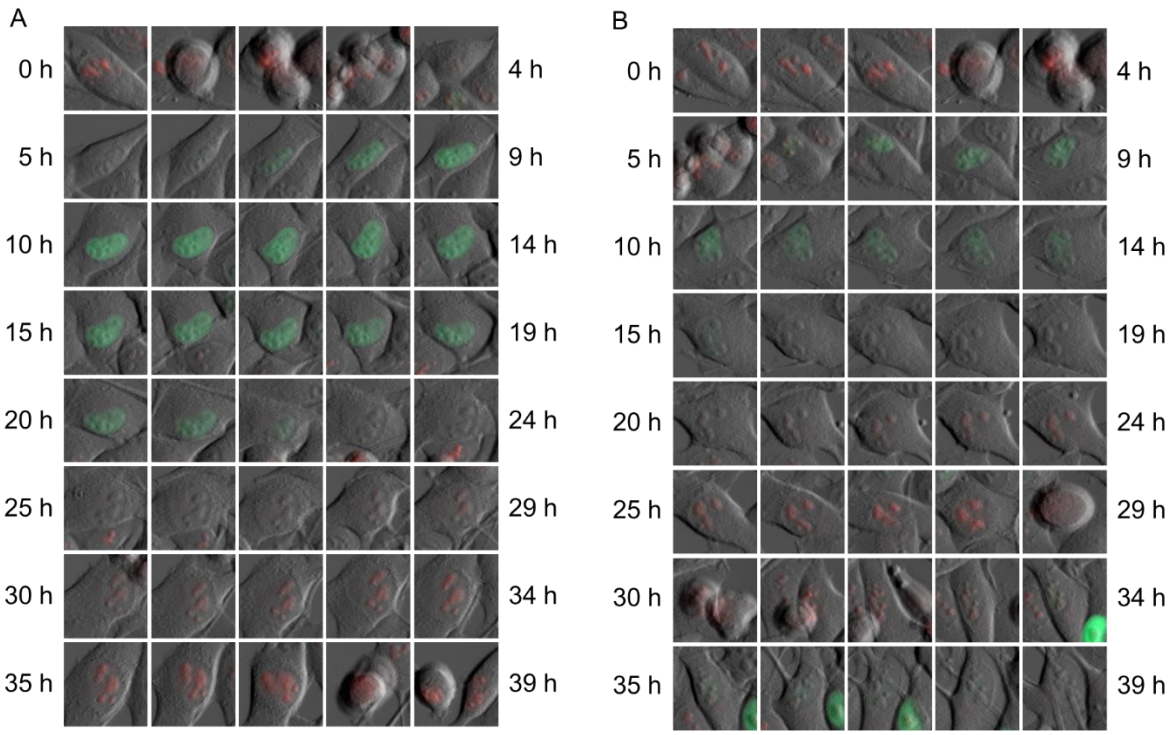


Figure 5.1. Reprehensive time-lapse photos of cycling Mel-RM.pK (RG28) cells. **A&B,** Two single cells with difference levels of p27 (GFP) after mitosis display different doubling time.

We also observed that some of the cells which showing extremely high levels p27 do not divide, or failed for dividing even they try with a frequent motion (Fig. 5.2A). We also can observe that some of these very green cells entered into cell cycle and finished two more mitosis (Fig.5.2B). This indicates

the dormant status of these cells are reversible and temporary, which means they are quiescent cells but not senescent cells.

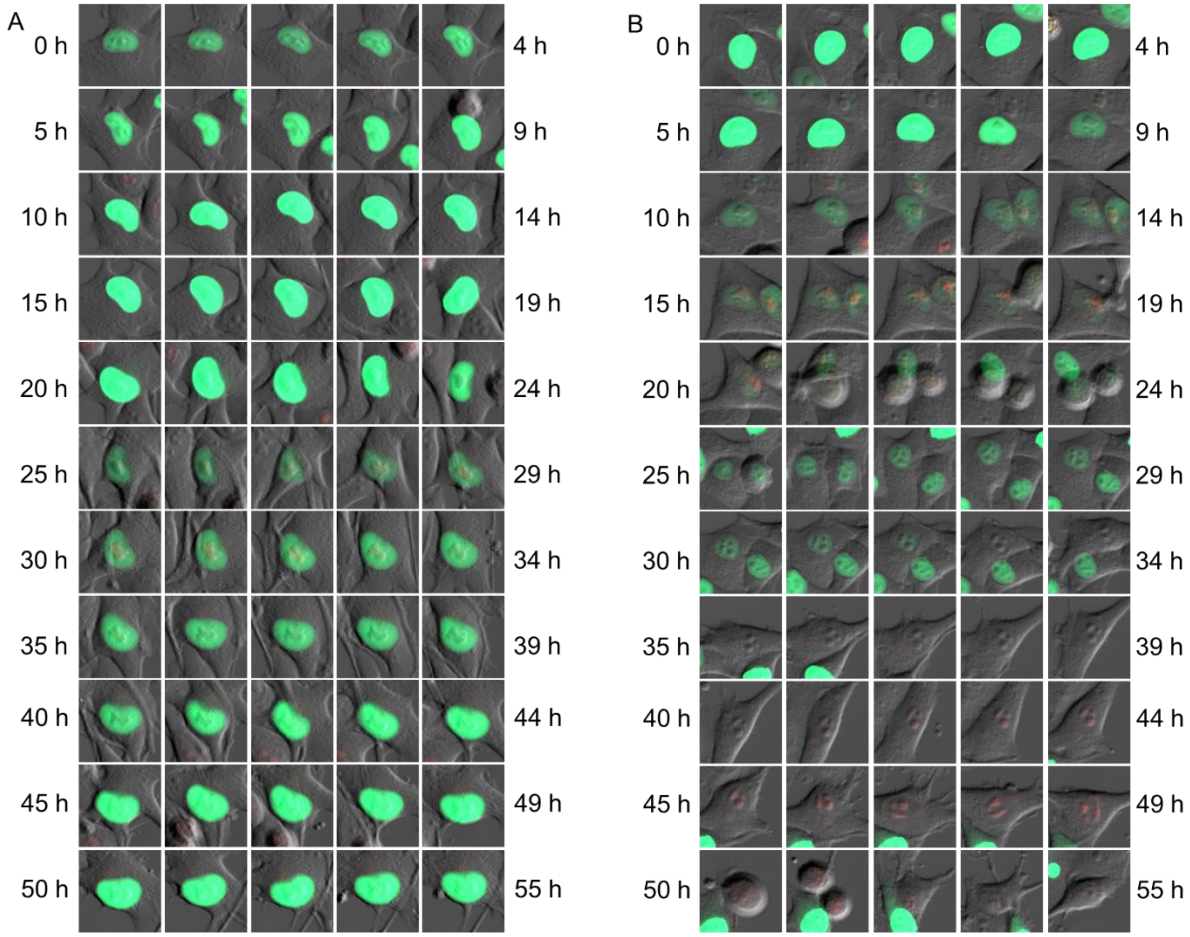


Figure 5.2. Reprehensive time-lapse photos of quiescent Mel-RM.pK (RG28) cells**.**

### 5.2.2 Isolation of human quiescent cancer cells by using Mel-RM.pK cells.

The Mel-RM.pK cells were analysed by flow cytometer. The $p27^{high}/Ki67^{low}$ cells were gated as quiescent cells. As can be seen in Figure 5.3, quiescent cells can be arrested by serum starvation and MEK inhibitor. The proportions of quiescent cells which arrested by MEK inhibitor are consistent with the results in Figure 4.12.

We sorted the cycling (C) and quiescent (Q) cells according to the gate is shown in Figure 5.4. The sorted cells were verified by Western bloting. In comparison with cycling cells, quiescent cells express less pRb and p-CDK2 (T160), which are two phosphorated protein happen in cycling cells. Cyclin A and Cyclin E are also downregulated in quiescent cells (Fig. 5.4).

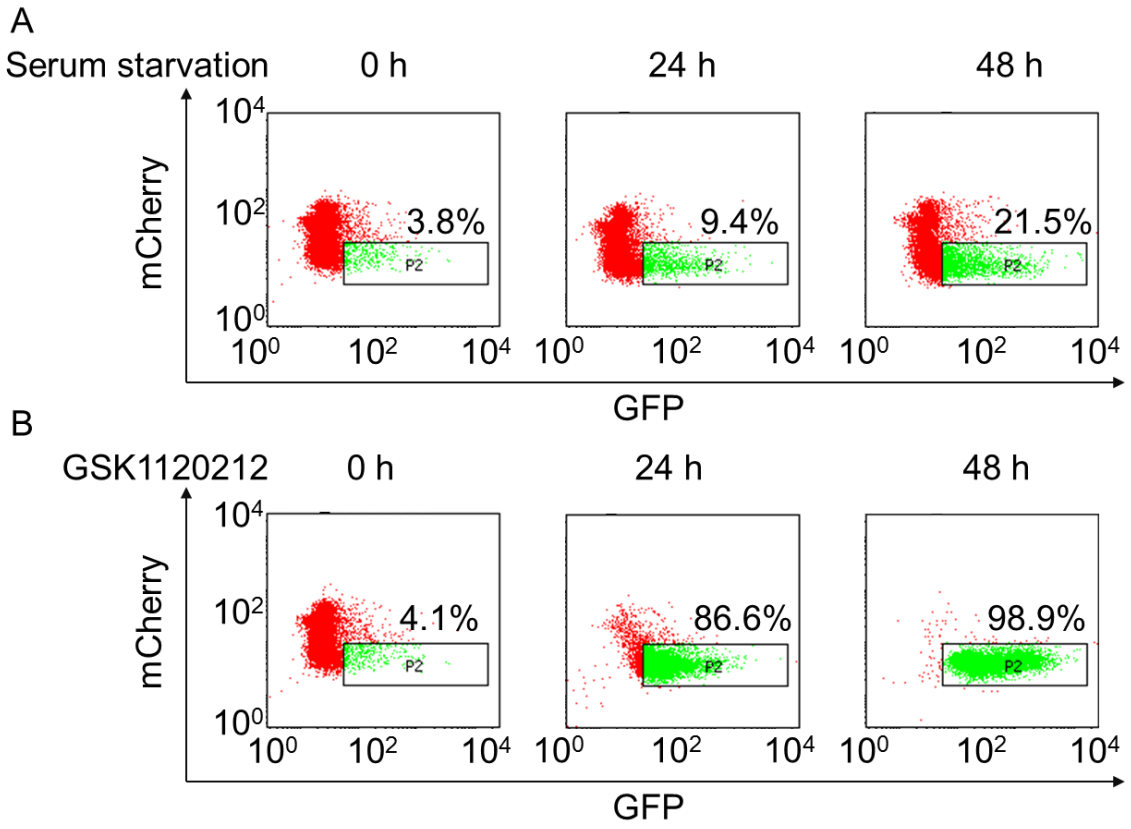


Figure 5.3. The fluorescence shift of Mel-RM.pK cells. **A & B,** The percentages of $p27^{high}/Ki67^{low}$ cells after serum starvation (A) and MEK inhibitor (B) treatment for indicated period.

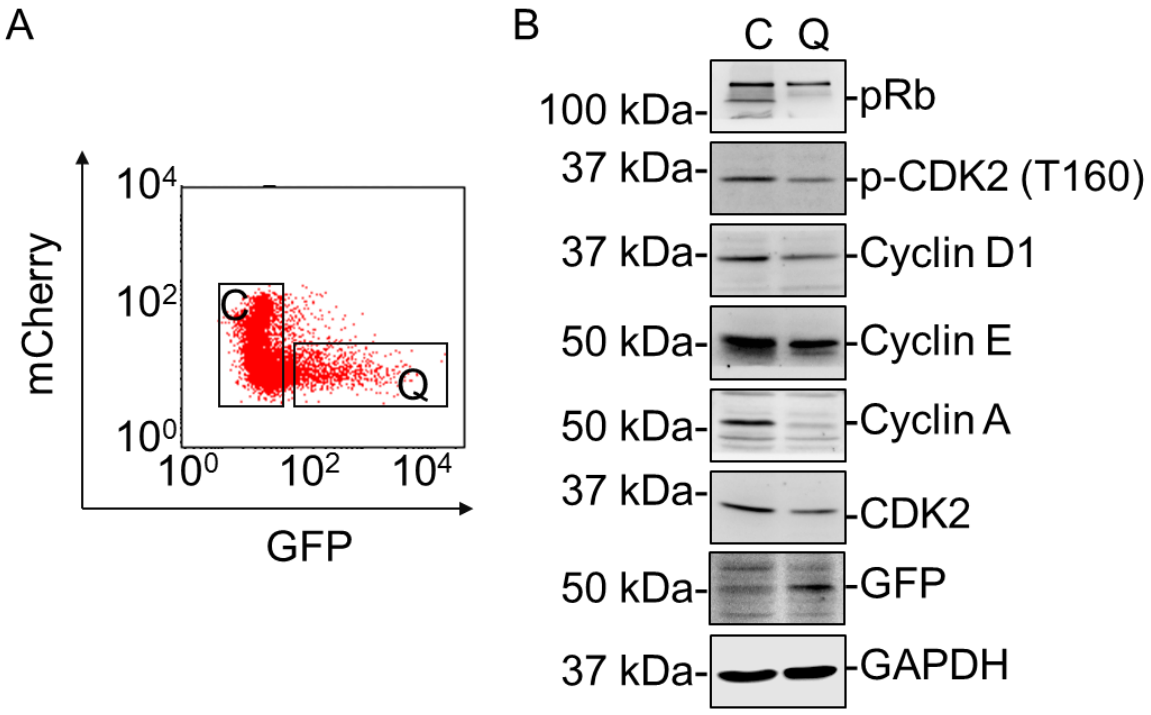


Figure 5.4. The isolation of quiescent (Q) and Cycling (C) cells in Mel-RM.pK cells. **A,** Mel-RM.pK cells were subjected to cell sorting after serum starvation for 72 hours. **B,** The isolated Q and C cell were subjected to Western blotting.

### 5.2.3 Characterization of the quiescent cells in transcriptional level.

The isolated cycling and quiescent cell pellets were subjected to whole transcriptome sequencing. At this stage, I just focus on coding genes. The differential expressed lncRNAs and circRNAs will be studied at postdoc stage.

Adjusted P value <0.05 and fold change>2 were set as a cut off. There are 496 genes significant downregulated in quiescent cells. While 359 genes upregulated in cycling cells (Fig. 5.5A).

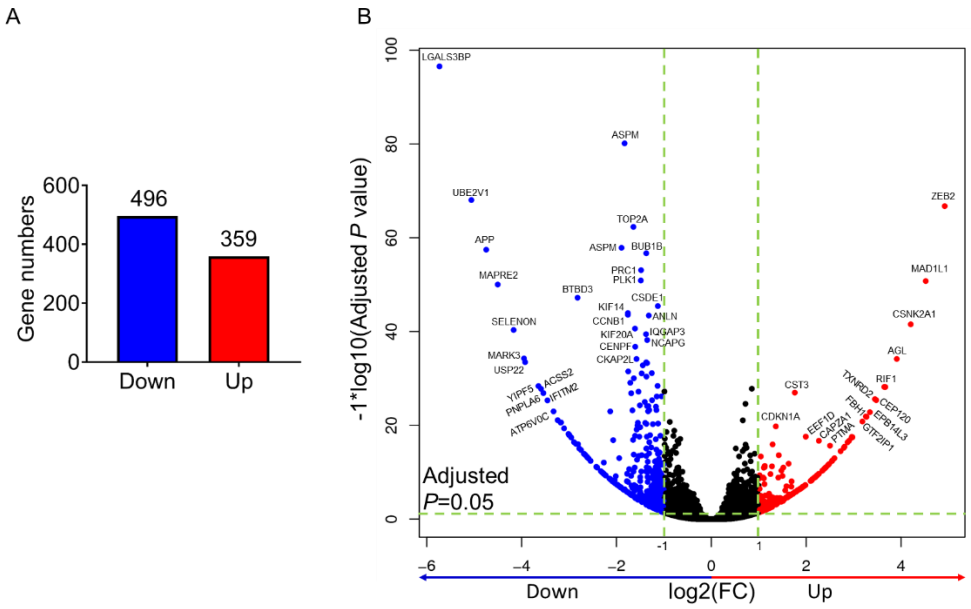


Figure 5.5. A summary of differential expressed coding genes in cycling and quiescent cells. **A,** Illustration of the gene numbers downregulated and upregulated in quiescent cancer cells. **B,** The volcano plot of the differential expression genes in quiescent and cycling cancer cells.

We analysed the differential expressed genes by IPA and found that mitotic roles of polo-like kinase pathway is inactive dramatically in the isolated quiescent cells (Fig. 5.6). The Polo-like protein kinases (Plks) are a conserved family of enzymes that play a variety of roles in the passage of cells through M phase[254]. This hints a clear splitting of mitotic and quiescent cells. The other pathway will be discussed in discussion part.

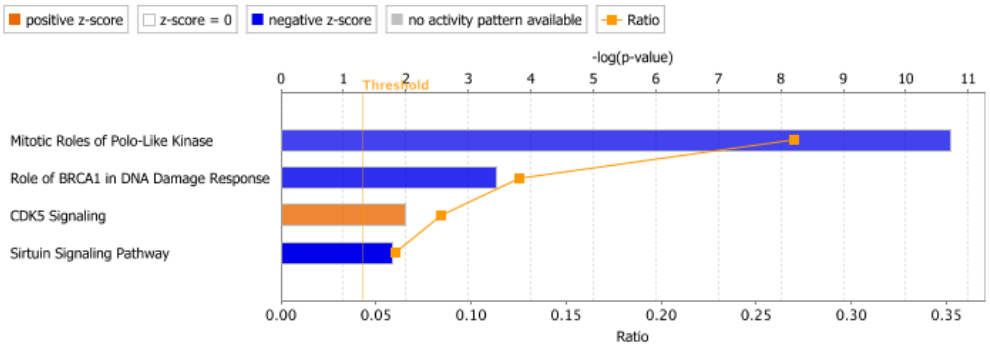


Figure 5.6. IPA analysis the dysregulated pathway in the isolated quiescent and cycling cells. The cut off of Z-score is 2.

GSEA analysed the total expression of 29562 mRNAs indicates that all the mitosis, E2F and G2M progression pathway were enriched in cycling cells rather than quiescent cells as expected (Fig. 5.7), which is consistent with the validation results in Figure 5.4.

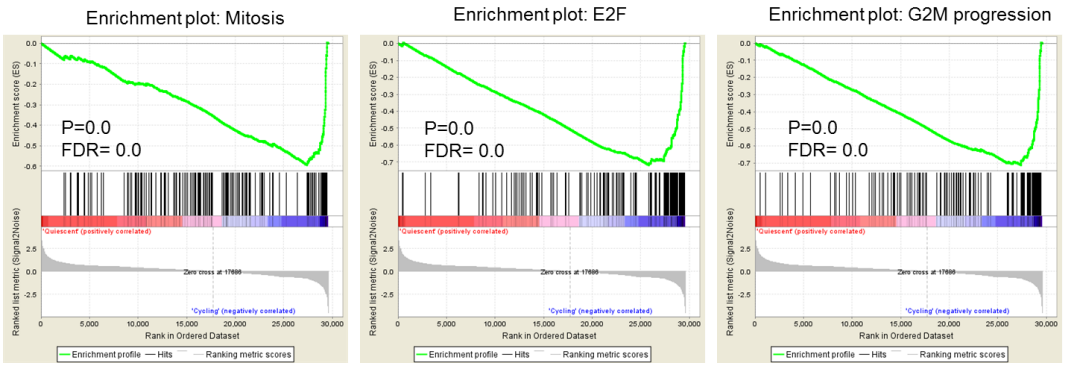


Figure 5.7. Differential expression of transcripts important for cell cycling between $p27^{high}/Ki67^{low}$ quiescent and $p27^{low}/Ki67^{high}$ cycling cells.

## 5.2.4 Characterization of the quiescent cells in protein level.

We also subjected the isolated pellets to iTRAQ 4-plex. GSEA also confirmed the enrichment of cell cycle associated pathway in cycling cells in comparison of quiescent cells (Figure 5.8).

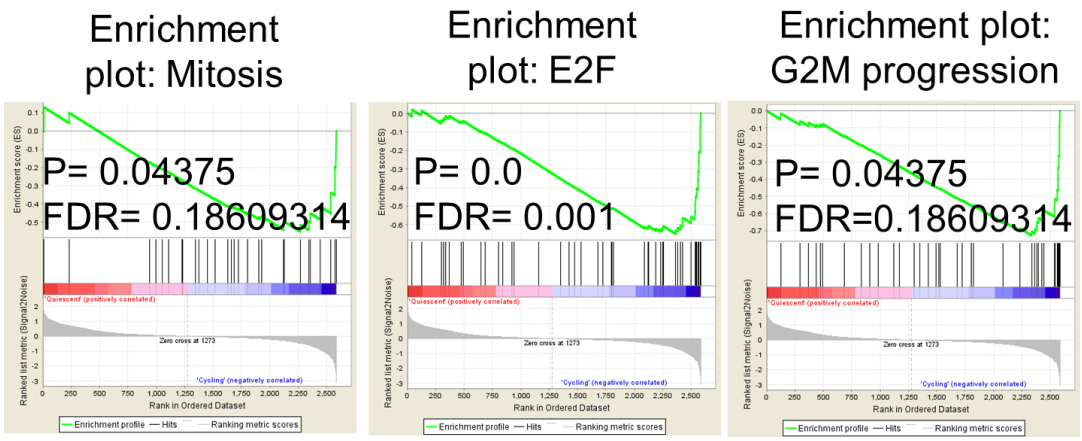


Figure 5.8. Differential expression of proteins important for cell cycling between $p27^{high}/Ki67^{low}$ quiescent and $p27^{low}/Ki67^{high}$ cycling cells.

### 5.4.5 Oxidative phosphorylation is enriched in quiescent cancer cells.

Interesting, Both RNA-seq and proteomics results hint that quiescent rely on oxidative phosphorylation (Fig.5.9).

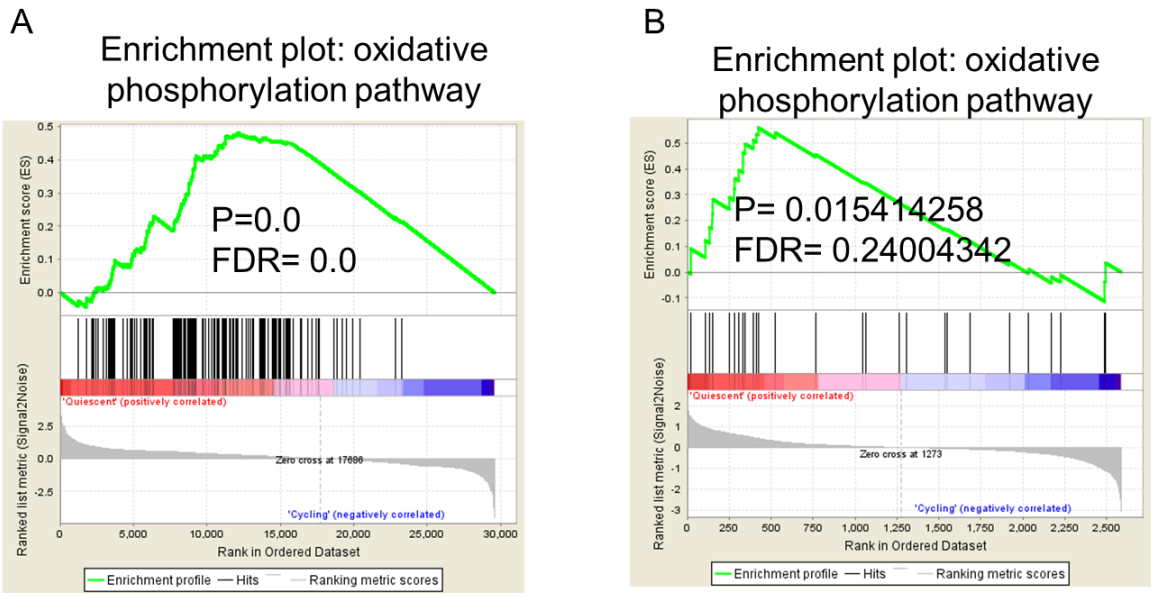


Figure 5.9. A subset of genes of the oxidative phosphorylation pathway are upregulated in quiescent melanoma cells. **A,** Oxidative phosphorylation pathway is enriched in quiescent cells at mRNA level. **B,** Oxidative phosphorylation pathway is enriched in quiescent cells at protein level.

## 5.3 Discussion

The secondary inactive pathway in quiescent cells is role of BRCA1 in DNA damage response. BRCA1 is a well-established tumour suppressor gene, which is frequently mutated in familial breast and ovarian cancers. The gene product of BRCA1 functions in a number of cellular pathways that maintain genomic stability, including DNA damage-induced cell cycle checkpoint activation, DNA damage repair, protein ubiquitination, chromatin remodelling, as well as transcriptional regulation and apoptosis[255]. BRCA1 is phosphorylated by ATM, ATR, and chk2 on several serines throughout the length of the protein in response to DNA damage, suggesting that phosphorylation of BRCA1 plays a role in DNA damage response.

The difference of DNA damage and repair between quiescent and proliferating cells has been studied since 1980s. In case of radiation induced DNA damage, quiescent cells were more sensitive to ionizing radiation than the proliferating cells. However, quiescent cells showed higher repair of potentially lethal damage (PLDR) than proliferating cells did[256]. DNA damage accumulation in hematopoietic stem cells (HSCs) during aging. This was associated with broad attenuation of DNA repair and response pathways that was dependent upon HSC quiescence[257]. In esophageal cancer, the damage-resistance ability of cancer stem cell is protective, likely attributed to their slow-cycling status and avoidance of apoptosis or senescence triggered by an excessive DNA damage response (DDR)[258]. Our data is consistent with the above publication. It seems the attenuation of DNA repair and response in quiescent cells play a protective role.

Cancers have the ability to develop resistance to traditional therapies. As it was reported, it maybe because of drug inactivation, drug target alteration, drug efflux, DNA damage repair, cell death inhibition, and the epithelial-mesenchymal transition, as well as how inherent tumour cell heterogeneity plays a role in drug resistance[259]. For tumour cells, one of the explanation about obtaining the ability to survival under the exposure of a specific kind of drug is the happening of beneficial mutation. We do not have the evidence that all the drugs can arrest tumour cells at quiescent status. But it is the truth that

in several kinds of drugs[260, 261, 262]. Combinational considering above, quiescent cancer cells may bear an attenuate but special repair mechanism. The mechanism can be dig further by study DDR associated genes which are differential expressed in quiescent and cycling cells.

Cancer cells rewire their metabolism to promote growth, survival, proliferation, and long-term maintenance. The common feature of this altered metabolism is increased glucose uptake and fermentation of glucose to lactate[263]. This is Warburg effect, which refers to the observation that even in aerobic condition, cancer cells tend to favour metabolism via glycolysis rather than the much more efficient oxidative phosphorylation pathway. Per unit of glucose, aerobic glycolysis is an inefficient means of generating ATP compared to the amount obtained by mitochondrial respiration. However, the Warburg Effect has been proposed to be an adaptation mechanism to support the biosynthetic requirements of uncontrolled proliferation. In this scenario, the increased glucose consumption is used as a carbon source for anabolic processes needed to support cell proliferation[264].

Here, we found that the favourite metabolism pathway of quiescent cancer cells are oxidative phosphorylation, which is different from cycling cancer cells. This maybe a promising target of killing quiescent cancer cells.

# Chapter Six The eradication of quiescent cancer cells by oxidative phosphorylation inhibitor

## 6.1 Introduction

As is mentioned in last chapter that human quiescent cancer cells are more rely on oxidative phosphorylation to obtain ATP. While aerobic glycolysis offer more building blocks to maintain the success of cell proliferation. For example, the biosynthesis of nucleotides, lipids and amino acids. It is also help to maintain cellular redox state. It is very easy to understand that the building blocks created by glycolysis is unnecessary for quiescent cells since they are not dividing. Even aerobic glycolysis is an inefficient means of generating ATP compared with the amount obtained by mitochondrial respiration[264], the rate of glucose metabolism through aerobic glycolysis is higher. It is reported that the amount of ATP synthesized over any given period of time is comparable when either form of glucose metabolism is utilized[265]. Thus, a reasonable hypothesis for why quiescent cancer cells would employ oxidative phosphorylation for ATP producer is that without the burden of proliferation, glucoses were consumed just for the basic energy needs by oxidative phosphorylation. This is a very efficient way to survival under strict environment when nutrition is not enough or the environment is toxic.

To balance the bioenergetic and biosynthetic need, cancer cells choose aerobic glycolysis as the majority route to generate ATP. To survival under strict environment, the cancer cells turn to quiescent state which suicide proliferation, alter to a more efficient way to meet the basic bioenergetics need. This suggests that inhibition of mitochondrial metabolism maybe the most efficient way to wipe out quiescent cells.

OXPHOS, especially the electron transfer chian can be inhibited by many molecules. Such as 2,4-Dinitrophenol (DNP), Oligomycin A, Rotenone, 2-Thenoyltrifluoroacetone (TTFA) and Carbonyl cyanide 3-chlorophenylhydrazone (CCCP). These available drugs have generally unfavourable pharmacologic properties, DNP had been used extensively in diet pills. However, Cases of dangerous side effects such as fatal hyperthermia led to its official discontinuation by 1938.

Metformin is famous as the first-line medication for the treatment of type 2 diabetes[266]. Potential mechanism of metformin action on cellular metabolism and cell proliferation. Metformin increases glucose uptake and glycolysis. It activates AMPK leading to the phosphorylation of ACC (acetyl CoA carboxylase) and ultimately increases fatty acid oxidation. Metformin also inhibits the mitochondrial complex 1[267]. Complex I in Electron transport chain (NADH:ubiquinone oxidoreductase, NADH-CoQ reductase, or NADH dehydrogenase;), pumped four protons from matrix to intermembrane space, which is very important to the generation of ATP in oxidative phosphorylation. Buzzai and colleagues have shown that metformin inhibited oxygen consumption in colon cancer cells, which is consistent with the inhibition of oxidative phosphorylation. It also reported that metformin can inhibit complex I and increases glycolysis in prostate cancer cells[268].

As a first-line drug in clinical, the side effect has been validated. We will test the killing effect of metformin on quiescent cells in this chapter. Once it works, as we have got a lot record in clinical trial, it will be a promising drug which can be utilized in clinical shortly to reduce cancer recurrence.

Furthermore, Bay 87 -2243[269] and IACS-010759[270, 271] are good candidates of OXPHOS inhibitors to kill quiescent cancer cells.

## 6.2 Results

### 6.2.1 IC 50 of various OXPHOS inhibitors

As the Mel-RM.pK subline is generated by Mel-RM melanoma cell line as well as Mel-RM can be significantly arrested in G0 phase by MEK inhibitor, we tested the killing of quiescent cancer cells by OXPHOS inhibitor in Mel-RM cells first. We tested the IC50 of 2,4-DNP, CCCP and Oligomycin A by MTS here. As can be seen in Figure 6.1. The IC50 of 2,4-DNP, CCCP and Oligomycin A are 500 μM, 4 μM and 10 μM, separately. Of note, we cannot see much floating cells in the treatment of these OXPHOS inhibitors at IC50 concentration. This hints that the inhibition of the viability of is mainly induced by the inhibition of proliferation but not apoptosis.

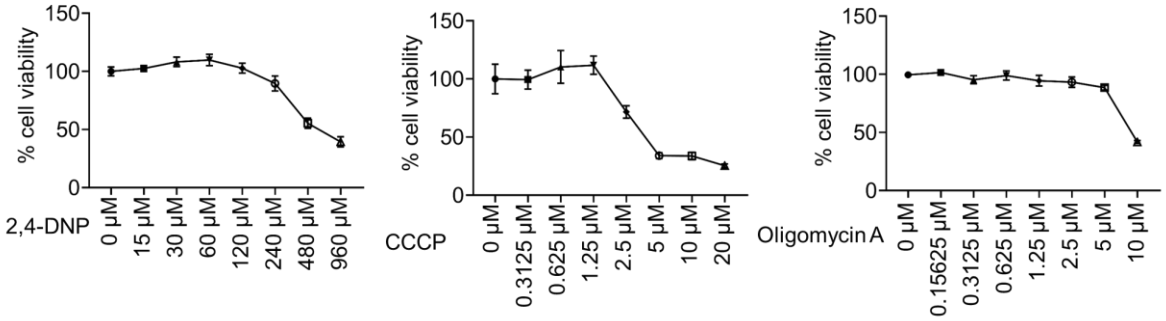


Figure 6.1. IC50 of OXPOS inhibitors. Mel-RM cells treated by three kinds of OXOHOS inhibitors for 48 hours were subjected to MTS assay.

### 6.2.2 OXPHOS inhibitors sensitized the killing of Mel-RM by MEK inhibitor

MEK inhibitor can dramatically arrest Mel-RM cells in G0 phase (Fig.4.12). Actually, neither MEK inhibitor nor OXPHOS inhibitor can induce much apoptotic cells (Fig. 6.2). In addition, the treated cells will re-growth when the inhibitors were got rid of (data not shown). In striking, the combination of these two kind of drugs induce apoptosis dramatically (Fig. 6.2).

### 6.2.3 OXPHOS inhibitors target quiescent cell

We analysed the cell cycle distribution under the treatment of 2, 4-DNP and found that it arrest Mel-RM cells at G2/M phase (Fig. 6.3). This implies that cells prefer stay at cycling phases rather than G0 phase with the treatment of OXPHOS inhibitor. We suppose that MEK inhibitor targets cycling cells so that quiescent cells are enriched after the treatment. While OXPHOS inhibitor targets quiescent cells so that cycling cells are enriched after the treatment. Neither of these two inhibitor can induce significant apoptosis. This maybe a survival mechanism that the cells escape from the phases that are harmful to themselves.

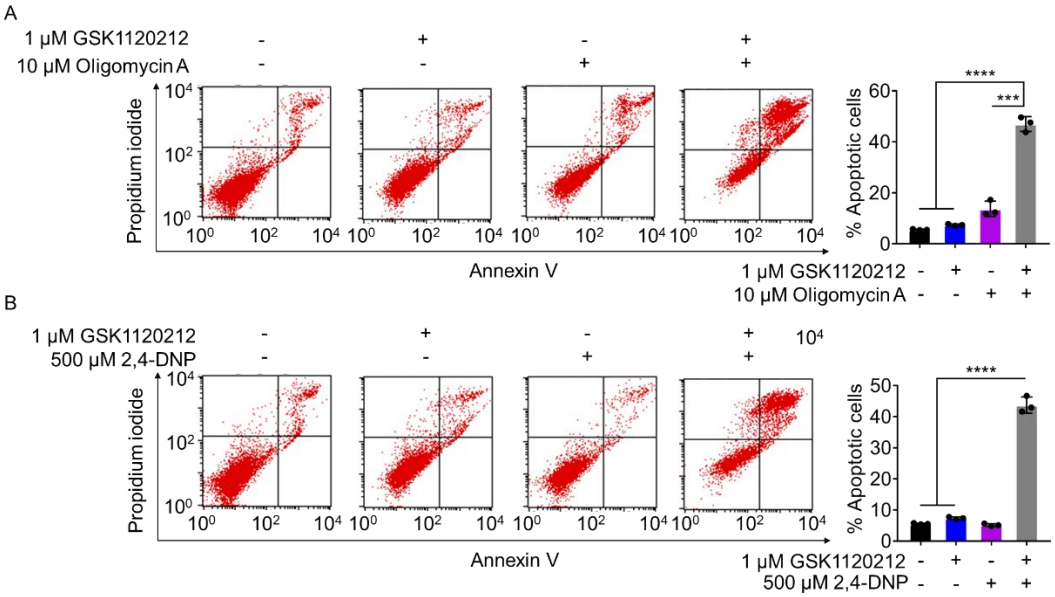


Figure 6.2. OXPHOS inhibitors boost the killing of Mel-RM cells by MEK inhibitor GSK1120212. **A & B,** Mel-RM cells were treated by the indicated drugs and subjected to PI-Annexin V staining following with flow cytometry analysis (A left & B left). The quantifications of the apoptotic cells are in right. Data shown are either representative (A left & B left) or mean±SEM (A right & B right) of three individual experiments. ***, $P<0.001$; ****, $P<0.0001$, Student *t* test.

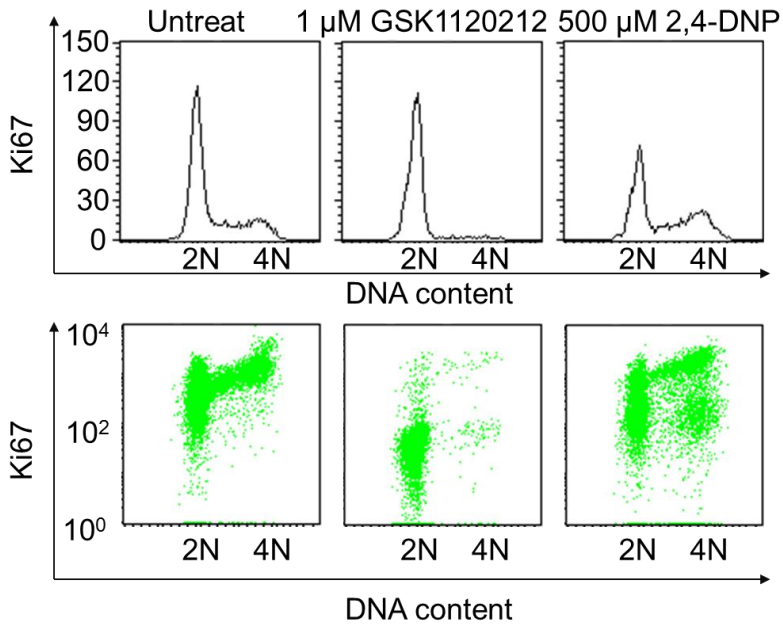


Figure 6.3. 2,4-DNP arrested Mel-RM cells at G2/M phase**.** Mel-RM treated by indicated drugs were subjected to Propidium iodide and Ki67 staining and flow cytometry analysis.

To confirm that the OXPHOS inhibitor induced killing was due to the quiescent state but not the combination of MEK inhibitor itself, we treated the serum starved cells with OXPHOS inhibitor. Serum starvation is a more gentle method to arrest quiescent cells in comparison with MEK inhibitor. Interestingly, serum starvation can also sensitize Mel-RM to be killed by OXPHOS inhibitor (Fig. 6.4). This means that it is the G0 phase determine the killing of Mel-RM cells by OXPHOS inhibitor.

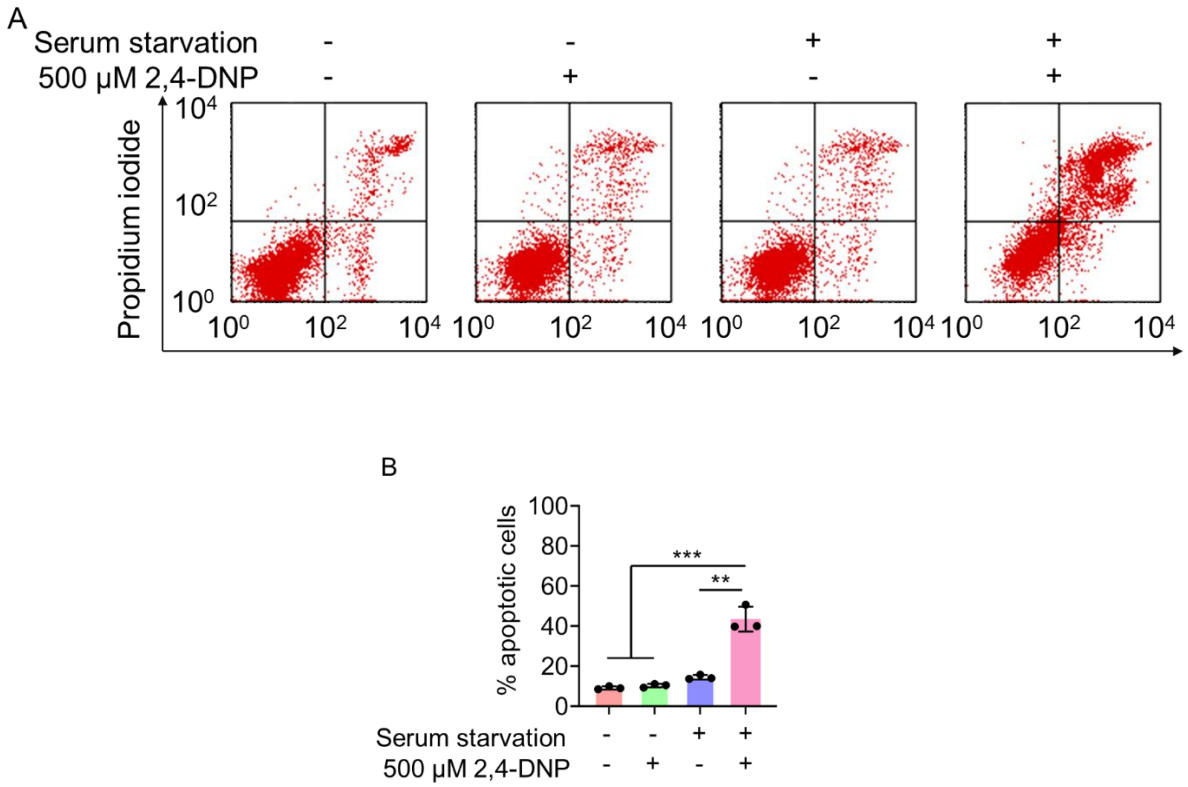


Figure 6.4. Serum starvation sensitized Mel-RM cells to the treatment of OXPHOS inhibitors. **A,** Mel-RM cells were treated as indicated and subjected to PI-Annexin V staining following with flow cytometry analysis. **B,** The quantification of the apoptotic cells in (A). Data shown are either representative (A) or mean±SEM (B) of three individual experiments. **, $P<0.01$; ***, $P<0.001$, Student *t* test.

### 6.2.4 Metformin target quiescent cell

We tested the IC50 of metformin in Mel-RM cells (Fig. 6.5). Further experiment utilized 20 mM metformin. Unfortunately, metformin did not promote the killing of Mel-RM cells by MAPK inhibitors (Fig. 6.6). Strikingly, the killing of melanoma cells by MEK inhibitor and metformin is antagonized.

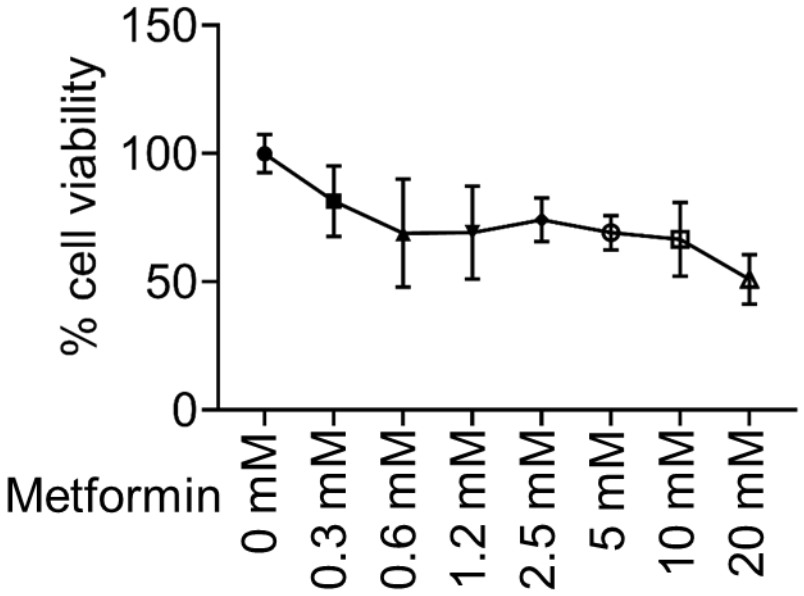


Figure 6.5. IC50 of metformin. Mel-RM cells treated by metformin for 48 hours were subjected to MTS assay.

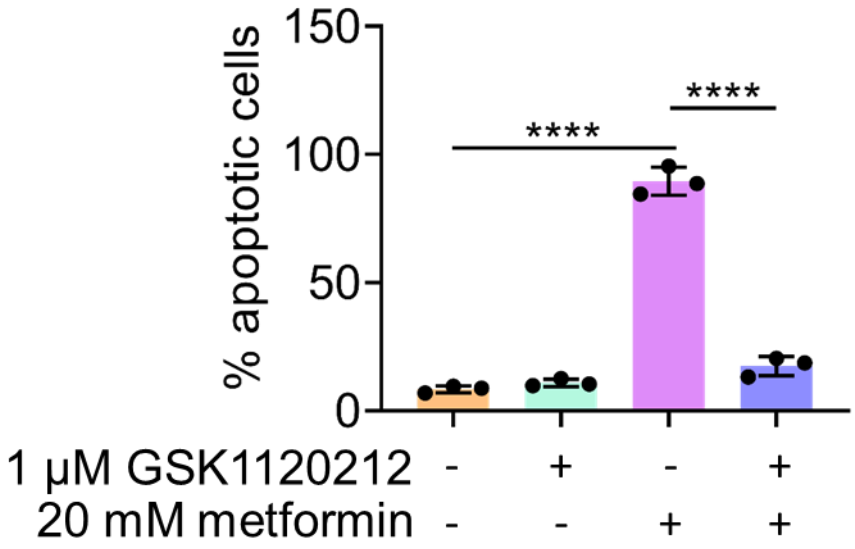


Figure 6.6. MEK inhibitor antagonized the killing of Mel-RM cells by metformin. Mel-RM cells were treated by the indicated drugs and subjected to PI-Annexin V staining following with flow cytometry analysis. The quantifications of the apoptotic cells are in right. Data shown are either representative mean±SEM of three individual experiments. ****, P<0.0001, Student *t* test.

## 6.3 Discussion

Despite the recent advance in the treatment of metastatic melanoma using MAPK inhibitors and immune checkpoint antibodies, relapse following initial remission remains an unsolved problem. We have found that the majority of mutant BRAF melanoma cells surviving acute exposure to the BRAF inhibitor vemurafenib or the MEK inhibitor trametinib are quiescent, similar to those resistant to cytotoxic drugs that primarily kill cycling (dividing) cells[83, 272]. Nevertheless, the mechanisms responsible for the resistance of quiescent melanoma cells to cell death remain largely undefined. This is primarily due to the lack of understanding of their biological characteristics as a consequence of technical hurdles in the isolation and analysis of viable quiescent cells. In this chapter, we found targeting OXPHOS by 2,4-DNP and Oligomycin A can dramatically increase the cell death that induced by MAPK inhibitors (Fig. 6.2). This is probably a promising way to improve the outcome of melanoma treatment.

In chapter 5, we also found the other pathways that active in quiescent cells. For example, CDK5 signalling pathway (Fig.5.6). CDK5 is a proline-directed serine/threonine kinase. Unlike other members of the CDK family, the protein encoded by this gene does not directly control cell cycle regulation, but acts as a regulatory kinase involved in other post-mitotic processes such as neuronal activity, neuronal migration during development and neurite outgrowth. During embryogenesis, CDK5 is indispensable for brain development and, in the adult brain, it is essential for numerous neuronal processes, including higher cognitive functions such as learning and memory formation[273]. However Cdk5 has been recently implicated in the development and progression of a variety of cancers including breast, lung, colon, pancreatic, melanoma, thyroid and brain tumours. This broad pro-tumorigenic role makes Cdk5 a promising drug target for the development of new cancer therapies[274]. Genes in CDK5 signalling pathways, but not CDK5 only, may also be good candidates of targeting quiescent cancer cells.

# Chapter Seven

# Discussion

Using the radioactive labelling technique to label newly synthesized DNA in early cell division studies, it was found that a population of cells are negative for the labelling, suggesting the existence of a nondividing, dormant state[275].

There are $10^{13}$–$10^{14}$ cells in the human body. At any given time, the vast majority of these cells are non-dividing and outside of an active cell cycle. Some of these non-dividing cells (e.g. senescent or terminally differentiated cells) are irreversibly arrested; they can no longer re-enter the cell cycle to proliferate under normal physiological conditions[276]. By contrast, a subset of non-dividing cells is 'reactivatable' and can enter the proliferative cell cycle in response to physiological growth signals; these cells are called quiescent cells. Examples of quiescent cells include many adult stem cells, progenitor cells, fibroblasts, lymphocytes, hepatocytes and some epithelial cells. The exact number of quiescent cells in the body is not well characterized[276].

Further to the pathways discussed in Chapter 1, additional pathways are involved in quiescence, including the Notch signalling pathway. Notch is an important regulator in tissue maintenance and regeneration during development[277] and is also involved in the regulation of cellular quiescence through its effector proteins, the transcriptional regulators RBPJ and HES1. Quiescent cells are associated with activation of autophagy pathways[278]. Many unicellular organisms reside in the quiescent state for a prolonged period of time to survive in unfavourable environments[279].

Quiescence is a universal status, not only occurring in functional somatic cells, but also in cancer cells to avoiding irreversible damage form suboptimal conditions. The moderate way of facing stress increases the difficulty of complete cancer cell eradication. As there are similarities in characteristics between quiescent somatic cells and quiescent cancer cells, identifying the difference between only quiescent cancer cells and cycling cancer cells is not enough. Therefore, the identification of differences in the characteristics of somatic quiescent cells and quiescent cancer cells is pivotal[280].

The metastatic cascade follows a series of steps that tumour cells need to take to reach distant organs and eventually form metastases. Metastatic tumours are more aggressive than primary tumours and are

the main cause of cancer-related death. Thus, it is more reasonable to study the metastatic quiescent cancer cells rather than primary quiescent cancer cells.

When cells leave the primary tumour and enter the blood stream, they become CTCs. However, once CTCs reach and lodge in a distant organ, they are termed DTCs, as they have already completed the steps of dissemination[281]. DTC biology has garnered great interest as it is becoming clear that these cells are the best explanation for the source of metastasis[30]. However, metastatic lesions can become symptomatic years or decades after primary tumour removal, suggesting that DTCs are not immediately competent to initiate growth and persist as minimal residual disease (MRD)[282]. A growing body of literature suggests that DTCs can be detected, for example, in the bone marrow (BM) of patients after years in remission[283]. Further, DTCs can recirculate throughout the body and enter and exit organs without initiating growth[37, 284].

Research on patient samples and mouse models showed that DTCs can be nonproliferative[285]. Aguirre-Ghiso and Sosa proposed that, even with interspersed events of cancer cell division, this quiescent state is the dominant phenotype during asymptomatic MRD phases and that this state ultimately controls the timing of metastasis[286, 287]. They further proposed that the biology of DTCs can be very different from that of growing primary tumours, that it can be deciphered, and more importantly, that it can be controlled to prevent metastasis.

Cancer dormancy is not yet fully understood. In addition to the limited knowledge regarding induction of tumour dormancy, there are large gaps in knowledge regarding how tumours escape from dormancy. There are three ways targeting tumour dormancy. The first way is keep a dormant tumour in a dormant state forever, which makes patients bear chronic diseases during their life. Secondly, to induce the quiescent cancer cells out of dormancy, making them sensitive to treatment by conventional drugs. This is a risky choice since the induced cycling cancer cells maybe become out of control. So the safe and direct way is to find approaches to target quiescent cancer cell to wipe them out. Therefore, uncovering the biological properties of quiescent cancer cells and seeking targets to kill them is the most promising way to overcome cancer recurrence.

Theoretically, there are four technical hurdles in targeting quiescent cancer cells. First, characterizing quiescent cancer cells and sorting out the difference between cycling and quiescent cancer cells. Secondly, designing drugs that specifically target quiescent cells based on the biological properties. Thirdly, the optimization of drugs to specialize them for quiescent cancer cells rather than other somatic cells. Fourthly, making sure the drugs can be delivered to the sites of the quiescent cancer cells in patients. It is imperative to understand the basic mechanisms of dormancy, as this will accelerate the development of new markers of progression and novel therapeutic opportunities to induce dormancy and/or eradicate dormant disease.

Christoph A. Klein and Dieter Hölzel have performed mathematical modelling to explain the occurrence of cancer dormancy, as a characteristic of all migrating tumour cells, as part of an evolutionary process of selection and mutation[288]. This is to say that tumour cells accumulate somatic mutations at the primary site and disseminate from large established tumours. According to their model, late disseminating tumour cells are more aggressive, have more genetic changes, and disseminate more frequently from large tumours[288].

Genetic mutations may account for the emergence of metastatic ability or for resistance to a specific therapy. However, they hardly explain the flexible adaptation of neoplasms to different environments/therapies. Francesco et al. suggest that epigenetic alterations in dormant cancer cells occur first and that some advantageous features are then fixed by genetic changes at a later stage[289]. According to the RNA-seq results, we found several hundred lncRNAs upregulated in quiescent cancer cells (Section 5.2.3, data not shown). Some of them may play vital role in the maintenance or drug resistance of quiescent cancer cells. It is worthy to study the regulations and functions of these lncRNAs to uncover the further mechanism of quiescence.

Further, it is thought that once tumour cells disseminate and begin to migrate to a new site to metastasize, the interaction of the tumour cells with the surrounding microenvironment determines whether the cells will proliferate and form metastases or undergo growth arrest and enter cancer cell dormancy[29]. Thus, the tumour microenvironment plays a pivotal role here to determine whether the tumour cells go on to dormancy or proliferation. The tumour microenvironment is the environment around a tumour,

including the surrounding blood vessels, immune cells, fibroblasts, signalling molecules and the ECM[290, 291]. On the other hand, tumours can influence the microenvironment by releasing extracellular signals, promoting tumour angiogenesis and inducing peripheral immune tolerance, while the immune cells in the microenvironment can affect the growth and evolution of cancerous cells.

There are three scenarios to explain the relationship between DTCs and the tumour microenvironment[287]. Scenario 1 supported that DTCs fate is instructed by reciprocal cross talk with the target organ and by epigenetic programs. Several studies identified that the dormancy is induced or reactivated by target organs[30, 282, 286]. In these studies, specific cues such as BMP7, TGFβ2, BMP4, and GAS6, all factors involved in adult stem cell fate regulation, were found to be inducers of dormancy in specific microenvironments like the lung and BM[292, 293, 294, 295, 296]. A recent study showed that, in a mouse model of melanoma, vaccination prevented tumour growth but did not stop tumour cell dissemination, and a residual fraction of tumour cells persisted in the animals[297]. This suggests that a subpopulation of melanoma cells could evade immune detection. Importantly, the residual DTCs were dormant for at least 1 year (>15 years in humans). The glucocorticoid-induced leucine zipper appeared to be low in dormant melanoma DTC-derived cultures, allowing for FOXO3A-mediated $p21^{CIP1}$ induction for quiescence; this same mechanism appeared to be associated with immune evasion. Changes in the immune microenvironment, adaptive or innate, may also influence the duration of dormancy. For example, it is known that BM-derived myeloid cells can be recruited to the lung upon lipopolysaccharide-mediated inflammation, and this alters the lung microenvironment in such a way that potent dormancy inducers, such as thrombospondin-1, are lost and enable expansion of metastasis[298, 299].

Scenario 2 is that primary tumour microenvironments might affect DTC dormancy. Microenvironmental factors present in growing primary tumours, and common to many cancers, could influence the existence of a pre-dormancy signature. This signature could then become functional as cells disseminate from their primary lesions to secondary organs. For example, estrogen receptor–positive BC patients have a risk of distant metastasis more than two decades after diagnosis[300, 301, 302]. A

few studies have defined signatures that predict longer metastasis-free periods in $ER^+$ but not $ER^-$ BC or that associate with EMT signatures[302, 303].

Scenario 3 is that early dissemination as a source of dormant disseminated tumour cells. This part was introduced in chapter 1 (1.1.2) and will not do more discussion here.

Metabolic reprogramming is a well-appreciated hallmark of cancer, and there has been extensive drug discovery research in this area. We have used 2,4-DNP and Oligomycin A to increase the killing of melanoma cells by MAPK inhibitors. Both of them worked well, however, both of the drugs have generally unfavourable pharmacologic properties, 2,4-DNP had been used extensively in diet[304], and over 100,000 people had been treated worldwide with the drug at the time of its discontinuation. Cases of dangerous side effects such as fatal hyperthermia led to its official discontinuation by 1938. Given the toxicities of the drugs, further development of alternative oxidative phosphorylation inhibitors should be considered.

There are plenty of commercial OXPHOS inhibitors, including atovaquone, which inhibits complex III of the mitochondrial electron transport chain in parasites, methylmalonate, a succinate dehydrogenase inhibitor, 3-Nitropropionic acid, an irreversible mitochondrial respiratory complex II inhibitor and rotenone, which inhibits complex I of the mitochondrial electron transport chain. There are also many kinds of uncouplers available, including BAM15, a mitochondrial protonophore uncoupler, CCCP, CCP and malonoben, which are oxidative phosphorylation uncouplers, and S3QEL 2, a suppressor of Complex III superoxide production.

Since metformin can target complex I of the mitochondrial electron transport chain, we used it in combination with MAPK inhibitors. We aimed to find a drug that had previously been verified as safe and tolerable in clinical trials as repurposing an existing drug or therapy shortens the translation of treatments into the clinic. Unfortunately, metformin does not boost the killing of MAPK inhibitors. In contrast, MAPK inhibitors can rescue the killing efficiency caused by metformin(Fig 6.6). As metformin must be used at millimolar concentrations to achieve complex I inhibition *in vitro*, doubts have been raised on its actual mechanism of action *in vivo*. Another possibility may be due to

incompletely understood molecular mechanisms. Multiple potential mechanisms of action have been proposed: inhibition of the mitochondrial respiratory chain (complex I), activation of AMP-activated protein kinase (AMPK), inhibition of glucagon-induced elevation of cyclic adenosine monophosphate (cAMP) with reduced activation of protein kinase A (PKA), inhibition of mitochondrial glycerophosphate dehydrogenase, and an effect on gut microbiota. Nevertheless, it is interesting to know the mechanism of the antagonistic relationship between metformin and MAPK inhibitors toward killing melanoma.

A recently developed, highly specific complex I inhibitor, 1-cyclopropyl-4-(4-[(5-methyl-3-(3-[4-(trifluoromethoxy)phenyl]-1,2,4-oxadiazol-5-yl)-1H-pyrazol-1-yl)methyl]pyridin-2-yl)piperazine (BAY87-2243, abbreviated as B87), inhibited the proliferation of human cancer cells, including melanoma cells, *in vitro*[305] and *in vivo*[306]. In contrast to the widely used experimental complex I inhibitor rotenone, B87 does not alter microtubular polymerization rates, hence lacking antimitotic (and hence toxic) activity. B87 operates via an exquisite on-target effect[305] and it failed to kill human cancer cells alone. However, it is toxic to cancer cells when simultaneously used with Dimethyl α-Ketoglutarate (DMKG)[307]. Thus, it is worth assessing B87 as an OXPHOS inhibitor to check the synergetic killing of melanoma with MAPK inhibitors. Another promising OXPHOS inhibitor is IACS-010759. IACS-010759 at nanomolar concentrations blocks cellular respiration through inhibition of complex I of the electron transport chain and is currently in Phase 1 clinical trial in AML (NCT #02882321)[270, 308].

During my PhD, I did two projects. In the first project (Chapter 3), we reported the identification of a p53-responsive microRNA network that promotes cancer cell quiescence. On the one hand, miRNA-27b-3p targets Cks1 leading to reduction in p27 polyubiquitination and subsequent degradation mediated by Skp2. Conversely, miRNA-455-3p targets CAC1 that enhances CDK2-mediated phosphorylation of p27 at Thr187 necessary for Skp2-mediated p27 polyubiquitination. Collectively, these results reveal that p53 is a driver of quiescence in cancer cells through two distinct but complementary miRNA pathways that stabilize p27. The enticing implications of the work involve the potential to improve the therapeutic efficacy of currently available therapeutic agents, in particular, those activating p53. Here promotion of miRNA-27b-3p/ miRNA-455-3p expression will presumably

force cells to remain in a harmless quiescent state. Alternatively, inhibition would drive quiescent cells to re-enter the cell cycle and render them sensitive to therapeutic agents.

The other project was “a genomic editing approach for isolation of viable quiescent melanoma cells”. We took advantage of the fact that quiescent cells are characteristically negative for the proliferation marker Ki67 to develop a CRISPR/Cas9-based system, in which a green fluorescent protein (EGFP) gene is fused with endogenous *CDKN1B*, the gene encoding p27, and a red fluorescent protein (mCherry) gene, with endogenous MKI67, the gene encoding Ki67 in the genome of human melanoma cells. By using this system, we have successfully isolated viable $p27^{high}/Ki67^{-}$ human melanoma cells using FACS that were verified to be authentic quiescent cells using dual nucleic acid staining. This system provides us with an exceptional tool and will be the basis of further characterization of the biological properties of quiescent melanoma cells in future studies.

# Reference


1. Davies H, Bignell GR, Cox C, Stephens P, Edkins S, Clegg S*, et al.* Mutations of the BRAF gene in human cancer. *Nature* 2002, **417**(6892)**:** 949-954.

2. Tietze JK, Forschner A, Loquai C, Mitzel-Rink H, Zimmer L, Meiss F*, et al.* The efficacy of re-challenge with BRAF inhibitors after previous progression to BRAF inhibitors in melanoma: A retrospective multicenter study. *Oncotarget* 2018, **9**(76)**:** 34336-34346.

3. Leman JA, Mac Kie RM. Late (> 10 years) recurrence of melanoma: the Scottish experience. *Br J Dermatol* 2003, **148**(2)**:** 372-373.

4. Goss PE, Chambers AF. Does tumour dormancy offer a therapeutic target? *Nat Rev Cancer* 2010, **10**(12)**:** 871-877.

5. Yeh AC, Ramaswamy S. Mechanisms of Cancer Cell Dormancy—Another Hallmark of Cancer? *Cancer Research* 2015, **75**(23)**:** 5014-5022.

6. Zeeshan R, Mutahir Z. Cancer metastasis - tricks of the trade. *Bosnian journal of basic medical sciences* 2017, **17**(3)**:** 172-182.

7. Jemal A, Bray F, Center MM, Ferlay J, Ward E, Forman D. Global cancer statistics. *CA: a cancer journal for clinicians* 2011, **61**(2)**:** 69-90.

8. Jemal A, Siegel R, Ward E, Hao Y, Xu J, Thun MJ. Cancer statistics, 2009. *CA: a cancer journal for clinicians* 2009, **59**(4)**:** 225-249.

9. Qian C-N, Mei Y, Zhang J. Cancer metastasis: issues and challenges. *Chinese journal of cancer* 2017, **36**(1)**:** 38-38.

10. Chaffer CL, Weinberg RA. A Perspective on Cancer Cell Metastasis. *Science* 2011, **331**(6024)**:** 1559-1564.

11. Gomis RR, Gawrzak S. Tumor cell dormancy. *Molecular oncology* 2016.

12. Obenauf AC, Massague J. Surviving at a Distance: Organ-Specific Metastasis. *Trends in cancer* 2015, **1**(1)**:** 76-91.

13. Kessenbrock K, Plaks V, Werb Z. Matrix metalloproteinases: regulators of the tumor microenvironment. *Cell* 2010, **141**(1)**:** 52-67.

14. Wolf K, Wu YI, Liu Y, Geiger J, Tam E, Overall C*, et al.* Multi-step pericellular proteolysis controls the transition from individual to collective cancer cell invasion. *Nature cell biology* 2007, **9**(8)**:** 893-904.

15. Dumont N, Liu B, Defilippis RA, Chang H, Rabban JT, Karnezis AN*, et al.* Breast fibroblasts modulate early dissemination, tumorigenesis, and metastasis through alteration of extracellular matrix characteristics. *Neoplasia (New York, NY)* 2013, **15**(3)**:** 249-262.

16. Joyce JA, Baruch A, Chehade K, Meyer-Morse N, Giraudo E, Tsai FY*, et al.* Cathepsin cysteine proteases are effectors of invasive growth and angiogenesis during multistage tumorigenesis. *Cancer Cell* 2004, **5**(5)**:** 443-453.

17. Tsuji T, Ibaragi S, Hu G-f. Epithelial-mesenchymal transition and cell cooperativity in metastasis. *Cancer research* 2009, **69**(18)**:** 7135-7139.

18. Lamouille S, Xu J, Derynck R. Molecular mechanisms of epithelial-mesenchymal transition. *Nature reviews Molecular cell biology* 2014, **15**(3)**:** 178-196.

19. Morikawa S, Baluk P, Kaidoh T, Haskell A, Jain RK, McDonald DM. Abnormalities in pericytes on blood vessels and endothelial sprouts in tumors. *The American journal of pathology* 2002, **160**(3)**:** 985-1000.

20. Giampieri S, Manning C, Hooper S, Jones L, Hill CS, Sahai E. Localized and reversible TGFbeta signalling switches breast cancer cells from cohesive to single cell motility. *Nature cell biology* 2009, **11**(11)**:** 1287-1296.

21. Massague J, Obenauf AC. Metastatic colonization by circulating tumour cells. *Nature* 2016, **529**(7586)**:** 298-306.

22. Muller V, Stahmann N, Riethdorf S, Rau T, Zabel T, Goetz A*, et al.* Circulating tumor cells in breast cancer: correlation to bone marrow micrometastases, heterogeneous response to systemic therapy and low proliferative activity. *Clin Cancer Res* 2005, **11**(10)**:** 3678-3685.

23. Miller MC, Doyle GV, Terstappen LWMM. Significance of Circulating Tumor Cells Detected by the CellSearch System in Patients with Metastatic Breast Colorectal and Prostate Cancer. *Journal of oncology* 2010, **2010:** 617421-617421.

24. Padua D, Zhang XH, Wang Q, Nadal C, Gerald WL, Gomis RR*, et al.* TGFbeta primes breast tumors for lung metastasis seeding through angiopoietin-like 4. *Cell* 2008, **133**(1)**:** 66-77.

25. Zhang XHF, Giuliano M, Trivedi MV, Schiff R, Osborne CK. Metastasis dormancy in estrogen receptor-positive breast cancer. *Clinical cancer research : an official journal of the American Association for Cancer Research* 2013, **19**(23)**:** 6389-6397.

26. Adam AP, George A, Schewe D, Bragado P, Iglesias BV, Ranganathan AC*, et al.* Computational identification of a p38SAPK-regulated transcription factor network required for tumor cell quiescence. *Cancer Res* 2009, **69**(14)**:** 5664-5672.

27. Malladi S, Macalinao DG, Jin X, He L, Basnet H, Zou Y*, et al.* Metastatic Latency and Immune Evasion through Autocrine Inhibition of WNT. *Cell* 2016, **165**(1)**:** 45-60.

28. Yeh AC, Ramaswamy S. Mechanisms of Cancer Cell Dormancy--Another Hallmark of Cancer? *Cancer Res* 2015, **75**(23)**:** 5014-5022.

29. Aguirre-Ghiso JA. Models, mechanisms and clinical evidence for cancer dormancy. *Nat Rev Cancer* 2007, **7**(11)**:** 834-846.

30. Giancotti FG. Mechanisms governing metastatic dormancy and reactivation. *Cell* 2013, **155**(4)**:** 750-764.

31. Hadfield G. The dormant cancer cell. *British medical journal* 1954, **2**(4888)**:** 607-610.

32. Crowley NJ, Seigler HF. Late recurrence of malignant melanoma. Analysis of 168 patients. *Ann Surg* 1990, **212**(2)**:** 173-177.

33. Hansel G, Schonlebe J, Haroske G, Wollina U. Late recurrence (10 years or more) of malignant melanoma in south-east Germany (Saxony). A single-centre analysis of 1881 patients with a follow-up of 10 years or more. *Journal of the European Academy of Dermatology and Venereology : JEADV* 2010, **24**(7)**:** 833-836.

34. Schmid-Wendtner MH, Baumert J, Schmidt M, Konz B, Holzel D, Plewig G*, et al.* Late metastases of cutaneous melanoma: an analysis of 31 patients. *Journal of the American Academy of Dermatology* 2000, **43**(4)**:** 605-609.

35. Tsao H, Cosimi AB, Sober AJ. Ultra-late recurrence (15 years or longer) of cutaneous melanoma. *Cancer* 1997, **79**(12)**:** 2361-2370.

36. Karrison TG, Ferguson DJ, Meier P. Dormancy of mammary carcinoma after mastectomy. *Journal of the National Cancer Institute* 1999, **91**(1)**:** 80-85.

37. Meng S, Tripathy D, Frenkel EP, Shete S, Naftalis EZ, Huth JF*, et al.* Circulating tumor cells in patients with breast cancer dormancy. *Clin Cancer Res* 2004, **10**(24)**:** 8152-8162.

38. Wang SH, Lin SY. Tumor dormancy: potential therapeutic target in tumor recurrence and metastasis prevention. *Experimental hematology & oncology* 2013, **2**(1)**:** 29.

39. Manjili MH. Tumor Dormancy and Relapse: From a Natural Byproduct of Evolution to a Disease State. *Cancer Res* 2017, **77**(10)**:** 2564-2569.

40. Nielsen M, Thomsen JL, Primdahl S, Dyreborg U, Andersen JA. Breast cancer and atypia among young and middle-aged women: a study of 110 medicolegal autopsies. *British journal of cancer* 1987, **56**(6)**:** 814-819.

41. Folkman J, Kalluri R. Cancer without disease. *Nature* 2004, **427**(6977)**:** 787.

42. Pavlidis N, Khaled H, Gaafar R. A mini review on cancer of unknown primary site: A clinical puzzle for the oncologists. *Journal of advanced research* 2015, **6**(3)**:** 375-382.

43. Schmidt-Kittler O, Ragg T, Daskalakis A, Granzow M, Ahr A, Blankenstein TJ*, et al.* From latent disseminated cells to overt metastasis: genetic analysis of systemic breast cancer progression. *Proc Natl Acad Sci U S A* 2003, **100**(13)**:** 7737-7742.

44. Huang Z, Bao S-D. Roles of main pro- and anti-angiogenic factors in tumor angiogenesis. *World journal of gastroenterology* 2004, **10**(4)**:** 463-470.

45. Bouïs D, Kusumanto Y, Meijer C, Mulder NH, Hospers GAP. A review on pro- and anti-angiogenic factors as targets of clinical intervention. *Pharmacological Research* 2006, **53**(2)**:** 89-103.

46. Naumov GN, Bender E, Zurakowski D, Kang SY, Sampson D, Flynn E*, et al.* A model of human tumor dormancy: an angiogenic switch from the nonangiogenic phenotype. *Journal of the National Cancer Institute* 2006, **98**(5)**:** 316-325.

47. Al-Mehdi AB, Tozawa K, Fisher AB, Shientag L, Lee A, Muschel RJ. Intravascular origin of metastasis from the proliferation of endothelium-attached tumor cells: a new model for metastasis. *Nat Med* 2000, **6**(1)**:** 100-102.

48. Vesely MD, Schreiber RD. Cancer immunoediting: antigens, mechanisms, and implications to cancer immunotherapy. *Annals of the New York Academy of Sciences* 2013, **1284:** 1-5.

49. Koebel CM, Vermi W, Swann JB, Zerafa N, Rodig SJ, Old LJ*, et al.* Adaptive immunity maintains occult cancer in an equilibrium state. *Nature* 2007, **450**(7171)**:** 903-907.

50. MacKie RM, Reid R, Junor B. Fatal melanoma transferred in a donated kidney 16 years after melanoma surgery. *The New England journal of medicine* 2003, **348**(6)**:** 567-568.

51. Pantel K, Brakenhoff RH, Brandt B. Detection, clinical relevance and specific biological properties of disseminating tumour cells. *Nat Rev Cancer* 2008, **8**(5)**:** 329-340.

52. Dey-Guha I, Wolfer A, Yeh AC, J GA, Darp R, Leon E*, et al.* Asymmetric cancer cell division regulated by AKT. *Proc Natl Acad Sci U S A* 2011, **108**(31)**:** 12845-12850.

53. Mellor HR, Ferguson DJ, Callaghan R. A model of quiescent tumour microregions for evaluating multicellular resistance to chemotherapeutic drugs. *British journal of cancer* 2005, **93**(3)**:** 302-309.

54. Smith JA, Martin L. Do cells cycle? *Proc Natl Acad Sci U S A* 1973, **70**(4)**:** 1263-1267.

55. Schie IW, Huser T. Methods and applications of Raman microspectroscopy to single-cell analysis. *Applied spectroscopy* 2013, **67**(8)**:** 813-828.

56. Dalton S. Linking the Cell Cycle to Cell Fate Decisions. *Trends Cell Biol* 2015, **25**(10)**:** 592-600.

57. Poon RY. Cell Cycle Control: A System of Interlinking Oscillators. *Methods Mol Biol* 2016, **1342:** 3-19.

58. Barnum KJ, O'Connell MJ. Cell cycle regulation by checkpoints. *Methods in molecular biology (Clifton, NJ)* 2014, **1170:** 29-40.

59. Kastan MB, Bartek J. Cell-cycle checkpoints and cancer. *Nature* 2004, **432**(7015)**:** 316-323.

60. John PC, Mews M, Moore R. Cyclin/Cdk complexes: their involvement in cell cycle progression and mitotic division. *Protoplasma* 2001, **216**(3-4)**:** 119-142.

61. Nakayama KI, Nakayama K. Ubiquitin ligases: cell-cycle control and cancer. *Nat Rev Cancer* 2006, **6**(5)**:** 369-381.

62. Peters JM. The anaphase-promoting complex: proteolysis in mitosis and beyond. *Mol Cell* 2002, **9**(5)**:** 931-943.

63. Starostina NG, Kipreos ET. Multiple degradation pathways regulate versatile CIP/KIP CDK inhibitors. *Trends Cell Biol* 2012, **22**(1)**:** 33-41.

64. Kumar A, Placone JK, Engler AJ. Understanding the extracellular forces that determine cell fate and maintenance. *Development (Cambridge, England)* 2017, **144**(23)**:** 4261-4270.

65. Irizarry RA, Warren D, Spencer F, Kim IF, Biswal S, Frank BC*, et al.* Multiple-laboratory comparison of microarray platforms. *Nat Methods* 2005, **2**.

66. Peters J-M. The Anaphase-Promoting Complex: Proteolysis in Mitosis and Beyond. *Molecular Cell* 2002, **9**(5)**:** 931-943.

67. Bashir T, Dorrello NV, Amador V, Guardavaccaro D, Pagano M. Control of the SCF(Skp2-Cks1) ubiquitin ligase by the APC/C(Cdh1) ubiquitin ligase. *Nature* 2004, **428**(6979)**:** 190-193.

68. Carrano AC, Eytan E, Hershko A, Pagano M. SKP2 is required for ubiquitin-mediated degradation of the CDK inhibitor p27. *Nature cell biology* 1999, **1:** 193.

69. Calvisi DF, Ladu S, Pinna F, Frau M, Tomasi ML, Sini M*, et al.* SKP2 and CKS1 promote degradation of cell cycle regulators and are associated with hepatocellular carcinoma prognosis. *Gastroenterology* 2009, **137**(5)**:** 1816-1826.e1811-1810.

70. Chen PL, Scully P, Shew JY, Wang JY, Lee WH. Phosphorylation of the retinoblastoma gene product is modulated during the cell cycle and cellular differentiation. *Cell* 1989, **58**(6)**:** 1193-1198.

71. Attwooll C, Lazzerini Denchi E, Helin K. The E2F family: specific functions and overlapping interests. *The EMBO journal* 2004, **23**(24)**:** 4709-4716.

72. Nevins JR. The Rb/E2F pathway and cancer. *Human molecular genetics* 2001, **10**(7)**:** 699-703.

73. Harbour JW, Dean DC. The Rb/E2F pathway: expanding roles and emerging paradigms. *Genes Dev* 2000, **14**(19)**:** 2393-2409.

74. Biggar KK, Storey KB. Perspectives in cell cycle regulation: lessons from an anoxic vertebrate. *Current genomics* 2009, **10**(8)**:** 573-584.

75. Wei W, Ayad NG, Wan Y, Zhang GJ, Kirschner MW, Kaelin WG, Jr. Degradation of the SCF component Skp2 in cell-cycle phase G1 by the anaphase-promoting complex. *Nature* 2004, **428**(6979)**:** 194-198.

76. Sakaue-Sawano A, Kurokawa H, Morimura T, Hanyu A, Hama H, Osawa H*, et al.* Visualizing spatiotemporal dynamics of multicellular cell-cycle progression. *Cell* 2008, **132**(3)**:** 487-498.

77. Arias EE, Walter JC. Strength in numbers: preventing rereplication via multiple mechanisms in eukaryotic cells. *Genes Dev* 2007, **21**(5)**:** 497-518.

78. Nishitani H, Lygerou Z, Nishimoto T. Proteolysis of DNA replication licensing factor Cdt1 in S-phase is performed independently of geminin through its N-terminal region. *J Biol Chem* 2004, **279**(29)**:** 30807-30816.

79. Sakaue-Sawano A, Ohtawa K, Hama H, Kawano M, Ogawa M, Miyawaki A. Tracing the silhouette of individual cells in S/G2/M phases with fluorescence. *Chemistry & biology* 2008, **15**(12)**:** 1243-1248.

80. Sakaue-Sawano A, Yo M, Komatsu N, Hiratsuka T, Kogure T, Hoshida T*, et al.* Genetically Encoded Tools for Optical Dissection of the Mammalian Cell Cycle. *Mol Cell* 2017, **68**(3)**:** 626-640.e625.

81. Zielke N, Edgar BA. FUCCI sensors: powerful new tools for analysis of cell proliferation. *Wiley interdisciplinary reviews Developmental biology* 2015, **4**(5)**:** 469-487.

82. Oki T, Nishimura K, Kitaura J, Togami K, Maehara A, Izawa K*, et al.* A novel cell-cycle-indicator, mVenus-p27K-, identifies quiescent cells and visualizes G0-G1 transition. *Sci Rep* 2014, **4:** 4012.

83. Schmidt M, Lu Y, Parant JM, Lozano G, Bacher G, Beckers T*, et al.* Differential roles of p21(Waf1) and p27(Kip1) in modulating chemosensitivity and their possible application in drug discovery studies. *Mol Pharmacol* 2001, **60**(5)**:** 900-906.

84. Makalowski W, Zhang J, Boguski MS. Comparative analysis of 1196 orthologous mouse and human full-length mRNA and protein sequences. *Genome Res* 1996, **6**(9)**:** 846-857.

85. Dai Y, Grant S. Cyclin-dependent kinase inhibitors. *Current Opinion in Pharmacology* 2003, **3**(4)**:** 362-370.

86. Abbastabar M, Kheyrollah M, Azizian K, Bagherlou N, Tehrani SS, Maniati M*, et al.* Multiple functions of p27 in cell cycle, apoptosis, epigenetic modification and transcriptional regulation for the control of cell growth: A double-edged sword protein. *DNA Repair (Amst)* 2018, **69:** 63-72.

87. Hnit SS, Xie C, Yao M, Holst J, Bensoussan A, De Souza P*, et al.* p27(Kip1) signaling: Transcriptional and post-translational regulation. *Int J Biochem Cell Biol* 2015, **68:** 9-14.

88. Polyak K, Lee MH, Erdjument-Bromage H, Koff A, Roberts JM, Tempst P*, et al.* Cloning of p27Kip1, a cyclin-dependent kinase inhibitor and a potential mediator of extracellular antimitogenic signals. *Cell* 1994, **78**(1)**:** 59-66.

89. Cusan M, Mungo G, De Marco Zompit M, Segatto I, Belletti B, Baldassarre G. Landscape of CDKN1B Mutations in Luminal Breast Cancer and Other Hormone-Driven Human Tumors. *Frontiers in Endocrinology* 2018, **9**(393).

90. Dijkers PF, Medema RH, Pals C, Banerji L, Thomas NSB, Lam EW-F*, et al.* Forkhead Transcription Factor FKHR-L1 Modulates Cytokine-Dependent Transcriptional Regulation of p27<sup>KIP1</sup>. *Molecular and Cellular Biology* 2000, **20**(24)**:** 9138-9148.

91. Gianani R. The Multiple Endocrine Neoplasia Type-1 (MEN-1) Syndrome and Its Effect on the Pancreas. *The Journal of Clinical Endocrinology & Metabolism* 2007, **92**(3)**:** 811-812.

92. Karnik SK, Hughes CM, Gu X, Rozenblatt-Rosen O, McLean GW, Xiong Y*, et al.* Menin regulates pancreatic islet growth by promoting histone methylation and expression of genes encoding p27<sup>Kip1</sup> and p18<sup>INK4c</sup>. *Proceedings of the National Academy of Sciences of the United States of America* 2005, **102**(41)**:** 14659-14664.

93. Yang W, Shen J, Wu M, Arsura M, FitzGerald M, Suldan Z*, et al.* Repression of transcription of the p27Kip1 cyclin-dependent kinase inhibitor gene by c-Myc. *Oncogene* 2001, **20:** 1688.

94. Chandramohan V, Mineva ND, Burke B, Jeay S, Wu M, Shen J*, et al.* c-Myc represses FOXO3a-mediated transcription of the gene encoding the p27Kip1 cyclin dependent kinase inhibitor. *Journal of Cellular Biochemistry* 2008, **104**(6)**:** 2091-2106.

95. le Sage C, Nagel R, Egan DA, Schrier M, Mesman E, Mangiola A*, et al.* Regulation of the p27(Kip1) tumor suppressor by miR-221 and miR-222 promotes cancer cell proliferation. *The EMBO journal* 2007, **26**(15)**:** 3699-3708.

96. Pineau P, Volinia S, McJunkin K, Marchio A, Battiston C, Terris B*, et al.* miR-221 overexpression contributes to liver tumorigenesis. *Proceedings of the National Academy of Sciences* 2010, **107**(1)**:** 264-269.

97. Pérez-Roger I, Solomon DLC, Sewing A, Land H. Myc activation of cyclin E/Cdk2 kinase involves induction of cyclin E gene transcription and inhibition of p27Kip1 binding to newly formed complexes. *Oncogene* 1997, **14:** 2373.

98. Müller D, Bouchard C, Rudolph B, Steiner P, Stuckmann I, Saffrich R*, et al.* Cdk2-dependent phosphorylation of p27 facilitates its Myc-induced release from cyclin E/cdk2 complexes. *Oncogene* 1997, **15:** 2561.

99. O'Hagan RC, Ohh M, David G, de Alboran IM, Alt FW, Kaelin WG, Jr*., et al.* Myc-enhanced expression of Cul1 promotes ubiquitin-dependent proteolysis and cell cycle progression. *Genes Dev* 2000, **14**(17)**:** 2185-2191.

100. Bretones G, Acosta JC, Caraballo JM, Ferrandiz N, Gomez-Casares MT, Albajar M*, et al.* SKP2 oncogene is a direct MYC target gene and MYC down-regulates p27(KIP1) through SKP2 in human leukemia cells. *J Biol Chem* 2011, **286**(11)**:** 9815-9825.

101. Gopfert U, Kullmann M, Hengst L. Cell cycle-dependent translation of p27 involves a responsive element in its 5'-UTR that overlaps with a uORF. *Human molecular genetics* 2003, **12**(14)**:** 1767-1779.

102. Tang HL, Zhang K, Guo K, Chen M. Quantification method of effects of uncertainty on component performance for turbo-shaft engine performance. *Tuijin Jishu/Journal of Propulsion Technology* 2015, **36**(8)**:** 1143-1150.

103. He X, Arslan AD, Ho TT, Yuan C, Stampfer MR, Beck WT. Involvement of polypyrimidine tract-binding protein (PTBP1) in maintaining breast cancer cell growth and malignant properties. *Oncogenesis* 2014, **3:** e84.

104. Kullmann M, Gopfert U, Siewe B, Hengst L. ELAV/Hu proteins inhibit p27 translation via an IRES element in the p27 5'UTR. *Genes Dev* 2002, **16**(23)**:** 3087-3099.

105. Zaharieva E, Haussmann IU, Bräuer U, Soller M. Concentration and localization of coexpressed ELAV/Hu proteins control specificity of mRNA processing. *Molecular and Cellular Biology* 2015, **35**(18)**:** 3104-3115.

106. Tsvetkov LM, Yeh KH, Lee SJ, Sun H, Zhang H. p27(Kip1) ubiquitination and degradation is regulated by the SCF(Skp2) complex through phosphorylated Thr187 in p27. *Current biology : CB* 1999, **9**(12)**:** 661-664.

107. Hao B, Zheng N, Schulman BA, Wu G, Miller JJ, Pagano M*, et al.* Structural basis of the Cks1-dependent recognition of p27(Kip1) by the SCF(Skp2) ubiquitin ligase. *Mol Cell* 2005, **20**(1)**:** 9-19.

108. Ganoth D, Bornstein G, Ko TK, Larsen B, Tyers M, Pagano M*, et al.* The cell-cycle regulatory protein Cks1 is required for SCF(Skp2)-mediated ubiquitinylation of p27. *Nature cell biology* 2001, **3**(3)**:** 321-324.

109. Spruck C, Strohmaier H, Watson M, Smith AP, Ryan A, Krek TW*, et al.* A CDK-independent function of mammalian Cks1: targeting of SCF(Skp2) to the CDK inhibitor p27Kip1. *Mol Cell* 2001, **7**(3)**:** 639-650.

110. Sheaff RJ, Groudine M, Gordon M, Roberts JM, Clurman BE. Cyclin E-CDK2 is a regulator of p27Kip1. *Genes Dev* 1997, **11**(11)**:** 1464-1478.

111. Bencivenga D, Caldarelli I, Stampone E, Mancini FP, Balestrieri ML, Della Ragione F*, et al.* p27(Kip1) and human cancers: A reappraisal of a still enigmatic protein. *Cancer letters* 2017, **403:** 354-365.

112. Ishida N, Hara T, Kamura T, Yoshida M, Nakayama K, Nakayama KI. Phosphorylation of p27Kip1 on serine 10 is required for its binding to CRM1 and nuclear export. *J Biol Chem* 2002, **277**(17)**:** 14355-14358.

113. Tomoda K, Kubota Y, Kato J. Degradation of the cyclin-dependent-kinase inhibitor p27Kip1 is instigated by Jab1. *Nature* 1999, **398**(6723)**:** 160-165.

114. Kamura T, Hara T, Matsumoto M, Ishida N, Okumura F, Hatakeyama S*, et al.* Cytoplasmic ubiquitin ligase KPC regulates proteolysis of p27(Kip1) at G1 phase. *Nature cell biology* 2004, **6**(12)**:** 1229-1235.

115. Susaki E, Nakayama K, Nakayama KI. Cyclin D2 translocates p27 out of the nucleus and promotes its degradation at the G0-G1 transition. *Mol Cell Biol* 2007, **27**(13)**:** 4626-4640.

116. Mishra A, Godavarthi SK, Jana NR. UBE3A/E6-AP regulates cell proliferation by promoting proteasomal degradation of p27. *Neurobiology of disease* 2009, **36**(1)**:** 26-34.

117. Shimada M, Kitagawa K, Dobashi Y, Isobe T, Hattori T, Uchida C*, et al.* High expression of Pirh2, an E3 ligase for p27, is associated with low expression of p27 and poor prognosis in head and neck cancers. *Cancer science* 2009, **100**(5)**:** 866-872.

118. Ye Y, Wang H, Chu JH, Chou GX, Chen SB, Mo H*, et al.* Atractylenolide II induces G1 cell-cycle arrest and apoptosis in B16 melanoma cells. *Journal of ethnopharmacology* 2011, **136**(1)**:** 279-282.

119. Wang D, Sun Q, Wu J, Wang W, Yao G, Li T*, et al.* A new Prenylated Flavonoid induces G0/G1 arrest and apoptosis through p38/JNK MAPK pathways in Human Hepatocellular Carcinoma cells. *Scientific Reports* 2017, **7**(1)**:** 5736.

120. Hashimoto T, Juso K, Nakano M, Nagano T, Kambayashi S, Nakashima A*, et al.* Preferential Fas-mediated apoptotic execution at G1 phase: the resistance of mitotic cells to the cell death. *Cell Death &Amp; Disease* 2012, **3:** e313.

121. Hiromura K, Pippin JW, Fero ML, Roberts JM, Shankland SJ. Modulation of apoptosis by the cyclin-dependent kinase inhibitor p27(Kip1). *J Clin Invest* 1999, **103**(5)**:** 597-604.

122. Gerdes J, Schwab U, Lemke H, Stein H. Production of a mouse monoclonal antibody reactive with a human nuclear antigen associated with cell proliferation. *International journal of cancer* 1983, **31**(1)**:** 13-20.

123. Inwald EC, Klinkhammer-Schalke M, Hofstadter F, Zeman F, Koller M, Gerstenhauer M*, et al.* Ki-67 is a prognostic parameter in breast cancer patients: results of a large population-based cohort of a cancer registry. *Breast cancer research and treatment* 2013, **139**(2)**:** 539-552.

124. Sotiriou C, Hayes DF, Penault-Llorca F, Viale G, Smith IE, Cuzick J*, et al.* Assessment of Ki67 in Breast Cancer: Recommendations from the International Ki67 in Breast Cancer Working Group. *JNCI: Journal of the National Cancer Institute* 2011, **103**(22)**:** 1656-1664.

125. Schlüter C, Duchrow M, Wohlenberg C, Becker MH, Key G, Flad HD*, et al.* The cell proliferation-associated antigen of antibody Ki-67: a very large, ubiquitous nuclear protein with numerous repeated elements, representing a new kind of cell cycle-maintaining proteins. *The Journal of Cell Biology* 1993, **123**(3)**:** 513-522.

126. Durocher D, Jackson SP. The FHA domain. *FEBS Letters* 2002, **513**(1)**:** 58-66.

127. Sueishi M, Takagi M, Yoneda Y. The forkhead-associated domain of Ki-67 antigen interacts with the novel kinesin-like protein Hklp2. *J Biol Chem* 2000, **275**(37)**:** 28888-28892.

128. Vanneste D, Takagi M, Imamoto N, Vernos I. The Role of Hklp2 in the Stabilization and Maintenance of Spindle Bipolarity. *Current Biology* 2009, **19**(20)**:** 1712-1717.

129. Lin TC, Su CY, Wu PY, Lai TC, Pan WA, Jan YH*, et al.* The nucleolar protein NIFK promotes cancer progression via CK1alpha/beta-catenin in metastasis and Ki-67-dependent cell proliferation. *eLife* 2016, **5**.

130. Sun X, Kaufman PD. Ki-67: more than a proliferation marker. *Chromosoma* 2018, **127**(2)**:** 175-186.

131. Booth DG, Takagi M, Sanchez-Pulido L, Petfalski E, Vargiu G, Samejima K*, et al.* Ki-67 is a PP1-interacting protein that organises the mitotic chromosome periphery. *eLife* 2014, **3:** e01641.

132. Takagi M, Nishiyama Y, Taguchi A, Imamoto N. Ki67 antigen contributes to the timely accumulation of protein phosphatase 1gamma on anaphase chromosomes. *J Biol Chem* 2014, **289**(33)**:** 22877-22887.

133. MacCallum DE, Hall PA. Biochemical Characterization of pKi67 with the Identification of a Mitotic-Specific Form Associated with Hyperphosphorylation and Altered DNA Binding. *Experimental Cell Research* 1999, **252**(1)**:** 186-198.

134. Saiwaki T, Kotera I, Sasaki M, Takagi M, Yoneda Y. In vivo dynamics and kinetics of pKi-67: Transition from a mobile to an immobile form at the onset of anaphase. *Experimental Cell Research* 2005, **308**(1)**:** 123-134.

135. Cuylen S, Blaukopf C, Politi AZ, Müller-Reichert T, Neumann B, Poser I*, et al.* Ki-67 acts as a biological surfactant to disperse mitotic chromosomes. *Nature* 2016, **535:** 308.

136. Endl E, Steinbach P, Knuchel R, Hofstadter F. Analysis of cell cycle-related Ki-67 and p120 expression by flow cytometric BrdUrd-Hoechst/7AAD and immunolabeling technique. *Cytometry* 1997, **29**(3)**:** 233-241.

137. Miller I, Min M, Yang C, Tian C, Gookin S, Carter D*, et al.* Ki67 is a Graded Rather than a Binary Marker of Proliferation versus Quiescence. *Cell reports* 2018, **24**(5)**:** 1105-1112.e1105.

138. Zambon AC. Use of the Ki67 promoter to label cell cycle entry in living cells. *Cytometry A* 2010, **77**(6)**:** 564-570.

139. Pei DS, Qian GW, Tian H, Mou J, Li W, Zheng JN. Analysis of human Ki-67 gene promoter and identification of the Sp1 binding sites for Ki-67 transcription. *Tumour biology : the journal of the International Society for Oncodevelopmental Biology and Medicine* 2012, **33**(1)**:** 257-266.

140. Li L, Qian G, Tian H, Di J, Chen F, Zheng J. Identification of hypomethylation profile of Ki-67 promoter in vitro and in vivo. *Int J Clin Exp Pathol* 2016, **9**(2)**:** 1311-1318.

141. Ishida S, Huang E, Zuzan H, Spang R, Leone G, West M*, et al.* Role for E2F in control of both DNA replication and mitotic functions as revealed from DNA microarray analysis. *Mol Cell Biol* 2001, **21**(14)**:** 4684-4699.

142. Brandeis M, Frank D, Keshet I, Siegfried Z, Mendelsohn M, Nemes A*, et al.* Sp1 elements protect a CpG island from de novo methylation. *Nature* 1994, **371**(6496)**:** 435-438.

143. Sobecki M, Mrouj K, Camasses A, Parisis N, Nicolas E, Lleres D*, et al.* The cell proliferation antigen Ki-67 organises heterochromatin. *eLife* 2016, **5:** e13722.

144. Cidado J, Wong HY, Rosen DM, Cimino-Mathews A, Garay JP, Fessler AG*, et al.* Ki-67 is required for maintenance of cancer stem cells but not cell proliferation. *Oncotarget* 2016, **7**(5)**:** 6281-6293.

145. Scholzen T, Endl E, Wohlenberg C, van der Sar S, Cowell IG, Gerdes J*, et al.* The Ki-67 protein interacts with members of the heterochromatin protein 1 (HP1) family: a potential role in the regulation of higher-order chromatin structure. *The Journal of pathology* 2002, **196**(2)**:** 135-144.

146. Plaat B, Kole A, Mastik M, Hoekstra H, Molenaar W, Vaalburg W. Protein synthesis rate measured with L-[1-11C]tyrosine positron emission tomography correlates with mitotic activity and MIB-1 antibody-detected proliferation in human soft tissue sarcomas. *European journal of nuclear medicine* 1999, **26**(4)**:** 328-332.

147. Van Hooser AA, Yuh P, Heald R. The perichromosomal layer. *Chromosoma* 2005, **114**(6)**:** 377-388.

148. Zizi-Sermpetzoglou A, Moustou E, Petrakopoulou N, Arkoumani E, Tepelenis N, Savvaidou V. Atypical polypoid adenomyoma of the uterus. A case report and a review of the literature. *European journal of gynaecological oncology* 2012, **33**(1)**:** 118-121.

149. Viale G. Pathological work up of the primary tumor: Getting the proper information out of it. *The Breast* 2011, **20:** S82-S86.

150. Ibrahim T, Farolfi A, Scarpi E, Mercatali L, Medri L, Ricci M*, et al.* Hormonal receptor, human epidermal growth factor receptor-2, and Ki67 discordance between primary breast cancer and paired metastases: clinical impact. *Oncology* 2013, **84**(3)**:** 150-157.

151. Chlebowski RT, Col N, Winer EP, Collyar DE, Cummings SR, Vogel VG, 3rd*, et al.* American Society of Clinical Oncology technology assessment of pharmacologic interventions for breast cancer risk reduction including tamoxifen, raloxifene, and aromatase inhibition. *Journal of clinical oncology : official journal of the American Society of Clinical Oncology* 2002, **20**(15)**:** 3328-3343.

152. Jonat W, Arnold N. Is the Ki-67 labelling index ready for clinical use? *Annals of oncology : official journal of the European Society for Medical Oncology* 2011, **22**(3)**:** 500-502.

153. Carroll D. Genome engineering with zinc-finger nucleases. *Genetics* 2011, **188**(4)**:** 773-782.

154. Miller JC, Tan S, Qiao G, Barlow KA, Wang J, Xia DF*, et al.* A TALE nuclease architecture for efficient genome editing. *Nature Biotechnology* 2010, **29:** 143.

155. Zhang F, Cong L, Lodato S, Kosuri S, Church GM, Arlotta P. Efficient construction of sequence-specific TAL effectors for modulating mammalian transcription. *Nat Biotechnol* 2011, **29**(2)**:** 149-153.

156. Naitou A, Kato Y, Nakanishi T, Matsuura T, Watanabe H. Heterodimeric TALENs induce targeted heritable mutations in the crustacean Daphnia magna. *Biology open* 2015, **4**(3)**:** 364-369.

157. Wiedenheft B, Sternberg SH, Doudna JA. RNA-guided genetic silencing systems in bacteria and archaea. *Nature* 2012, **482**(7385)**:** 331-338.

158. Bhaya D, Davison M, Barrangou R. CRISPR-Cas systems in bacteria and archaea: versatile small RNAs for adaptive defense and regulation. *Annual review of genetics* 2011, **45:** 273-297.

159. Makarova KS, Haft DH, Barrangou R, Brouns SJ, Charpentier E, Horvath P*, et al.* Evolution and classification of the CRISPR-Cas systems. *Nature reviews Microbiology* 2011, **9**(6)**:** 467-477.

160. Qi LS, Larson MH, Gilbert LA, Doudna JA, Weissman JS, Arkin AP*, et al.* Repurposing CRISPR as an RNA-guided platform for sequence-specific control of gene expression. *Cell* 2013, **152**(5)**:** 1173-1183.

161. Jinek M, Chylinski K, Fonfara I, Hauer M, Doudna JA, Charpentier E. A programmable dual-RNA-guided DNA endonuclease in adaptive bacterial immunity. *Science* 2012, **337**(6096)**:** 816-821.

162. Cong L, Ran FA, Cox D, Lin S, Barretto R, Habib N*, et al.* Multiplex genome engineering using CRISPR/Cas systems. *Science* 2013, **339**(6121)**:** 819-823.

163. Mali P, Yang L, Esvelt KM, Aach J, Guell M, DiCarlo JE*, et al.* RNA-guided human genome engineering via Cas9. *Science (New York, NY)* 2013, **339**(6121)**:** 823-826.

164. DiCarlo JE, Norville JE, Mali P, Rios X, Aach J, Church GM. Genome engineering in Saccharomyces cerevisiae using CRISPR-Cas systems. *Nucleic acids research* 2013, **41**(7)**:** 4336-4343.

165. Zhang G-C, Kong II, Kim H, Liu J-J, Cate JHD, Jin Y-S. Construction of a quadruple auxotrophic mutant of an industrial polyploid saccharomyces cerevisiae strain by using RNA-guided Cas9 nuclease. *Applied and environmental microbiology* 2014, **80**(24)**:** 7694-7701.

166. Vyas VK, Barrasa MI, Fink GR. A Candida albicans CRISPR system permits genetic engineering of essential genes and gene families. *Science advances* 2015, **1**(3)**:** e1500248-e1500248.

167. Ng H, Dean N. Dramatic Improvement of CRISPR/Cas9 Editing in Candida albicans by Increased Single Guide RNA Expression. *mSphere* 2017, **2**(2)**:** e00385-00316.

168. Hwang WY, Fu Y, Reyon D, Maeder ML, Tsai SQ, Sander JD*, et al.* Efficient genome editing in zebrafish using a CRISPR-Cas system. *Nature biotechnology* 2013, **31**(3)**:** 227-229.

169. Gratz SJ, Cummings AM, Nguyen JN, Hamm DC, Donohue LK, Harrison MM*, et al.* Genome engineering of Drosophila with the CRISPR RNA-guided Cas9 nuclease. *Genetics* 2013, **194**(4)**:** 1029-1035.

170. Bassett AR, Tibbit C, Ponting CP, Liu J-L. Highly efficient targeted mutagenesis of Drosophila with the CRISPR/Cas9 system. *Cell reports* 2013, **4**(1)**:** 220-228.

171. Yan H, Opachaloemphan C, Mancini G, Yang H, Gallitto M, Mlejnek J*, et al.* An Engineered orco Mutation Produces Aberrant Social Behavior and Defective Neural Development in Ants. *Cell* 2017, **170**(4)**:** 736-747.e739.

172. Trible W, Olivos-Cisneros L, McKenzie SK, Saragosti J, Chang NC, Matthews BJ*, et al.* orco Mutagenesis Causes Loss of Antennal Lobe Glomeruli and Impaired Social Behavior in Ants. *Cell* 2017, **170**(4)**:** 727-735.e710.

173. Kistler KE, Vosshall LB, Matthews BJ. Genome engineering with CRISPR-Cas9 in the mosquito Aedes aegypti. *Cell reports* 2015, **11**(1)**:** 51-60.

174. Friedland AE, Tzur YB, Esvelt KM, Colaiácovo MP, Church GM, Calarco JA. Heritable genome editing in C. elegans via a CRISPR-Cas9 system. *Nature methods* 2013, **10**(8)**:** 741-743.

175. Jiang W, Zhou H, Bi H, Fromm M, Yang B, Weeks DP. Demonstration of CRISPR/Cas9/sgRNA-mediated targeted gene modification in Arabidopsis, tobacco, sorghum and rice. *Nucleic acids research* 2013, **41**(20)**:** e188-e188.

176. Wang H, Yang H, Shivalila CS, Dawlaty MM, Cheng AW, Zhang F*, et al.* One-step generation of mice carrying mutations in multiple genes by CRISPR/Cas-mediated genome engineering. *Cell* 2013, **153**(4)**:** 910-918.

177. Guo X, Li X-J. Targeted genome editing in primate embryos. *Cell research* 2015, **25**(7)**:** 767-768.

178. Baltimore D, Berg P, Botchan M, Carroll D, Charo RA, Church G*, et al.* Biotechnology. A prudent path forward for genomic engineering and germline gene modification. *Science (New York, NY)* 2015, **348**(6230)**:** 36-38.

179. Zhang C, Wang J, Quan R. Development and application of CRISPR/Cas9 technologies in genomic editing. *Human molecular genetics* 2018, **27**(R2)**:** R79-R88.

180. Komor AC, Kim YB, Packer MS, Zuris JA, Liu DR. Programmable editing of a target base in genomic DNA without double-stranded DNA cleavage. *Nature* 2016, **533**(7603)**:** 420-424.

181. Komor AC, Zhao KT, Packer MS, Gaudelli NM, Waterbury AL, Koblan LW*, et al.* Improved base excision repair inhibition and bacteriophage Mu Gam protein yields C:G-to-T:A base editors with higher efficiency and product purity. *Sci Adv* 2017, **3**(8)**:** eaao4774.

182. Maeder ML, Linder SJ, Cascio VM, Fu Y, Ho QH, Joung JK. CRISPR RNA-guided activation of endogenous human genes. *Nat Methods* 2013, **10**(10)**:** 977-979.

183. Perez-Pinera P, Kocak DD, Vockley CM, Adler AF, Kabadi AM, Polstein LR*, et al.* RNA-guided gene activation by CRISPR-Cas9-based transcription factors. *Nat Methods* 2013, **10**(10)**:** 973-976.

184. Gilbert LA, Larson MH, Morsut L, Liu Z, Brar GA, Torres SE*, et al.* CRISPR-mediated modular RNA-guided regulation of transcription in eukaryotes. *Cell* 2013, **154**(2)**:** 442-451.

185. Chen B, Gilbert LA, Cimini BA, Schnitzbauer J, Zhang W, Li GW*, et al.* Dynamic imaging of genomic loci in living human cells by an optimized CRISPR/Cas system. *Cell* 2013, **155**(7)**:** 1479-1491.

186. Kearns NA, Pham H, Tabak B, Genga RM, Silverstein NJ, Garber M*, et al.* Functional annotation of native enhancers with a Cas9-histone demethylase fusion. *Nat Methods* 2015, **12**(5)**:** 401-403.

187. Kwon DY, Zhao Y-T, Lamonica JM, Zhou Z. Locus-specific histone deacetylation using a synthetic CRISPR-Cas9-based HDAC. *Nature Communications* 2017, **8:** 15315.

188. Lei Y, Zhang X, Su J, Jeong M, Gundry MC, Huang Y-H*, et al.* Targeted DNA methylation in vivo using an engineered dCas9-MQ1 fusion protein. *Nature Communications* 2017, **8:** 16026.

189. Huang Y-H, Su J, Lei Y, Brunetti L, Gundry MC, Zhang X*, et al.* DNA epigenome editing using CRISPR-Cas SunTag-directed DNMT3A. *Genome Biology* 2017, **18**(1)**:** 176.

190. Konermann S, Brigham MD, Trevino AE, Hsu PD, Heidenreich M, Le C*, et al.* Optical control of mammalian endogenous transcription and epigenetic states. *Nature* 2013, **500:** 472.

191. Jackson AL, Bartz SR, Schelter J, Kobayashi SV, Burchard J, Mao M*, et al.* Expression profiling reveals off-target gene regulation by RNAi. *Nat Biotechnol* 2003, **21**(6)**:** 635-637.

192. Liu Y, Cao Z, Wang Y, Guo Y, Xu P, Yuan P*, et al.* Genome-wide screening for functional long noncoding RNAs in human cells by Cas9 targeting of splice sites. *Nat Biotechnol* 2018.

193. Zhu S, Li W, Liu J, Chen CH, Liao Q, Xu P*, et al.* Genome-scale deletion screening of human long non-coding RNAs using a paired-guide RNA CRISPR-Cas9 library. *Nat Biotechnol* 2016, **34**(12)**:** 1279-1286.

194. Dai X, Park JJ, Du Y, Kim HR, Wang G, Errami Y*, et al.* One-step generation of modular CAR-T cells with AAV-Cpf1. *Nat Methods* 2019, **16**(3)**:** 247-254.

195. Barrangou R, Doudna JA. Applications of CRISPR technologies in research and beyond. *Nat Biotechnol* 2016, **34**(9)**:** 933-941.

196. Yamano T, Zetsche B, Ishitani R, Zhang F, Nishimasu H, Nureki O. Structural Basis for the Canonical and Non-canonical PAM Recognition by CRISPR-Cpf1. *Mol Cell* 2017, **67**(4)**:** 633-645.e633.

197. Cox DBT, Gootenberg JS, Abudayyeh OO, Franklin B, Kellner MJ, Joung J*, et al.* RNA editing with CRISPR-Cas13. *Science* 2017, **358**(6366)**:** 1019-1027.

198. Abudayyeh OO, Gootenberg JS, Essletzbichler P, Han S, Joung J, Belanto JJ*, et al.* RNA targeting with CRISPR–Cas13. *Nature* 2017, **550:** 280.

199. Schindele P, Wolter F, Puchta H. Transforming plant biology and breeding with CRISPR/Cas9, Cas12 and Cas13. *FEBS Lett* 2018, **592**(12)**:** 1954-1967.

200. Wang JY, Liu GZ, Wilmott JS, La T, Feng YC, Yari H*, et al.* Skp2-Mediated Stabilization of MTH1 Promotes Survival of Melanoma Cells upon Oxidative Stress. *Cancer Research* 2017, **77**(22)**:** 6226.

201. Pantel K, Brakenhoff RH. Dissecting the metastatic cascade. *Nat Rev Cancer* 2004, **4**(6)**:** 448-456.

202. Hirata Y, Furuhashi K, Ishii H, Li HW, Pinho S, Ding L*, et al.* CD150(high) Bone Marrow Tregs Maintain Hematopoietic Stem Cell Quiescence and Immune Privilege via Adenosine. *Cell stem cell* 2018, **22**(3)**:** 445-453.e445.

203. Sampath SC, Sampath SC, Ho ATV, Corbel SY, Millstone JD, Lamb J*, et al.* Induction of muscle stem cell quiescence by the secreted niche factor Oncostatin M. *Nat Commun* 2018, **9**(1)**:** 1531.

204. Lee HJ, Jedrychowski MP, Vinayagam A, Wu N, Shyh-Chang N, Hu Y*, et al.* Proteomic and Metabolomic Characterization of a Mammalian Cellular Transition from Quiescence to Proliferation. *Cell reports* 2017, **20**(3)**:** 721-736.

205. Coller HA, Sang L, Roberts JM. A new description of cellular quiescence. *PLoS Biol* 2006, **4**(3)**:** e83.

206. Scholzen T, Gerdes J. The Ki-67 protein: from the known and the unknown. *J Cell Physiol* 2000, **182**(3)**:** 311-322.

207. Besson A, Dowdy SF, Roberts JM. CDK Inhibitors: Cell Cycle Regulators and Beyond. *Developmental Cell* 2008, **14**(2)**:** 159-169.

208. Aguirre-Ghiso JA, Estrada Y, Liu D, Ossowski L. ERK(MAPK) activity as a determinant of tumor growth and dormancy; regulation by p38(SAPK). *Cancer Res* 2003, **63**(7)**:** 1684-1695.

209. Bjornson CR, Cheung TH, Liu L, Tripathi PV, Steeper KM, Rando TA. Notch signaling is necessary to maintain quiescence in adult muscle stem cells. *Stem Cells* 2012, **30**(2)**:** 232-242.

210. Brown JA, Yonekubo Y, Hanson N, Sastre-Perona A, Basin A, Rytlewski JA*, et al.* TGF-beta-Induced Quiescence Mediates Chemoresistance of Tumor-Propagating Cells in Squamous Cell Carcinoma. *Cell stem cell* 2017, **21**(5)**:** 650-664.e658.

211. Kwon JS, Everetts NJ, Wang X, Wang W, Della Croce K, Xing J*, et al.* Controlling Depth of Cellular Quiescence by an Rb-E2F Network Switch. *Cell reports* 2017, **20**(13)**:** 3223-3235.

212. Brien GL, Healy E, Jerman E, Conway E, Fadda E, O'Donovan D*, et al.* A chromatin-independent role of Polycomb-like 1 to stabilize p53 and promote cellular quiescence. *Genes Dev* 2015, **29**(21)**:** 2231-2243.

213. Cheung TH, Quach NL, Charville GW, Liu L, Park L, Edalati A*, et al.* Maintenance of muscle stem-cell quiescence by microRNA-489. *Nature* 2012, **482**(7386)**:** 524-528.

214. Roche B, Arcangioli B, Martienssen RA. RNA interference is essential for cellular quiescence. *Science* 2016, **354**(6313).

215. Raffel S, Trumpp A. miR-126 Drives Quiescence and Self-Renewal in Leukemic Stem Cells. *Cancer Cell* 2016, **29**(2)**:** 133-135.

216. Sato T, Yamamoto T, Sehara-Fujisawa A. miR-195/497 induce postnatal quiescence of skeletal muscle stem cells. *Nat Commun* 2014, **5:** 4597.

217. Suh EJ, Remillard MY, Legesse-Miller A, Johnson EL, Lemons JMS, Chapman TR*, et al.* A microRNA network regulates proliferative timing and extracellular matrix synthesis during cellular quiescence in fibroblasts. *Genome Biology* 2012, **13**(12)**:** R121-R121.

218. Kong Y, Nan K, Yin Y. Identification and characterization of CAC1 as a novel CDK2-associated cullin. *Cell Cycle* 2009, **8**(21)**:** 3552-3561.

219. Montagnoli A, Fiore F, Eytan E, Carrano AC, Draetta GF, Hershko A*, et al.* Ubiquitination of p27 is regulated by Cdk-dependent phosphorylation and trimeric complex formation. *Genes Dev* 1999, **13**(9)**:** 1181-1189.

220. Xi Z, Yao M, Li Y, Xie C, Holst J, Liu T*, et al.* Guttiferone K impedes cell cycle re-entry of quiescent prostate cancer cells via stabilization of FBXW7 and subsequent c-MYC degradation. *Cell Death Dis* 2016, **7**(6)**:** e2252.

221. Zhang YY, Tabataba H, Liu XY, Wang JY, Yan XG, Farrelly M*, et al.* ACTN4 regulates the stability of RIPK1 in melanoma. *Oncogene* 2018.

222. Nishitani H, Taraviras S, Lygerou Z, Nishimoto T. The human licensing factor for DNA replication Cdt1 accumulates in G1 and is destabilized after initiation of S-phase. *J Biol Chem* 2001, **276**(48)**:** 44905-44911.

223. Hara T, Kamura T, Nakayama K, Oshikawa K, Hatakeyama S, Nakayama K. Degradation of p27(Kip1) at the G(0)-G(1) transition mediated by a Skp2-independent ubiquitination pathway. *J Biol Chem* 2001, **276**(52)**:** 48937-48943.

224. Gos M, Miloszewska J, Swoboda P, Trembacz H, Skierski J, Janik P. Cellular quiescence induced by contact inhibition or serum withdrawal in C3H10T1/2 cells. *Cell proliferation* 2005, **38**(2)**:** 107-116.

225. Kim KH, Sederstrom JM. Assaying Cell Cycle Status Using Flow Cytometry. *Curr Protoc Mol Biol* 2015, **111:** 28 26 21-11.

226. Schaaf MB, Garg AD, Agostinis P. Defining the role of the tumor vasculature in antitumor immunity and immunotherapy. *Cell Death Dis* 2018, **9**(2)**:** 115.

227. Kossatz U, Dietrich N, Zender L, Buer J, Manns MP, Malek NP. Skp2-dependent degradation of p27kip1 is essential for cell cycle progression. *Genes Dev* 2004, **18**(21)**:** 2602-2607.

228. Jin L, Hu WL, Jiang CC, Wang JX, Han CC, Chu P*, et al.* MicroRNA-149*, a p53-responsive microRNA, functions as an oncogenic regulator in human melanoma. *Proc Natl Acad Sci U S A* 2011, **108**(38)**:** 15840-15845.

229. Suzuki HI, Yamagata K, Sugimoto K, Iwamoto T, Kato S, Miyazono K. Modulation of microRNA processing by p53. *Nature* 2009, **460**(7254)**:** 529-533.

230. Niculescu AB, Chen X, Smeets M, Hengst L, Prives C, Reed SI. Effects of p21(Cip1/Waf1) at Both the G(1)/S and the G(2)/M Cell Cycle Transitions: pRb Is a Critical Determinant in Blocking DNA Replication and in Preventing Endoreduplication. *Molecular and Cellular Biology* 1998, **18**(3)**:** 1763-1763.

231. Rufini A, Tucci P, Celardo I, Melino G. Senescence and aging: the critical roles of p53. *Oncogene* 2013, **32**(43)**:** 5129-5143.

232. Liu Y, Elf SE, Miyata Y, Sashida G, Liu Y, Huang G*, et al.* p53 Regulates Hematopoietic Stem Cell Quiescence. *Cell stem cell* 2009, **4**(1)**:** 37-48.

233. Denkert C, Furstenberg A, Daniel PT, Koch I, Kobel M, Weichert W*, et al.* Induction of G0/G1 cell cycle arrest in ovarian carcinoma cells by the anti-inflammatory drug NS-398, but not by COX-2-specific RNA interference. *Oncogene* 2003, **22**(54)**:** 8653-8661.

234. Barr AR, Cooper S, Heldt FS, Butera F, Stoy H, Mansfeld J*, et al.* DNA damage during S-phase mediates the proliferation-quiescence decision in the subsequent G1 via p21 expression. *Nat Commun* 2017, **8:** 14728.

235. Linke SP, Clarkin KC, Di Leonardo A, Tsou A, Wahl GM. A reversible, p53-dependent G0/G1 cell cycle arrest induced by ribonucleotide depletion in the absence of detectable DNA damage. *Genes Dev* 1996, **10**(8)**:** 934-947.

236. Almog N, Briggs C, Beheshti A, Ma L, Wilkie KP, Rietman E*, et al.* Transcriptional changes induced by the tumor dormancy-associated microRNA-190. *Transcription* 2013, **4**(4)**:** 177-191.

237. Galardi S, Mercatelli N, Giorda E, Massalini S, Frajese GV, Ciafre SA*, et al.* miR-221 and miR-222 expression affects the proliferation potential of human prostate carcinoma cell lines by targeting p27Kip1. *J Biol Chem* 2007, **282**(32)**:** 23716-23724.

238. Tang Y, Reed SI. The Cdk-associated protein Cks1 functions both in G1 and G2 in Saccharomyces cerevisiae. *Genes Dev* 1993, **7**(5)**:** 822-832.

239. Diaz-Perales A, Quesada V, Sanchez LM, Ugalde AP, Suarez MF, Fueyo A*, et al.* Identification of human aminopeptidase O, a novel metalloprotease with structural similarity to aminopeptidase B and leukotriene A4 hydrolase. *J Biol Chem* 2005, **280**(14)**:** 14310-14317.

240. Kyle AH, Baker JH, Minchinton AI. Targeting quiescent tumor cells via oxygen and IGF-I supplementation. *Cancer Res* 2012, **72**(3)**:** 801-809.

241. Li T, Kon N, Jiang L, Tan M, Ludwig T, Zhao Y*, et al.* Tumor suppression in the absence of p53-mediated cell cycle arrest, apoptosis, and senescence. *Cell* 2012, **149**(6)**:** 1269-1283.

242. O'Brate A, Giannakakou P. The importance of p53 location: nuclear or cytoplasmic zip code? *Drug resistance updates : reviews and commentaries in antimicrobial and anticancer chemotherapy* 2003, **6**(6)**:** 313-322.

243. Ratz M, Testa I, Hell SW, Jakobs S. CRISPR/Cas9-mediated endogenous protein tagging for RESOLFT super-resolution microscopy of living human cells. *Sci Rep* 2015, **5:** 9592.

244. Jiang Z, Zhou X, Li R, Michal JJ, Zhang S, Dodson MV*, et al.* Whole transcriptome analysis with sequencing: methods, challenges and potential solutions. *Cell Mol Life Sci* 2015, **72**(18)**:** 3425-3439.

245. Wang Z, Gerstein M, Snyder M. RNA-Seq: a revolutionary tool for transcriptomics. *Nat Rev Genet* 2009, **10**.

246. Wang Z, Gerstein M, Snyder M. RNA-Seq: a revolutionary tool for transcriptomics. *Nat Rev Genet* 2009, **10**(1)**:** 57-63.

247. James P. Protein identification in the post-genome era: the rapid rise of proteomics. *Quarterly reviews of biophysics* 1997, **30**(4)**:** 279-331.

248. Thrall B, Wiley HS, Waters KM, Girolami M, Rogers S, Liu T*, et al.* Investigating the correspondence between transcriptomic and proteomic expression profiles using coupled cluster models. *Bioinformatics* 2008, **24**(24)**:** 2894-2900.

249. Casey TM, Khan JM, Bringans SD, Koudelka T, Takle PS, Downs RA*, et al.* Analysis of Reproducibility of Proteome Coverage and Quantitation Using Isobaric Mass Tags (iTRAQ and TMT). *Journal of proteome research* 2017, **16**(2)**:** 384-392.

250. Tabb DL, Vega-Montoto L, Rudnick PA, Variyath AM, Ham A-JL, Bunk DM*, et al.* Repeatability and reproducibility in proteomic identifications by liquid chromatography-tandem mass spectrometry. *Journal of proteome research* 2010, **9**(2)**:** 761-776.

251. Washburn MP, Ulaszek RR, Yates JR. Reproducibility of Quantitative Proteomic Analyses of Complex Biological Mixtures by Multidimensional Protein Identification Technology. *Analytical Chemistry* 2003, **75**(19)**:** 5054-5061.

252. Röst HL, Malmström L, Aebersold R. Reproducible quantitative proteotype data matrices for systems biology. *Molecular Biology of the Cell* 2015, **26**(22)**:** 3926-3931.

253. Hidalgo-Galiana A, Monge M, Biron DG, Canals F, Ribera I, Cieslak A. Reproducibility and consistency of proteomic experiments on natural populations of a non-model aquatic insect. *PLoS One* 2014, **9**(8)**:** e104734.

254. Donaldson MM, Tavares AAM, Hagan IM, Nigg EA, Glover DM. The mitotic roles of Polo-like kinase. *Journal of Cell Science* 2001, **114**(13)**:** 2357-2358.

255. Wu J, Lu LY, Yu X. The role of BRCA1 in DNA damage response. *Protein & cell* 2010, **1**(2)**:** 117-123.

256. Wilson KM, Keng PC. Radiation-induced DNA damage and repair in quiescent and proliferating human tumor cells in vitro. *International journal of radiation biology* 1989, **55**(3)**:** 385-395.

257. Beerman I, Seita J, Inlay Matthew A, Weissman Irving L, Rossi Derrick J. Quiescent Hematopoietic Stem Cells Accumulate DNA Damage during Aging that Is Repaired upon Entry into Cell Cycle. *Cell stem cell* 2014, **15**(1)**:** 37-50.

258. Chen Y, Li D, Wang D, Liu X, Yin N, Song Y*, et al.* Quiescence and attenuated DNA damage response promote survival of esophageal cancer stem cells. *J Cell Biochem* 2012, **113**(12)**:** 3643-3652.

259. Housman G, Byler S, Heerboth S, Lapinska K, Longacre M, Snyder N*, et al.* Drug resistance in cancer: an overview. *Cancers* 2014, **6**(3)**:** 1769-1792.

260. Zhou Q, You C, Zheng C, Gu Y, Gu H, Zhang R*, et al.* 3-Nitroacridine derivatives arrest cell cycle at G0/G1 phase and induce apoptosis in human breast cancer cells may act as DNA-target anticancer agents. *Life Sciences* 2018, **206:** 1-9.

261. Wang X, Tian J, Jiao X, Geng J, Wang R, Liu N*, et al.* The novel mechanism of anticancer effect on gastric cancer through inducing G0/G1 cell cycle arrest and caspase-dependent apoptosis in vitro and in vivo by methionine enkephalin. *Cancer management and research* 2018, **10:** 4773-4787.

262. Ehrhardt H, Wachter F, Grunert M, Jeremias I. Cell cycle-arrested tumor cells exhibit increased sensitivity towards TRAIL-induced apoptosis. *Cell Death &Amp; Disease* 2013, **4:** e661.

263. Liberti MV, Locasale JW. The Warburg Effect: How Does it Benefit Cancer Cells? *Trends in biochemical sciences* 2016, **41**(3)**:** 211-218.

264. Vander Heiden MG, Cantley LC, Thompson CB. Understanding the Warburg effect: the metabolic requirements of cell proliferation. *Science* 2009, **324**(5930)**:** 1029-1033.

265. Shestov AA, Liu X, Ser Z, Cluntun AA, Hung YP, Huang L*, et al.* Quantitative determinants of aerobic glycolysis identify flux through the enzyme GAPDH as a limiting step. *eLife* 2014, **3**.

266. Thomas I, Gregg B. Metformin; a review of its history and future: from lilac to longevity. *Pediatric diabetes* 2017, **18**(1)**:** 10-16.

267. El-Mir MY, Nogueira V, Fontaine E, Averet N, Rigoulet M, Leverve X. Dimethylbiguanide inhibits cell respiration via an indirect effect targeted on the respiratory chain complex I. *J Biol Chem* 2000, **275**(1)**:** 223-228.

268. Ben Sahra I, Laurent K, Giuliano S, Larbret F, Ponzio G, Gounon P*, et al.* Targeting cancer cell metabolism: the combination of metformin and 2-deoxyglucose induces p53-dependent apoptosis in prostate cancer cells. *Cancer Res* 2010, **70**(6)**:** 2465-2475.

269. Schockel L, Glasauer A, Basit F, Bitschar K, Truong H, Erdmann G*, et al.* Targeting mitochondrial complex I using BAY 87-2243 reduces melanoma tumor growth. *Cancer Metab* 2015, **3:** 11.

270. Yang H, Tabe Y, Sekihara K, Saito K, Ma H, Ruvolo V*, et al.* Novel Oxidative Phosphorylation Inhibitor IACS-010759 Induces AMPK-Dependent Apoptosis of AML Cells. *Blood* 2017, **130**(Suppl 1)**:** 1245-1245.

271. An OXPHOS Inhibitor Has Antitumor Activity in Multiple Tumor Models. *Cancer discovery* 2018.

272. Touil Y, Igoudjil W, Corvaisier M, Dessein AF, Vandomme J, Monte D*, et al.* Colon cancer cells escape 5FU chemotherapy-induced cell death by entering stemness and quiescence associated with the c-Yes/YAP axis. *Clin Cancer Res* 2014, **20**(4)**:** 837-846.

273. Shah K, Lahiri DK. Cdk5 activity in the brain – multiple paths of regulation. *Journal of Cell Science* 2014, **127**(11)**:** 2391-2400.

274. Pozo K, Bibb JA. The Emerging Role of Cdk5 in Cancer. *Trends in cancer* 2016, **2**(10)**:** 606-618.

275. Patt HM, Quastler H. Radiation effects on cell renewal and related systems. *Physiological reviews* 1963, **43:** 357-396.

276. Yao G. Modelling mammalian cellular quiescence. *Interface Focus* 2014, **4**(3)**:** 20130074.

277. Artavanis-Tsakonas S, Rand MD, Lake RJ. Notch Signaling: Cell Fate Control and Signal Integration in Development. *Science* 1999, **284**(5415)**:** 770-776.

278. Valentin M, Yang E. Autophagy is activated, but is not required for the G0 function of BCL-2 or BCL-xL. *Cell Cycle* 2008, **7**(17)**:** 2762-2768.

279. Gray JV, Petsko GA, Johnston GC, Ringe D, Singer RA, Werner-Washburne M. "Sleeping beauty": quiescence in Saccharomyces cerevisiae. *Microbiology and molecular biology reviews : MMBR* 2004, **68**(2)**:** 187-206.

280. Shi Y, Lim SK, Liang Q, Iyer SV, Wang H-Y, Wang Z*, et al.* Gboxin is an oxidative phosphorylation inhibitor that targets glioblastoma. *Nature* 2019, **567**(7748)**:** 341-346.

281. Dasgupta A, Lim AR, Ghajar CM. Circulating and disseminated tumor cells: harbingers or initiators of metastasis? *Molecular oncology* 2017, **11**(1)**:** 40-61.

282. Linde N, Fluegen G, Aguirre-Ghiso JA. Chapter Two - The Relationship Between Dormant Cancer Cells and Their Microenvironment. In: Welch DR, Fisher PB (eds). *Advances in Cancer Research*, vol. 132. Academic Press, 2016, pp 45-71.

283. Chery L, Lam HM, Coleman I, Lakely B, Coleman R, Larson S*, et al.* Characterization of single disseminated prostate cancer cells reveals tumor cell heterogeneity and identifies dormancy associated pathways. *Oncotarget* 2014, **5**(20)**:** 9939-9951.

284. Moody SE, Sarkisian CJ, Hahn KT, Gunther EJ, Pickup S, Dugan KD*, et al.* Conditional activation of Neu in the mammary epithelium of transgenic mice results in reversible pulmonary metastasis. *Cancer Cell* 2002, **2**(6)**:** 451-461.

285. Polzer B, Klein CA. Metastasis awakening: the challenges of targeting minimal residual cancer. *Nat Med* 2013, **19**(3)**:** 274-275.

286. Sosa MS, Bragado P, Aguirre-Ghiso JA. Mechanisms of disseminated cancer cell dormancy: an awakening field. *Nat Rev Cancer* 2014, **14**(9)**:** 611-622.

287. Aguirre-Ghiso JA, Sosa MS. Emerging Topics on Disseminated Cancer Cell Dormancy and the Paradigm of Metastasis. *Annual Review of Cancer Biology* 2018, **2**(1)**:** 377-393.

288. Klein CA, Holzel D. Systemic cancer progression and tumor dormancy: mathematical models meet single cell genomics. *Cell Cycle* 2006, **5**(16)**:** 1788-1798.

289. Crea F, Nur Saidy NR, Collins CC, Wang Y. The epigenetic/noncoding origin of tumor dormancy. *Trends in molecular medicine* 2015, **21**(4)**:** 206-211.

290. Joyce JA, Fearon DT. T cell exclusion, immune privilege, and the tumor microenvironment. *Science* 2015, **348**(6230)**:** 74-80.

291. Spill F, Reynolds DS, Kamm RD, Zaman MH. Impact of the physical microenvironment on tumor progression and metastasis. *Current opinion in biotechnology* 2016, **40:** 41-48.

292. Bragado P, Estrada Y, Parikh F, Krause S, Capobianco C, Farina HG*, et al.* TGF-beta2 dictates disseminated tumour cell fate in target organs through TGF-beta-RIII and p38alpha/beta signalling. *Nature cell biology* 2013, **15**(11)**:** 1351-1361.

293. Gao H, Chakraborty G, Lee-Lim AP, Mo Q, Decker M, Vonica A*, et al.* The BMP inhibitor Coco reactivates breast cancer cells at lung metastatic sites. *Cell* 2012, **150**(4)**:** 764-779.

294. Kobayashi A, Okuda H, Xing F, Pandey PR, Watabe M, Hirota S*, et al.* Bone morphogenetic protein 7 in dormancy and metastasis of prostate cancer stem-like cells in bone. *The Journal of experimental medicine* 2011, **208**(13)**:** 2641-2655.

295. Kumar R, Langer JC, Snoeck HW. Transforming growth factor-beta2 is involved in quantitative genetic variation in thymic involution. *Blood* 2006, **107**(5)**:** 1974-1979.

296. Langer JC, Henckaerts E, Orenstein J, Snoeck HW. Quantitative trait analysis reveals transforming growth factor-beta2 as a positive regulator of early hematopoietic progenitor and stem cell function. *The Journal of experimental medicine* 2004, **199**(1)**:** 5-14.

297. Touil Y, Segard P, Ostyn P, Begard S, Aspord C, El Machhour R*, et al.* Melanoma dormancy in a mouse model is linked to GILZ/FOXO3A-dependent quiescence of disseminated stem-like cells. *Sci Rep* 2016, **6:** 30405.

298. Catena R, Bhattacharya N, El Rayes T, Wang S, Choi H, Gao D*, et al.* Bone marrow-derived Gr1+ cells can generate a metastasis-resistant microenvironment via induced secretion of thrombospondin-1. *Cancer discovery* 2013, **3**(5)**:** 578-589.

299. El Rayes T, Catena R, Lee S, Stawowczyk M, Joshi N, Fischbach C*, et al.* Lung inflammation promotes metastasis through neutrophil protease-mediated degradation of Tsp-1. *Proc Natl Acad Sci U S A* 2015, **112**(52)**:** 16000-16005.

300. Colleoni M, Sun Z, Price KN, Karlsson P, Forbes JF, Thurlimann B*, et al.* Annual Hazard Rates of Recurrence for Breast Cancer During 24 Years of Follow-Up: Results From the International Breast Cancer Study Group Trials I to V. *Journal of clinical oncology : official journal of the American Society of Clinical Oncology* 2016, **34**(9)**:** 927-935.

301. Guzvic M, Klein CA. Cancer dormancy: time to explore its clinical relevance. *Breast cancer research : BCR* 2013, **15**(6)**:** 321.

302. Kim RS, Avivar-Valderas A, Estrada Y, Bragado P, Sosa MS, Aguirre-Ghiso JA*, et al.* Dormancy signatures and metastasis in estrogen receptor positive and negative breast cancer. *PLoS One* 2012, **7**(4)**:** e35569.

303. Cheng Q, Chang JT, Gwin WR, Zhu J, Ambs S, Geradts J*, et al.* A signature of epithelial-mesenchymal plasticity and stromal activation in primary tumor modulates late recurrence in breast cancer independent of disease subtype. *Breast cancer research : BCR* 2014, **16**(4)**:** 407.

304. CUTTING WC, TAINTER ML. METABOLIC ACTIONS OF DINITROPHENOL: WITH THE USE OF BALANCED AND UNBALANCED DIETS. *JAMA* 1933, **101**(27)**:** 2099-2102.

305. Ellinghaus P, Heisler I, Unterschemmann K, Haerter M, Beck H, Greschat S*, et al.* BAY 87-2243, a highly potent and selective inhibitor of hypoxia-induced gene activation has antitumor activities by inhibition of mitochondrial complex I. *Cancer Medicine* 2013, **2**(5)**:** 611-624.

306. Schöckel L, Glasauer A, Basit F, Bitschar K, Truong H, Erdmann G*, et al.* Targeting mitochondrial complex I using BAY 87-2243 reduces melanoma tumor growth. *Cancer Metab* 2015, **3**.

307. Sica V, Bravo-San Pedro JM, Izzo V, Pol J, Pierredon S, Enot D*, et al.* Lethal Poisoning of Cancer Cells by Respiratory Chain Inhibition plus Dimethyl alpha-Ketoglutarate. *Cell reports* 2019, **27**(3)**:** 820-834.e829.

308. Molina JR, Sun Y, Protopopova M, Gera S, Bandi M, Bristow C*, et al.* An inhibitor of oxidative phosphorylation exploits cancer vulnerability. *Nat Med* 2018, **24**(7)**:** 1036-1046.